

Regulation of *Toxoplasma gondii* bradyzoite differentiation in terminally differentiated skeletal muscle cells

Dissertation

for the award of the degree

‘Doctor of Philosophy’ Ph.D. Division of Mathematics and Natural Sciences
of the Georg-August-Universität Göttingen

Within the doctoral program of Biology
of the Georg-August University School of Science (GAUSS)

Submitted by

Md. Taibur Rahman

Born in Dinajpur, Bangladesh

Göttingen, 2017

Thesis Committee:

Professor Dr. Uwe Groß

Institute for Medical Microbiology

Professor Dr. Gerhard Braus

Department of Molecular Microbiology and Genetics

Professor Dr. Carsten Lüder

Institute for Medical Microbiology

Members of the Examination board:

1. First Reviewer:

Professor Dr. Uwe Groß

Institute for Medical Microbiology

2. Second Reviewer:

Professor Dr. Gerhard Braus

Department of Molecular Microbiology and Genetics

Further members of the Examination Board:

3. Professor Dr. Carsten Lüder

Institute for Medical Microbiology

4. Professor Dr. Rolf Daniel

Department of Genomic and Applied Microbiology

5. Professor Dr. Stefan Pöhlmann

Infection Biology Unit,
German Primate Center

6. Dr. Fabian Moritz Commichau

Department of General Microbiology

Date of oral examination: 24 November 2017

Declaration:

I hereby declare that I prepared the PhD thesis entitled ‘Regulation of *Toxoplasma gondii* bradyzoite differentiation in terminally differentiated skeletal muscle cells’ on my own work and to the best of my knowledge with no other sources and aids than quoted.

Göttingen, 26 September 2017

Md. Taibur Rahman

Dedication:

‘To my family’

Acknowledgment:

First of all, I would like to thank my creator and merciful Allah for helping me to complete this PhD thesis. I have to express my heartfelt thank and gratitude to my supervisor Professor Dr. Carsten Lüder for providing me the opportunity to do this PhD work in his laboratory. I am very much grateful for his excellent mentoring, guidance in experimental work, proof-reading the thesis and sharing scientific knowledge throughout my PhD studies. It would not be possible to finish this work without his constant support with patient and love. I believe the experience and knowledge that I gathered here will certainly help me to contribute in science and welfare for human being in future. I would also thank the members of my thesis advisory committee Professor Dr. Uwe Groß and Professor Dr. Gerhard Braus for their invaluable suggestions, helpful feedback and evaluation of my thesis. I am also greatfull to Professor Dr. Rolf Daniel, Professor Dr. Stefan Pöhlmann, and Dr. Fabian Moritz Commichau for accepting to be examiner of my PhD thesis examination committee.

I want to thank Dr. Wolfgang Bohne, Dr. Oliver Bader and Dr. Raimond Lugert for their cordial support during my study. My special thanks to labmates and good friends Roswitha Nast, Sabrina Minatelli and Emilia Gomez for helping and discussing various scientific and daily life problems as well as for creating excellent environment for research. I also want to thank Vincent Buschatzky, Anastasia Lübke, Julian Schwanbeck, Pia Sternisek for creating nice atmosphere in the laboratory. Furthermore, I am deeply grateful to the staff of Institute for Medical Microbiology for the continuous help in maintaining and supplying reagents and equipments for my laboratory works.

I am extremely grateful to my parents, wife Afroza Sultana, my cute and lovely daughter Tamara Ambreen Rahman and other family members for their sacrifice and cordial support during this study. Special thanks to my wife for her sacrifice, continuous care and support in every single moment. I would also like to thank all of my Bangladeshi friends, seniors/juniors here in Göttingen for making nice atmosphere in daily life. And of course, many thanks to my home institution University of Dhaka for providing me the advance knowledge in the field of Biochemistry and Molecular Biology and granting leave for earning this PhD degree. In addition, I want to thank faculty members of the department of Biochemistry and Molecular Biology, University of Dhaka particularly to Prof. Dr. Mustafizur Rahman, Prof. Dr. Mamun Rashid Chowdhury, Prof. Dr. Hussain Uddin

Shekhar, Prof. Dr. A H M Nurun Nabi, Prof. Dr. A K M Mahbub Hasan for helping me to obtain the grant of my study.

Last but not least, I want to thank the collaborators of my studies, namely Dr. Martin Blume and Dr. Izabela Swierzy for helping in mass spectrometric analysis and Bryan Downie and Dr. Gabriela Salinas-Riester for transcriptome analysis.

I am indebted to my funding authority, the members of Interweave Erasmus Mundus scholarship commission and Professor Dr. Uwe Gross, head of Institute for Medical Microbiology for providing the financial support throughout the study period. In principle, it would not be possible to complete my PhD studies without these funding sources. Thank you very much for being part of my PhD studies at University of Göttingen.

Table of Content:

Acknowledgment.....	(I-II)
Table of content.....	(III-VII)
List of Figures.....	(VIII-X)
List of Tables.....	(XI-XII)
Abbreviations.....	(XIII-XVI)
Abstract.....	(XVII-XX)
Chapter 1: Introduction.....	1
1.1 <i>Toxoplasma gondii</i>	2
1.2 Life cycle of <i>Toxoplasma gondii</i>	3
1.3 Epidemiology and importance of meat from livestock in transmission of <i>T. gondii</i> to humans	5
1.4 Developmental biology of skeletal muscle cells (SkMCs).....	6
1.5 Glucose metabolism in proliferating and differentiating cells and its impact on ROS	8
1.6 Host factors regulating <i>T. gondii</i> stage conversion	10
1.6.1 Host immune responses can trigger <i>T. gondii</i> stage conversion	10
1.6.2 Exogenous stress factors can induce <i>T. gondii</i> stage conversion	11
1.6.3 Cell type-specific <i>T. gondii</i> stage conversion.....	12
1.6.4 Host cell cycle withdrawal is associated with <i>T. gondii</i> bradyzoite differentiation	13
1.6.5 Host cell metabolism and <i>T. gondii</i> stage conversion	14
1.7 Importance of the study	16
1.8 Hypothesis and aims of study.....	17

Chapter 2: Materials & Methods	18
2.1 Materials	19
2.1.1 Cell lines and organisms.....	19
2.1.2 Cell culture media.....	19
2.1.3 Cell culture dishes and plastic ware	20
2.1.4 Inhibitors/modulators used for experimental analysis.....	21
2.1.5 Lysis buffer for protein isolation	22
2.1.6 SDS-PAGE gel and buffer.....	22
2.1.7 Western blot buffer and solutions.....	23
2.1.8 Immunofluorescence staining buffer and solutions.....	24
2.1.9 Agarose gel buffer	24
2.1.10 Other chemicals	25
2.1.11 Reagents/ kits for experimental analysis	26
2.1.12 Antibodies for immunofluorescence and Western blot staining	26
2.1.13 List of primers used in qPCR	28
2.1.14 Instruments	29
2.1.15 Software and online tools	30
2.2 Methods	31
2.2.1 L929 cell culture	31
2.2.2 Parasite-L929 co-culture.....	31
2.2.3 C2C12 cell culture	32
2.2.4 Parasite isolation for infection assays.....	32
2.2.5 Myotubes and myoblasts preparation for experimental work	33
2.2.6 Treatment of myotubes and myoblasts with pharmacological inhibitors or modulators and parasite infection	34
2.2.7 P21 knockdown in C2C12 myoblasts by RNA interference	35
2.2.8 Quantitative reverse transcription PCR.....	40

2.2.9	Immunofluorescence staining.....	44
2.2.10	Bromodeoxyuridine (BrdU) incorporation assay	46
2.2.11	P21 expression examined by Western blotting.....	46
2.2.12	Measurement of intracellular NADP ⁺ /NADPH	49
2.2.13	Determination of intracellular Reactive Oxygen Species (ROS) levels.....	51
2.2.14	RNA sequencing.....	51
2.2.15	Isotope labeling and metabolite analysis via gas chromatography- coupled mass spectrometry (GC-MS)	54
2.2.16	Statistical analysis	55
Chapter 3: Results		56
3.1	Terminally differentiated SkMCs support <i>T. gondii</i> bradyzoite differentiation	57
3.1.1	<i>T. gondii</i> bradyzoite differentiation is accelerated in myotubes as compared to myoblasts	57
3.2	Transcriptome analysis of SkMCs.....	58
3.2.1	RT-qPCR confirms higher BAG1 mRNA expression in <i>T. gondii</i> within myotubes as compared to those in myoblasts	58
3.2.2	Parasite replication and myosin heavy chain expression in myotubes and myoblasts	60
3.2.3	Gene expression profiles of myoblasts and myotubes before and after <i>T. gondii</i> infection	60
3.2.4	DEGs in non-infected or infected myoblasts versus myotubes.....	61
3.2.5	Gene ontology analysis of differentially regulated genes in infected myoblasts versus myotubes	63
3.2.6	Biological processes associated with DEGs uniquely upregulated in infected myoblasts versus infected myotubes	64
3.2.7	GO term analysis of DEGs uniquely downregulated in infected myoblasts versus infected myotubes	65

3.2.8	Differential gene expression in non-infected and <i>T. gondii</i> -infected myotubes and myoblasts.....	66
3.2.9	Differential gene expression of distinct glucose metabolizing enzymes and cell cycle regulators in myotubes and myoblasts	67
3.3	Impact of differential glucose metabolism in SkMCs on <i>T. gondii</i> stage conversion.....	72
3.3.1	Differences in carbohydrate metabolism in <i>T. gondii</i> -infected and non-infected myotubes and myoblasts	72
3.3.2	Myotubes preferentially channel glycolytic pyruvate into the TCA cycle via anaplerotic reactions.....	74
3.3.3	Dehydroepiandrosterone accelerates <i>T. gondii</i> bradyzoite differentiation in myotubes and myoblasts.....	75
3.3.4	NADP ⁺ /NADPH levels in <i>T. gondii</i> -infected myoblasts and myotubes and their modulation by DHEA-mediated inhibition of G6PDH.....	79
3.3.5	6-aminonicotinamide induces <i>T. gondii</i> bradyzoite differentiation in myoblasts and myotubes.....	80
3.3.6	Phenyl acetic acid accelerates <i>T. gondii</i> BAG1 expression in myotubes but not in myoblasts	83
3.3.7	Dimethyl- α -ketoglutarate accelerates <i>T. gondii</i> BAG1 expression in myoblasts.....	85
3.3.8	Sodium-L-lactate induces <i>T. gondii</i> BAG1 expression in myoblasts but not in myotubes	87
3.4	Impact of redox homeostasis on <i>T. gondii</i> bradyzoite differentiation in SkMCs	90
3.4.1	Myotubes produce lower NADPH levels and higher ratio of NADP ⁺ /NADPH than myoblasts.....	90
3.4.2	CellROX staining indicates higher ROS levels in <i>T. gondii</i> -infected myoblasts than in myotubes	91
3.4.3	Modulation of ROS in SkMCs using antioxidants and its impact on <i>T. gondii</i> bradyzoite differentiation	93

3.4.4	N-acetyl cysteine induces extracellular <i>T. gondii</i> BAG1 mRNA expression	99
3.4.5	Modulation of ROS in SkMCs using ROS inducer and its impact on <i>T. gondii</i> bradyzoite differentiation	100
3.5	Impact of host cell cycle on <i>T. gondii</i> bradyzoite differentiation in SkMCs.....	104
3.5.1	Pharmacological cell cycle inhibitors accelerate <i>T. gondii</i> bradyzoite differentiation in SkMCs	104
3.5.2	Cell cycle inhibitors strongly arrest host cell proliferation	107
3.5.3	RNA interference mediated knock-down of cell cycle regulator p21 ^{Waf1/Cip1} and its impact on <i>T. gondii</i> bradyzoite differentiation on SkMCs	108
Chapter 4: Discussion.....		116
4.1	Terminally differentiated SkMCs support <i>T. gondii</i> stage conversion	117
4.2	Transcriptome analyses provide candidates for experimental proof on <i>T. gondii</i> stage conversion in SkMCs	118
4.3	Differences in host glucose metabolism impacts <i>T. gondii</i> stage conversion in SkMCs	124
4.4	Redox homeostasis modulate <i>T. gondii</i> stage conversion in SkMCs	129
4.5	Host cell cycle and its impact on <i>T. gondii</i> bradyzoite differentiation in SkMCs	132
Chapter 5: References		137
Chapter 6: Supplementary Tables.....		156
Chapter 7: Curriculum Vitae.....		166

List of Figures:

Figure No	Title	Page No
Figure 1.1:	Life cycle of <i>Toxoplasma gondii</i>	04
Figure 1.2:	Differentiation of myoblasts into myotubes	08
Figure 2.1:	Structure of MISSION [®] pLKO.1 plasmid	36
Figure 2.2:	Protein transfer by Western blotting	48
Figure 3.1:	<i>T. gondii</i> bradyzoite differentiation and tissue cyst formation is preferentially triggered in mature myotubes	58
Figure 3.2:	Myotubes support higher <i>T. gondii</i> BAG1 mRNA expression but similar parasite replication as compared to myoblasts	59
Figure 3.3:	Heatmap illustrating differential gene expression in non-infected and <i>T. gondii</i> -infected myoblasts and myotubes	61
Figure 3.4:	Identification of DEGs in non-infected and <i>T. gondii</i> -infected myoblasts and myotubes	63
Figure 3.5:	GO term enrichment analysis of differentially regulated genes in <i>T. gondii</i> -infected myoblasts and myotubes	63
Figure 3.6:	GO term enrichment analysis of DEGs uniquely upregulated in <i>T. gondii</i> -infected myoblasts versus infected myotubes	64
Figure 3.7:	GO term enrichment analysis of uniquely downregulated DEGs in infected myoblasts vs infected myotubes	65
Figure 3.8:	RNAseq gene expression data of selected metabolic enzymes and cell cycle protein p21 in <i>T. gondii</i> -infected and non-infected myotubes and myoblasts	69
Figure 3.9:	Validation of gene expression of selected metabolic enzymes and cell cycle protein p21 using RT-qPCR	70
Figure 3.10:	Mass spectrometric analysis of glucose catabolism in non-infected and <i>T. gondii</i> -infected myotubes and myoblasts	73

Figure 3.11:	Myotubes channel glycolytic carbon into the TCA cycle more readily through anaplerotic reactions than myoblasts	74
Figure 3.12:	Schematic diagram of glucose metabolism via pentose phosphate pathway, glycolysis and TCA cycle	77
Figure 3.13:	Dehydroepiandrosterone (DHEA) induces <i>T. gondii</i> bradyzoite differentiation and tissue cyst formation in myoblasts and myotubes	78
Figure 3.14:	NADP ⁺ /NADPH measurement in <i>T. gondii</i> -infected myotubes and myoblasts	80
Figure 3.15:	6-aminonicotinamide (6-AN) accelerates <i>T. gondii</i> bradyzoite differentiation in myoblasts and myotubes	82
Figure 3.16:	Impact of phenyl acetic acid on <i>T. gondii</i> BAG1 mRNA expression, parasite replication and cyst formation in myotubes and myoblasts	84
Figure 3.17:	Dimethyl- α -ketoglutarate induces <i>T. gondii</i> BAG1 expression and reduces parasite replication in myoblasts	86
Figure 3.18:	Lactate can increase BAG1 expression and cyst formation and can inhibit parasite replication in <i>T. gondii</i> within myoblasts but not in myotubes	88
Figure 3.19:	Myotubes produce reduced levels of NADPH as compared to myoblasts and have a higher NADP ⁺ /NADPH ratio	91
Figure 3.20:	ROS staining in <i>T. gondii</i> -infected and non-infected myotubes and myoblasts	92
Figure 3.21:	N-Acetyl cysteine inhibits <i>T. gondii</i> bradyzoite differentiation in myotubes and myoblasts but tissue cyst formation in myotubes only	95
Figure 3.22:	Tiron induces <i>T. gondii</i> BAG1 mRNA expression in myotubes and myoblasts but does not induce cyst formation	97
Figure 3.23:	Tiron inhibits DNA synthesis and proliferation of SkMCs	98

Figure 3.24:	N-acetyl cysteine induces BAG1 mRNA expression in extracellular parasites	99
Figure 3.25:	Luperox induce bradyzoite differentiation in myotubes and myoblasts	101
Figure 3.26:	H ₂ O ₂ induces BAG1 mRNA expression in <i>T. gondii</i> inside myotubes and myoblasts	103
Figure 3.27:	Cell cycle inhibitors can accelerate bradyzoite differentiation in myotubes and myoblasts	106
Figure 3.28:	Cell cycle inhibitors inhibit host cells proliferation	107
Figure 3.29:	Validation of RNA interference-mediated knock-down of p21 ^{Waf1/Cip1} in SkMCs and its impact on myotubes formation	110
Figure 3.30:	P21 knockdown in SkMCs does not generally accelerate host cell proliferation	112
Figure 3.31:	P21 knockdown in SkMCs does not impair bradyzoite differentiation but accelerates parasite replication	114
Figure 4.1:	Scheme on factors that induce <i>T. gondii</i> bradyzoite differentiation in myotubes	135

List of Tables:

Table No	Title	Page No
Table 2.1:	Inhibitors/modulators used for experimental analysis	34
Table 2.2:	Sequences of p21-targeted shRNA. Nucleotides forming the RNA loop within the shRNA are indicated in red	36
Table 2.3:	Transfection of C2C12 myoblasts cells with p21-shRNA or negative control pLKO.1 plasmids	39
Table 2.4:	Reaction components for cDNA synthesis	41
Table 2.5:	Real time qPCR reaction mixture	42
Table 2.6:	Real time qPCR programs for gene expression analysis	43
Table 2.7:	Antibodies used in immunofluorescence staining	45
Table 2.8:	Primary and secondary antibodies used in western blotting	49
Table 2.9:	Major components of the NADP ⁺ /NADPH quantification kit	49
Supplementary Table 3.1:	Top30 uniquely upregulated DEGs in <i>T. gondii</i> -infected myoblasts versus myotubes	155
Supplementary Table 3.2:	Top30 uniquely downregulated DEGs in <i>T. gondii</i> -infected myoblasts versus myotubes	156
Supplementary Table 3.3:	List of differentially regulated genes in <i>T. gondii</i> -infected myotubes versus non-infected myotubes	157
Supplementary Table 3.4:	List of differentially regulated genes in <i>T. gondii</i> -infected myoblasts versus non-infected myoblasts	158
Supplementary Table 3.5:	List of DEGs involved in glycolysis in non-infected and <i>T. gondii</i> -infected myotubes and myoblasts	160
Supplementary Table 3.6:	List of DEGs involved in TCA cycle in non-infected and <i>T. gondii</i> -infected myotubes and myoblasts	161

Supplementary Table 3.7:	List of DEGs involved in the pentose phosphate pathway in non-infected and <i>T. gondii</i> -infected myotubes and myoblasts	162
Supplementary Table 3.8:	List of DEGs involved in glycogen metabolism in non-infected and <i>T. gondii</i> -infected myotubes and myoblasts	162
Supplementary Table 3.9:	List of DEGs involved in cell cycle regulation in non-infected and <i>T. gondii</i> -infected myotubes and myoblasts	163

Abbreviations:

Ab	Antibody
APH	Aphidicolin
APS	Ammonium persulfate
ANOVA	Analysis of variance
ATP	Adenosine triphosphate
6-AN	6-Aminonicotinamide
BAG1	Bradyzoite antigen1
BrdU	Bromodeoxyuridine
BSA	Bovine serum albumin
BSTFA	N, O-Bistrifluoroacetamide
Cy	Cyanine
C	Carbon
Ca	Calcium
CCL	Chemokine ligand
CDA	Cell division autoantigen
CDK	Cyclin-dependent kinase
cDNA	Complementary DNA
°C	Degree Celsius
CHO	Chinese hamster ovary
CO ₂	Carbon dioxide
CP	Crossing point
DABCO	1,4-Diazabicyclo[2.2.2]octane
DAVID	Database for Annotation, Visualization and Integrated Discovery
DBL	<i>Dolichos biflorus</i> lectin
DEGs	Differentially expressed genes
DGE	Deutsche Gesellschaft für Ernährung
DHEA	Dehydroepiandrosteron
DMEM	Dulbecco's modified Eagle's medium
DMKG	Dimethyl- α -ketoglutarate

DMSO	Dimethyl sulfoxide
DNA	Deoxyribonucleic acid
DNaseI	Deoxyribonuclease I
dNTP	Deoxynucleotide triphosphate
E	Efficiency
<i>E. coli</i>	<i>Escherichia coli</i>
ECACC	European Collection of Authenticated Cell Cultures
EDTA	Ethylene diamine tetra-acetic acid
ERK	Extracellular signal regulated kinase
FCS	Fetal calf serum
For	Forward
FV	Field of vision
g	Gravity
G6PDH	Glucose-6-phosphate dehydrogenase
GAPDH	Glyceraldehyde-3-phosphate dehydrogenase
GC-MS	Gas chromatographic mass spectrometry
H ₂ O ₂	Hydrogen peroxide
•OH	Hydroxyl radicals
HCl	Hydrochloric acid
HFF	Human foreskin fibroblasts
HIV	Human immune deficiency virus
HS	Horse serum
IFN	Interferon
IgG	Immunoglobulin G
IL	Interleukin
iNOS	Inducible nitric oxide synthase
KDa	Kilodalton
LB	Luria-Bertani
LDL	Low-density lipoprotein
LPS	Lipopolysaccharides
M	Molar
MAPK	Mitogen-activated protein kinase
MCP	Monocyte chemoattractant protein

Mg	Magnesium
µg	Microgram
MIM	Mimosine
ml	Milliliter
mM	Milimolar
MRF	Myogenic regulatory factor
mRNA	Messenger RNA
NAC	N-acetyl cystein
NADP	Nicotinamide adenine dinucleotide phosphate
NADPH	Reduced nicotinamide adenine dinucleotide phosphate
NaN ₃	Sodium azide
NAP	Nucleosome assembly protein
NCBI	National Center for Biotechnology Information
NF-κB	Nuclear factor kappa-beta
NH ₄ Cl	Ammonium chloride
NO	Nitric oxide
NOX-4	NADPH oxidase-4
<i>p</i>	Probability
PAA	Phenyl acetic acid
6PGDH	6-Phosphogluconate dehydrogenase
PAGE	Polyacrylamide gel electrophoresis
PBS	Phosphate-buffered saline
PC	Pyruvate carboxylase
PCNA	Proliferating cell nuclear antigen
PCR	Polymerase chain reaction
PDH	Pyruvate dehydrogenase
PEP	Phosphoenol pyruvate
PFA	Paraformaldehyde
PGC1-α	Proliferator-activated receptor-gamma coactivator 1 alpha
PI3K	Phosphoinositide-3-kinase
PLA2	PhospholipaseA2
PMSF	Phenylmethylsulfonylfluorid
PPP	Pentose phosphate pathway

qPCR	Quantitative polymerase chain reaction
RB	Retinoblastoma
Rev	Reverse
RISC	RNA-induced silencing complex
RNA	Ribonucleic acid
RNAi	RNA interference
RNAseq	RNA sequencing
ROS	Reactive oxygen species
RPKM	Reads per kilobase per million reads
RQN	RNA quality number
RT	Reverse transcriptase
SDS	Sodium dodecyl sulfate
SEM	Standard error mean
shRNA	Short hairpin RNA
siRNA	Small interfering RNA
SkMCs	Skeletal muscle cells
SNP	Sodium nitroprusside
<i>spp.</i>	Species
<i>T. gondii</i>	<i>Toxoplasma gondii</i>
TAE	Tris-acetate-EDTA
TBS	Tris-buffered saline
TCA	Tricarboxylic acid cycle
TEMED	Tetramethylethylenediamine
Tg	<i>Toxoplasma gondii</i>
TGF	Transforming growth factor
TMS	Trimethylsilyl
Tspyl2	Testis-specific Y-encoded-like protein-2
U	unit
χ^2	Chi-squared

Abstract

Toxoplasma gondii is an intracellular protozoan parasite that infects warm-blooded animals including an estimated thirty percent of humans world-wide. In immunocompetent host, primary infection is usually asymptomatic but fast-replicating tachyzoites partially undergo developmental switching into slow-replicating, dormant bradyzoites preferentially within muscular and neural tissues. Stage differentiation from tachyzoites to bradyzoites enables the parasite to establish chronic infection and facilitates transmission of the parasite to new hosts via predation or ingestion of raw or undercooked meat from infected livestock. Bradyzoite differentiation and tissue cyst development is spontaneously triggered in terminally differentiated skeletal muscle cells (SkMCs), i.e in myotubes but not in proliferating myoblasts or fibroblasts. The factors that trigger bradyzoite differentiation in myotubes are only partially known. Herein, host cell transcriptomes, metabolomes and cell cycle regulation were determined to identify host cell factors that might regulate bradyzoite differentiation in myotubes.

RNA sequencing-based transcriptome analysis of non-infected and *T. gondii*-infected myotubes and myoblasts revealed that these cell types differed significantly in the expression of ~6500 genes (DEGs) irrespective of *T. gondii* infection. Gene ontology analysis revealed that these DEGs predominantly regulated cellular component organization or biogenesis, cell cycle processes including mitotic cell cycle, muscle structure development and cellular metabolic processes. Surprisingly, infection with *T. gondii* had only a minor impact on gene expression in myoblasts and myotubes. Further analyses of the transcriptomes from infected and non-infected myoblasts and myotubes showed differential expression of various enzymes of the central carbohydrate metabolism. For example, genes encoding most glycolytic enzymes, some tricarboxylic acid (TCA) cycle enzymes, particularly the pyruvate carboxylase of TCA cycle anaplerosis, and multiple genes encoding glycogen metabolic enzymes were upregulated in myotubes as compared to myoblasts. In contrast, genes encoding enzymes of the pentose phosphate pathway (PPP) including glucose-6-phosphate dehydrogenase (G6PDH)2 or G6PDH(X-linked) and 6-phosphogluconate dehydrogenase (6PGDH) were upregulated in myoblasts compared to myotubes. In addition, myotubes showed upregulation of various cell cycle inhibitors including p21^{Waf1/Cip1} as compared to myoblasts whereas many cyclin-dependent kinases and their cyclins were upregulated in myoblasts compared to myotubes irrespective of whether the cells were non-infected or infected with *T. gondii*. Differential expression of

these molecules in myoblasts and myotubes irrespective of infection was further confirmed by RT-qPCR.

GC-MS analyses of non-infected and *T. gondii*-infected myotubes and myoblasts after labeling with ^{13}C -glucose indeed indicated increased PPP activities in myoblasts, accelerated TCA cycle anaplerosis via the pyruvate carboxylase in myotubes, but no differences in glycolysis between the cell types. Remarkably, pharmacological inhibition of the PPP using the G6PDH inhibitor dehydroepiandrosterone and the 6PGDH inhibitor 6-aminonicotinamide upregulated *T. gondii* bradyzoite antigen (BAG) 1 mRNA expression and tissue cyst formation while it reduced parasite replication in both cell types but to a higher extent in myoblasts. This indicated that lower PPP activities as observed in myotubes compared to myoblasts favors *T. gondii* stage conversion. In contrast, addition of the TCA cycle intermediate analogue dimethyl- α -ketoglutarate accelerated BAG1 mRNA expression without increasing tissue cyst formation by *T. gondii* in myoblasts but not in myotubes. Modulation of anaerobic glycolysis using sodium-L-lactate showed a trend of increased *T. gondii* bradyzoite differentiation in myoblasts only. Lower PPP activity as observed in myotubes led to reduced levels of NADPH and higher $\text{NADP}^+/\text{NADPH}$ ratios in myotubes than in myoblasts. Despite lower NADPH levels in myotubes, reactive oxygen species (ROS) levels were however nearly doubled in myoblasts than in myotubes. Modulation of endogenous ROS using the antioxidant N-acetyl cysteine inhibited *T. gondii* bradyzoite differentiation in both myotubes and myoblasts. Interestingly, inducing ROS in myotubes and myoblasts using the oxidants luperox or H_2O_2 accelerated *T. gondii* bradyzoite differentiation in both cell types. Thus, physiological concentration of endogenous ROS as observed in myotubes but not myoblasts might favor *T. gondii* stage conversion in myotubes.

Modulation of the host cell cycle of *T. gondii*-infected myotubes and myoblasts using pharmacological inhibitors aphidicolin and mimosine accelerated BAG1 mRNA expression in *T. gondii* within SkMCs but only partially induced tissue cyst formation. Furthermore, complete halting of parasite replication by higher concentrations of these inhibitors suggested a possibly direct effect on the parasites. To specifically modulate the host cell cycle and since myotubes showed upregulation of the cell cycle inhibitor $\text{p21}^{\text{Waf1/Cip1}}$ as compared to myoblasts, p21 was inhibited in SkMCs using RNA interference. Knock-down of p21 in myoblasts sustained cell cycle progression and

inhibited differentiation of myoblasts into myotubes. However, host cell p21 knock-down surprisingly even increased BAG1 mRNA expression by *T. gondii* but also strongly accelerated parasite replication in SkMCs. Thus, differentiation of SkMCs to myotubes promotes *T. gondii* bradyzoite formation independently of p21^{Waf1/Cip1}.

Together these data unravel large differences in the transcriptomes, the central carbohydrate metabolism and the cell cycle regulation between myoblasts and myotubes before and after infection with *T. gondii*. Out of these differences, the lower PPP activities, the higher TCA cycle activities and the physiological concentrations of endogenous ROS as observed in mature myotubes can regulate *T. gondii* bradyzoite formation in SkMCs.

Chapter 1: Introduction

1.1 *Toxoplasma gondii*

Toxoplasma gondii (*T. gondii*) is an obligate intracellular protozoan parasite of the phylum *Apicomplexa*. Other important parasites of the *Apicomplexa* include *Plasmodium spp.* (malaria), *Eimeria spp.* (coccidiosis), *Neospora spp.* (neosporosis), *Babesia spp.* (babesiosis), *Theileria spp.* (theileriosis) and *Cryptosporidium spp.* (cryptosporidiosis) (Kim and Weiss, 2004). Among them, *T. gondii* is the most prevalent and successful parasite in nature that can infect a wide variety of warm-blooded animals including humans and is responsible for the disease toxoplasmosis (Tenter *et al.*, 2000; Montoya and Liesenfeld, 2004). More than 100 years ago, *T. gondii* was initially identified by Nicolle and Manceaux in the blood and tissues of a North African rodent, namely *Ctenodactylus gundi* (Nicolle and Manceaux, 1908). *T. gondii* and other parasites of the phylum *Apicomplexa* contain distinct structures at their apical end as for instance the conoid, the micronemes and the rhoptries which are essential for invasion into host cells (Dubey *et al.*, 1998; Baum *et al.*, 2008). *T. gondii* uses diverse strategies to circumvent or to inhibit effective host defense mechanisms and thereby is able to lead to lifelong persistence in the host (Lüder *et al.*, 1999).

Acute toxoplasmosis by *T. gondii* infections is regularly asymptomatic or a mild disease with flu-like symptoms in immunocompetent host. However, infection of pregnant women can lead to transmission of actively proliferating parasites (i.e. the tachyzoites) to the fetus through vertical transmission that can cause congenital toxoplasmosis (Havelaar *et al.*, 2007; Pappas *et al.*, 2009) with severe neurological disability, retinochorioiditis, physical deformities (hydrocephalus) and severe tissue destruction (toxoplasmic encephalitis) or even death of the fetus (Tenter *et al.*, 2000; Gross *et al.*, 2004; Moncada and Montoya, 2012). Importantly, latent reactivated toxoplasmosis can also cause severe symptoms in immunocompromised patients such as those with acquired immune deficiency syndrome (AIDS) (Luft and Remington, 1992), transplant recipients (Barcan *et al.*, 2002; Grosu *et al.*, 2007) and cancer patients (Lu *et al.*, 2015).

Phylogenetic analysis of *T. gondii* isolates from Europe and North America showed that the parasite population consists of three major clonal lineages that are called type-I, type-II and type-III (Howe and Sibley, 1995). Among these, type-II strains predominate in infected human and domestic animals and are prevalent from Northern Europe (Jokelainen *et al.*, 2011) to Southern Europe (Sousa *et al.*, 2006). In Germany, 71%

isolates from infected humans are type-II strains (Maksimov *et al.*, 2012) whereas in France, more than 90% of isolates from humans and animals are type-II strains (Ajzenberg *et al.*, 2002; Aubert *et al.*, 2010). Similar prevalences of type-II strains of *T. gondii* have been found in North America (Howe and Sibley, 1995). While type-III strain are abundant in animals and are rarely seen in humans (Howe and Sibley, 1995; Ajzenberg *et al.*, 2002), type-I strains and atypical strains are mostly isolated from HIV-infected toxoplasmosis patients particularly from Africa and South America (Ajzenberg *et al.*, 2009). According to virulence, type-I strains are highly virulent in mice whereas type-II and III are less virulent (Sibley and Ajioka, 2008).

1.2 Life cycle of *Toxoplasma gondii*

T. gondii has a complex life cycle that takes place in two different hosts. It has both sexual and asexual stages in its life cycle where sexual reproduction takes place in definitive feline hosts such as the cat and asexual reproduction takes place in a wide variety of intermediate mammalian and avian hosts including humans. Sexual reproduction takes place in the intestine of cats after ingestion of bradyzoite-containing tissue cysts that are present in the tissues of chronically infected intermediate hosts. After destruction of the cyst wall by gastric enzymes, bradyzoites undergo self-limiting asexual multiplication within enterocytes to produce merozoites that lead to the formation of male and female gametes (Dubey, 1998; Ferguson, 2002). After fertilization, oocysts are formed within enterocytes followed by the release of unsporulated oocysts into the environment through cat feces. Shedding of oocysts starts within 3-15 days after the ingestion of tissue cysts and may continue up to 20 days (Dubey and Frenkel, 1972). Within the environment, the unsporulated oocysts undergo meiosis and division to yield eight haploid sporozoites contained within the infective oocysts. Oocysts are capable of surviving in the environment for more than a year and can contaminate food and water which are taken up by the intermediate host (Figure 1.1) where asexual reproduction occurs. After the release of sporozoites in the intestine of intermediate hosts and infection of enterocytes, acute infection with *T. gondii* is characterized by proliferation of fast-replicating tachyzoites which can disseminate throughout the body via the blood and lymphatic systems (Dubey, 1997). Robust innate and adaptive immunity in the intermediate host is able to largely eliminate the proliferating tachyzoites during acute infection but a portion of them

transform into slowly replicating bradyzoites preferentially in neural and muscular tissue (Dubey *et al.*, 1998). Developmental switching from tachyzoites into bradyzoites in brain and skeletal muscle is responsible for the long term chronic infection and transmission of the parasite to new hosts. Ingestion of tissue cysts via omnivorous or carnivorous feeding can lead to transmission of the parasite to either other intermediate hosts or to a cat for reinitiating the sexual phase of the cycle. Humans become infected by eating bradyzoite-containing undercooked meat (Cook *et al.*, 2000), by ingesting sporulated oocyst contaminating food and water (de Moura *et al.*, 2006; Jones and Dubey, 2012) and/or by vertical transmission from infected pregnant women to their fetus (Dunn *et al.*, 1999). This clearly shows that stage conversion from tachyzoites to bradyzoites is a key factor for parasite pathogenesis and provides a major route of transmission between intermediate hosts including humans due to long term persistence in skeletal muscle or brain cells.

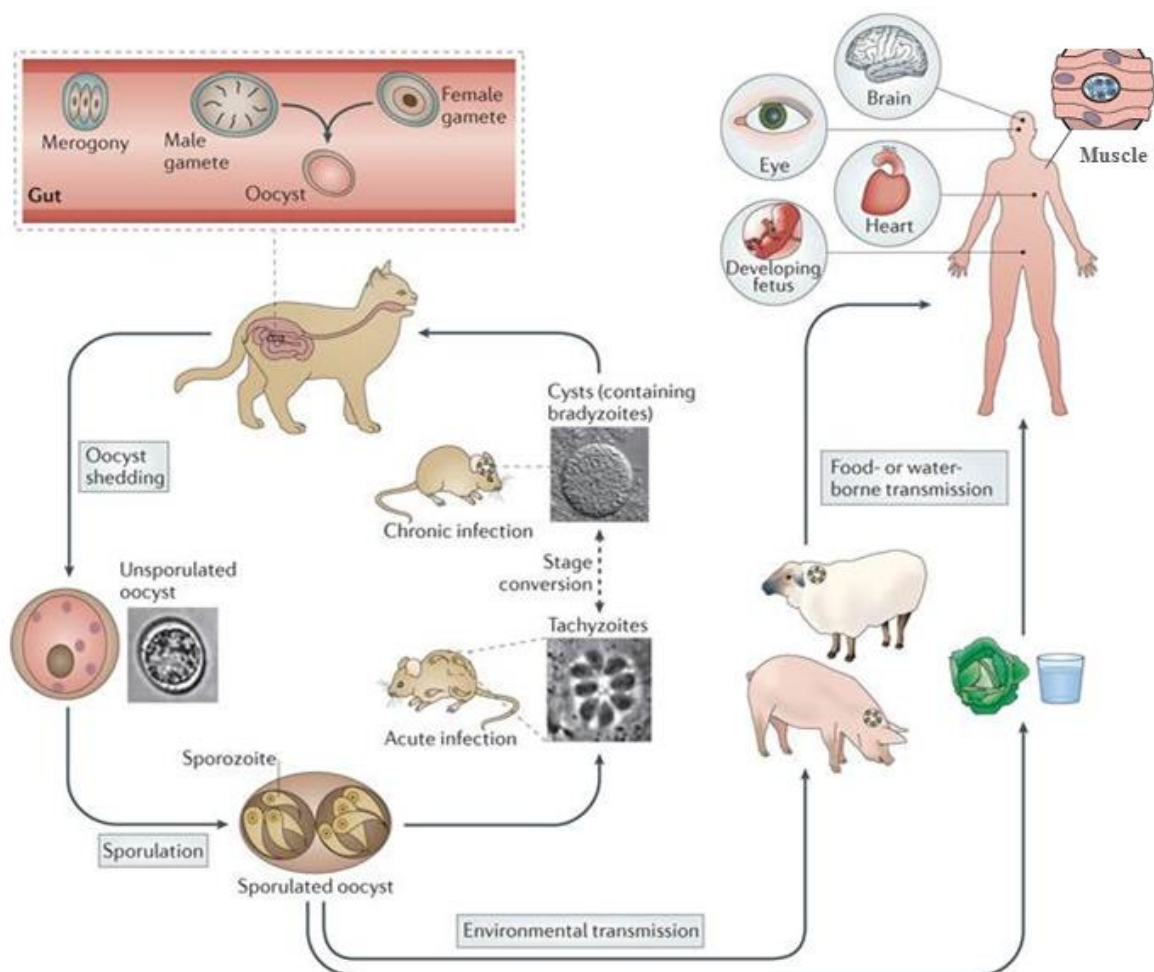


Figure 1.1: Life cycle of *Toxoplasma gondii* (Modified from Hunter & David Sibley 2012).

1.3 Epidemiology and importance of meat from livestock in transmission of *T. gondii* to humans

As *T. gondii* can infect any warm-blooded animal including livestock and humans, it is both of medical and veterinary importance. Congenital toxoplasmosis for example can lead to abortions in humans and animals, particularly in sheep (Tenter *et al.*, 2000). Recently, it has been reported that approximately 30-50 % of the human population is infected by *T. gondii* world-wide (Flegr *et al.*, 2014). The infection rate varies from 10 to 80% depending on environmental and socioeconomic factors including food habits, health-related practices and geographic areas (Pappas *et al.*, 2009). Relatively low prevalences (10-30%) of *T. gondii* infections have been found in North America, South East Asia, Northern Europe and Sahelian countries of Africa whereas moderate prevalences (30-50%) have been observed in countries of central and southern Europe, and in parts of Asia and Middle East. High prevalences (50-80%) have been found in some countries of Europe, Latin America and in tropical countries of Africa (Pappas *et al.*, 2009). Recently, a nationwide cross-sectional study was conducted in Germany, which showed that 55% of adult individuals are seropositive for *T. gondii* thus indicating a high prevalence in Germany. The rate of seroprevalence was found to increase with age from 20% in younger adults (age group 18-29 years) to 77% in older ones (age group 70-79 years). Furthermore, males showed a higher prevalence than females possibly because males are considered to consume more meat (Wilking *et al.*, 2016).

As discussed above, bradyzoite-containing tissue cysts in skeletal muscle of warm-blooded animals including livestock (pigs, sheep, goats, poultry, cattle) provide a major source of *T. gondii* infection in humans (Schlüter *et al.*, 2014). It has been shown before that eating raw and undercooked meat is one of the major routes of *T. gondii* transmission to humans (Tenter *et al.*, 2000; Ferguson, 2004). According to a European multicenter case control study, 30-63% of acute *Toxoplasma* infections of pregnant women were due to consumption of undercooked or cured meat products (Cook *et al.*, 2000). Another study conducted in the USA identified eating raw and cured meat as significant risk factor for *T. gondii* infection (Jones *et al.*, 2009; Jones and Dubey, 2012). This clearly points out the importance of meat and particularly skeletal muscles from chronically infected livestock for the transmission of *T. gondii* to humans. It has to be stressed that pig, cattle and poultry are the three major meat-producing animals consumed in Germany (Voth, 2015) and in the USA (Daniel *et al.*, 2011) that can harbor *T. gondii*. According to the German nutrition

society (DGE) from 2012, the average consumption of meat and meat products has been estimated to range from ~0.6 kg/person/week (women) to 1.1 kg/person/week (men). The amount of consumption of selected meat per capita in 2012 has been estimated ~52 kg for pork, ~18 kg for poultry and ~12 kg for beef (Voth, 2015). In Europe and USA, infected pork meat has been considered a major source of *T. gondii* infection in humans (Tenter, 2009; Dubey *et al.*, 2012). The reason is that pork is more likely to be infected with *T. gondii* than cattle and poultry due to a higher susceptibility of infection (Hill and Dubey, 2013). In Germany, the seroprevalence of *T. gondii* in pigs ranges from 2.8% (finishing pigs) to 31.6% (sows pigs) (De Buhr *et al.*, 2008). Consumption of infected poultry meat is also likely to play an important role in transmission of *T. gondii* to humans (Dubey *et al.*, 2005). A seroprevalence study conducted with chicken showed that 60% of chicken carried antibodies against *T. gondii* (Aigner *et al.*, 2010). Like the seroprevalence of pigs, it depends on the species and housing conditions where nearly 100% of backyard chickens are infected with *T. gondii* (Dubey, 2010a). For this reason, chickens are also considered an important source for transmission of *T. gondii* to humans. Prevalences of *T. gondii* in other meat-producing animals such as sheep, goats and horses vary with age. In Europe, the seroprevalence of *T. gondii* in farm sheep is increasing with age and ranges from 18% (lambs) to 89% (adults) (Halos *et al.*, 2010). Rates of seropositivity reported for goats vary from 4-77% (Dubey *et al.*, 2011) while they are generally lower in horses (Dubey, 2010b). These above data emphasize the importance of transmission of *T. gondii* through meat from chronically infected livestock to humans and request for an urgent attention to study mechanism of *T. gondii* persistence in skeletal muscle in order to limit spreading of the disease.

1.4 Developmental biology of skeletal muscle cells (SkMCs)

Skeletal muscle, a complex and heterogeneous tissue of animals, is mostly composed of highly specialized and large syncytial myotubes or muscle fibers. Myotubes are polynucleated and terminally differentiated SkMCs which develop from pluripotent progenitor cells during embryonic myogenesis or from uncommitted satellite stem cells during adult myogenesis (Bentzinger *et al.*, 2012). During embryonic myogenesis, pluripotent progenitor cells skip the uncommitted satellite cell stage and directly become committed satellite cells or proliferating myoblasts which further differentiate into myotubes

(Bentzinger *et al.*, 2012). Furthermore, some progenitor cells develop as a heterogeneous population of uncommitted and committed stem cells where the committed stem cells can eventually return into the uncommitted cell pool to compensate for the loss of terminally differentiated myotubes in adult skeletal muscles. However, adult myogenesis proceeds from uncommitted satellite stem cells to committed proliferating myoblasts which differentiate into non-proliferating mature myotubes (Bentzinger *et al.*, 2012). This *in vivo* muscle developmental process can be replicated *in vitro* using C2C12 murine myoblasts (Burattini *et al.*, 2004; Curci *et al.*, 2008; Abmayr and Pavlath, 2012). Subsequently, murine SkMCs has been used for studying the host-parasite interaction of *T. gondii* (Takács *et al.*, 2012; Swierzy and Lüder, 2014). Actively proliferating C2C12 myoblasts can be propagated *in vitro* in medium containing growth factors. C2C12 myoblasts start differentiating into myocytes in medium with reduced serum concentration referred to as differentiation medium. During differentiation, individual myocytes migrate, adhere and fuse with one another to form nascent myotubes with few nuclei. Afterwards, nascent myotubes fuse with other myocytes to form multinucleated, myosin heavy chain positive, mature myotubes (Abmayr and Pavlath, 2012; Bentzinger *et al.*, 2012; Swierzy and Lüder, 2014). Differentiation of C2C12 myoblasts into myotubes has been studied before by using differentiation medium comprising 2% horse serum (Rajan *et al.*, 2012). Both *in vivo* and *in vitro* differentiation of myoblasts into myotubes is regulated through several interconnected processes including (i) expression of four muscle-specific basic helix-loop-helix transcription factors, i.e MyoD, Myf5, myogenin, and myogenic regulatory factor (MRF4) (Huang and Thayer, 2002; Swierzy and Lüder, 2014), (ii) a permanent cell cycle withdrawal by upregulating the cell cycle inhibitors p21^{Waf1/Cip1} and p27, inhibition of cyclin-dependent kinases CDK1, CDK2, CDK4 and phosphorylation of retinoblastoma (RB) protein (Shen *et al.*, 2003; Casadei *et al.*, 2009), (iii) expression of muscle specific contractile proteins and (iv) fusion of mono-nucleated myoblasts together with myocytes (Huang and Thayer, 2002). *In vitro* differentiation of myoblasts into myotubes is shown in Figure 1.2.

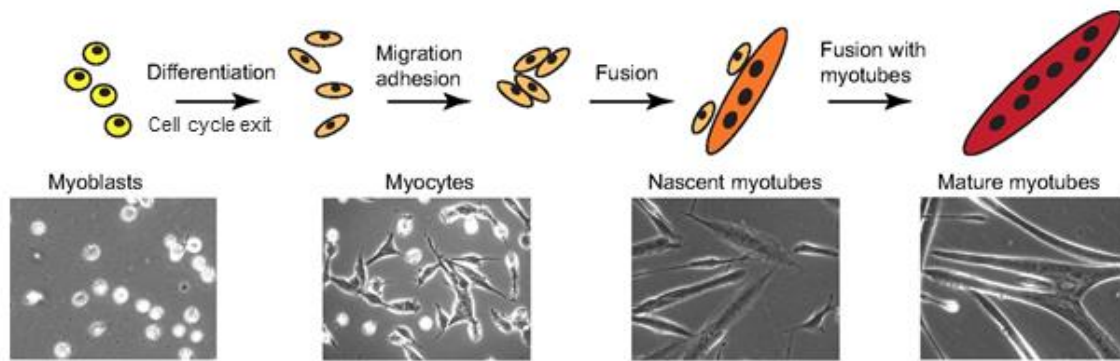


Figure 1.2: Differentiation of myoblasts into myotubes (Modified from Abmayr & Pavlath 2012).

1.5 Glucose metabolism in proliferating and differentiating cells and its impact on ROS

As a general rule, cell proliferation and differentiation is accompanied by a high demand on carbon sources, preferentially glucose, for the synthesis of membranes, organelles, biomass and energy (Fajas, 2013). After entering into cells, glucose can be metabolized in three major pathways; (i) it can undergo complete oxidation via glycolysis, tricarboxylic acid (TCA) cycle and oxidative phosphorylation, (ii) it can be metabolized through the pentose phosphate pathway (PPP) to produce ribose sugars for synthesis of nucleotides or reduced nicotinamide adenine dinucleotide phosphate (NADPH) for anabolic reactions and to defeat oxidative stress, (iii) and it can shift into glycogen synthesis for storage (Gottlieb, 2011). In proliferative cells, glucose metabolism is directed towards either glycolysis to rapidly generate energy equivalents and/or can be oxidized in the PPP to produce NADPH for synthesis of macromolecules including lipids, proteins and nucleotides (Aguilar and Fajas, 2010; Fajas, 2013). In contrast, carbohydrates in most differentiated cells are primarily completely oxidized to produce carbon dioxide through glycolysis in the cytoplasm followed by TCA cycle in mitochondria (Heiden *et al.*, 2009; Aguilar and Fajas, 2010). This metabolic shift is a key event for initiating cellular differentiation. This has been demonstrated by increased mitochondrial function and enzyme activity during differentiation of myoblasts to myotubes (Barbieri and Sestili, 2012; Wagatsuma and Sakuma, 2013). The evidences suggest that the metabolic shift from glycolysis to oxidative phosphorylation is the major energy source required for myogenesis. Aguilar and colleagues have described that cell proliferation requires an adaptive change of metabolism

and thereby have established a link between cell cycle regulation and metabolic control (Aguilar and Fajas, 2010). Cell cycle progression of proliferating cells from G1 into S-phase depends on the activation of G1 phase-specific cyclins/cyclin-dependent kinases (CDKs) and retinoblastoma (RB) protein pRB-E2F (Aguilar and Fajas, 2010). As myoblasts and myotubes differ largely in their cell cycle regulation (Shen *et al.*, 2003), they might also have different metabolic activities to support cellular proliferation and differentiation.

Differences of metabolic activities in a cell may generate differences in the redox homeostasis. Reactive oxygen species (ROS) are considered metabolic byproducts of normal cellular metabolism and are mainly composed of superoxide anions (O_2^-), hydroxyl radicals ($\bullet OH$) and H_2O_2 . Initially, ROS was identified as a deleterious species in SkMCs (Barbieri and Sestili, 2012). However, accumulating evidence suggest that ROS at physiological concentration may play beneficial roles in cells through multiple cellular functions using a wide variety of signaling cascades. For example, low levels of cellular ROS may act on cell survival, proliferation and differentiation, immune responses and other factors. On the contrary, high levels of ROS may create oxidative stress for the cell thereby contributing to deleterious effects as for instance muscle atrophy, apoptosis, inhibition of differentiation, and mitochondrial dysfunction (Barbieri and Sestili, 2012). In addition, ROS has recently been identified as a key modulator for microbial persistence and chronic infection (Spooner and Yilmaz, 2011). However, the beneficial or detrimental functions of ROS depend on multiple intrinsic and extrinsic factors as for instance concentration and duration of ROS signals in target cells, the site of ROS production, or the antioxidant status of the cell. In SkMCs, ROS can be produced from a variety of sources. Among these, mitochondria are considered the major source of ROS production as oxidative metabolism occurs to a large extent in mitochondria (Davies *et al.*, 1982). Complex-I and complex-III of the electron transport chain are indeed important sites for mitochondrial ROS production (Barja, 1999; Muller *et al.*, 2004). Another important source of ROS production is the enzyme NADPH oxidase (NOX) which is located in the sarcoplasmic reticulum and in transverse tubules of SkMCs (Piao *et al.*, 2005; Acharya *et al.*, 2013). Membrane-bound phospholipaseA2 (PLA2) may also play a passive role in intracellular ROS production by releasing membrane phospholipids, i.e. arachidonic acid which is a substrate for the ROS generating enzyme lipooxygenase-2 (Zuo *et al.*, 2004). In

addition, xanthine oxidase which is an important enzyme for purine metabolism also contributes to ROS production in SkMCs (Steinbacher and Eckl, 2015).

1.6 Host factors regulating *T. gondii* stage conversion

T. gondii establishes chronic infections in animals and humans through stage conversion from its fast-replicating tachyzoite stage to its slow-replicating bradyzoite stage. This stage conversion of the parasite is a complex process where tachyzoite-specific genes are switched off and bradyzoite-specific genes are upregulated (Lyons *et al.*, 2002). Upregulation of bradyzoite-specific gene expression leads to the development of bradyzoites and conversion of parasitophorous vacuoles into tissue cysts that may contain several hundreds of bradyzoites. Importantly, the tissue cyst distribution during chronic infection shows a predilection for distinct tissues with a preferential localization in skeletal muscles and brain (Dubey *et al.*, 1998). The factors that induce stage conversion in SkMCs and brain are not completely known. Nevertheless, research of the last decade has brought significant contributions to understand the biology of bradyzoite development in SkMCs.

1.6.1 Host immune responses can trigger *T. gondii* stage conversion

The host immune response is important for controlling any type of microbial infection. During acute *T. gondii* infection, the interferon (IFN)- γ -dependent cell-mediated host immune response eliminates the majority of *T. gondii* tachyzoites and controls pathogenesis (Suzuki *et al.*, 1988). However, IFN- γ can also induce tachyzoite-to-bradyzoite differentiation *in vitro* in certain cell types. This has been demonstrated by treatment of murine macrophages with IFN- γ and/or lipopolysaccharides (LPS) that inhibits parasite replication and induces bradyzoite differentiation (Bohne *et al.*, 1993, 1994). It has to be stressed that intermediate levels of macrophage activation are important because reduced parasite replication is required for induction of bradyzoite differentiation (Bohne *et al.*, 1994). This can be explained by the fact that too strongly activated macrophages may completely halt parasite cell cycle progression prior to reaching a cell cycle checkpoint that is required for *T. gondii* to enter into the bradyzoite-inducing

developmental program or may even kill the parasite. In contrast, non-activated macrophages support tachyzoite replication by directing cell cycle progression through S-phase to mitosis (Radke *et al.*, 2001). A key determinant of IFN- γ -mediated bradyzoite differentiation in murine macrophages is the production of nitric oxide (NO) by stimulation of the inducible nitric oxide synthase (iNOS) (Bohne *et al.*, 1994; Ibrahim *et al.*, 2009). This view is supported by using sodium nitroprusside (SNP), a donor of NO which induces bradyzoite differentiation not only in murine macrophage (Bohne *et al.*, 1994) but also in other cell types, i.e in rat brain cells (Lüder *et al.*, 1999) and human foreskin fibroblast (HFF) (Kirkman *et al.*, 2001) *in vitro*. NO is possibly exerting its effect by acting on mitochondrial functions of the host cell and/or the parasite by reacting with iron-sulfur centers of enzymes. It provides a link between mitochondrial metabolism and *T. gondii* bradyzoite differentiation.

In SkMCs, a number of cytokines and chemokines including chemokine ligand (CCL)-2, monocyte chemoattractant protein (MCP)-1, interleukin (IL)-1 α , IL-1 β and IL-23 are upregulated in mature myotubes as compared to myoblasts after *T. gondii* infection (Swierzy *et al.*, 2014). Whether these cytokines and chemokines induce *T. gondii* stage conversion in myotubes has not been determined. However, pro-inflammatory IL-6 has been shown to induce bradyzoite differentiation and tissue cysts formation in human fibroblasts (Weiss *et al.*, 1995). This raises the possibility that one or more of the above proinflammatory molecules may initiate bradyzoite development in myotubes which needs experimental validation.

1.6.2 Exogenous stress factors can induce *T. gondii* stage conversion

Several *in vitro* studies have shown that *T. gondii* stage conversion can also occur in the absence of inflammatory factors (McHugh *et al.*, 1993; Bohne *et al.*, 1994). Ferreira de Silva and colleagues have summarized numerous *in vitro* studies where stress factors were identified as inducers of bradyzoite development (Ferreira da Silva *et al.*, 2008). For example alkaline pH (pH 8.0-8.2) induces bradyzoite differentiation if infected cells are continuously exposed to this conditions (Soête *et al.*, 1994; Weiss *et al.*, 1995; Fux *et al.*, 2007). However, bradyzoite differentiation via alkaline pH does not provide sufficient evidence about the *in vivo* condition since such a high pH does not represent a

physiological condition. Applying heat shock (temperature $>43^{\circ}\text{C}$) is another factor that induces bradyzoite development in *T. gondii*-infected cells (Soête *et al.*, 1994). Here, the author exposed host cells to a heat shock at 43°C before and after *T. gondii* infection (Soête *et al.*, 1994). Besides, many chemicals and drugs have been shown to restrict parasite replication but also to induce bradyzoite-specific gene expression. For example, a combination of pyrimethamine and sulfadiazine has been shown to be most effective in the reduction of parasite replication and induction of bradyzoite antigen (BAG) 1 expression (Bohne *et al.*, 1994; Gross and Pohl, 1996). Similarly, hydronaphthoquinone and atovaquone show significant reduction of parasite replication and strong effect on BAG1 expression (Araujo *et al.*, 1992; Ferguson *et al.*, 1994). Other chemicals as for example sodium arsenite has been studied *in vitro* and shown to induce bradyzoite-specific genes but not to lead to development of tissue cysts (Soête *et al.*, 1994). Several mitochondrial inhibitors (oligomycin, antimycin-A, rotenone, myxothiazole) have been studied previously and found to induce bradyzoite-specific antigens without development of tissue cysts (Bohne *et al.*, 1994; Tomavo and Boothroyd, 1995).

T. gondii stage differentiation via these stress factors raises the question whether they act directly on the parasite or indirectly through the host cell or both. Nevertheless, the data provide useful information for *T. gondii* stage differentiation in infected cells *in vitro* and offer a link between stage conversion and host stress factors. But whether these factors induce bradyzoite development *in vivo* remains unclear.

1.6.3 Cell type-specific *T. gondii* stage conversion

T. gondii can infect any nucleated cell of mammalian and avian intermediate hosts including humans and stage conversion can occur in multiple tissues or cell types including brain, skeletal and heart muscle, eye, liver, kidney and others. However, it has to be stressed that *T. gondii* stage conversion preferentially occurs in skeletal muscle and brain, thereby leading to chronic infection. One explanation could be reduced inflammatory responses within both tissues which may allow *T. gondii* cyst development and survival. Another reason might be that they are post-mitotic, terminally differentiated cells which are permanently withdrawn from cell cycle progression and may thus present characteristics that are particularly suitable for parasite differentiation (Swierzy and Lüder,

2014; Lüder and Rahman, 2017). Primary SkMCs has been used as a model for studying development of *T. gondii* *in vitro* (Guimarães *et al.*, 2008). At the same time it has been shown that SkMCs support bradyzoite differentiation and tissue cyst formation. Remarkably, *T. gondii* stage conversion from its tachyzoite stage to the bradyzoite stage spontaneously occurs in primary SkMCs more readily than in fibroblasts and this does not require any exogenous stress factor (Guimarães *et al.*, 2008; Ferreira-da-Silva *et al.*, 2009). Recently, Swierzy and colleagues have shown that mouse SkMCs after differentiation into myosin heavy chain (MyHC)-positive poly-nucleated myotubes accelerate bradyzoite differentiation and tissue cysts formation whereas proliferating and MyHC-negative myoblasts support parasite growth and tachyzoite replication. This clearly shows that not only the cell type but the state of host cell is important for *T. gondii* stage conversion (Swierzy and Lüder, 2014).

1.6.4 Host cell cycle withdrawal is associated with *T. gondii* bradyzoite differentiation

One of the major differences between myoblasts and myotubes is the permanent cell cycle arrest of myotubes at G1/G0 phase (Shen *et al.*, 2003), which has been confirmed by lack of incorporation of Bromodeoxyuridine (BrdU) in DNA in myotubes (Swierzy and Lüder, 2014). Here the authors have thus confirmed that myotubes do not enter into the S phase of the cell cycle and hence do not replicate their DNA (Swierzy and Lüder, 2014). Since myotubes but not myoblasts trigger stage differentiation in *T. gondii*, it is therefore of great importance to study the impact of the host cell cycle on *T. gondii* bradyzoite differentiation in myotubes and myoblasts. Radke and colleagues have shown for the first time that overexpression of a host cell cycle regulator, namely human cell division autoantigen (CDA)-1 by using a trisubstituted pyrrole (designated compound-1) inhibits parasite growth and induces bradyzoite-specific proteins in *T. gondii* and formation of the cyst wall (Radke *et al.*, 2006). Consequently, knock-down of host CDA-1 prevented compound-1-mediated inhibition of parasite growth and bradyzoite differentiation (Radke *et al.*, 2006). CDA-1 in mice is known as testis specific Y-encoded like protein 2 (Tspyl2). It is a negative cell cycle regulator which inhibits cell growth and proliferation by inducing expression of p21^{Waf1/Cip1} via activation of p53 and extracellular signal regulated kinase (ERK)1/2 (Tu *et al.*, 2007; Tao *et al.*, 2011). Recently, the role of host CDA-1/Tspyl2 in

regulating stage differentiation in *T. gondii* has been confirmed under more physiological conditions using mouse SkMCs for *T. gondii* bradyzoite differentiation (Swierzy and Lüder, 2014). Here, the authors showed that differentiation of C2C12 murine myoblasts into poly-nucleated myotubes induces CDA-1/Tspsyl2 mRNA expression, and this was accompanied by cell cycle arrest in myotubes. Remarkably, siRNA-mediated knockdown of CDA-1/Tspsyl2 in C2C12 myoblasts accelerated host cell cycle progression even after induction of differentiation with low serum medium (2% horse serum) and this was accompanied with sustained parasite growth and abolished *T. gondii* stage conversion. The state of differentiation and withdrawal from cell cycle progression in SkMCs thus impact *T. gondii* stage conversion (Swierzy and Lüder, 2014). It is important to note that knockdown of CDA-1/Tspsyl2 in C2C12 myoblasts also inhibits myotubes formation suggesting multiple effects on host cells including cell cycle acceleration along with inhibition of myotube formation and others (Swierzy and Lüder, 2014). However, these studies provide a link between the host cell cycle and *T. gondii* stage conversion. The mechanism of how CDA-1/Tspsyl2 impacts *T. gondii* stage conversion is currently unknown. Importantly, CDA-1/Tspsyl2 upregulates the negative cell cycle regulator p21^{Waf1/Cip1} mRNA in myotubes (Swierzy and Lüder, 2014). However, whether increased levels of p21^{Waf1/Cip1} have any role in *T. gondii* bradyzoite differentiation in myotubes is still unknown.

1.6.5 Host cell metabolism and *T. gondii* stage conversion

T. gondii is an obligatory intracellular protozoan parasite. It must thus satisfy nutritional needs for replication and survival from its host cell. Through genome and transcriptome sequencing it has been revealed that *T. gondii* is auxotrophic for some metabolites (Blader et al. 2001; Gail et al. 2001; Crawford et al. 2006). Thus, they are unable to synthesize some essential metabolites and have to scavenge them from the host cell as for example arginine (Fox *et al.*, 2004), tryptophan (Pfefferkorn, 1984), phospholipids (Charron and Sibley, 2002), cholesterol (Coppens and Joiner, 2003; Sehgal *et al.*, 2005), polyamines (Cook *et al.*, 2007), purines (Krug *et al.*, 1989; Chaudhary *et al.*, 2004), cysteine and other essential amino acids except lysine (Chaudhary and Roos, 2005). They have to take up also basic nutrients such as glucose and glutamine (Blader and Koshy, 2014) and metal ions as for example iron (Gail *et al.*, 2004). Limited availability of these essential molecules from

host cells may thus inhibit parasite growth and favor *T. gondii* bradyzoite differentiation. For instance, starvation for arginine (Fox *et al.*, 2004) or pyrimidine in limited (0.03%) CO₂ concentration (Dzierszynski *et al.*, 2004) induces *T. gondii* bradyzoite differentiation. Similarly, it has been confirmed that starvation for low-density lipoprotein (LDL)-derived cholesterol also induces bradyzoite differentiation in chinese hamster ovary (CHO) cells (Ihara and Nishikawa, 2014). In addition to starvation for essential nutrients, there are some other metabolites that can induce stage conversion. For example, expression of ecto-5'-nucleotidase (CD73) which is needed for synthesis of adenosine, i.e. a major component of purines for which *T. gondii* is auxotrophic (Chaudhary *et al.*, 2004) promotes *T. gondii* bradyzoite differentiation and tissue cysts formation in the brain (Mahamed *et al.*, 2012). This has been confirmed through *in vivo* studies where mice lacking CD73 were protected from *T. gondii* chronic infection suggesting their inability to bradyzoite differentiation (Mahamed *et al.*, 2012).

As *T. gondii* uses glucose from host cells as a major carbon source for its energy metabolism and for biosynthesis of macromolecules (Blader and Koshy, 2014), glucose metabolism in different host cells may also play a role in *T. gondii* stage differentiation. An impact of the host glucose metabolism in *T. gondii* stage differentiation is indeed beginning to emerge. Recently, Weilhammer and co-workers have shown that the metabolic state of the host cell may play role in growth and differentiation of *T. gondii* (Weilhammer *et al.*, 2012). Here, the authors identified the glycolytic end product lactate as an inhibitory metabolite for *T. gondii* stage conversion in distinct host cells. Indeed, increased lactate secretion in supernatant was judged as indicator of higher glycolytic activities of NIH/3T3 fibroblasts and 293T embryonic kidney cells that are resistant to stage conversion under stress conditions. More importantly, supernatant from these cells transmitted the inhibitory activities for bradyzoite differentiation in Vero kidney cells but not in HFF which are normally permissive for *T. gondii* stage differentiation (Weilhammer *et al.*, 2012). Furthermore, upregulation of glycolysis in HFF and Vero cells by either increasing glucose concentration or by overexpression of the host kinase Akt also inhibited stage conversion (Weilhammer *et al.*, 2012). This data provide a link between higher levels of glycolysis in host cells and inhibition of *T. gondii* stage conversion which ultimately leads to continuous growth of the parasite. Since myotubes are terminally differentiated cells whereas myoblasts are actively proliferating cells, glucose metabolism may differ between these cell types. The complete picture of glucose metabolism in non-infected and

T. gondii-infected myotubes and myoblasts is thus a promising approach to understand the impact of host metabolic pathways on *T. gondii* stage conversion in myotubes.

1.7 Importance of the study

T. gondii appears to have a predilection for developmental switching from proliferative tachyzoites to dormant bradyzoites particularly in skeletal muscle and brain. The stage conversion in these tissues leads to the development of chronic infection in warm-blooded animals including livestock (Dubey *et al.*, 1998; Ferreira-da-Silva *et al.*, 2009). Furthermore, persistence of *T. gondii* in skeletal muscle of livestock animals (pigs, cattle, poultry, sheep and goat) provides a major route of parasite transmission to humans by eating raw or undercooked meat and meat products (Cook *et al.*, 2000; Jones *et al.*, 2009). This demonstrates the importance of *T. gondii* stage conversion and parasite persistence in skeletal muscle cell (SkMCs). It is thus important to identify the factors that induce *T. gondii* stage conversion in SkMCs. These factors are only partially known. *In vitro*, *T. gondii* can be induced to transform from tachyzoites to bradyzoites by exposure to external stress including alkaline pH, heat stress or chemicals (Ferreira da Silva *et al.*, 2008). Recently, Swierzy *et al.* have demonstrated that in differentiated SkMCs, i.e myotubes, *T. gondii* spontaneously differentiates from tachyzoites to bradyzoites in the absence of exogenous stress factors. In contrast, this did not occur in proliferating myoblasts or fibroblasts (Swierzy and Lüder, 2014). In addition, inactivation of the negative cell cycle regulator Tspyl2 by RNA interference largely abolished stage differentiation in SkMCs. These results indicate that terminal differentiation and/or cell cycle arrest of SkMCs is critical in regulating stage conversion. However, the exact factor(s) that induces *T. gondii* to transform to the bradyzoite stage is (are) not yet known.

1.8 Hypothesis and aims of study

It was hypothesized that *T. gondii* may encounter a distinct cellular microenvironment in myotubes that induces stage conversion in terminally differentiated SkMCs.

Therefore, the major aim of this study was to identify the factors which favor spontaneous stage conversion of *T. gondii* in SkMCs. The following issues were of particular interest to be addressed in this study:

- i. To unravel transcriptome differences of non-infected and *T. gondii*-infected myotubes and myoblasts.
- ii. To identify differences in glucose metabolism via glycolysis, TCA cycle and pentose phosphate pathway in non-infected and *T. gondii*-infected myotubes and myoblasts.
- iii. To determine the impact of metabolic pathways, i.e glycolysis, TCA cycle and pentose phosphate pathway on *T. gondii* stage conversion in myotubes and myoblasts using pharmacological inhibitors or modulators.
- iv. To unravel differences in NADPH production and ROS levels in non-infected and *T. gondii*-infected myotubes and myoblasts and to determine the effect ROS on *T. gondii* stage conversion.
- v. To determine the impact of pharmacological cell cycle inhibitors on *T. gondii* stage conversion in SkMCs.
- vi. To knock-down the negative cell cycle inhibitor p21^{Waf1/Cip1} and to determine its impact on *T. gondii* stage conversion in SkMCs.

Together, it was expected that the results of this study will further enhance our understanding of host cell factors which might provide the appropriate signal(s) that induces parasite stage differentiation and enables long term persistence of *T. gondii* in SkMCs

Chapter 2: Materials & Methods

2.1 Materials

2.1.1 Cell lines and organisms

- L929 murine fibroblasts from mouse C3H (Institute for Medical Microbiology, Göttingen).
- Murine C2C12 myoblasts from mouse C3H (European Collection of Authenticated Cell Cultures (ECACC), UK).
- Murine C2C12 mutant myoblasts (p21 knock-down) after transfection with p21-shRNA-pLKO.1 plasmids.
- Murine C2C12 mutant myoblasts (negative control) after transfection with pLKO.1-puro plasmid.
- Competent *Escherichia coli* NEB-5 α (New England Bio-Lab, Frankfurt/Main).
- Mission p21-shRNA bacterial glycerol stocks (Sigma-Aldrich, Munich).
- *Toxoplasma gondii* mouse-avirulent NTE strain (type II).

2.1.2 Cell culture media

Growth/Differentiation medium	Composition	Company
L929-growth medium	Dulbecco's modified Eagle's medium (DMEM) 1.0% FCS (Fetal calf serum) Penicillin-streptomycin (100 U/ml-100 μ g/ml) 1x Non-essential amino acid 1 mM Sodium pyruvate	Biochrom, Berlin
C2C12 growth medium	DMEM 10% FCS Penicillin-streptomycin (100 U/ml-100 μ g/ml)	Biochrom, Berlin
C2C12 differentiation medium	DMEM 2.0% Horse serum Penicillin-streptomycin (100 U/ml-100 μ g/ml)	Biochrom, Berlin

C2C12 transfection medium	DMEM 3.0% FCS Penicillin-streptomycin (100 U/ml-100 µg/ml)	Biochrom, Berlin
C2C12 metabolic labelling medium	Glucose-free DMEM 10% FCS Penicillin-streptomycin (100 U/ml-100 µg/ml)	Biochrom, Berlin
<i>Toxoplasma</i> medium	RPMI1640 (Roswell Park Memorial Institute) 1.0% FCS Penicillin-streptomycin (100 U/ml-100 µg/ml)	Biochrom, Berlin
Luria-Bertani (LB) broth/ LB-Agar (for <i>E. coli</i>)	1.0% Bacto-tryptone 0.5% Bacto-yeast extract 1.0% NaCl 1.5% Agar (LB-Agar only) Ampicillin (100 µg/ml)	Becton Dickinson, Heidelberg Becton Dickinson, Heidelberg Carl Roth, Karlsruhe Carl Roth, Karlsruhe Sigma-Aldrich, Munich
Terrific Broth (TB) medium	1.2% Bacto-tryptone 2.4% Bacto-yeast extract 0.4% Glycerol 1.0% Phosphate buffer (0.17M KH ₂ PO ₄ , 0.72M K ₂ HPO ₄)	Becton Dickinson, Heidelberg Becton Dickinson, Heidelberg Merck, Darmstadt Merck, Darmstadt Merck, Darmstadt

2.1.3 Cell culture dishes and plastic ware

Name	Company
Multi-well cell culture plates (6,12 and 24 well)	Greiner, Frickenhausen
96-well polystyrene cell culture plates	Greiner, Frickenhausen
96-well polystyrene flat bottom plates	Greiner, Frickenhausen
Cell culture flask (25cm ² and 75cm ²)	Greiner, Frickenhausen
Glass cover slips (diameter 13 mm, round)	Thermo Scientific, Braunschweig

Cryogenic vials (Nunc, 2mL)	Thermo Scientific, Braunschweig
Eppendorf tubes (1.5 ml and 2 ml)	Sarstedt, Nümbrecht
Centrifuge tubes (15 ml and 50 ml)	Sarstedt, Nümbrecht
Cell scrapers (24 cm)	Biochrom, Berlin
Nitrocellulose membrane	GE Healthcare, Buckinghamshire, UK
Whatman filter papers	GE Healthcare, Buckinghamshire, UK
Parafilm	BEMIS, Wisconsin, USA
Glass slides (76x26 mm)	Thermo Scientific, Braunschweig
Hemocytometer grid (cell counting chamber)	Sigma-Aldrich, Munich
Viva-spin filter (10 kDa cutoff)	Sartorius, Göttingen
Kimtech science kimwipes	Kimberly Clark professional, Surrey, UK
Star guard gloves	STARLAB GmbH, Hamburg
Pipette filter tips	Sarstedt, Nümbrecht

2.1.4 Inhibitors/modulators used for experimental analysis

Name	Company
Aphidicolin	Sigma-Aldrich, Munich
L-Mimosine	
Dehydroepiandrosterone	
6-Aminonicotinamide	
Phenylacetic acid	
Sodium-L-lactate	
Dimethyl- α -ketoglutarate	
N-acetylcystein	
Tiron	
Luperox (Tert-butyl hydroperoxide solution, 70 wt. % in H ₂ O)	
Hydrogen peroxide solution (30% w/v in H ₂ O)	

2.1.5 Lysis buffer for protein isolation

Item and Composition	Company
<u>2x Stock solution:</u>	
2% Triton-X 100	Sigma-Aldrich, Munich
300 mM NaCl	Merck, Darmstadt
100 mM Tris-HCl (pH 8.0)	Merck, Darmstadt
<u>Other components:</u>	
50 mM Sodium fluoride	Merck, Darmstadt
25 mM Sodium pyrophosphate	Sigma-Aldrich, Munich
1 mM Phenylmethylsulfonylfluoride (PMSF)	Sigma-Aldrich, Munich
10 µM Leupeptin	Sigma-Aldrich, Munich
5 µg/ml Aprotinin	Sigma-Aldrich, Munich
5 µg/ml Pepstatin	Sigma-Aldrich, Munich
1 mM Sodium orthovanadate	Sigma-Aldrich, Munich
1 mM Ethylene diamine tetra-acetic acid (EDTA)	Sigma-Aldrich, Munich
Sterile dd H ₂ O	

2.1.6 SDS-PAGE gel and buffer

Item	Composition	Company
Separating gel (12%)	0.375 M Tris-HCl (pH 8.8)	Carl Roth, Karlsruhe
	0.2% SDS	Carl Roth, Karlsruhe
	12% Acrylamide/Bis-acrylamide (30%/0.8% w/v)	Carl Roth, Karlsruhe
	0.04% APS	Merck, Darmstadt
	0.02% TEMED	Carl Roth, Karlsruhe
	ddH ₂ O	
Stacking gel (5%)	0.125 M Tris-HCl (pH 6.8)	Carl Roth, Karlsruhe
	0.2% SDS	Carl Roth, Karlsruhe
	5% Acrylamide/Bis-acrylamide (30%/0.8% w/v)	Carl Roth, Karlsruhe
	0.02% APS	Merck, Darmstadt
	0.02% TEMED	Carl Roth, Karlsruhe
	0.01% Bromophenol blue	Ameresco, Solon, USA
	ddH ₂ O	

1x Running buffer (pH 8.5)	25 mM Tris-HCl 192 mM Glycine 0.1% SDS	Carl Roth, Karlsruhe Carl Roth, Karlsruhe Carl Roth, Karlsruhe
5x SDS sample buffer	0.3125 M Tris-HCl, pH 6.8 10 % SDS 162.5 mM Dithiothreitol 50 % (v/v) Glycerol 0.05% (w/v) Bromophenol blue ddH ₂ O	Carl Roth, Karlsruhe Carl Roth, Karlsruhe Sigma-Aldrich, Munich Merck, Darmstadt Ameresco, Solon, USA

2.1.7 Western blot buffer and solutions

Item	Composition	Company
Tris-HCl buffer (0.3M)	20 ml 1.5 M Tris-HCl (pH 10.4) 20 ml 99% Methanol 60 ml ddH ₂ O	Carl Roth, Karlsruhe Carl Roth, Karlsruhe
Tris-HCl buffer (25mM)	20 ml 125 mM Tris-HCl (pH 10.4) 20 ml 99% Methanol 60 ml ddH ₂ O	Carl Roth, Karlsruhe Carl Roth, Karlsruhe
Aminocaproic acid buffer (40mM)	20 ml 200 mM Aminocaproic acid (pH 7.4) 20 ml 99% Methanol 60 ml ddH ₂ O	Sigma-Aldrich, Munich Carl Roth, Karlsruhe
Wash solution	1x TBS (Tris-buffered saline) 0.05% Tween 20 pH 7.4	Carl Roth, Karlsruhe Sigma-Aldrich, Munich
Blocking solution	5% Dry skimmed milk powder 1x TBS 0.05% Tween 20 pH 7.4	Carl Roth, Karlsruhe Carl Roth, Karlsruhe Sigma-Aldrich, Munich
Antibody incubation buffer	5% BSA 1x TBS 0.05% Tween 20 pH 7.4	Carl Roth, Karlsruhe Carl Roth, Karlsruhe Sigma-Aldrich, Munich

2.1.8 Immunofluorescence staining buffer and solutions

Item	Composition	Company
Washing buffer	1x PBS, pH 7.4 0.1 mg/ml Saponin	Biochrom, Berlin Sigma-Aldrich, Munich
Blocking buffer	1% BSA 1x PBS (pH 7.4) 0.02% NaN ₃ 0.1 mg/ml Saponin	Carl Roth, Karlsruhe Biochrom, Berlin Sigma-Aldrich, Munich Sigma-Aldrich, Munich
Propidium iodide solution	5 µg/ml propidiumiodide 1x PBS, pH 7.4	Sigma-Aldrich, Munich
Cell fixation solution	4% Paraformaldehyde 0.1 M Sodium- cacodylate/HCl pH 7.4	Merck, Darmstadt Carl Roth, Karlsruhe Merck, Darmstadt
Blocking solution for BrdU assay	5% BSA 0.3% Triton-X100 1x PBS (pH 7.4)	Carl Roth, Karlsruhe Sigma-Aldrich, Munich Biochrom, Berlin
Antibody incubation solution for BrdU assay	5% BSA 0.3% Triton-X100 1x PBS (pH 7.4)	Carl Roth, Karlsruhe Sigma-Aldrich, Munich Biochrom, Berlin
Wash solution for BrdU assay	1% BSA 1x PBS (pH 7.4)	Carl Roth, Karlsruhe Biochrom, Berlin

2.1.9 Agarose gel buffer

Item	Composition	Company
1x TAE buffer	40 mM Tris-HCl 20 mM Acetic acid 1.0 mM EDTA ddH ₂ O pH 8.0	Carl Roth, Karlsruhe Carl Roth, Karlsruhe Sigma-Aldrich, Munich

2.1.10 Other chemicals

Name	Company
Trypsin (0.25% in PBS w/o Ca ²⁺ and Mg ²⁺)	Biochrom, Berlin
EDTA (1.0% in PBS w/o Ca ²⁺ and Mg ²⁺)	Biochrom, Berlin
Trypanblue	Ferac, Berlin
Dimethyl sulfoxide (DMSO)	Sigma-Aldrich, Munich
Mowiol® 4-88	Merck, Darmstadt
Immersion oil	Sigma-Aldrich, Munich
Sodium azide (NaN ₃)	Sigma-Aldrich, Munich
PBS Dulbecco (w/o Ca ²⁺ and Mg ²⁺)	Biochrom, Berlin
Ethanol	Carl Roth, Karlsruhe
Laminine (murine)	Sigma-Aldrich, Munich
L-Polyornithine hydrobromide	Sigma-Aldrich, Munich
1,4-Diazabicyclo[2.2.2]octane (DABCO)	Sigma-Aldrich, Munich
Paraformaldehyde	Merck, Darmstadt
Sodium cacodylate	Carl Roth, Karlsruhe
Propidium iodide	Sigma-Aldrich, Munich
DNA Loading dye	Thermo Scientific, Braunschweig.
Gene Ruler (1 Kb)	Thermo Scientific, Braunschweig.
PonceauS solution (0.1 % (w/v) in 5% acetic acid)	Sigma-Aldrich, Munich
Prestained protein marker	Thermo Scientific, Braunschweig.
Glycerol	Merck, Darmstadt
Saponin	Sigma-Aldrich, Munich
HCl	Merck, Darmstadt
Glycine	Carl Roth, Karlsruhe
ECL Western blot detecting solution	GE Healthcare, Buckinghamshire, UK
¹³ C-D-glucose (uniform labelling of all Cs)	Euriso-top GmbH, Saarbrücken
Scyllo-Inositol	Sigma-Aldrich, Munich

2.1.11 Reagents/ kits for experimental analysis

Name of Analysis	Name of kits	Company
RNA isolation	GenElute Mammalian Total RNA Miniprep Kit	Sigma-Aldrich, Munich
DNase-I treatment	Deoxyribonuclease I Amplification Grade	Sigma-Aldrich, Munich
Reverse transcription	Omniscript Reverse Transcription Kit	Qiagen, Hilden
RNase inhibitor	RNasin 40 U/ μ l	Promega, Madison, USA
LightCycler qPCR	LightCycler FastStart DNA MasterPlus SYBR Green I	Roche, Mannheim
NADP ⁺ /NADPH measurement	NADP ⁺ /NADPH Assay Kit	Sigma-Aldrich, Munich
Plasmid isolation	GenElute Plasmid Miniprep Kit	Sigma-Aldrich, Munich
Transfection	FuGENE® HD Transfection Reagent	Roche, Mannheim
RNA analysis	RNA analysis kit, 15nt	Advance Analytical Technologies, California, USA
RNA sequencing kit	Illumina® TruSeq® RNA Sample Preparation Kit v2	Illumina, California, USA.
SOC outgrowth medium	Transformation	New England Bio-Lab, Frankfurt am Main

2.1.12 Antibodies for immunofluorescence and Western blot staining

Name	Company
<u>Primary antibodies:</u>	
Rabbit anti- <i>Toxoplasma</i> (serum)	Prof. Dr. Uwe Groß, Institute for Medical Microbiology, Göttingen

Mouse anti- <i>Toxoplasma</i> (serum)	Prof. Dr. Uwe Groß, Institute for Medical Microbiology, Göttingen
Biotin-conjugated <i>Dolichos biflorus</i> lectin (DBL)	Sigma-Aldrich, Saint Louis, USA
Mouse anti-BrdU antibody	Cell Signalling Technology, Massachusetts, USA
Rabbit anti-mouse myosin heavy chain antibody	Santa-Cruz Biotechnology, Heidelberg
Mouse anti-mouse p21(F5) antibody	Santa-Cruz Biotechnology, Heidelberg
Mouse anti-mouse β -actin antibody	Prof. Dr. James Lessard, Children's Hospital Medical Center in Cincinnati, Ohio, USA

Secondary antibodies:

Cy5-conjugated donkey F(ab') ₂ anti-rabbit IgG (H+L)	Jackson ImmunoResearch, Hamburg
Cy2-conjugated streptavidin	Jackson ImmunoResearch, Hamburg
DyLight488-conjugated donkey F(ab') ₂ anti-rabbit IgG (H+L)	Jackson ImmunoResearch, Hamburg
Cy5-conjugated goat anti-mouse IgG (Fc γ -specific)	Jackson ImmunoResearch, Hamburg
DyLight488-conjugated donkey F(ab') ₂ anti-mouse IgG (H+L)	Jackson ImmunoResearch, Hamburg
Peroxidase-conjugated goat F(ab') ₂ anti-mouse IgG (H+L)	Jackson ImmunoResearch, Hamburg

2.1.13 List of primers used in qPCR

Name of primers	Primer sequence (5'→3')	AnT (°C)	Company
TgBAG1-for TgBAG1-rev	AGCGGAGAAAGTGGACGATG TGATTTGTTGCTTTGCGCCC	66	
TgActin-for TgActin-rev	GGCGAACCGTGAGAGAATGA GCGTCCAGCAAGATCCAAAC	68	
TgGAPDH-for TgGAPDH-rev	GTCAATCATTCTGTCAATTCGA ACACCATGTAGTCCAGGGACATG	68	
mP21 ^{WAF1/Cip1} -for mP21 ^{WAF1/Cip1} -rev	CCGAGAGGTGTGAGCCGCCG GCATCGCAATCACGGCGCAA	68	
mG6PDH2-for mG6PDH2-rev	AGGACCTACCCATGGTCACA GGCAAGGAGGCTGTCCATAG	62	
mG6PDH(X-linked)-for mG6PDH(X-linked)-rev	GAGAGTGGGCTTCCAGTACG GGACAAAATGGCGGTCCAAG	63	Sigma- Aldrich, Munich
m6PGDH-for m6PGDH-rev	TGCCATGTGGACCAGACAAG AGGCACACCCAGAGAGTGTA	62	
mGlycogen phosphorylase-for mGlycogen phosphorylase-rev	GAGTGGACACGGATGGTGAT TAGAGACTGGGGAAAGTGGGT	62	
mGlycogen synthase 1-for mGlycogen synthase 1-rev	CCGTGCCTTTCTTGGATTGC GATTCGGGAAGCCACACAGA	65	
mActin-for mActin-rev	GTACCACCATGTACCCAGGC AAGGGTGTAACACGCAGCTC	72	
mPyruvate carboxylase-for mPyruvate carboxylase-rev	ATGACTCTGGAAGGCGACGA GCCATTGCAGGTAGTGTGTG	63	
pLKO.1-puro plasmid-for pLKO.1-puro plasmid-rev	TACGATACAAGGCTGTTAGAGAG CCGGTGTTTCGTCTTTCCA	61	

AnT: Annealing temperature

2.1.14 Instruments

Name	Company
LightCycler 1.5	Roche, Mannheim
Nanodrop-2000c Spectrophotometer	Thermo Scientific, Schwerte
Leica confocal microscope SP2	Leica Microsystem, Heidelberg
Leica microsystem (Light microscope)	Wetzlar GmbH, Wetzlar
Axiostar plus microscope	Carl Zeiss, Göttingen
Luminescent image analyzer (LAS-4000)	Fujifilm Life Science, Düsseldorf
Victor multilabel plate reader	Thermo Scientific, Schwerte
Gel doc XR system	Bio-Rad, Munich
Centrifuge megafuge 2.0 RS	Thermo Scientific, Schwerte
Eppendorf centrifuge 5417R	Eppendorf, Hamburg
Eppendorf thermomixer compact	Eppendorf, Hamburg
Heraeus CO ₂ incubator	Thermo Scientific, Schwerte
Refrigerators	Liebherr, Dortmund
Hemocytometer grid	Sigma-Aldrich, Munich
Biohazard safety hoods	BDK, Sonnenbühl-Genkingen
Reax top test tube shaker	Heidolph, Schwabach
Duomax 1030 Rocker shaker	Heidolph, Schwabach
Electrophoretic chamber	Bio-Rad, Munich
Electrophoresis power supply EPS 500/400	PharmaciaBiotech, Freiburg
Comb	Bio-Rad, Munich
Semidry western-blotter	Biometra, Göttingen
CP224S Analytical balance	Sartorius, Göttingen
pH meter	Mettler-Toledo, Giesen
Fragment Analyzer TM	Advance Analytical Technologies, California, USA
Illumina Hiseq TM 4000	Illumina, California, USA

2.1.15 Software and online tools

Name	Company
LightCycler software 1.5	Roche, Mannheim
Leica confocal microscope software	Leica Microsystem, Heidelberg
ImageQuant LAS-4000	Fujifilm Life Science, Düsseldorf
Wallac 1420 workstation	Thermo Scientific, Schwerte
QuantityOne (Gel doc image analysis software)	Bio-Rad, Munich
DAVID (Database for Annotation, Visualization and Integrated Discovery) online tool (version 6.8)	National Cancer Institute, Frederick, USA
Venn diagram tool	Gent, Belgium
Microsoft Office 2010	Microsoft Corporation, Washington, USA
GraphPadPrism 5	GraphPad software, California, USA
Mendeley Reference Manager	Mendeley, New York, USA
Primer designing tools	National Center for Biotechnology Information (NCBI), Bethesda, USA

2.2 Methods

2.2.1 L929 cell culture

L929 fibroblast cells from a C3H mouse were used as host cells for co-culturing of *T. gondii* in order to maintain steady supply of parasites for experimental work. To avoid excessive confluency, L929 cells were sub-cultured twice a week in a 6-well cell culture plate. To this end, cells were examined microscopically to confirm their appropriate density and viability. Then, cells were scraped off with a cell scraper in order to detach them from the culture dish. They were then resuspended, followed by adding eight drops of cell suspension into each well of a 6-well plate. Thereafter, ~4.0 ml of L929 growth medium was added into each well. L929 cultures were kept in an incubator at 37°C with 5% CO₂ and humidified atmosphere.

2.2.2 Parasite-L929 co-culture

The mouse-avirulent *T. gondii* type II strain NTE (Gross *et al.*, 1991) was used throughout this study. Parasites were maintained as viable, highly replicating and metabolically active tachyzoites through co-culturing with L929 host fibroblasts. To this end, different amounts of L929 cell suspension (see above) were distributed into the wells of a 12-well cell culture plate using 10 ml glass pipettes as follows: 5 drops in the first row, 4 drops in the second row and 3 drops in the third row. Thereafter, different amounts of viable extracellular parasites of appropriate density from previous co-cultures were added accordingly: 6 drops of parasite suspension into the 1st column, 4 drops into the 2nd and 3rd column and 2 drops into the 4th column of that 12-well plate. Finally, *Toxoplasma* medium was added into each well to a final volume of ~1.5 ml and plates were kept in a humidified atmosphere at 37°C with 5% CO₂.

2.2.3 C2C12 cell culture

The mouse skeletal muscle cell line C2C12 (seeding 1×10^5 cells/flask) were propagated as myoblasts in 75cm^2 cell culture flasks with ~ 30 ml C2C12 growth medium in a humidified atmosphere at 37°C with 5% CO_2 . C2C12 cells were grown and maintained in a proliferative state by keeping them subconfluent and by sub-culturing in fresh medium twice a week. To this end, cells were rinsed with EDTA (1.0% in PBS w/o Ca^{2+} and Mg^{2+}) and were then detached from the culture dish using trypsin (0.25% in PBS w/o Ca^{2+} and Mg^{2+}). Trypsin was inactivated by adding C2C12 growth medium and cells were then centrifuged at 400g for 5 minutes at room temperature. After discarding the supernatant, pellets were resuspended in 2.0 ml C2C12 growth medium and ~ 25 μl of cell suspension was added into the culture flask containing ~ 30 ml of fresh C2C12 growth medium. In order to maintain the ability to form myotubes, a frozen stock aliquot of C2C12 cells (frozen in liquid nitrogen in 70% DMEM medium, 20% FCS and 10% DMSO) were thawed every 1 to 2 months. To this end, the vial with the frozen cells was thawed in a 37°C water bath and its content immediately poured into a centrifuge tube containing ~ 40 ml C2C12 medium to neutralize the toxic effect of DMSO. The cells were then centrifuged at 400g for 5 minutes at room temperature and pellets were resuspended in 10 ml C2C12 growth medium and transferred into the flask containing additional 20 ml of medium. Cells were kept in a humidified atmosphere at 37°C with 5% CO_2 .

2.2.4 Parasite isolation for infection assays

Parasites were isolated from L929-*Toxoplasma* co-cultures by differential centrifugation and were thoroughly washed in C2C12 growth medium as described (Goebel *et al.*, 2001). Briefly, contaminating host cells were pelleted by centrifugation at 35g for 5 minutes at room temperature. Then the supernatant was collected and centrifuged at 1350g for 10 minutes to pellet parasites. After discarding the supernatant, the parasites were washed with C2C12 growth medium and were centrifuged again at 1350g for 10 minutes. After discarding the supernatant, the parasites were finally resuspended in 1.0 ml medium and an aliquot was diluted 1:20 and counted in a hemocytometer grid.

2.2.5 Myotubes and myoblasts preparation for experimental work

(A) Terminal differentiation of C2C12 myoblasts to myotubes was performed by using differentiation medium containing 2.0% horse serum (Rajan *et al.*, 2012). Briefly, C2C12 myoblasts were isolated by rinsing with EDTA (1.0% in PBS w/o Ca²⁺ and Mg²⁺) and by detaching with trypsin (0.25% in PBS w/o Ca²⁺ and Mg²⁺). They were then centrifuged at 400g for 5 minutes at room temperature. After discarding the supernatant, the cells were resuspended in 2.0 ml C2C12 growth medium and counted in a hemocytometer grid using a 1:2 diluted samples in trypan blue. C2C12 myoblasts were then plated at a density of 1.0-1.5×10⁵ cells/well of a 6-well plate with 3.0 ml/well of C2C12 growth medium.

After ~24 hours of seeding, when the cells were attached to the surface, the C2C12 growth medium was replaced with differentiation medium. The differentiation medium was exchanged every 48 hours until day 7 of seeding when proliferating myoblasts have largely differentiated into poly-nucleated myotubes. Differentiation medium of myotubes was then replaced by C2C12 growth medium in order to maintain the same experimental condition as with myoblasts. In parallel, C2C12 myoblasts (1-2×10⁵ cells/well) were isolated as described above and were seeded in another 6-well plate. On the following day, both myotubes and myoblasts were subjected to treatment with different inhibitors or modulators (if required) and/or were parasite-infected with *T. gondii* tachyzoites.

(B) For immunofluorescence microscopy, myotubes were similarly formed on 13 mm round glass coverslips within 24-well plates coated with laminin or a combination of poly-L-ornithine and laminin. Briefly, sterile glass coverslips were placed into 24-well cell culture plates and treated with laminin (15 µg/ml in PBS, pH 7.4) for 2 hours at 37°C in a 5% CO₂ incubator. Alternatively, coverslips were first treated with poly-L-ornithine (0.5 mg/ml in 125 mM borate buffer, pH 8.3) for 3 hours at 37°C in a 5% CO₂ incubator. After having been washed with PBS three times, coverslips were further treated with laminin as described above. Thereafter, cover slips were washed again three times in PBS, and C2C12 myoblasts cells (2×10⁴ cells/well) were plated in 0.5 ml of C2C12 growth medium. After ~24 hours of seeding, when the cells had attached to the coverslips, the C2C12 growth medium was replaced with differentiation medium and cells were differentiated to myotubes as described above until day7 of seeding. Differentiation medium of myotubes

was then replaced by C2C12 growth medium and C2C12 myoblasts (2×10^4 cells/well) were seeded on coverslips in 24-well plates in parallel. On the following day, both myotubes and myoblasts were subjected to treatment with different inhibitors or modulators (if required) and/or parasite-infected with *T. gondii* tachyzoites.

2.2.6 Treatment of myotubes and myoblasts with pharmacological inhibitors or modulators and parasite infection

C2C12 myotubes were generated as described (see 2.2.5). Both myotubes and myoblasts were treated with pharmacological inhibitors or modulators of the cell cycle, metabolic pathways or redox homeostasis at concentrations as indicated (Table 2.1) or were mock-treated with the respective vehicle. One hour later (unless otherwise stated), cells were infected with *T. gondii* tachyzoites at a host cell-to-parasite ratio of 1:3.5. Total RNA was isolated at 4, 24 or 48 hours post infection for RT-qPCR or cell fixation was performed at 48 and 72 hours post infection for immunofluorescence analysis.

Table 2.1: Inhibitors/modulators used for experimental analysis

Inhibitor/ modulator	Concentration	Target enzyme/function	Associated pathway
Aphidicolin	250-500 ng/ml	Inhibits DNA polymerase	Cell cycle
Mimosine	100-250 μ M	Inhibits DNA synthesis	Cell cycle
Dehydroepiandrosteron	50-100 μ M	Inhibits Glucose-6P-dehydrogenase2	Pentose phosphate pathway
6-Aminonicotinamide	20-100 μ M	Inhibits 6-phosphogluconate dehydrogenase	Pentose phosphate pathway
Phenylacetic acid	1-5 mM	Inhibits pyruvate carboxylase	TCA cycle anaplerosis
Sodium-L-lactate	1-3 mM	Modulates lactate dehydrogenase	Anaerobic glycolysis
Dimethyl- α -ketoglutarate	5-10 mM	Modulates TCA cycle	TCA cycle

N-acetyl cystein	5-10 mM	ROS scavenger	Redox signaling
Tiron	1-5 mM	ROS scavenger	Redox signaling
Luperox	20-40 μ M, 200 μ M	ROS inducer	Redox signaling
Hydrogen peroxide	50-100 μ M	ROS inducer	Redox signaling

2.2.7 P21 knockdown in C2C12 myoblasts by RNA interference

RNA interference (RNAi) has emerged as a widely used method for studying gene functions. In this study, RNAi was used to knockdown the p21 cell cycle inhibitor gene in C2C12 myoblasts in order to understand the impact of p21 on *T. gondii* stage conversion in myoblasts and myotubes.

2.2.7.1 Structure of Mission® TRC1-pLKO.1 plasmid vector and p21-shRNA sequences

In order to knockdown p21 gene in murine C2C12 myoblasts, TRC1-pLKO.1 lentiviral plasmid vectors encoding p21 targeted short hairpin RNA (shRNA) were used. The shRNA is processed intracellularly through the enzyme Dicer to create 18-22 nucleotides short small interfering RNA (siRNA), which then degrades p21 mRNA via p21-targeted siRNA/RISC complex.

To increase the likelihood of obtaining an efficient p21 mRNA knockdown and to produce a stable transfectant, five different p21-targeted shRNA Mission® TRC1-pLKO.1 plasmids were commercially obtained as bacterial glycerol stocks. As a negative control, Mission® TRC1-pLKO.1-empty vector containing plasmid DNA without a p21-targeted shRNA insert was used where the RISC complex is not activated. The sequence of the p21-shRNA fragments and the structure of pLKO.1 plasmids are shown in Table 2.2 and in Figure 2.1, respectively. Ampicillin and puromycin resistance genes encoded markers for selection of successfully transformed bacteria or successfully transfected C2C12 eukaryotic cells, respectively.

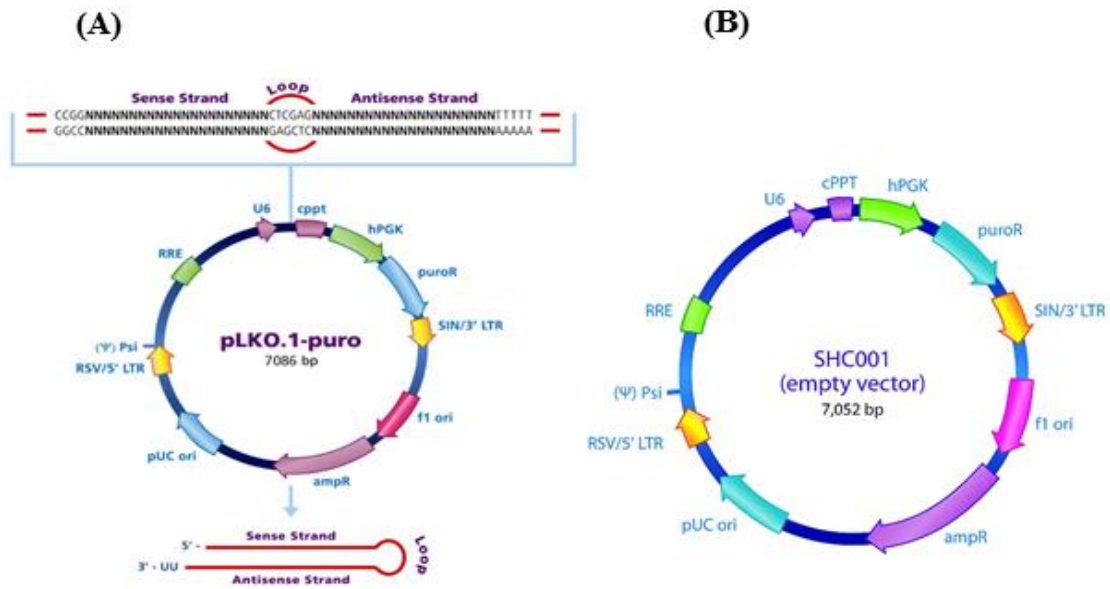


Figure 2.1: (A) Structure of MISSION[®]pLKO.1 plasmid. Five lentiviral plasmid vectors carried different p21-shRNA sequences between the polymerase III promoter (U6) and the central polypurine tract (CPPT). Selection markers were encoded by the ampicillin and puromycin resistance genes. (B) Structure of MISSION[®]pLKO.1-puro Empty Vector Plasmid used as a negative control. This plasmid did not carry a p21-targeted shRNA sequence. Selection markers were encoded by the ampicillin and puromycin resistance genes. Both pictures were collected from <http://www.sigmaldrich.com>.

Table 2.2: Sequences of p21-targeted shRNA. Nucleotides forming the RNA loop within the shRNA are indicated in red

Name of plasmid	p21-shRNA sequence
MISSION [®] pLKO.1-shRNA1	CCGGCCCCGAGAACGGTGGAACTTTCTCGAGAA AGTTCACCGTTCTCGGGCTTTTTG
MISSION [®] pLKO.1-shRNA2	CCGGCCGGAACATCTCAGGGCCGAACTCGAGTT CGGCCCTGAGATGTTCCGGTTTTTG
MISSION [®] pLKO.1-shRNA3	CCGGACAGGAGCAAAGTGTGCCGTTCTCGAGAA CGGCACACTTTGCTCCTGTTTTTTG
MISSION [®] pLKO.1-shRNA4	CCGGAGTGAGCAGTTGCGCCGTGATCTCGAGAT CACGGCGCAACTGCTCACTTTTTTG
MISSION [®] pLKO.1-shRNA5	CCGGGAACCTTTGACTTCGTCACGGACTCGAG TCCGTGACGAAGTCAAAGTTCTTTTTG
MISSION [®] pLKO.1-puro (negative control)	No p21-targeted shRNA insert

2.2.7.2 Propagation of p21-shRNA pKLO.1 plasmid vectors

Escherichia coli bacterial glycerol stocks were used for propagation of lentiviral plasmid vectors encoding p21-shRNA sequences. Fifty to one hundred μl of bacterial stock were added into sterile culture tubes containing 0.5 ml pre-warmed Terrific Broth (TB) medium without antibiotics. The culture was incubated at 37°C with shaking for 15-30 minutes. Using a sterile inoculation loop, 25-50 μl of the incubated culture were streaked onto freshly prepared plates containing Luria-Bertani (LB) agar and 100 $\mu\text{g/ml}$ ampicillin. The plates were then incubated in a humidified atmosphere overnight (15-20 hours) at 37 °C. Thereafter, a single bacterial colony from overnight culture plates was inoculated and grown in a test tube with 5.0 mL of LB broth containing 100 $\mu\text{g/ml}$ ampicillin. Then the bacterial culture was incubated overnight at 37°C with shaking at 200 rpm for propagation.

2.2.7.3 Plasmid DNA isolation

For transfection of C2C12 myoblasts, p21-shRNA pLKO.1 plasmid DNA was isolated from *E. coli* using the GenElute™ Plasmid Miniprep Kit as recommended by the manufacturer (Sigma-Aldrich). Five milliliters of bacterial overnight culture (see above) were centrifuged at 12000g for 1 minute at room temperature. The cell pellet was then mixed with 200 μl of resuspension solution and vortexed vigorously. Subsequently, the cells were lysed by addition of 200 μl of lysis buffer and gently inverted for 5 minutes to clear the solution. Three hundred and fifty μl neutralizing solution were added and again gently inverted six times and then centrifuged for 10 minutes at 12000g to pellet cell debris. In parallel, a binding column was prepared using 500 μl of column preparation solution, spun down at 12000g for 30 seconds, and the flow-through was discarded. Subsequently, the clear cell lysate was transferred to the binding column and spun through the column filter for 30 seconds at 12000g. The binding filter was then washed with 750 μl of wash buffer and centrifuged briefly at 12000g. After discarding the filtrate, the binding membrane was dried by re-centrifugation to remove residual ethanol. The plasmid DNA was then eluted by addition of 100 μl of elution solution and stored at -20 ° C for transfection into C2C12 myoblasts cells.

2.2.7.4 Transformation using p21-shRNA negative pKLO.1-puro plasmid vector

In order to propagate negative control pKLO.1-puro plasmid DNA, *E. coli* NEB 5-alpha competent cells were transformed with the respective plasmid. To this end, *E. coli* NEB 5-alpha competent cells were defrosted on ice for 10 minutes. After mixing gently, 50 µl of cells were carefully transferred into a transformation tube on ice. Then 1.0 µl containing 100 ng of pKLO.1 empty vector plasmid DNA was added to the cells. After mixing the cells and DNA by flicking, the tubes were placed on ice for 30 minutes. Thereafter, cells were heat-shocked at 42°C for 30 seconds and then incubated on ice for 5 minutes. Thereafter, 950 µl pre-warmed (37°C) SOC medium was added to the mixture and the cells were incubated at 37°C for 60 minutes with vigorous shaking (250 rpm). The cells were thoroughly mixed by flicking the tube and inverting, and then 10-fold serial dilutions were prepared in SOC medium. Cells (50-100 µl) at each dilution were spread onto pre-warmed LB-agar plates with 100 µg/ml ampicillin and incubated overnight at 37°C. A single bacterial colony from overnight culture plates was used for propagation (see 2.2.7.2) and DNA isolation (see 2.2.7.3) of negative control pKLO.1-puro plasmid.

2.2.7.5 Agarose gel electrophoresis

To confirm negative control pLKO.1-puro plasmid isolated from transformed *E. coli* cells, qPCR was used to amplify DNA using specific primers of the pLKO.1-puro plasmid (see 2.1.13). Amplified DNA fragments and water as negative control were resolved in a 1.0 % agarose gel in 1x Tris-acetate-EDTA buffer. The agarose suspension was boiled until agarose particles were completely dissolved. After briefly cooling of the agarose solution, 5.0 µl/100 ml of Midori Green were added, followed by gentle mixing, and poured into a gel chamber with a plastic comb. After polymerization of the gel, 4.0 µl of qPCR amplicons were mixed with 4 µl of DNA Loading Dye and pipetted into the agarose gel well. In addition, 8.0 µl of 1 kb Gene Ruler DNA marker was used as a size standard. The electrophoretic separation of nucleic acid fragments was carried out at 110-120 V for 1 hour. Nucleic acid bands were visualized using a UV trans-illuminator.

2.2.7.6 Transfection of C2C12 myoblasts with pLKO.1 plasmids

The transfection of C2C12 myoblasts with pLKO.1 plasmids encoding p21-shRNAs or with an empty vector as a negative control was performed using the FuGENE® transfection reagent (Roche). To this end, C2C12 myoblasts were seeded at a concentration of 7×10^4 per well in 24-well plates with 0.5 ml C2C12 growth medium (see above) and incubated at 37°C in a humidified 5% CO₂ atmosphere. After 24 hours, the C2C12 growth medium was replaced by transfection medium for 30 minutes. In parallel, 2 µg of each plasmid was mixed with 3 µl or 6 µl of transfection reagent (Table 2.3) and incubated at 37°C for 15 minutes. Next, the plasmid-transfection reagent mixture was cautiously dropped onto the cells. After 4 hours of transfection at 37°C, the transfection medium was replaced again by C2C12 growth medium. After 48 hours of cell growth, 2.5 µg/ml puromycin were added to the transfected cells for selection. Surviving cells were propagated and were then cloned by limiting dilution in 96-well plates after adding one or two cells per well. Two different clones of each cell pool carrying the different p21 shRNA or negative control plasmids were selected and frozen in 70% DMEM, 20% FCS, 10% DMSO in liquid N₂ for future experiments. During experimental analysis but not after infection with *T. gondii*, p21-shRNA knockdown clones and negative control clones were cultured (see 2.2.3) in C2C12 growth medium (see 2.1.2) with 2.5 µg/ml puromycin.

Table 2.3: Transfection of C2C12 myoblasts cells with p21-shRNA or negative control pLKO.1 plasmids

Plasmid name	Plasmid	Transfection reagent
pLKO.1-p21-shRNA 1	2 µg	3 µl or 6 µl
pLKO.1-p21-shRNA 2	2 µg	3 µl or 6 µl
pLKO.1-p21-shRNA 3	2 µg	3 µl or 6 µl
pLKO.1-p21-shRNA 4	2 µg	3 µl or 6 µl
pLKO.1-p21-shRNA 5	2 µg	3 µl or 6 µl
pLKO.1-puro (negative control)	2 µg	3 µl or 6 µl

2.2.8 Quantitative reverse transcription PCR

2.2.8.1 RNA isolation

Total RNA was isolated using the GenElute™ Mammalian Total RNA Miniprep Kit as recommended by the manufacturer (Sigma-Aldrich) with slight modifications. Briefly, myotubes and myoblasts grown in 6-well plates and treated and/or infected as described above were washed gently with 1.0 ml of cold PBS and then 350 µl of lysis solution supplemented with 2-mercaptoethanol (1:100, stock solution provided with the kit) was added into each well. The plates were shaken smoothly to ensure complete lysis of all cells followed by transfer of cell lysate into a filtration column. Columns were centrifuged at 14000g for 2 minutes at room temperature, filtrates were mixed with an equal volume (350 µl) of 70% ethanol and were then transferred into binding columns. Binding columns were centrifuged for 15 seconds at 14000g and after discarding the flow-through, the binding membranes were washed by centrifuging 500 µl of wash solution-I for 15 seconds through the membranes. Thereafter, the columns were transferred into new collection tubes and washed twice with 500 µl each of wash solution-II previously supplemented with ethanol as indicated by the manufacturer. For the last washing step, columns were centrifuged for 2 minutes at 14000g to remove residual ethanol. Finally, the columns were transferred into new collection tubes and RNA was eluted with 50 µl of elution solution by centrifuging at 14000g for 1 minute.

2.2.8.2 DNase I treatment

After isolation, RNA samples were treated with DNaseI Amplification grade as recommended by the manufacturer (Sigma Aldrich) to remove contaminating genomic DNA. Briefly, 50 µl of RNA sample were mixed with 5.0 µl of 10x reaction buffer and 5.0 µl of DNaseI Amplification grade (1 unit/ml) and incubated at room temperature for 15 minutes. Thereafter, 5.0 µl of stop solution (provided with the kit) were added to bind calcium and magnesium ions and to inactivate DNase I. Samples were heated at 70°C for 10 minutes to denature DNase I and were then stored immediately at -80°C.

2.2.8.3 Quantification of RNA

RNA was quantitated by measuring its absorbance at 260 nm (A₂₆₀) using a NanoDrop-2000c instrument. NanoDrop is a full spectrum spectrophotometer that can measure DNA/RNA/protein concentrations within 1.0 µl of sample with high accuracy and reproducibility. To this end, 1-2 µl of RNA sample was pipetted onto the end of a fiber optic cable and a second optic cable was then brought into contact with the sample to measure the concentration of RNA. The ratio between the absorbance values at 260 and 280 nm estimated the RNA purity with a reference value of pure RNA being ~2.0.

2.2.8.4 Reverse transcription (cDNA synthesis)

Complementary DNA (cDNA) synthesis was carried out using the Omniscript Reverse Transcription kit as recommended by the manufacturer (Qiagen). Briefly, 1-2 µg RNA were mixed with variable amounts of RNase-free water and 6.4 µl (for total reaction volume of 20 µl) or 7.4 µl (for total reaction volume of 30 µl) of freshly prepared master mix (Table 2.4). Samples were then incubated at 37°C for 90 minutes with constant shaking. cDNAs were stored at -20°C for further analysis.

Table 2.4: Reaction components for cDNA synthesis

Component	Volume/sample	Final concentration (for 30 µl reactions in parenthesis)
	<u>Master Mix</u>	
10x Buffer RT	2.0 µl or 3.0 µl	1.0 x
dNTP Mix (5 mM each dNTP)	2.0 µl	0.5 mM (0.33 mM) each dNTP
Oligo-dT primer (50 µM)	0.4 µl	1.0 µM (0.6 µM)
RNase inhibitor (10 units/µl)	1.0 µl	10 units
Omniscript Reverse Transcriptase (4 units/µl)	1.0 µl	4.0 units
RNase-free water	Variable	
Template RNA	1-2 µg	

2.2.8.5 Real Time qPCR

In order to determine differences in mRNA levels, cDNA samples were diluted two-fold and twenty-fold and were amplified by real time quantitative PCR using SYBR Green FastStart[®] DNA Master Plus kit as recommended by the manufacturer (Roche). First, 14.0 µl of FastStart[®]Taq DNA polymerase were added to 114 µl premix containing reaction buffer, SYBR Green I dye, dNTP mix and MgCl₂. Thereafter, a PCR master mix (15 µl per sample) was prepared using premix, forward and reverse primers and PCR grade water (Table 2.5). Fifteen µl of master mix was then added to each of the LightCycler capillaries followed by adding 5.0 µl diluted template cDNA (1:2 or 1:20) or PCR grade water as negative control before sealing the capillaries by a plug. The capillaries were then gently centrifuged for 10 seconds and samples were amplified in a LightCycler1.5. For each primer pair target gene, different amplification programs were used as specified in Table 2.6.

Table 2.5: Real time qPCR reaction mixture

Component	Concentration	Volume/sample
<u>Master Mix</u>		
Premix		4.0 µl
Forward primer (10 µM)	0.5 µM	0.5 µl
Reverse primer (10 µM)	0.5 µM	0.5 µl
PCR grade water		10 µl
<u>Sample</u>		
cDNA or PCR grade water as control		5.0 µl
Total volume		20 µl

Table 2.6: Real time qPCR programs for gene expression analysis

Step	Temperature	Duration	Cycle
Denaturation	95 °C	10 minutes	
Amplification	95 °C	10 seconds	
	61-72 (depending on different target gene)	10 seconds	
	72 °C	10-20 seconds (depending on amplicon length)	40 or 45 cycles
Melting curve	95 °C	0	
	65 °C	20 seconds	
	99 °C	0	
End	40 °C	10 seconds	

The relative fold change of mRNA levels as a measure of gene expression was calculated according to the following formula (unless stated otherwise):

$$\text{Ratio} = \frac{(E_{\text{Target}})^{\Delta\text{CP}_{\text{target gene (control-inhibitor)}}}}{(E_{\text{Reference}})^{\Delta\text{CP}_{\text{reference gene (control-inhibitor)}}}}$$

Herein, the fold change of the mRNA level of a target gene was normalized to a reference gene and the efficiency of amplification (E) was set 2. The reference gene corresponds to a 'housekeeping' gene; for gene expression analysis in the parasite *T. gondii* actin (TgActin) or *T. gondii* glyceraldehyde-3-phosphate dehydrogenase (TgGAPDH) and for that of host genes mouse β -actin was used.

2.2.9 Immunofluorescence staining

2.2.9.1 Cell fixation

After treatment of cells with inhibitors/modulators (see 2.2.6) and/or *T. gondii* infection, cells on coverslips of 24-well plates were fixed at 48 and/or 72 hours post infection using 4% paraformaldehyde in 0.1 M sodium cacodylate/HCl, pH 7.4 (PFA) (or methanol or 70% ethanol if indicated). To this end, cells were washed twice with PBS for 5 minutes each and were then fixed with 350µl/well of PFA for 60 minutes at room temperature. After that, PFA was removed and cells were washed three times with PBS for 5 minutes each.

2.2.9.2 Immunostaining

After removing the PBS, cells were quenched for 10 minutes with 50 mM NH₄Cl in PBS and then washed once with PBS for 5 minutes at room temperature. Cells were permeabilised and unspecific binding sites were blocked with blocking buffer (1.0% BSA, 0.1 mg/ml saponin in PBS) for one hour at room temperature. Thereafter, cells were washed once with washing buffer (0.1 mg/ml saponin in PBS) and incubated with primary antibodies or lectin (Table 2.7) diluted in blocking buffer for one hour at room temperature. After washing three times for 10 minutes each with washing buffer, cells were incubated for one hour with secondary antibodies or streptavidin (Table 2.7) diluted in blocking buffer. For both primary and secondary antibody incubations, cover slips were removed from the 24-well plate and inverted onto 30-40 µl drops of antibody solution on parafilm. In order to wash cells, coverslips were put back cell-side up into the wells of the 24-well plate. Unbound antibodies were then removed by washing three times for 10 minutes each with washing buffer and finally once with PBS for 5 minutes. To visualize the total cell population, cells were incubated with 5 µg/ml propidium iodide in PBS for 4 minutes. After washing with PBS twice for 5 minutes each, coverslips were rinsed in demineralized water and mounted on slides with 10 µl mowiol per cover slip. Slides were kept in the dark to dry overnight at room temperature. The samples were stored at 4°C until examination using a Leica SP2 confocal laser scanning microscope.

Table 2.7: Antibodies used in immunofluorescence staining

Antibodies	Dilution (Concentration)
<u>Primary antibodies:</u>	
Rabbit anti- <i>Toxoplasma</i> (serum)	1:400 (in case of Cy5-conjugated sec. Ab) , 1: 2000 (in case of DyLight488-conjugated sec. Ab)
Mouse anti- <i>Toxoplasma</i> (serum)	1:200
Biotin-conjugated <i>Dolichos biflorus</i> lectin (DBL)	1:400 (3.125 µg/ml)
Mouse anti-BrdU antibody	1:1000
Rabbit anti-mouse myosin heavy chain antibody	1:100 (2.0 µg/ml)
Mouse anti-mouse p21(F5) antibody	1:200 (1.0 µg/ml)
<u>Secondary antibodies:</u>	
Cy5-conjugated donkey F(ab') ₂ anti-rabbit IgG (H+L)	1:100 (7.5 µg/ml)
Cy2-conjugated streptavidin	1:200 (4.0µg/ml)
DyLight488-conjugated donkey F(ab') ₂ anti- rabbit IgG (H+L)	1:200 (3.75 µg/ml)
Cy5-conjugated goat anti-mouse IgG (Fcγ-specific)	1:100 (6.0 µg/ml)
DyLight488-conjugated donkey F(ab') ₂ anti-mouse IgG (H+L)	1:200 (3.75 µg/ml)

2.2.10 Bromodeoxyuridine (BrdU) incorporation assay

Myotubes were prepared from C2C12 myoblasts on coverslips within 24-well plates as described in section 2.2.5B. Both myotubes and myoblasts were treated with inhibitors or vehicle and/or were infected with *T. gondii* at a host cell-to-parasite ratio of 1:3.5. BrdU incorporation assay was also performed with undifferentiated and differentiated p21-shRNA transfectants (see above) and wildtype C2C12 cells where BrdU was added at day 1, day 3, day 5 and day 7 of differentiation. During the last two hours prior to fixation, cells were treated with 10 µg/ml BrdU at 37°C. Thereafter, BrdU containing medium was removed and 500 µl/well of 70% ethanol were added for 5 minutes at room temperature. The cells were washed three times in PBS and then incubated in 500 µl/well of 1.5 M HCl for 30 minutes at room temperature. After removal of HCl, cells were washed again three times in PBS and stored in PBS at 4°C for immunostaining (see 2.2.9.2) using blocking solution, antibody incubation solution and wash solution as specified in 2.1.8.

2.2.11 P21 expression examined by Western blotting

Western blotting is a fundamental technique used to separate and identify proteins from a complex mixture of proteins based on molecular weight through gel electrophoresis followed by transferring them onto a membrane and staining of protein of interest using appropriate antibodies.

2.2.11.1 Sample preparation and protein isolation

Proteins were isolated from p21-shRNA transfectants, negative control transfectants and wildtype C2C12 cells at 3, 5 and 7 days after onset of differentiation from myoblasts to myotubes. To this end, cells were seeded at a concentration of 1.0×10^5 /well in 6-well plates. After 24 hours, cells were induced to differentiate using differentiation medium as described (2.2.5). Proteins were isolated from differentiated cells at the indicated time points as well as from wild-type myoblasts. To this end, cells were collected from the culture dish by EDTA-trypsin treatment as described (2.2.3) and transferred into cold C2C12 medium and then centrifuged at 400g for 5 minutes. The supernatants were discarded and pellets were resuspended in 1.0 ml of C2C12 medium. An aliquot of cells

was then counted in a hemocytometer grid and remaining cells transferred into a microcentrifuge tube and centrifuged at 6000g for 5 minutes at 4°C. After discarding the supernatants, cell pellets were resuspended in 50 µl/1x10⁶ cells ice cold lysis buffer (see 2.1.5). Cells were lysed on ice for 60 minutes with vortexing after every 15 minutes. Finally, cell lysates were centrifuged at 14000g for 5 minutes at 4°C and soluble proteins within the supernatant were stored at -80°C for further analysis.

2.2.11.2 SDS-PAGE

Proteins were separated by SDS-PAGE for subsequent detection by Western blotting. The separating and stacking gels comprised 12% and 5% acrylamide, respectively (see 2.1.6). Samples were diluted with 5x SDS sample buffer to a final concentration of 1x SDS sample buffer and heated with shaking at 99°C for 5 minutes. Thereafter, samples were shortly centrifuged and 20 µl of each sample were loaded onto the gel. Five µl of prestained protein markers were also loaded onto each gel. Proteins were separated in 1x SDS-PAGE running buffer (see 2.1.6) at 25 mA per gel for approximately 60 minutes. Following electrophoresis, proteins were transferred onto nitrocellulose membrane.

2.2.11.3 Western blotting

After protein separation by SDS-PAGE, proteins were transferred onto nitrocellulose membranes by semi-dry blotting using a discontinuous buffer system. To this end, the polyacrylamide gel and the nitrocellulose membrane were placed between filter papers that have been previously soaked in different buffer solutions (see 2.1.7 and Figure 2.2). Proteins were transferred at 32 mA per gel for 90 minutes towards the anode as indicated in Figure 2.2.

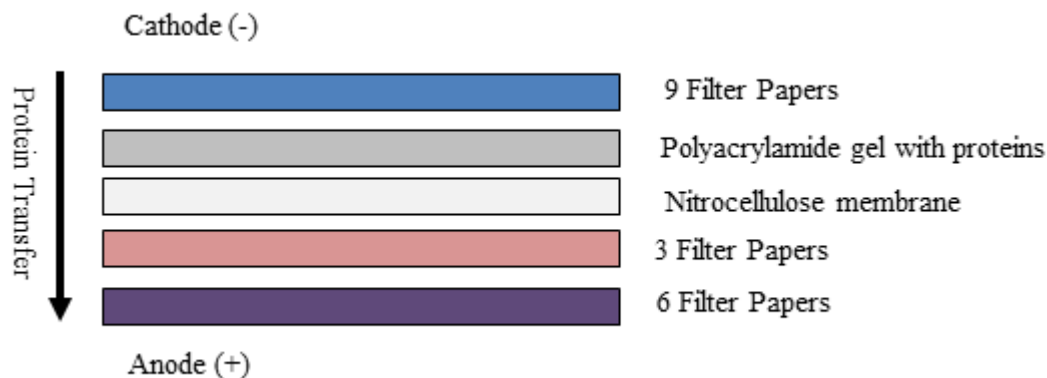


Figure 2.2: Protein transfer by Western blotting. Proteins were transferred from cathode (-) to anode (+). Filter papers were soaked in different buffer solutions as follows: 9 filter papers in aminocaproic acid buffer (40 mM), 3 filter papers in Tris-HCl buffer (25 mM) and 6 filter papers in Tris-HCl buffer (0.3 M) (from cathode to anode). Filter papers were used to prepare a sandwich of filter papers, polyacrylamide gel with proteins and nitrocellulose membrane.

2.2.11.4 Immunostaining of nitrocellulose membrane

To confirm protein transfer during Western blotting, the nitrocellulose membrane was stained with ponceauS solution. For this, the membrane was incubated in ponceauS solution for 3 minutes and then washed with ddH₂O until the background was destained and the protein bands were visible. An image of the protein bands was recorded using a gel documentation system with white top light illumination. Thereafter, unspecific binding sites were blocked in blocking solution containing 5% skimmed milk powder (see 2.1.7) for two hours with gentle shaking at room temperature. Primary antibodies, i.e. anti-mouse p21 (1.0 µg/ml) or anti-mouse β-actin antibody (1.0 µg/ml) were diluted in antibody incubation buffer (see 2.1.7 and Table 2.8) and then added to the membrane for overnight incubation with shaking at 4°C. Thereafter, unbound antibodies were removed by washing three times 10 minutes each with wash solution (see 2.1.7). Then the membranes were incubated with peroxidase-conjugated anti-mouse IgG secondary antibodies diluted in antibody incubation buffer (see 2.1.7) for 90 minutes, followed by washing again three times 10 minutes each with wash solution. After adding chemiluminescent detection reagents, the presence of p21 and beta-actin proteins was detected on the membrane using Fujifilm Image reader.

Table 2.8: Primary and secondary antibodies used in western blotting

Antibodies	Type	Dilution (Concentration)
Mouse anti-mouse p21(F5) antibody	Primary antibody	1:200 (1.0µg/ml)
Mouse anti-mouse β-actin antibody	Primary antibody	1:5000 (1.0µg/ml)
Peroxidase conjugated goat F(ab') ₂ anti-mouse IgG (H+L)	Secondary antibody	1:2000 (0.2 µg/ml)

2.2.12 Measurement of intracellular NADP⁺/NADPH

Intracellular NADP⁺/NADPH were measured in non-infected and *T. gondii*-infected and/or DHEA/solvent-treated myotubes and myoblasts by using the NADP⁺/NADPH quantification kit as recommended by the manufacturer (Sigma-Aldrich). This assay is specific for NADP⁺ and NADPH and does not detect NAD⁺ or NADH. The principle of this method is based on a colorimetric measurement of NADP_{total} (NADP⁺ and NADPH) or NADPH at 450 nm.

Table 2.9: Major components of the NADP⁺/NADPH quantification kit

Components	Preparation
NADP ⁺ /NADPH extraction buffer	The extraction buffer was allowed to reach room temperature before use.
NADP ⁺ cycling buffer	NADP ⁺ cycling buffer was allowed to reach room temperature before use.
NADP cycling enzyme mix	
NADPH developer	NADPH developer was reconstituted in 1.2 ml of ddH ₂ O, and stored at -80 ⁰ C until use.
NADPH standard	NADPH standard was reconstituted in 200 µl of DMSO to generate 1.0 nmole/µl (1 mM) solution, and stored at -80 ⁰ C until use.

2.2.12.1 Sample preparation

C2C12 myoblasts were differentiated into myotubes using 2% HS for 7 days as described in section 2.2.5A. Then both myotubes and myoblasts were treated with DHEA or solvent (if required) and were infected with *T. gondii* at a host cell-to-parasite ratio of 1:3.5 or left non-infected. After 48 hours of infection, cells were washed gently with cold 1x PBS (pH 7.4). Next, non-infected and *T. gondii*-infected cells were isolated using EDTA-trypsin as described (see 2.2.3). After counting, 1×10^6 - 1.5×10^6 cells from each sample were pelleted in a microcentrifuge tube by centrifuging at 376g for 5 minutes at 4°C. Cells were then extracted with 300 μ l of NADP⁺/NADPH extraction buffer and placed on ice for 10 minutes. Samples were centrifuged at 10000g for 10 minutes to remove insoluble material and the supernatants were filtered through a 10 kDa cut-off viva spin filter to largely deproteinize them in order to avoid consumption of NADPH by enzymes. Finally, samples were stored at -80°C for further analysis.

2.2.12.2 Detection of NADP⁺/NADPH

In order to determine NADPH concentration only, 100 μ l of extracted samples were heated at 60°C for 30 minutes in a heating block. Under these conditions NADP⁺ will be decomposed leaving NADPH only within the samples. Then samples were cooled on ice and spun down at 15000g for 30 seconds to remove any precipitates.

Colorimetric detection of NADP⁺/NADPH was performed in 96-well flat bottom plates. To this end, 10 μ l of the NADPH standard stock solution (1.0 nmole/ μ l) was diluted with 990 μ l of NADP⁺/NADPH extraction buffer to generate 10 picomol/ μ l standard solution. Then different volumes of NADPH standard solution (0, 2, 4, 6, 8, and 10 μ l) were added in duplicate into wells of the 96-well flat bottom plate. Thereafter, extraction buffer was added to a final volume of 50 μ l to generate 0 (blank), 20, 40, 60, 80 and 100 picomole/well of standards. Fifty microliters of unknown samples either pretreated as described above for NADPH only determination or untreated for total NADP⁺/NADPH determination were added in duplicate into wells of the 96-well plate. Hundred μ l of the master reaction mix (composed out of 98 μ l of NADP⁺ cycling buffer and 2 μ l of NADP⁺ cycling enzyme mix per reaction) were added to each of the standards and samples and mixed using an orbital rotator. The samples were incubated for 5 minutes at room

temperature to convert all NADP⁺ (if present) to NADPH. Finally, 10 µl of NADPH developer were added into each well and incubated for ~30 minutes for color development. The absorbance at 450 nm was finally recorded repeatedly during 1 hour using a Victor multilabel plate reader. Concentrations of NADPH only or NADP⁺/NADPH in unknown samples were calculated from the formula of a standard curve obtained after linear regression of the values of NADPH standard concentrations.

2.2.13 Determination of intracellular Reactive Oxygen Species (ROS) levels

In order to determine the accumulation of intracellular reactive oxygen species (ROS) in C2C12 myotubes and myoblasts, the CellROX Green reagent (Thermo Scientific) was used. CellROX Green reagent is a DNA dye which upon oxidation, binds to DNA and thus localizes primarily in the nucleus and mitochondria. C2C12 myoblasts were differentiated to myotubes using 2% HS (see 2.2.5B). Both myotubes and myoblasts were infected by *T. gondii* at a host cell-to-parasite ratio of 1:3.5, leaving some samples as non-infected controls. After 48 hours of infection, infected or non-infected myoblasts and myotubes were treated with 200 µM luperox (tert-butyl hydroperoxide; as a positive control) for 1 hour at 37°C and 5% CO₂ or were left untreated. Thereafter, 5 µM CellROX Green reagent was added to each sample for another 30 minutes. Cells were then washed three times with 1x PBS and fixed in 4% paraformaldehyde for 15 minutes at room temperature. After having been washed with 1x PBS twice, cells were incubated in 5 µg/ml propidium iodide for 5 minutes followed by washing twice with 1x PBS. Finally, coverslips were mounted onto glass slides using mowiol and analyzed by confocal laser scanning microscopy.

2.2.14 RNA sequencing

RNA sequencing (RNAseq) is a technique used for studying regulation of gene expression at the transcriptome level. It is considered a highly sensitive and accurate tool for measuring gene expression patterns in a cell population before and after any treatment including infection with pathogens and can provide an overview of the total changes in gene expression due to infection. Here, RNA sequencing was performed with *T. gondii*-infected and non-infected myotubes and myoblasts to unravel their differences in gene expression at mRNA levels.

2.2.14.1 Sample preparation and quality control analyses

Myotubes were prepared from C2C12 myoblasts in 6-well culture plates through differentiation using 2% HS (see 2.2.5A). Both myotubes and myoblasts were infected with *T. gondii* tachyzoites at a host cell-to-parasite ratio of 1:5 or were left non-infected. After twenty-four hours of infection, total RNA was isolated from both non-infected and *T. gondii*-infected samples using the GenElute™ Mammalian Total RNA Miniprep kit as described above (2.2.8.1) and a portion of RNA was used for cDNA synthesis and qPCR to determine relative BAG1 mRNA expression (see 2.2.8).

In parallel, both cell types were differentiated or seeded on laminin-coated glass coverslips in 24-well plates to determine the extent of myotube formation and *T. gondii* infection by means of an immunofluorescence test. To this end, both cell types were infected with *T. gondii* tachyzoites (host cell-to-parasite ratio 1:5) or were left non-infected. After 24 hours of infection, cells were washed twice with 1x PBS and fixed with 4% paraformaldehyde for one hour at room temperature. Then cells were washed again with 1x PBS three times and stored at 4 °C until immunofluorescence staining as described (see 2.2.9).

After confirming the expected results by RT-qPCR and immunofluorescence microscopy, the RNA samples of non-infected and infected myotubes as well as myoblasts from three independent experiments were used for subsequent RNA sequencing analysis. RNAseq was performed in collaboration with Gabriela Salinas-Riester and Bryan Downie at the Transcriptome and Genome Analysis Laboratory of the Georg-August-University of Göttingen.

2.2.14.2 Measurement of RNA quality and quantity

Before starting RNA sequencing at the transcriptome laboratory, the integrity/quality and the quantity of all RNA samples were determined in a Fragment Analyzer™ Automated CE system using the DNF-471 standard sensitivity RNA analysis kit and the Nanodrop-2000 spectrophotometer, respectively. The Fragment Analyzer™ provides a RNA quality number (RQN) between 1 and 10 for each RNA sample based on an algorithm that uses three values of the electropherogram, i.e the intensity in front of the 18S peak, the total intensity of the 18S and 28S peaks and the ratio of 28S and 18S peaks. The higher the RQN number, the better is the quality of the RNA sample.

2.2.14.3 Preparation of cDNA library and sequencing

RNA sequencing of samples from non-infected and *T. gondii*-infected myotubes and myoblasts from three independent experiments was performed using the Illumina® TruSeq® RNA Sample Preparation Kit v2 and the Illumina HiSeq™ 4000 sequencer. Briefly, 0.1-1 µg RNA of each sample was used to construct transcriptome libraries. First, polyA-containing eukaryotic mRNA was purified using oligo-dT-conjugated magnetic beads. After purification, the mRNA was fragmented into small pieces using divalent cations under elevated temperature. The cleaved RNA fragments were reversely transcribed into first strand cDNA using reverse transcriptase and random primers followed by second strand cDNA synthesis using DNA polymerase I and RNase H. The cDNA fragments then underwent an end repair process, before addition of a single 'A' and the ligation of adapters. After binding of the libraries to the flow cells, cDNA fragments were amplified and clusters of amplified fragments were then sequenced by means of sequential addition of specific fluorescently labelled nucleotides. After excitation of the sequentially added fluorescent nucleotides, the emission for each nucleotide within each cDNA cluster was recorded until a length of 50 bases was reached. Thirty to 100 million sequences per sample were mapped to the mouse and the *Toxoplasma* reference genomes (read mapping).

2.2.14.4 Analysis and statistical evaluation of the transcriptome data

To normalize the transcripts, 'reads per kilobase per million reads' (RPKM) values were calculated for each gene. The RPKM value expresses the ratio of the number of read within a transcript to the length of the transcript/exons in kilobases and the total amount of the sequencing reads in millions. For further analysis, significantly regulated transcripts were identified by the χ^2 test. For graphical representation of the expression profiles, heat maps of differentially expressed genes (DEGs) between cell types before or after infection were constructed. Functional analyzes of the genes/transcripts were carried out using the DAVID analysis tool (<https://david-d.ncifcrf.gov/>) and the Venn diagram software of the VIB/UGent (<http://bioinformatics.psb.ugent.be/webtools/Venn/>).

2.2.15 Isotope labeling and metabolite analysis via gas chromatography-coupled mass spectrometry (GC-MS)

Stable isotope labeling experiments were carried out in collaboration with Izabela Swierzy, Göttingen and Martin Blume, Melbourne as described previously (Blume *et al.*, 2015) with the following modifications. Briefly, myotubes were prepared from 6×10^5 C2C12 myoblasts in 92mm cell culture plates through differentiation using 2% HS (see 2.2.5). One day before infection, differentiation medium was exchanged by glucose-free DMEM supplemented with 1 g/l ^{12}C -glucose, 10% FCS and penicillin and streptomycin at concentrations as indicated (see 2.1.2). Myoblasts were seeded in parallel in the same medium. Both myotubes and myoblasts were infected with *T. gondii* tachyzoites at a host cell-to-parasite ratio of 1:3.5 or were left non-infected as controls. Six hours later, the medium was exchanged by medium where ^{12}C -glucose was replaced by ^{13}C -glucose and cells were incubated for additional four hours. Thereafter, cellular metabolism was terminated by rapid exchange of labeling media with 2.1 ml/sample cold 80% GC-MS grade methanol supplemented with 0.5 nmol *scyllo*-inositol as internal standard and transferring the plate onto an ice-water slurry. Cells were scraped and were transferred into a centrifuge tube. After washing each plate with 2.1 ml 80% methanol containing 0.5 nmol *scyllo*-inositol and transfer into the tubes, cells were sonicated in a water bath four times for 30 seconds with intermittent cooling on ice. After addition of chloroform and water to a ratio of chloroform:methanol:water of 1:11:6 (v/v), metabolites were extracted for 20 minutes in a water bath at 60°C. Insoluble material was then pelleted at 14000g and 0°C for 10 minutes. Phase separation was induced by addition of water and by sonication in a water bath 4 times 10 seconds each. After centrifugation at 14000g and 0°C for 10 minutes, the aqueous phase was dried in a heated speedvac and was shipped at room temperature to the University Of Melbourne, Australia. Polar metabolites were re-dried with methanol in a speed-vac and methoxymated with 20 mg/ml methoxyamine in pyridine at room temperature overnight prior to trimethylsilylation with N,O-bis (trimethylsilyl) trifluoroacetamide with 1% trimethylsilyl (BSTFA-1% TMS) (Sigma-Aldrich) for 1 hour at room temperature. Samples were then analysed by gas chromatography mass spectrometry (GC-MS) using Agilents 7890A-5975C system equipped with a DB-5MS + DG column (J&W, Agilent, 30m \times 0.25 mm, with 10 gap). Chromatograms were processed in MSD Chemstation D.01.02.16 software (Agilent). The incorporation of ^{13}C -atoms was estimated as the percentage of the metabolite pool containing one or more ^{13}C -

atoms after correction for natural abundance. Total metabolite counts were normalized to *scyllo*-inositol as an internal standard and to total protein content of each sample.

2.2.16 Statistical analysis

Each experiment was performed at least two times (unless otherwise stated). Data are expressed as means \pm standard error of the mean (means \pm SEM) from replicate experiments. The differences between two groups were considered significant if the *p*-values were less than 0.05. The *p*-values between the means of two groups were calculated by means of the Student *t*-test using Microsoft Excel. In case of more than two groups, *p* values were calculated through analysis of variance (ANOVA). χ^2 test was used to calculate *p*-values for analyzing RNA sequencing data. Graphs were prepared using Graphpad prism version5 and Microsoft Excel.

Chapter 3: Results

3.1 Terminally differentiated SkMCs support *T. gondii* bradyzoite differentiation

It has been established that skeletal muscle cells (SkMCs) and neurons are the preferred cell types for *T. gondii* bradyzoite differentiation and tissue cyst formation (Dubey *et al.*, 1998; Ferreira-da-Silva *et al.*, 2009; Guimarães *et al.*, 2009). Recently, Swierzy *et al.* have shown that *T. gondii* stage conversion from tachyzoites to bradyzoites occurs spontaneously in terminally differentiated SkMCs, i.e. in myotubes, but not in proliferating myoblasts (Swierzy and Lüder, 2014). In this study, it has been further confirmed that *T. gondii* stage conversion is accelerated in myotubes compared to myoblasts, prior to identifying factors which might induce tachyzoites to bradyzoites differentiation in myotubes (see below).

3.1.1 *T. gondii* bradyzoite differentiation is accelerated in myotubes as compared to myoblasts

In order to determine *T. gondii* stage conversion in myotubes, RT-qPCR was performed with *T. gondii*-infected myotubes and myoblasts to examine upregulation of bradyzoite antigen-1 (BAG1) mRNA between 4 and 48 hours post infection. Results showed that BAG1 mRNA increased five-fold in *T. gondii* residing in myotubes compared to those in myoblasts, although this was not statistically significant due to variable results from experiment to experiment suggesting some difficulties in reproducibility (Figure 3.1A). As bradyzoite development regularly leads to the formation of tissue cysts, fluorescence staining was performed to label cyst wall of *T. gondii* tissue cysts with *Dolichos biflorus* lectin. Data showed that cyst formation was increased in myotubes compared to myoblasts after 48 and 72 hours of infection (Figure 3.1B). Therefore, it was concluded that *T. gondii* stage conversion occurs preferentially in myotubes but not in myoblasts.

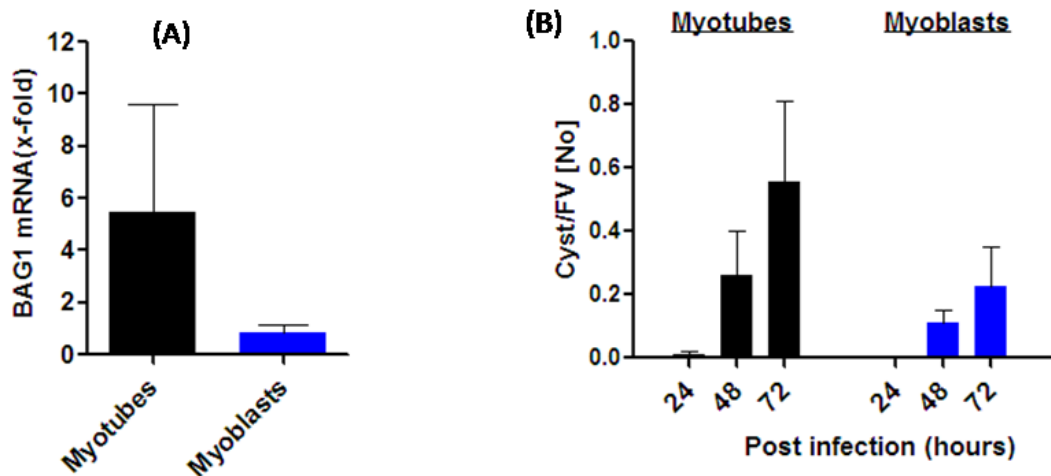


Figure 3.1: *T. gondii* bradyzoite differentiation and tissue cyst formation is preferentially triggered in mature myotubes. C2C12 myoblasts were induced to differentiate into poly-nucleated myotubes. Both differentiated myotubes and proliferating myoblasts were infected with *T. gondii* tachyzoites at a host cell-to-parasite ratio of 1:3.5. (A) Total RNA was isolated at 4 and 48 hours post infection, followed by cDNA synthesis. Subsequently, cDNA was amplified using specific primers for *T. gondii* bradyzoite antigen 1 (BAG1) and *T. gondii* actin (TgActin) by quantitative real-time PCR. The increase in BAG1 mRNA was calculated ($\Delta\Delta$ CP method) in myotubes and myoblasts and was normalized to that of TgActin mRNA. Results are depicted as means \pm S.E.M. from five independent experiments. (B) Cells were fixed at 48 and 72 hours post infection with 4 % paraformaldehyde. After fixation, tissue cysts of *T. gondii* were labeled with biotin-conjugated *Dolichos biflorus* lectin and Cy2-conjugated streptavidin, and parasites were labeled with a polyclonal *anti-T. gondii* antiserum and Cy5-conjugated secondary antibodies, and host cells were visualized using propidium iodide. The number of cysts was counted in 100 fields of vision (FV). Data represent means \pm S.E.M. from two independent experiments.

3.2 Transcriptome analysis of SkMCs

Transcriptome analysis is an important approach to identify differences between cells at the RNA level. In this study, the transcriptomes of non-infected and *T. gondii*-infected myotubes and myoblasts were analyzed in order to identify possible candidate genes or pathways that might regulate developmental switching of tachyzoites to bradyzoites in myotubes.

3.2.1 RT-qPCR confirms higher BAG1 mRNA expression in *T. gondii* within myotubes as compared to those in myoblasts

Before analyzing transcriptomes through RNA sequencing, RNA samples from non-infected and *T. gondii*-infected myotubes and myoblasts were assessed by RT-qPCR to determine relative *T. gondii* BAG1 mRNA expression in both cell types.

To this end, RNA was isolated from non-infected and *T. gondii*-infected myotubes and myoblasts at 24 hours post infection and after reverse transcription, equal amounts of cDNA were used to determine *T. gondii* BAG1 mRNA expression. Results showed more than 35-fold higher BAG1 mRNA levels in myotubes compared to myoblasts, indicating clearly higher bradyzoite differentiation in myotubes than in myoblasts as expected (Figure 3.2A).

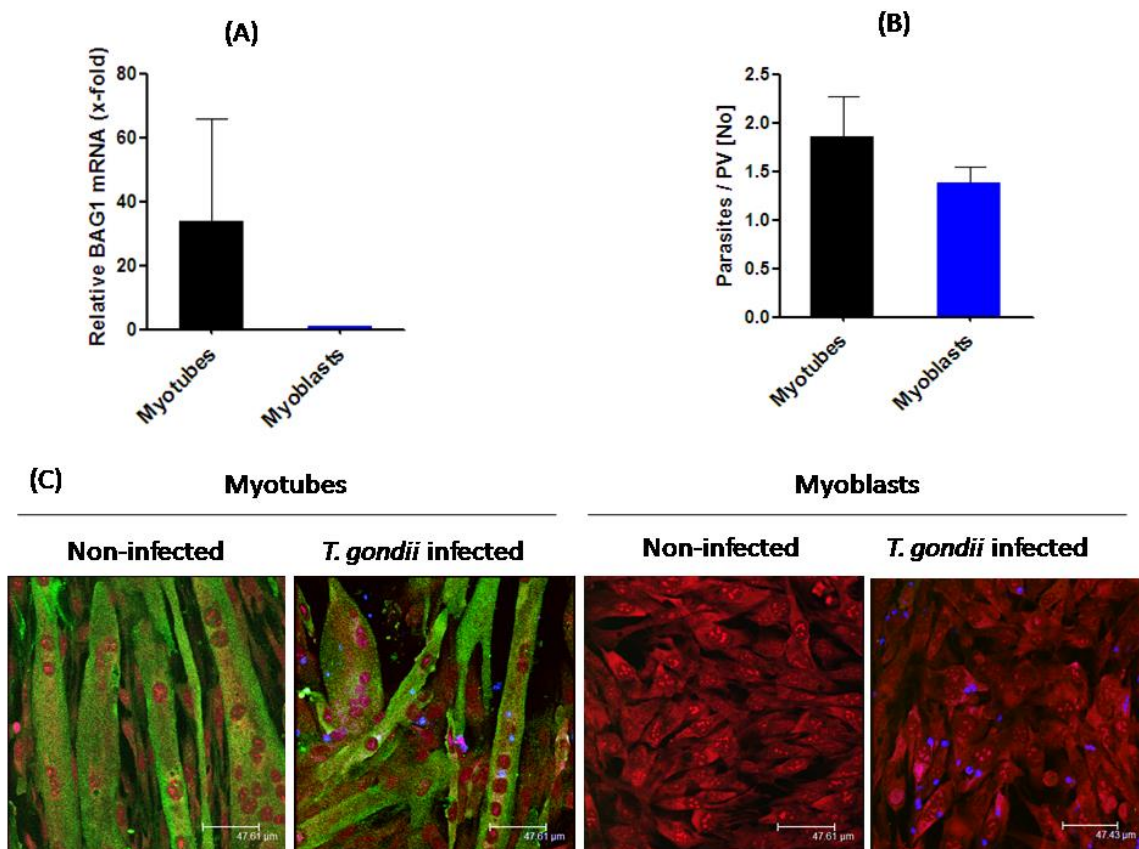


Figure 3.2: Myotubes support higher *T. gondii* BAG1 mRNA expression but similar parasite replication as compared to myoblasts. C2C12 myoblasts were induced to differentiate into poly-nucleated myotubes. Both myotubes and myoblasts were infected with *T. gondii* tachyzoites at a host cell-to-parasite ratio of 1:5. (A) Total RNA was isolated at 24 hours post infection, followed by cDNA synthesis by reverse transcription. Subsequently, cDNA was amplified using specific primers for *T. gondii* bradyzoite antigen 1 (BAG1) and *T. gondii* actin (TgActin) by quantitative real-time PCR. The relative BAG1 mRNA expression in myotubes as compared to myoblasts was calculated ($\Delta\Delta\text{CP}$ method) and was normalized to TgActin mRNA. Results are depicted as means \pm S.E.M. from three independent experiments. (B-C) Cells were fixed after 24 hours of infection using 4% PFA. Cells were labeled with anti-myosin heavy chain primary antibodies and Cy2-conjugated secondary antibodies (green fluorescence), and parasites were immunolabelled using a polyclonal anti-*T. gondii* antiserum and Cy5-conjugated secondary antibodies (blue fluorescence). Host cells were visualized using propidium iodide (red fluorescence). After cells had been fluorescently labeled, the average size of parasitophorous vacuoles (PVs) in each sample was determined by counting the number of parasites in 100 PVs (B). Data represent means \pm S.E.M. from three independent experiments. (C) Representative images of the labellings were recorded by confocal laser scanning microscopy and were superimposed.

3.2.2 Parasite replication and myosin heavy chain expression in myotubes and myoblasts

It has been shown before that reduced parasite replication is a prerequisite for *T. gondii* bradyzoite differentiation (Bohne *et al.*, 1994; Radke *et al.*, 2003). It was thus important to determine parasite replication in myotubes and myoblasts. In order to evaluate parasite replication, the infection rate of both cell types was evaluated by immunofluorescence staining. In both myotubes and myoblasts, parasite infection could clearly be detected (Figure 3.2C). Parasite replication was slightly higher in myotubes than in myoblasts after 24 hours of infection (Figure 3.2B). This data showed that the parasite was able to replicate in both myotubes and myoblasts to a similar extent. Lower parasite replication was expected in myotubes compared to myoblasts as reduced parasite replication is a hallmark of *T. gondii* bradyzoite differentiation in myotubes (Swierzy and Lüder, 2014). Immunofluorescence microscopy also revealed myosin heavy chain (MyHC) expression (green fluorescence) in poly-nucleated myotubes but not in myoblasts indicating formation of mature myotubes after *in vitro* differentiation in differentiation medium with 2 % horse serum (Figure 3.2C).

3.2.3 Gene expression profiles of myoblasts and myotubes before and after *T. gondii* infection

RNA sequencing was performed with non-infected and *T. gondii*-infected myoblasts and myotubes in order to identify genes that are differentially regulated in proliferating myoblasts or differentiated myotubes before and after *T. gondii* infection. To this end, RNA was isolated from three replicates of non-infected and *T. gondii*-infected myoblasts and myotubes at 24 hours post infection and was used for sequencing after confirming quality of the samples as described above. RNA sequencing data revealed that 6351 to 6592 genes were differentially expressed in myoblasts versus myotubes irrespective of infection (Figure 3.4A). Surprisingly, *T. gondii* had only a minor impact on regulation of gene expression in myotubes and myoblasts. To visualize expression pattern of differentially regulated genes (DEGs), a heatmap of the top 50 DEGs with the lowest *p*-values was constructed to visualize overall transcriptome differences between non-infected and *T. gondii*-infected myoblasts versus myotubes. Results confirmed that myotubes

largely differ from myoblasts in their gene expression pattern irrespective of infection. Within the group of these 50 genes, there were hardly any differences between non-infected and infected myoblasts or myotubes (Figure 3.3).

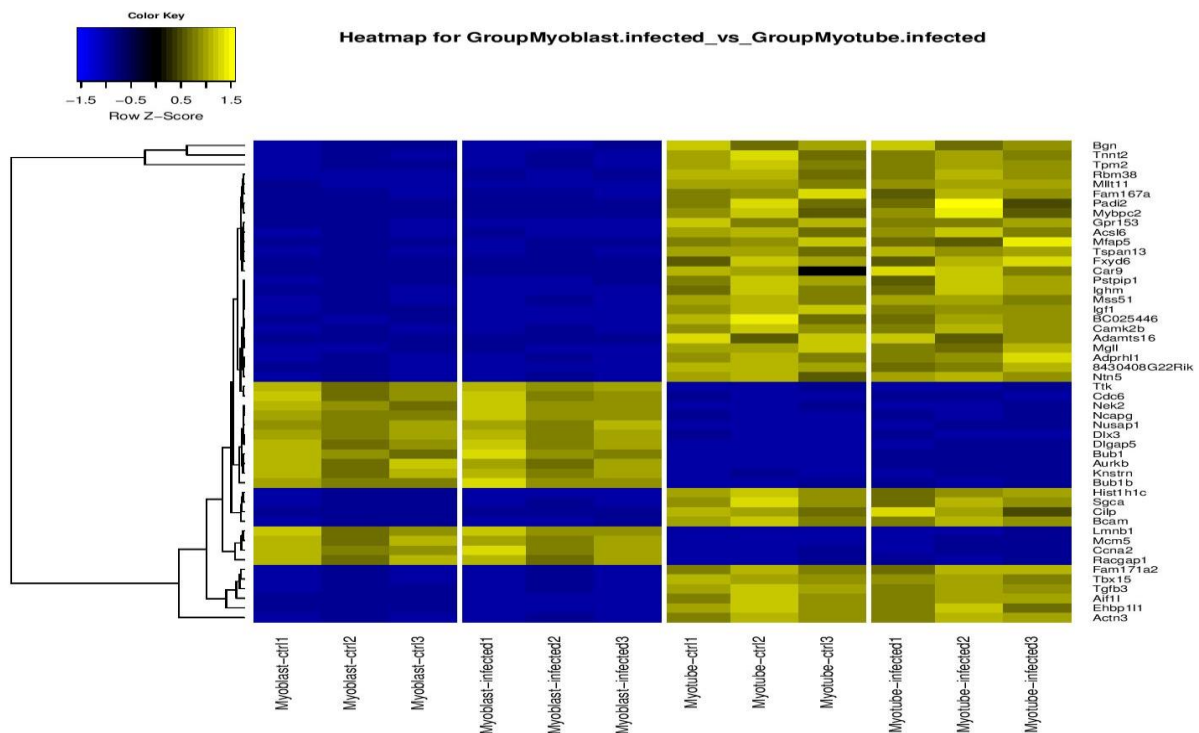


Figure 3.3: Heatmap illustrating differential gene expression in non-infected and *T. gondii*-infected myoblasts and myotubes. Three replicates each of non-infected (control) and *T. gondii*-infected myoblasts versus myotubes were hierarchically clustered based on an average linkage analysis using Pearson correlation coefficients as the distance measure. Up to 6592 differentially regulated genes were identified in myoblasts and myotubes irrespective of infection. From these, the top 50 genes with the highest significance levels of regulation between infected myoblasts and infected myotubes were clustered in this heatmap. Levels of gene expression were visualized using a Z-score color code ranging from -1.5 to +1.5 where yellow color indicates highest expression and blue color indicates lowest expression of genes.

3.2.4 DEGs in non-infected or infected myoblasts versus myotubes

Among the total number of DEGs (6351) that were differentially expressed in non-infected myoblasts versus non-infected myotubes 2872 were upregulated and 3479 DEGs were downregulated. Besides, of the 6592 total DEGs that were identified in *T. gondii*-infected myoblasts versus infected myotubes 3013 DEGs were upregulated and 3579 DEGs were downregulated (Figure 3.4A). Venn analysis was then performed to identify DEGs that were uniquely regulated in non-infected myoblasts versus myotubes as compared to infected myoblasts versus myotubes. Results identified 657 and 897 DEGs that were

uniquely regulated between the two non-infected or *T. gondii*-infected cell types, respectively. Both non-infected and infected myoblasts versus myotubes shared a majority of 5657 DEGs (Figure 3.4B). Among the 657 DEGs uniquely regulated in non-infected myoblasts versus non-infected myotubes 343 DEGs were upregulated and 314 DEGs were downregulated. Similarly, among the 897 DEGs uniquely regulated in infected myoblasts versus infected myotubes 485 DEGs were upregulated and 412 DEGs were downregulated (Figure 3.4C).

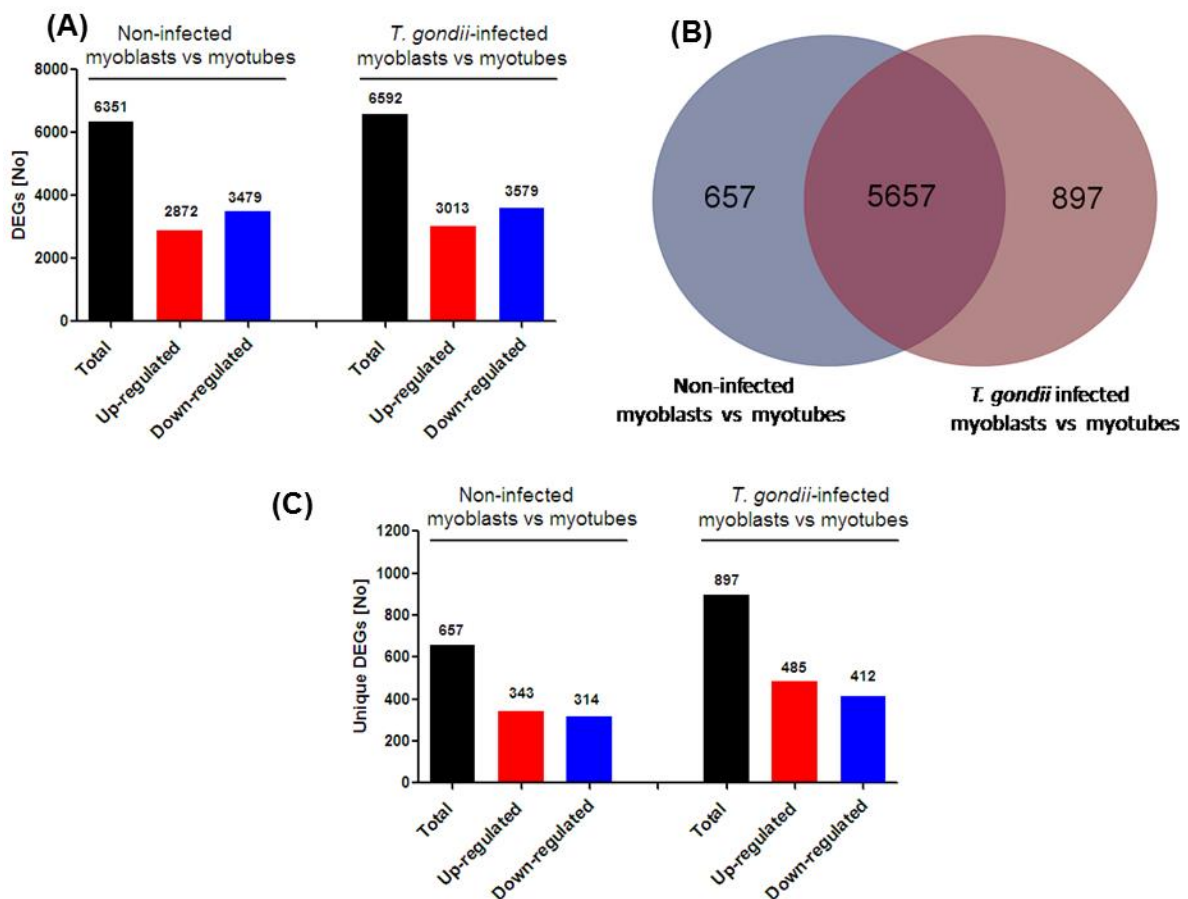


Figure 3.4: Identification of DEGs in non-infected and *T. gondii*-infected myoblasts versus myotubes. (A) DEGs ($p < 0.05$) were identified after RNAseq by comparing non-infected myoblasts and myotubes or *T. gondii*-infected myoblasts and myotubes. Among total DEGs numbers of those up- or downregulated in myoblasts as compared to myotubes were identified. (B) Venn diagram showing the number of DEGs commonly regulated in both non-infected and infected myoblasts versus myotubes within the overlap area of both circles. Numbers outside the overlap correspond to unique DEGs of non-infected myoblasts versus myotubes (left) and infected myoblasts versus myotubes (right). (C) DEGs uniquely regulated in either non-infected or infected myoblasts versus myotubes were grouped into genes up- and downregulated.

3.2.5 Gene ontology analysis of differentially regulated genes in infected myoblasts versus myotubes

Gene ontology term enrichment analysis was performed with DEGs identified in *T. gondii*-infected myoblasts versus infected myotubes in order to identify biological processes that differ between both cell types. Results showed that DEGs were highly enriched for genes predominantly associated with cellular component organization or biogenesis, the mitotic cell cycle including organelle fission, muscle structure development and metabolic processes including primary metabolic process, organic substance metabolic process and cellular nitrogen compound metabolic process (Figure 3.5). This clearly indicated that muscle development, the cell cycle and metabolism are important biological processes that largely differ between *T. gondii*-infected myoblasts and myotubes.

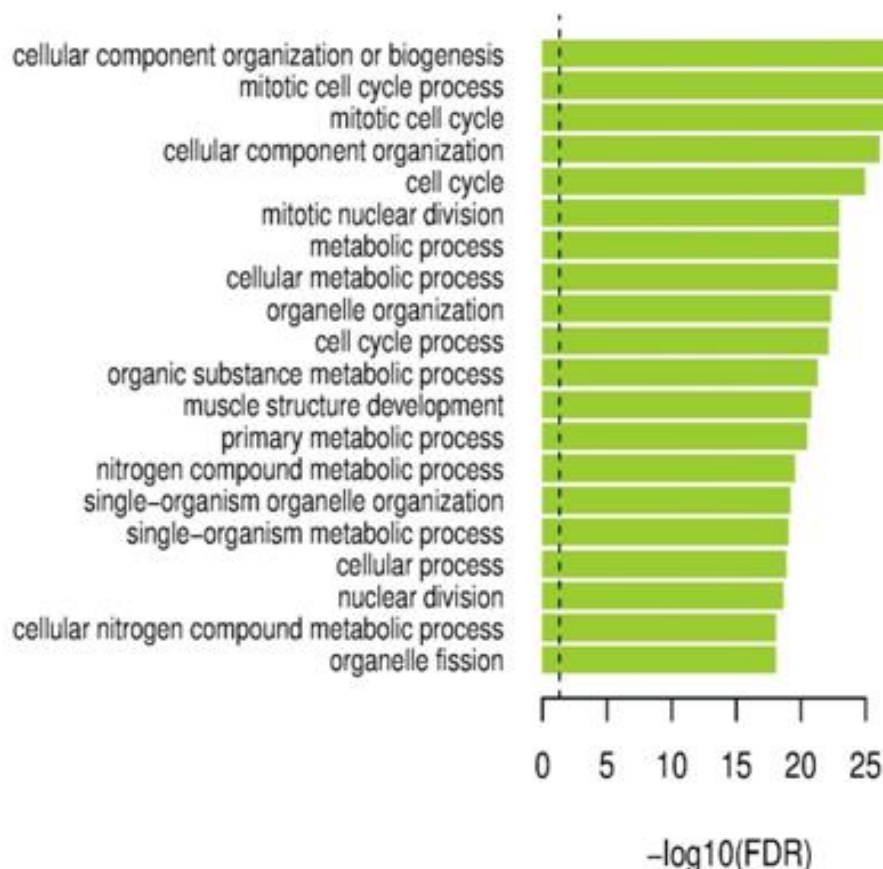


Figure 3.5: GO term enrichment analysis of differentially regulated genes in *T. gondii*-infected myoblasts and myotubes. The top 20 biological processes with the most significant enrichments among DEGs as compared to the reference genome are indicated.

3.2.6 Biological processes associated with DEGs uniquely upregulated in infected myoblasts versus infected myotubes

In order to identify biological processes that are specifically associated with the 485 DEGs that were uniquely upregulated in infected but not non-infected myoblasts versus myotubes (Figure 3.4C) the Database for Annotation, Visualization and Integrated Discovery (DAVID) online tools were used. Results showed that these DEGs were enriched in genes involved in various biological processes. Among these, the most prominent biological processes were transcription including mRNA processing, regulation of transcription, covalent chromatin modification, phosphorylation and protein phosphorylation, DNA repair and cellular responses to DNA damage stimulation (Figure 3.6). A list of the 30 most strongly uniquely upregulated DEGs in infected myoblasts versus infected myotubes but not in non-infected myoblasts versus myotubes are shown in supplementary Table 3.1.

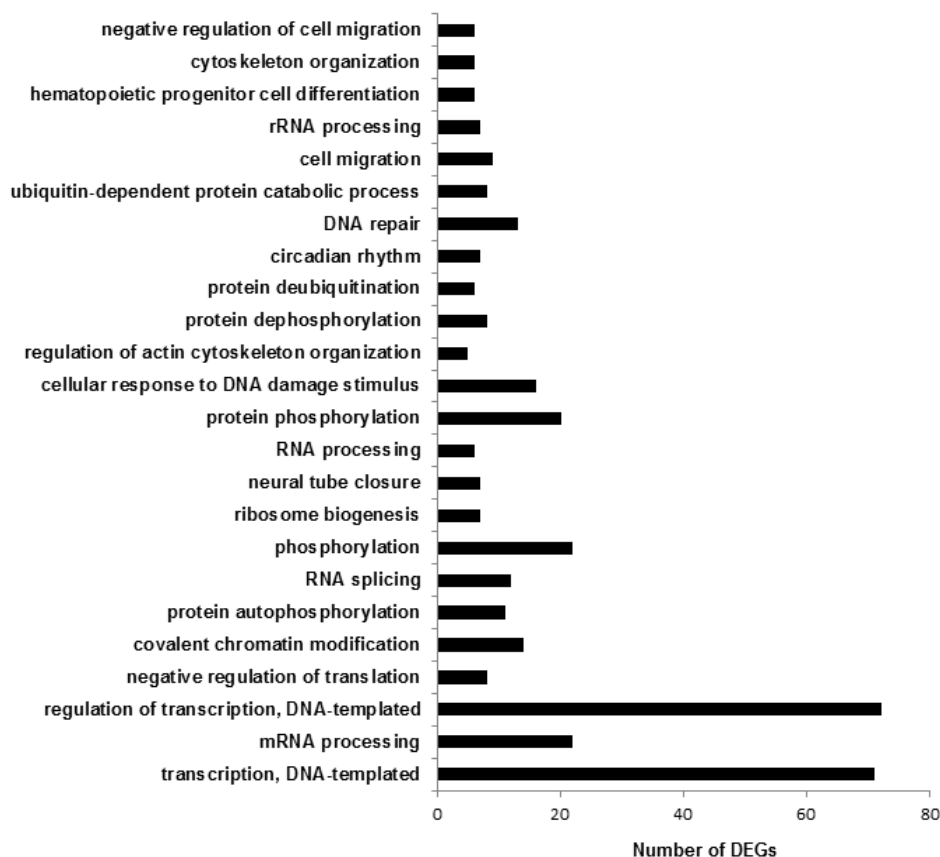


Figure 3.6: GO term enrichment analysis of DEGs uniquely upregulated in *T. gondii*-infected myoblasts versus infected myotubes. Uniquely upregulated DEGs were identified from total DEGs of *T. gondii*-infected myoblasts versus infected myotubes based on the fold regulation value of gene expression data. Thereafter, the DAVID online tools were used to identify association of these DEGs to different biological pathways (<https://david.ncifcrf.gov/tools.jsp>).

3.2.7 GO term analysis of DEGs uniquely downregulated in infected myoblasts versus infected myotubes

GO term enrichment analysis was also performed with those 412 DEGs that were uniquely downregulated in *T. gondii*-infected but not non-infected myoblasts versus myotubes (Figure 3.4C) using the DAVID tool. Results showed that differentially regulated genes were mainly involved in regulation of oxidation-reduction processes, axon guidance, transport, cell proliferation and others (Figure 3.7). A list of the 30 most strongly uniquely downregulated DEGs in infected myoblasts versus infected myotubes but not non-infected myoblasts versus myotubes are shown in supplementary Table 3.2.

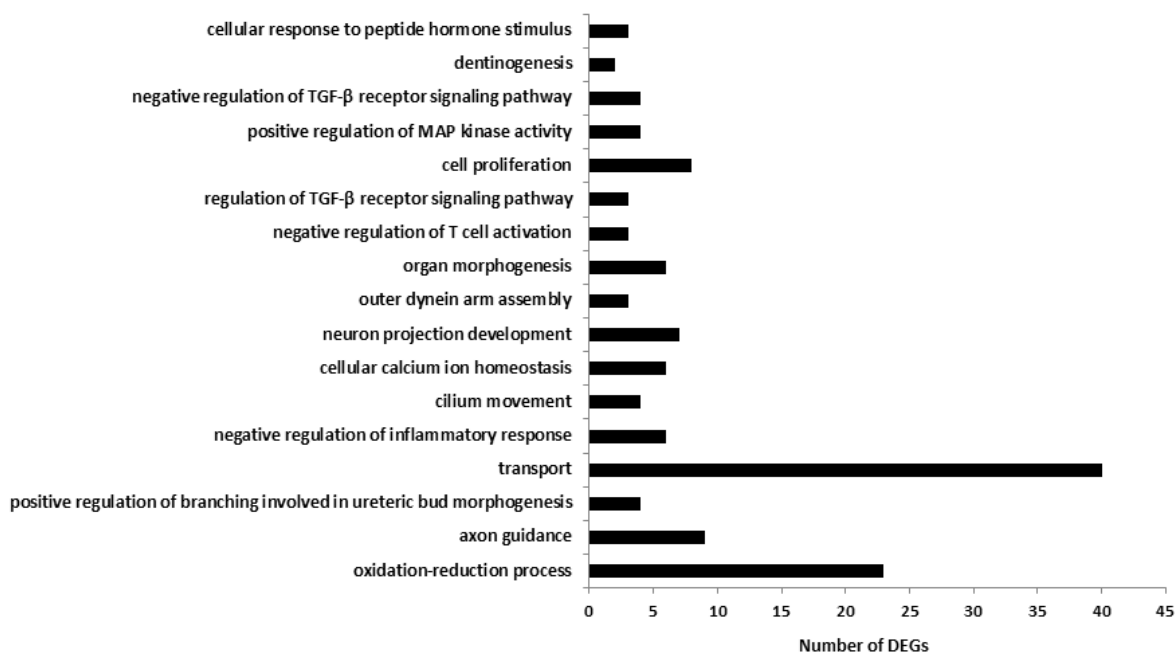


Figure 3.7: GO term enrichment analysis of uniquely downregulated DEGs in infected myoblasts vs infected myotubes. Uniquely downregulated DEGs were identified from total DEGs in *T. gondii*-infected myoblasts versus infected myotubes based on the fold regulation value of gene expression data. Thereafter, DAVID online tools were used to identify the association of these DEGs to different biological pathways (<https://david.ncifcrf.gov/tools.jsp>).

3.2.8 Differential gene expression in non-infected and *T. gondii*-infected myotubes and myoblasts

Whereas myotubes and myoblasts differed largely in their gene expression pattern (see Figure 3.3), *T. gondii*-infection had only a minor impact on these transcriptome. In total, only 38 genes were differentially regulated ($p < 0.05$) by *T. gondii* in myotubes after infection. Most genes were identified as predicted or pseudogenes. Nevertheless, a list of the differentially regulated genes in *T. gondii*-infected versus non-infected myotubes is shown in supplementary Table 3.3. Similarly, 70 genes were differentially regulated ($p < 0.05$) by *T. gondii* infection in myoblasts. Most genes were identified as predicted or pseudogenes. However, a list of the differentially regulated genes in *T. gondii* infected versus non-infected myoblasts is shown in supplementary Table 3.4.

Because a main aim of this study was to identify candidates that might regulate differential development of *T. gondii* in myotubes versus myoblasts, I next concentrated on those genes that were differentially expressed in myoblasts and myotubes irrespective of infection. Since GO term enrichment analysis has identified the cell cycle and metabolism of the host cell largely differing between myoblasts and myotubes (Figure 3.5) I concentrated on expression of glucose metabolism enzymes and cell cycle regulators in non-infected and *T. gondii*-infected myotubes and myoblasts. Upregulation or downregulation of genes associated with glucose metabolic pathways and cell cycle regulation was calculated as fold change (FC) using their RPKM values in *T. gondii*-infected myotubes versus myoblasts. Most of the genes encoding for glycolytic enzymes were significantly upregulated in infected myotubes as compared to infected myoblasts except glyceraldehyde-3-phosphate dehydrogenase, triphosphate isomerase-I and phosphoglycerate kinase-I and pyruvate kinase. The list of genes of glycolytic enzymes including their FC and p -value are shown in supplementary Table 3.5. Distinct genes encoding for enzymes of the TCA cycle, namely pyruvate dehydrogenase complex, aconitase-II, isocitrate dehydrogenase2 and pyruvate carboxylase were upregulated in infected myotubes as compared to infected myoblasts. Other genes such as citrate synthase and phosphoenol pyruvate (PEP) carboxykinase2 were downregulated in myotubes compared to myoblasts while most genes, i.e. ketoglutarate dehydrogenase, succinate-CoA ligase, succinate dehydrogenase, fumarate hydratase-I and malate dehydrogenase-II were not differentially regulated between infected myotubes and myoblasts. The list of genes

encoding for TCA cycle enzymes including their FC and *p*-value are shown in supplementary Table 3.6. Interestingly, most of the genes encoding enzymes of both the oxidative and non-oxidative phases of the pentose phosphate pathway (PPP) including glucose-6-phosphate dehydrogenase2, glucose-6-phosphate dehydrogenase (X-linked), 6-phosphogluconate dehydrogenase, ribose-5-phosphate isomerase and transketolase were downregulated in infected myotubes compared to myoblasts, suggesting their upregulation in infected myoblasts as compared to myotubes. The list of genes involved in the PPP including their FC and *p*-value are shown in supplementary Table 3.7. Genes encoding for enzymes of glycogen synthesis as for instance hexokinase-II, phosphoglucomutase-II, UDP-glucose pyrophosphorylase2, glycogenin, glycogen synthase-I and genes for glycogen degradation including glycogen phosphorylase and debranching enzymes were upregulated in myotubes as compared to myoblasts while the gene encoding for branching enzyme was not regulated. The list of genes involved in glycogen metabolism and their FC and *p*-value are shown in supplementary Table 3.8. Finally, gene expression data for proteins of cell cycle regulation were analysed. Results showed that genes encoding different CDK inhibitors as for instance p21, p57, p27 and cell cycle proteins i.e p53 and DNA damage regulated-I, retinoblastoma (RB)-1 were upregulated in infected myotubes compared to myoblasts. In contrast, genes encoding various cyclins including cyclinA2, cyclinB1/B2, cyclinC, cyclinD1/D2, cyclinE1/E2 and cyclin dependent kinases i.e CDK1, CDK2, CDK4, CDK6, CDK8 and p18, CWF-19 like1, proliferating cell nuclear antigen were downregulated in infected myotubes as compared to myoblasts. The list of genes involved in cell cycle regulation and their FC and *p*-value are shown in supplementary Table 3.9.

3.2.9 Differential gene expression of distinct glucose metabolizing enzymes and cell cycle regulators in myotubes and myoblasts

Since GO term analysis and expression data indicated major differences in cell cycle and primary metabolism regulation between infected myoblasts versus myotubes (see Figure 3.5), RNAseq data were further analyzed for expression of selected individual genes related to these pathways. Furthermore, their expression at the mRNA level was further validated by RT-qPCR. Glucose-6-phosphate dehydrogenase (G6PDH) 2 is an important enzyme of the pentose phosphate pathway (PPP) and catalyses the rate limiting reaction,

i.e. conversion of glucose-6-phosphate into 6-phosphogluconolactone. RNAseq data showed that the mRNA level of this enzyme was higher in myoblasts compared to myotubes. Interestingly, *T. gondii* further upregulated expression of G6PDH2 in both myoblasts and myotubes (Figure 3.8A). RT-qPCR was performed with mRNA isolated at 4, 24 and 48 hours post infection. Results confirmed higher levels of G6PDH2 mRNA in myoblasts compared to myotubes at 4 and to a lesser extent also at 24 hours after infection in both infected and non-infected control myoblasts. However, the levels of G6PDH2 mRNA did not differ between myoblasts and myotubes at 48 hours of infection (Figure 3.9A). RT-qPCR analysis did not confirm increased G6PDH2 mRNA levels after *T. gondii*-infection as indicated by RNAseq (Figure 3.8A). G6PDH (X-linked) mRNA was 4-fold higher in myoblasts as compared to myotubes irrespective of infection as revealed by RNAseq analysis (Figure 3.8B). RT-qPCR data confirmed upregulation of mRNA of this enzyme in myoblasts compared to myotubes at 4 and 24, but not at 48 hours post infection (Figure 3.9B). Messenger RNA of 6-phosphogluconate dehydrogenase (6PGDH) which catalyzes another important reaction of the PPP, i.e. decarboxylation of 6-phosphogluconate into ribulose-5-phosphate was 2-fold higher in myoblasts compared to myotubes irrespective of infection as indicated by RNAseq analysis (Figure 3.8C). Surprisingly, RT-qPCR revealed upregulation of 6PGDH mRNA in myoblasts as compared to myotubes at 4 hours post infection only but not at 24 and 48 hours (Figure 3.9C). In contrast to the enzymes of the PPP, mRNA expression of pyruvate carboxylase, i.e. an enzyme of TCA cycle anaplerosis which catalyzes the conversion of pyruvate into oxaloacetate, was upregulated in both *T. gondii*-infected and non-infected myotubes as compared to myoblasts as indicated by RNAseq analysis (Figure 3.8D). A similar pattern of relative mRNA expression of this enzyme was verified by RT-qPCR in myotubes and myoblasts at 24 and 48 hours post infection whereas such difference was not obvious at 4 hours of infection (Figure 3.9D). Transcripts of the glycogen synthase-I which is a rate limiting enzyme of glycogen synthesis were 4-fold upregulated in myotubes compared to myoblasts irrespective of infection as revealed by RNAseq (Figure 3.8E). RT-qPCR confirmed higher mRNA levels of this enzyme in infected and non-infected myotubes at 4, 24 and 48 hours of infection (Figure 3.9E). Similarly, expression of glycogen phosphorylase, an important enzyme of glycogen breakdown was upregulated in myotubes compared to myoblasts as observed after RNAseq (Figure 3.8F) and RT-qPCR (Figure 3.9F).

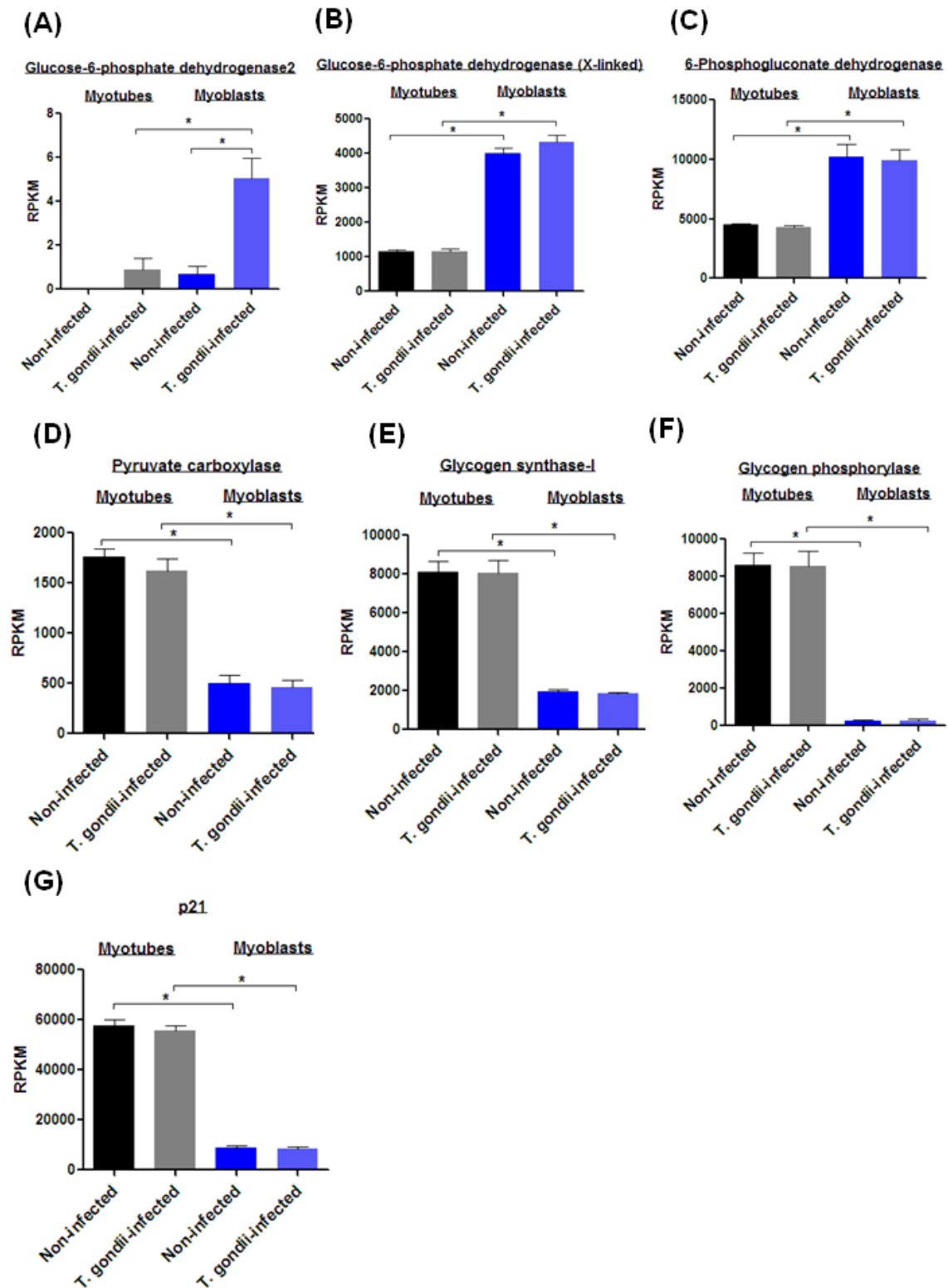


Figure 3.8: RNAseq gene expression data of selected metabolic enzymes and cell cycle protein p21 in *T. gondii*-infected and non-infected myotubes and myoblasts. Gene expression levels are indicated based on ‘reads per kilobase per million reads’ (RPKM) for metabolic enzymes and cell cycle protein p21 (A) glucose-6-phosphate dehydrogenase2 (B) glucose-6-phosphate dehydrogenase (X-linked) (C) 6-phosphogluconate dehydrogenase (D) pyruvate carboxylase (E) glycogen synthase-I (F) glycogen phosphorylase (G) p21. Results are depicted as means \pm S.E.M. from three independent biological replicates. Significant differences were identified by χ^2 test (* $p < 0.05$).

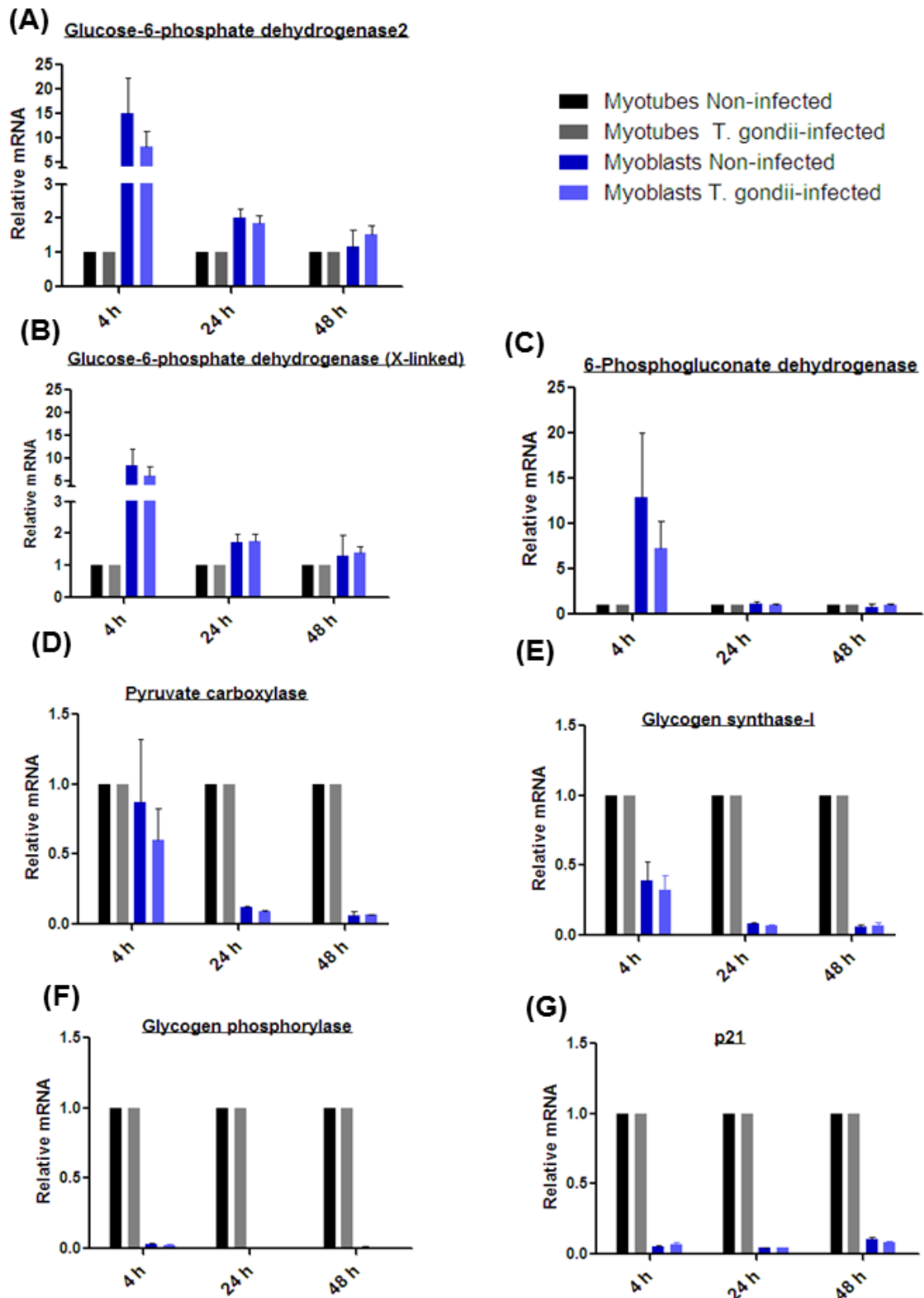


Figure 3.9: Validation of gene expression of selected metabolic enzymes and cell cycle protein p21 using RT-qPCR. C2C12 myoblasts were induced to differentiate into poly-nucleated myotubes. Both differentiated myotubes and proliferating myoblasts were infected with *T. gondii* tachyzoites at a host cell-to-parasite ratio of 1:3.5 or were left as non-infected control. Total RNA was isolated at 4, 24 and 48 hours post infection, followed by cDNA synthesis. Subsequently, cDNA was amplified using host cell specific primers for different metabolic enzymes- and cell cycle inhibitor p21 (A) glucose-6-phosphate dehydrogenase2

(B) glucose-6-phosphate dehydrogenase (X-linked) (C) 6-phosphogluconate dehydrogenase (D) pyruvate carboxylase (E) glycogen synthase-I (F) glycogen phosphorylase (G) p21. The relative mRNA expression in myoblasts as compared to myotubes was calculated ($\Delta\Delta\text{CP}$ method) and was normalized to mouse β -actin mRNA. Results are depicted as means \pm S.E.M. from three independent experiments.

Finally, p21, a potent cyclin-dependent kinase inhibitor which can halt cell cycle progression was upregulated in infected and non-infected myotubes compared to myoblasts and this was consistently observed after RNAseq analysis (Figure 3.8G) and RT-qPCR (Figure 3.9G). The differences in gene expression pattern of glucose metabolic enzymes and cell cycle proteins in myotubes and myoblasts provided initial hints for analyzing metabolic characteristics of these cell types and their role in *T. gondii* bradyzoite differentiation in myotubes.

3.3 Impact of differential glucose metabolism in SkMCs on *T. gondii* stage conversion

Since myoblasts and myotubes strongly differed in the mRNA levels of several key enzymes of the central carbohydrate metabolism further analyses were performed in order to validate differences in the metabolomes of both cell types. Furthermore, the impact of a differential glucose metabolism in SkMCs on *T. gondii* bradyzoite formation was assessed.

3.3.1 Differences in carbohydrate metabolism in *T. gondii*-infected and non-infected myotubes and myoblasts

Glucose is the most important hexose sugar and has a central role as an energy source in most organisms including mammals and *T. gondii*. Glucose can be catabolized via the pentose phosphate pathway (PPP) to generate reduced nicotinamide adenine dinucleotide phosphate (NADPH) and ribose sugars for synthesis of nucleotides. Alternatively, it may undergo complete oxidation via glycolysis and the TCA cycle for energy production. Finally, it can be utilized for synthesis of glycogen. In this study, glucose catabolism was monitored in non-infected and *T. gondii*-infected myotubes and myoblasts to determine differences in central carbohydrate metabolic pathways and their modulation by *T. gondii* in both cell types. To this end, gas chromatography-mass spectrometry (GC-MS) analysis of cells previously labeled with ^{13}C -glucose was performed to measure labeled carbon incorporation into metabolites of the PPP, glycolysis and the TCA cycle (in collaboration with Izabela Swierzy, Göttingen and Martin Blume, Melbourne). Consistent with the increased expression of PPP enzymes in myoblasts as compared to myotubes (see 3.2.9), the percentage of ^{13}C -incorporation into the PPP metabolite ribulose-5-phosphate was significantly higher in myoblasts compared to myotubes irrespective of infection. This suggested that myoblasts exhibit higher PPP activities than myotubes (Figure 3.10A). On the other hand, no significant differences in the percentages of labeled carbon incorporation into intermediates of glycolysis were detected between both non-infected or infected myotubes and myoblasts thus suggesting similar glycolytic activities in both cell types (Figure 3.10B). In contrast, statistically increased percentages of labeled carbon incorporation into the intermediates of the TCA cycle (i.e., citric acid, glutamic acid, succinic acid, fumaric acid, malic acid and aspartic acid) were detected in infected and

non-infected myotubes as compared to infected and non-infected myoblasts. Infection of both cell types with *T. gondii* had no impact on the percentages of ^{13}C incorporation into TCA cycle metabolites. This indicated that myotubes exhibit higher TCA cycle activities than myoblasts (Figure 3.10C). From these results it can be concluded that myoblasts and myotubes largely differ in glucose metabolism via PPP and TCA cycle but not through glycolysis.

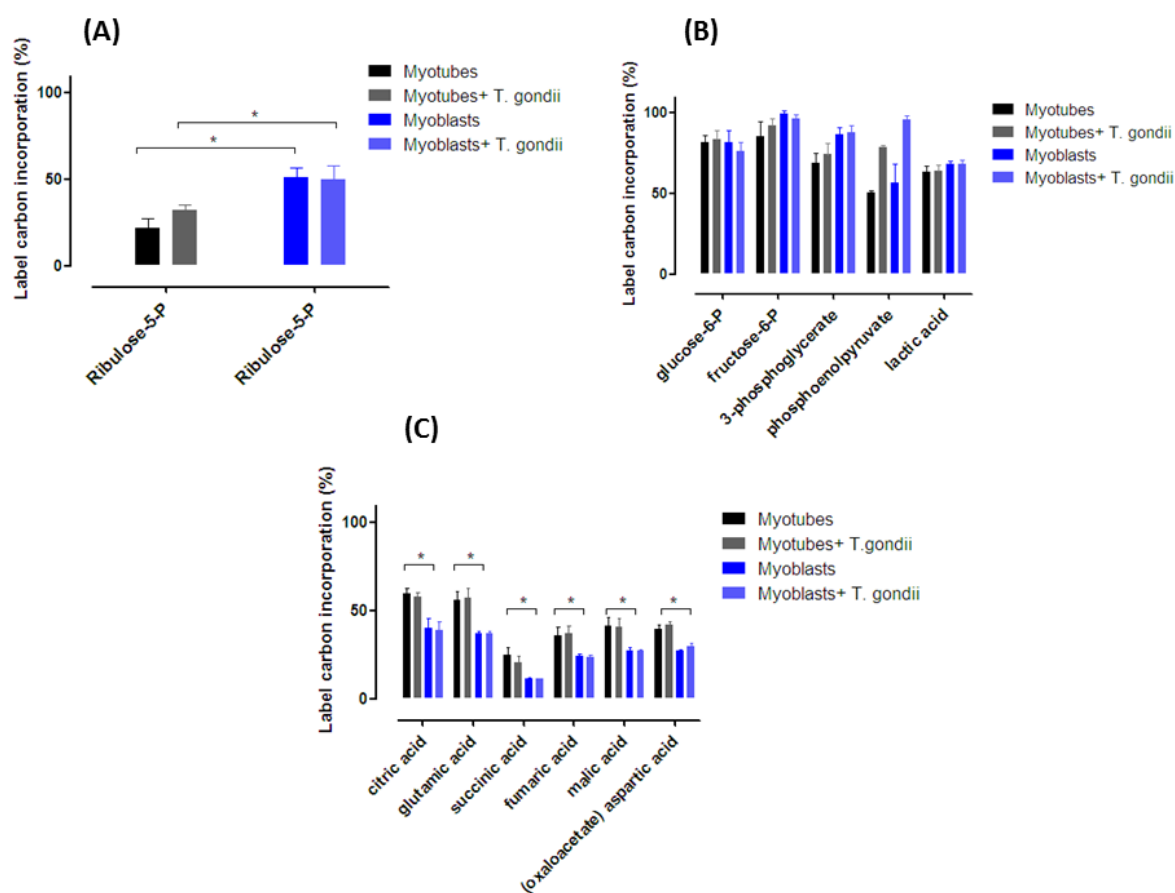


Figure 3.10: Mass spectrometric analysis of glucose catabolism in non-infected and *T. gondii*-infected myotubes and myoblasts. C2C12 myoblasts were induced to differentiate into poly-nucleated myotubes. Both myotubes and myoblasts were infected with *T. gondii* tachyzoites or were left non-infected. Six hours after infection, infected and non-infected myoblasts and myotubes were incubated in medium supplemented with ^{13}C -Glucose for additional 4 hours. After metabolite extraction, incorporation of ^{13}C into metabolites of the pentose phosphate pathway, glycolysis and the TCA cycle was analyzed by GC-MS. (A) Percentage of labeled carbon incorporation into ribulose-5-P generated by the pentose phosphate pathway. (B) Percentages of labeled carbon incorporation in metabolites of glycolysis. (C) Percentages of labeled carbon incorporation in metabolites of the TCA cycle. Results are depicted as means \pm S.E.M. from three independent experiments. Significant differences were identified by Student's *t*-test and ANOVA (* $p < 0.05$).

3.3.2 Myotubes preferentially channel glycolytic pyruvate into the TCA cycle via anaplerotic reactions

Since myotubes showed higher incorporation of ^{13}C from glucose into TCA cycle metabolites than myoblasts, it was important to understand how the labeled carbon atom of ^{13}C -glucose entered into the TCA cycle. Glucose-derived pyruvate can enter the TCA cycle via acetyl-CoA and the pyruvate dehydrogenase complex or through the anaplerotic reaction of the pyruvate carboxylase.

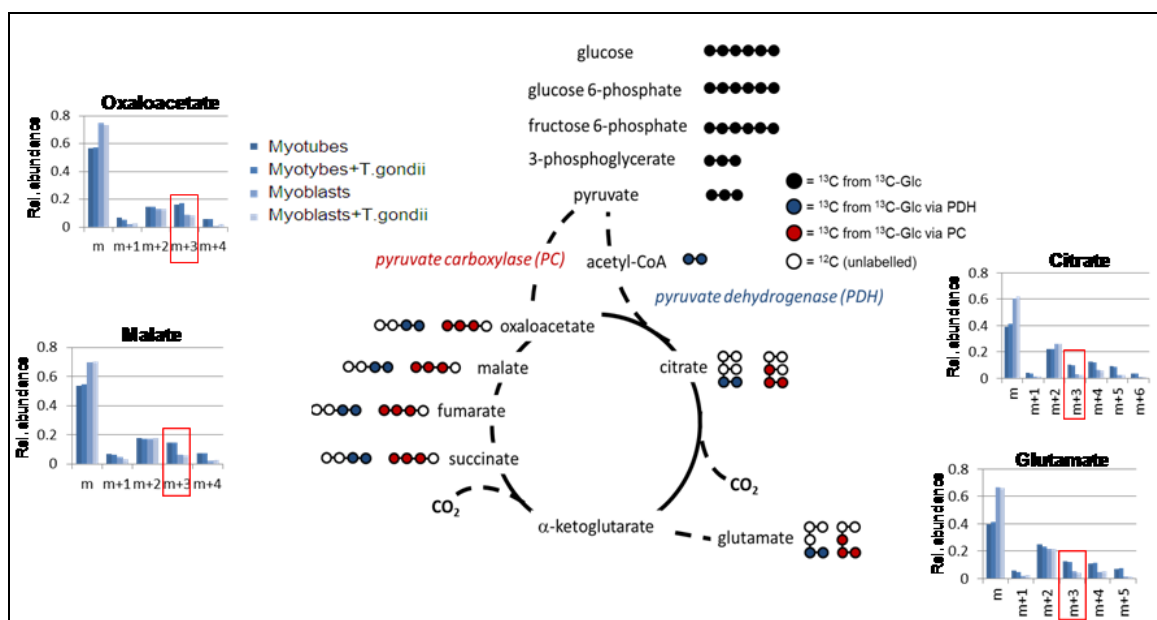


Figure 3.11: Myotubes channel glycolytic carbon into the TCA cycle more readily through anaplerotic reactions than myoblasts. C2C12 myoblasts were induced to differentiate into poly-nucleated myotubes. Both myotubes and myoblasts were infected with *T. gondii* tachyzoites. Six hours after infection, *T. gondii*-infected and non-infected myoblasts and myotubes were incubated in medium supplemented with ^{13}C -glucose for additional 4 hours. After metabolite extraction, incorporation of ^{13}C into metabolites of TCA cycle was analyzed by GC-MS. Relative abundance of labelled carbon (^{13}C) within individual intermediates of the TCA cycle as for instance citrate, glutamate (right panel) and oxaloacetate, malate (left panel) are indicated. Data are derived from one experiment. The diagram in middle shows glucose metabolic pathways through glycolysis and TCA cycle. The abundance of glucose-derived ^{13}C within TCA cycle intermediates are depicted when pyruvate preferentially enters into the TCA cycle through the pyruvate carboxylase reaction (red circles) or the pyruvate dehydrogenase complex reaction (blue circles). Higher abundance of three ^{13}C atoms each within TCA cycle intermediates in myotubes as compared to myoblasts is highlighted by red boxes within the bar graphs.

To answer the question, SkMCs were fed with ^{13}C -glucose and after extraction, masses of TCA cycle metabolites were measured by GC-MS. Data showed that oxaloacetate, malate, glutamate and citrate from infected and non-infected myotubes more readily presented masses that indicated the presence of three heavy carbon atoms (^{13}C , indicated by red circles in Figure 3.11) but not two ^{13}C (indicated by blue circles) when compared to myoblasts (Figure 3.11). This indicated that in myotubes, glucose-derived ^{13}C entered into the TCA cycle more preferentially through the pyruvate carboxylase reaction (TCA cycle anaplerosis) than in myoblasts. Again, no differences were observed between *T. gondii*-infected and non-infected SkMCs (Figure 3.11).

3.3.3 Dehydroepiandrosterone accelerates *T. gondii* bradyzoite differentiation in myotubes and myoblasts

Results of this study have shown that enzymes of the PPP including G6PDH2 and G6PDH (X-linked) were upregulated in infected and non-infected myoblasts as compared to myotubes (Figures 3.8A,B and 3.9A,B). Furthermore, GC-MS analysis suggested higher PPP activities in myoblasts than in myotubes (Figure 3.10A). These results raised questions on the importance of the PPP on *T. gondii* bradyzoite development in SkMCs since differentiated myotubes but not proliferating myoblasts support bradyzoite differentiation (Figure 3.1; Swierzy & Lüder 2014). Therefore, I next established pharmacological inhibition of G6PDH, i.e. the rate-limiting enzyme of the PPP in *T. gondii*-infected myoblasts as well as myotubes to determine its impact on bradyzoite differentiation in the parasite. For this purpose, dehydroepiandrosterone (DHEA) was used as an inhibitor of G6PDH (Figure 3.12; Schwartz & Pashko 2004). Myoblasts and myotubes were treated with 50 μM and 100 μM of DHEA or were mock-treated, followed by *T. gondii* infection one hour later. At 2 days of infection, total RNA was isolated and the expression of *T. gondii* BAG1 was examined by RT-qPCR. Interestingly, data showed significant upregulation of BAG1 mRNA from parasites in DHEA-treated myoblasts and myotubes compared to mock-treated cells. Furthermore, BAG1 induction by DHEA was much stronger in *T. gondii* within myoblasts than in myotubes (Figure 3.13A). This result suggested that inhibition of G6PDH by DHEA favor *T. gondii* bradyzoite development particularly in myoblasts and to a lesser extent also in myotubes.

As reduced parasite replication is considered a prerequisite for increased bradyzoite differentiation (Bohne *et al.*, 1994), I also determined the effect of DHEA on parasite replication in myotubes and myoblasts. Parasite replication was assessed in DHEA-treated or mock-treated myoblasts and myotubes after 48 hours of infection by immunofluorescence staining. Increased replication of *T. gondii* was confirmed to occur in mock-treated myoblasts as compared to mock-treated myotubes as previously described (Swierzy and Lüder, 2014). DHEA at 100 μ M reduced parasite replication by two-fold in myotubes as compared to treatment with the solvent. Interestingly, a three- and four-fold reduction in parasite replication was observed after treatment of myoblasts with 50 μ M or 100 μ M DHEA (Figure 3.13C). Consistently, parasitophorous vacuoles were smaller in DHEA-treated samples compared to mock-treated ones in both myotubes and myoblasts (Figure 3.13B). Therefore, it can be concluded that inhibiting the G6PDH by DHEA inhibits parasite replication and enhances bradyzoite differentiation primarily in myoblasts but to a lesser extent also in myotubes.

I next determined whether increased expression of bradyzoite specific genes (BAG1) and reduced parasite replication after DHEA treatment would also lead to the formation of tissue cysts. Cyst formation was thus evaluated in DHEA- or solvent-treated myoblasts and myotubes by staining of the cyst wall using the *Dolichos biflorus* lectin. Results showed a trend towards increasing numbers of cysts in DHEA-treated myoblasts and myotubes compared to mock treatment after 48 and 72 hours of infection. Cysts numbers were significantly increased in myoblasts treated with 100 μ M DHEA at 72 hours of infection (Figure 3.13D).

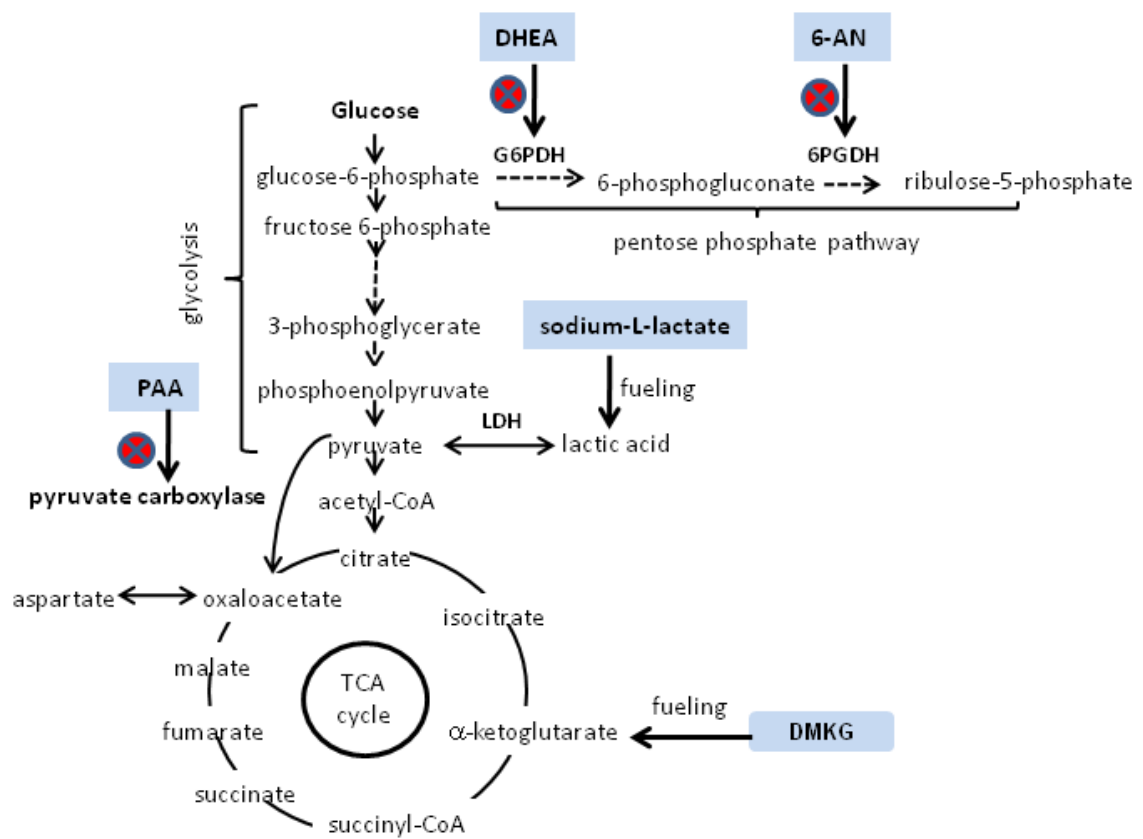


Figure 3.12: Schematic diagram of glucose metabolism via pentose phosphate pathway, glycolysis and TCA cycle. Different inhibitors/modulators were used to analyse the impact of metabolic pathways on *T. gondii* bradyzoite differentiation in myotubes and myoblasts. Dehydroepiandrosterone (DHEA) and 6-aminonicotinamide (6-AN) inhibits glucose-6-phosphate dehydrogenase (G6PDH) and 6-phosphogluconate dehydrogenase (6PGDH), respectively. Phenylacetic acid (PAA) inhibits pyruvate carboxylase whereas sodium-L-lactate and dimethyl- α -ketoglutarate (DMKG) are used as modulators of anaerobic glycolysis and TCA cycle, respectively. LDH indicates lactate dehydrogenase which catalyses reversible conversion of pyruvate to lactic acid, the last reaction of anaerobic glycolysis.

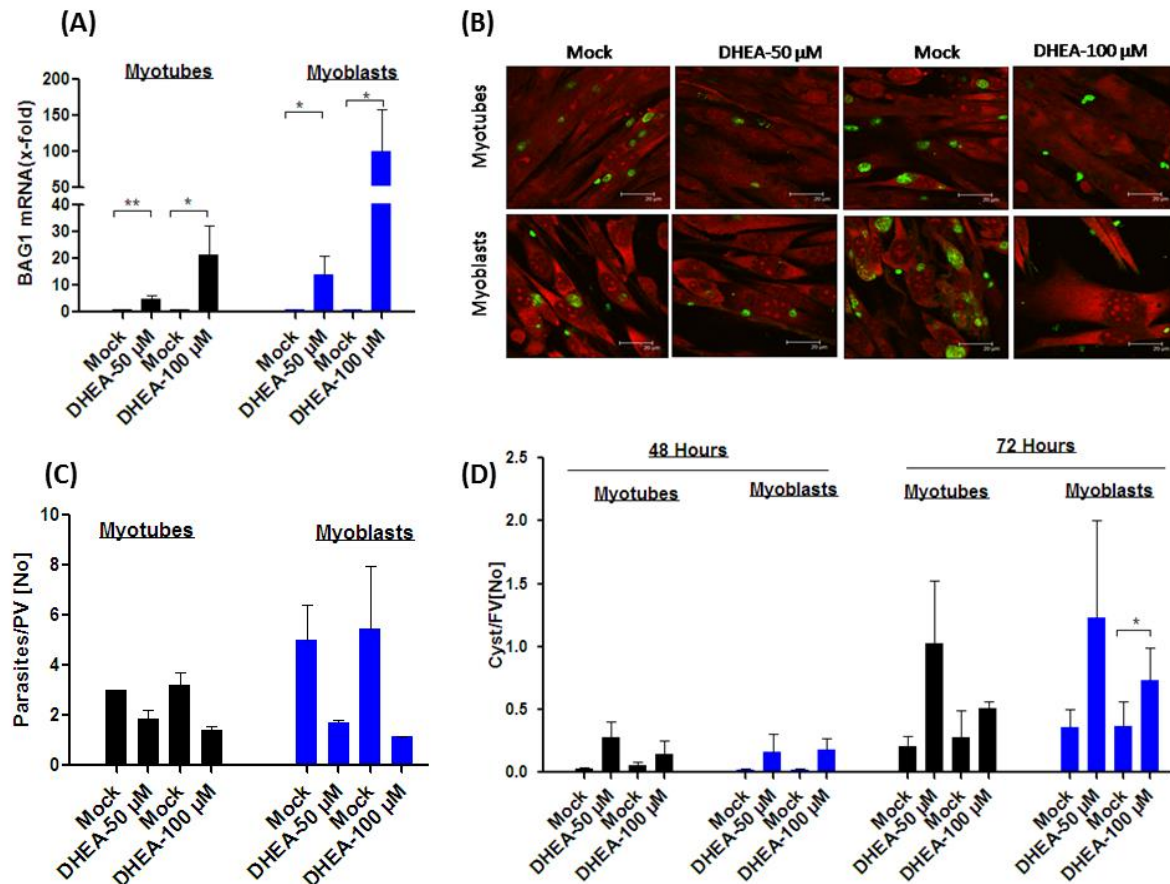


Figure 3.13: Dehydroepiandrosterone (DHEA) induces *T. gondii* bradyzoite differentiation and tissue cyst formation in myoblasts and myotubes. C2C12 myoblasts were induced to differentiate into myotubes. Both myotubes and myoblasts were treated with 50 μ M and 100 μ M of DHEA or were mock-treated, followed by *T. gondii* infection 1 hour later at a host cell-to-parasite ratio of 1:3.5. **(A)** After 48 hours of infection, total RNA was isolated, mRNA was reverse transcribed and cDNA was amplified using specific primers for *T. gondii* bradyzoite antigen 1 (BAG1) and *T. gondii* actin (TgActin) by quantitative real-time PCR. The relative increase in BAG1 mRNA by DHEA as compared to mock treatment was calculated and was normalized to TgActin mRNA. Results were depicted as means \pm S.E.M. from six independent experiments. Significant differences were identified by Student's *t*-test (* $p < 0.05$ and ** $p < 0.01$). **(B)** Cells were fixed at 48 hours post infection with 4 % paraformaldehyde and parasites were immunolabeled using a polyclonal *anti-T. gondii* antiserum and Cy2-conjugated secondary antibodies (green fluorescence). Host cells were visualized using propidium iodide (red fluorescence). Representative images of both labelings were recorded by confocal laser scanning microscopy and were superimposed. **(C)** After cells had been fluorescently labeled as described in (B), the average size of parasitophorous vacuoles (PVs) in each sample was determined by counting the number of parasites in 100 PVs. Data represent means \pm S.E.M. from two independent experiments. **(D)** Cells were fixed at 48 and 72 hours post infection with 4 % paraformaldehyde. Tissue cysts of *T. gondii* were labeled with biotin-conjugated *Dolichos biflorus* lectin and Cy2-conjugated streptavidin, parasites were labeled with a polyclonal *anti-T. gondii* antiserum and Cy5-conjugated secondary antibodies and host cells were visualized using propidium iodide. The numbers of cyst were counted in 100 fields of vision (FV). Data represent means \pm S.E.M. from two independent experiments. Significant differences were identified by Student's *t*-test (* $p < 0.05$).

3.3.4 NADP⁺/NADPH levels in *T. gondii*-infected myoblasts and myotubes and their modulation by DHEA-mediated inhibition of G6PDH

A main function of the PPP is to provide NADPH for synthesis purposes and regulation of cellular redox homeostasis. In order to determine differences in NADP⁺/NADPH levels in *T. gondii*-infected myoblasts and myotubes their levels were measured using a colorimetric test system. Furthermore, this test was used to determine the relative impact of DHEA on providing NADPH through the PPP. To this end, relative amounts of NADP(total), NADPH and the NADP⁺/NADPH ratios were measured in DHEA-treated or mock-treated *T. gondii*-infected myoblasts and myotubes. The results showed similar NADP(total) levels (NADP⁺ and NADPH) in infected control myoblasts and myotubes whereas NADPH levels were clearly higher in myoblasts than in myotubes as expected (Figure 3.14A). Consequently, the NADP⁺/NADPH ratio was clearly higher in myotubes as compared to myoblasts (Figure 3.14B). Treatment of parasite-infected myoblasts and myotubes with 50 or 100 µM of DHEA had no obvious impact on total NADP levels in both cell types. The NADPH level was slightly reduced in myotubes treated with 50 µM but not 100 µM of DHEA as compared to the mock control. However, reduced levels of NADPH were observed in DHEA-treated myoblasts (50 µM, 100 µM) as compared to the control and this was statistically significant when treated with 100 µM DHEA (Figure 3.14A). This confirmed that DHEA at least in myoblasts inhibited PPP-derived NADPH levels by inhibiting the G6PDH. Furthermore, the ratio of NADP⁺/NADPH was increasing after treatment of myoblasts with increasing amounts of DHEA ($p < 0.05$ at 100 µM of DHEA) and after treatment of myotubes with 100 µM of DHEA (Figure 3.14B). In general, however, DHEA had only a limited impact on NADPH levels in *T. gondii*-infected myoblasts and myotubes.

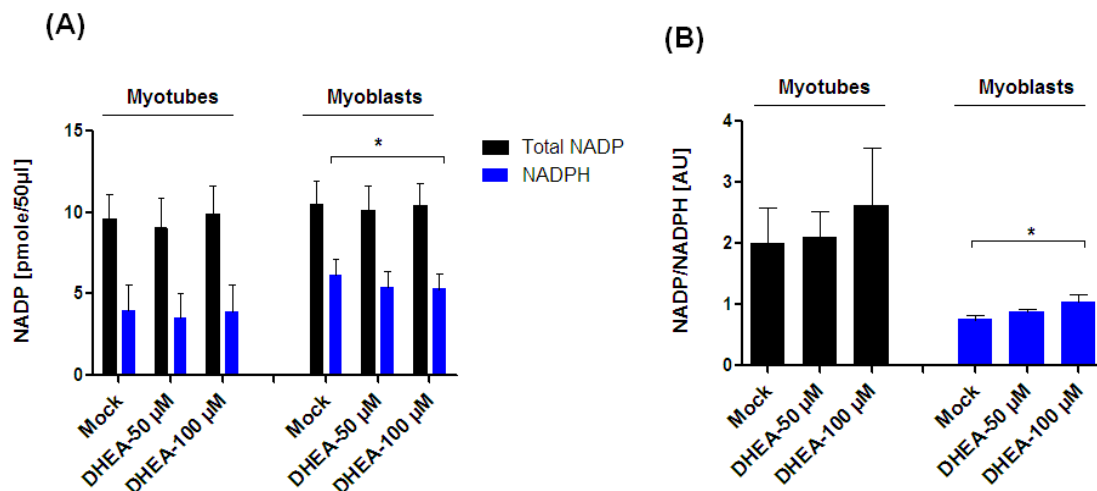


Figure 3.14: NADP⁺/NADPH measurement in *T. gondii*-infected myotubes and myoblasts. C2C12 myoblasts were induced to differentiate into myotubes. Both myotubes and myoblasts were treated with different concentration of DHEA (50 µM and 100 µM) or were mock-treated. Following one hour of treatment, cells were subjected to *T. gondii* infection at a host cell-to-parasite ratio of 1:3.5. After 48 hours of infection, cells were isolated and NADP (total) was extracted using NADP⁺/NADPH extraction buffer. Then samples were filtered through 10 kDa spin filter to deproteinize them in order to avoid consumption of NADPH by the enzymes. The samples were then used for colorimetric measurement of NADP total (NADP⁺ and NADPH) or NADPH at 450 nm using a multilabel plate reader. Levels of total NADP (NADP⁺ and NADPH) and NADPH are shown in (A) and the ratio of NADP⁺ to NADPH in (B). Results are depicted as means ± S.E.M. from four independent experiments. Significant differences were identified by Student's *t*-test (* *p*<0.05).

3.3.5 6-aminonicotinamide induces *T. gondii* bradyzoite differentiation in myoblasts and myotubes

To further validate that the effect of DHEA on *T. gondii* bradyzoite formation in myoblasts and myotubes was due to an inhibition of the PPP, an inhibitor of a second enzyme of the PPP, i.e. 6-aminonicotinamide (6-AN) was used. This inhibitor inhibits the 6-phosphogluconate dehydrogenase (6PGDH) (see Figure 3.12; Lange & Proft 1970) which was also upregulated in myoblasts as compared to myotubes as shown in Figure 3.8C. RT-qPCR was performed with 6-AN-treated *T. gondii*-infected myotubes and myoblasts to determine its impact on *T. gondii* BAG1 expression. Twenty and 100 µM of 6-AN induced BAG1 mRNA expression in *T. gondii* residing in both myotubes and myoblasts as compared to mock-treated controls. Remarkably, by far the highest induction of BAG1 mRNA was observed in myoblasts treated with 100 µM of 6-AN (Figure 3.15A). Thus,

results obtained after inhibition of 6PGDH mirrored those as observed after inhibition of G6PDH. This result further indicated that pharmacologically reducing PPP activity in SkMCs can favor *T. gondii* bradyzoite development particularly in myoblasts, but also myotubes.

As reduced parasite replication is a prerequisite for increased bradyzoite differentiation (Bohne *et al.*, 1994), the impact of 6-AN on parasite replication was determined. To this end, both myotubes and myoblasts were treated with different concentrations of 6-AN or DMSO as the solvent. Then, parasite replication was assessed in inhibitor- and solvent-treated cells by immunolabeling of the parasite and fluorescence confocal microscopy. Results indicated that parasite replication was moderately reduced in myotubes treated with 20 or 100 μM of 6-AN as compared to treatment with the solvent DMSO. In myoblasts which sustained higher parasite replication in mock-treated cells as compared to myotubes (Swierzy and Lüder, 2014), treatment with 20 μM and 100 μM of 6-AN inhibited parasite replication in a dose-dependent manner. Furthermore, 6-AN inhibited parasite replication in myoblasts to a clearly higher extent than in myotubes (Figure 3.15C). The parasitophorous vacuoles were smaller in 6-AN-treated samples compared to mock-treated ones in both myotubes and myoblasts (Figure 3.15B). Inhibiting the PPP in myotubes and particularly in myoblasts by 6-AN thus slows down parasite replication and enhances bradyzoite differentiation.

Next, the impact of 6-AN on *T. gondii* cyst formation was determined as bradyzoite differentiation regularly leads to the formation of a cyst wall surrounding the parasitophorous vacuole. Cyst formation was evaluated in 6-AN-treated or mock-treated myotubes and myoblasts by staining of the cyst wall using *Dolichos biflorus* lectin. Results showed mostly increased numbers of cysts in 6-AN-treated myotubes and myoblasts at 48 and 72 hours of infection as compared to the solvent-treated control (Figure 3.15D).

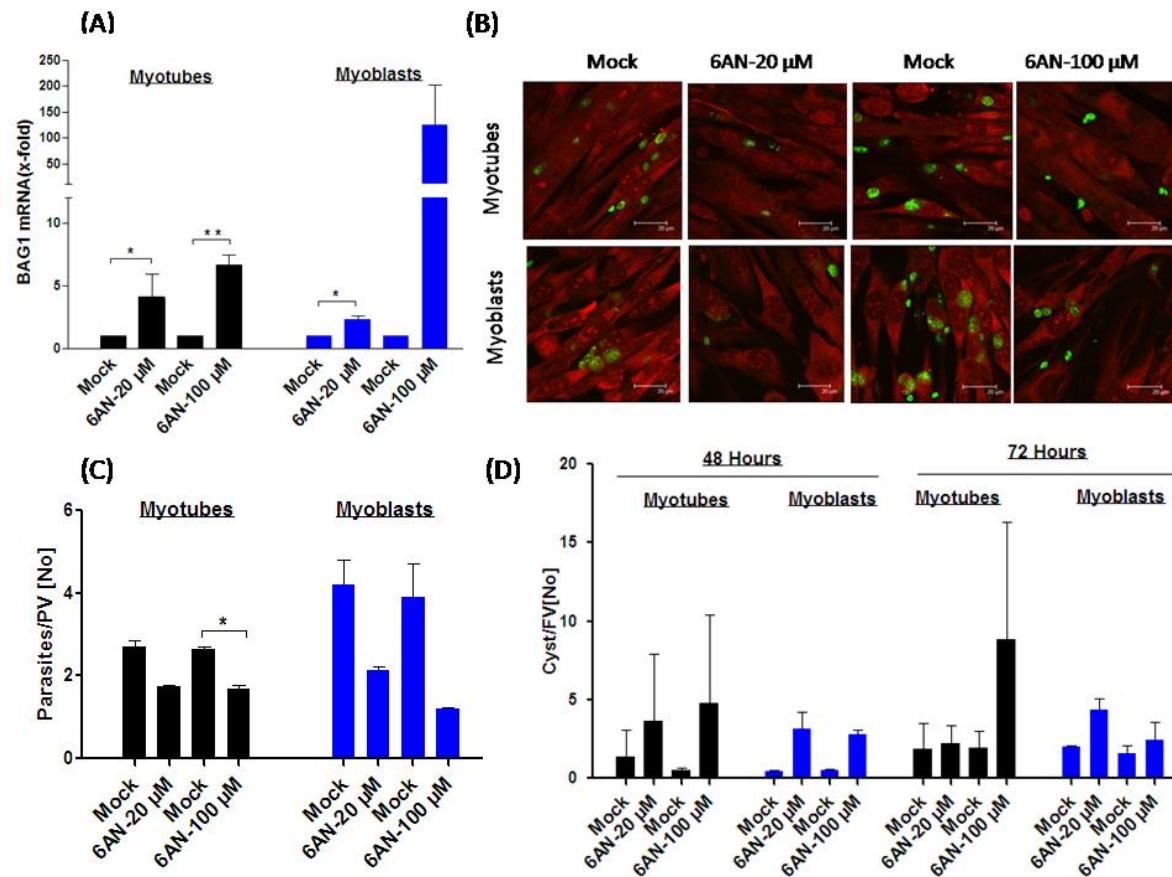


Figure 3.15: 6-aminonicotinamide (6-AN) accelerates *T. gondii* bradyzoite differentiation in myotubes and myoblasts. C2C12 myoblasts were induced to differentiate into myotubes. Both myotubes and myoblasts were treated with 20 μ M and 100 μ M of 6-AN or were mock-treated with DMSO, followed by *T. gondii* infection at a host cell-to-parasite ratio of 1:3.5. **(A)** After 48 hours of infection, total RNA was isolated, mRNA was reverse transcribed, and cDNA was amplified using specific primers for *T. gondii* bradyzoite antigen 1 (BAG1) and *T. gondii* actin (TgActin) by quantitative real-time PCR. The fold increase in BAG1 mRNA between 6-AN-treated cells and mock-treated cells was calculated using the $\Delta\Delta$ CP method and was normalized to TgActin mRNA. Results are depicted as means \pm S.E.M. from three independent experiments. Significant differences were identified by Student's *t*-test (* $p < 0.05$, ** $p < 0.01$). **(B)** Cells were fixed at 48 hours post infection with 4 % paraformaldehyde and parasites were immunolabeled (green fluorescence) using a polyclonal anti-*T. gondii* antiserum. Host cells were visualized using propidium iodide (red fluorescence). Representative images of both labelings were recorded by confocal laser scanning microscopy and were superimposed. **(C)** After cells had been fluorescently labeled as indicated above, the average size of the parasitophorous vacuoles (PVs) in each sample was determined by counting the number of parasites in 100 PVs. Data represent means \pm S.E.M. from two independent experiments. **(D)** Cells were fixed at 48 and 72 hours post infection with 4 % paraformaldehyde. After fixation, tissue cysts of *T. gondii* were labeled with biotin-conjugated *Dolichos biflorus* lectin and Cy2-conjugated streptavidin, parasites were labeled with a polyclonal anti-*T. gondii* antiserum and Cy5-conjugated secondary antibodies and host cells were visualized using propidium iodide. The numbers of cysts were counted in 100 fields of vision (FV). Data represent means \pm S.E.M. from two independent experiments.

3.3.6 Phenyl acetic acid accelerates *T. gondii* BAG1 expression in myotubes but not in myoblasts

Results presented before suggested that the activity of the TCA cycle enzymes were higher in *T. gondii*-infected and non-infected myotubes than in myoblasts (see Figure 3.10C). Furthermore, results suggested that myotubes channel glucose-derived carbohydrates more readily through the pyruvate carboxylase into the TCA cycle than myoblasts (Figure 3.11). Since myotubes and myoblasts differentially sustain bradyzoite formation in *T. gondii*, it was therefore important to unravel the impact of the pyruvate carboxylase on *T. gondii* bradyzoite differentiation in both cell types. Phenyl acetic acid (PAA) was used as an inhibitor of that enzyme (see Figure 3.12; Bahl et al. 1997) which catalyzes the carboxylation of pyruvate to oxaloacetate, an important anaplerotic reaction of the TCA cycle. RT-qPCR was performed using mRNA from *T. gondii*-infected myotubes and myoblasts treated with 1 and 5 mM PAA or mock-treated to see its impact on BAG1 expression. Unexpectedly, results indicated that PAA slightly (~1.5-fold) upregulated BAG1 mRNA expression in myotubes compared to mock. In contrast, PAA did not considerably affect BAG1 mRNA expression in *T. gondii*-infected myoblasts compared to mock with a ~20% reduction in BAG1 mRNA being observed (Figure 3.16A). In order to determine the effect of PAA on parasite replication in myotubes and myoblasts, immunofluorescence staining was performed. To this end, both myotubes and myoblasts were treated with concentrations of PAA as above or with ethanol as the vehicle. After 48 hours of infection, parasite replication was assessed in inhibitor- and solvent-treated samples by immunolabeling of the parasite followed by confocal fluorescence microscopy. Results revealed no clear trend towards an altered parasite replication after PAA treatment with the strongest effect being a decline of parasite replication in myoblasts treated with 5 mM PAA (Figure 3.16C). Representative images of the parasitophorous vacuoles in mock- and PAA-treated myotubes and myoblasts are shown in Figure 3.16B.

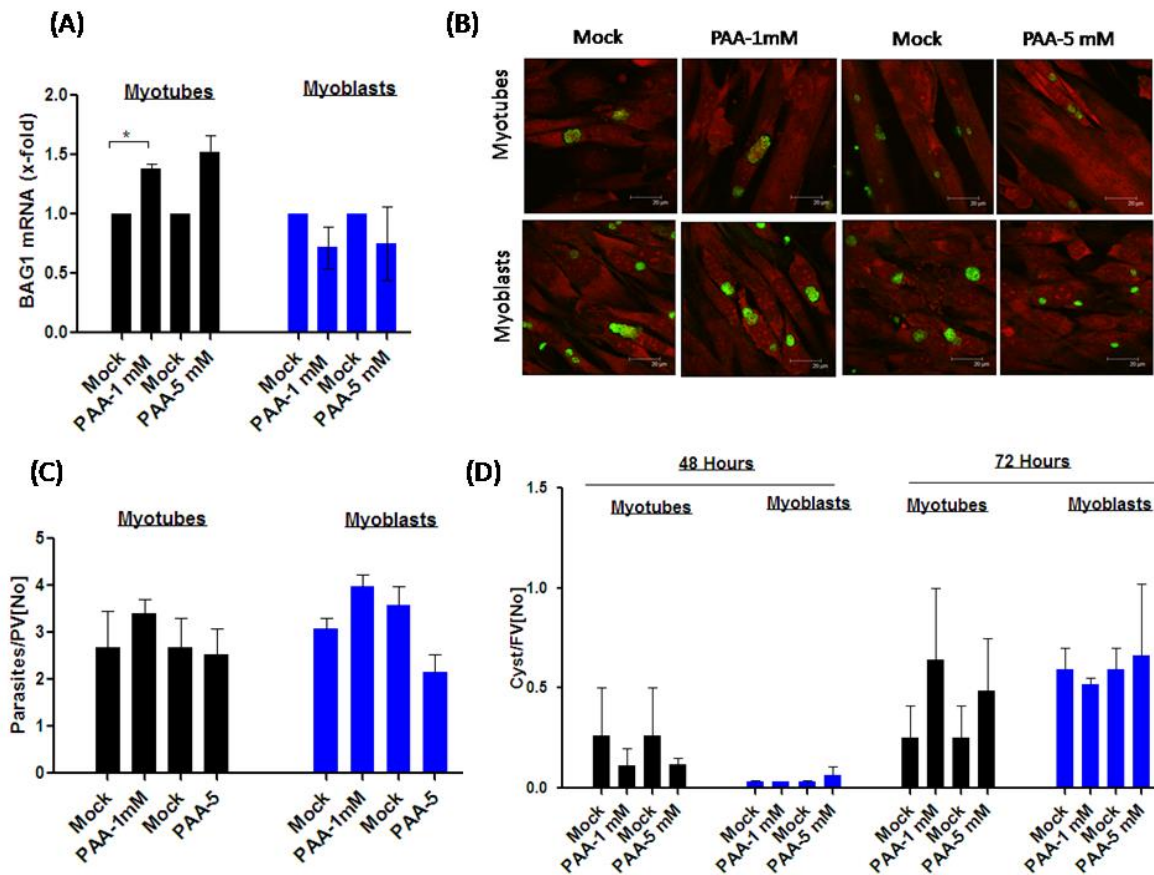


Figure 3.16: Impact of phenyl acetic acid on *T. gondii* BAG1 mRNA expression, parasite replication and cyst formation in myotubes and myoblasts. C2C12 myoblasts were induced to differentiate into myotubes. Both myotubes and myoblasts were treated with 1 mM and 5 mM of PAA or were mock-treated. After one hour of treatment, cells were infected with *T. gondii* at a host cell-to-parasite ratio of 1:3.5. **(A)** At 48 hours post infection, total RNA was isolated, mRNA was reverse transcribed and cDNA was amplified using specific primers for *T. gondii* bradyzoite antigen 1 (BAG1) and *T. gondii* actin (TgActin) by quantitative real-time PCR. The fold increase in BAG1 mRNA between PAA-treated and mock-treated cells was calculated according to the $\Delta\Delta\text{CP}$ method in myotubes and myoblasts and was normalized to TgActin mRNA. Results are depicted as means \pm S.E.M. from three independent experiments. Significant differences were identified by Student's *t*-test (* $p < 0.05$). **(B)** Cells were fixed at 48 hours post infection with 4 % paraformaldehyde and parasites were immunolabeled (green fluorescence) using a polyclonal anti-*T. gondii* antiserum. Host cells were visualized using propidium iodide (red fluorescence). Representative images of both labelings were recorded by confocal laser scanning microscopy and were superimposed. **(C)** After cells had been fluorescently labeled as indicated above, the average size of parasitophorous vacuoles (PVs) in each sample was determined by counting the number of parasites in 100 PVs. Data represent means \pm S.E.M. from two independent experiments. **(D)** Cells were fixed at 48 and 72 hours post infection with 4 % paraformaldehyde. After fixation, tissue cysts of *T. gondii* were labeled with biotin-conjugated *Dolichos biflorus* lectin and Cy2-conjugated streptavidin, parasites were labeled with a polyclonal anti-*T. gondii* antiserum and Cy5-conjugated secondary antibodies and host cells were visualized using propidium iodide. The numbers of cysts were counted in 100 fields of vision (FV). Data represent means \pm S.E.M. from two independent experiments.

In order to determine the impact of PAA on *T. gondii* cyst formation, immunofluorescence and lectin-based staining was performed as described above. Surprisingly, cyst counts were decreased in PAA-treated myotubes after 48 hours of infection whereas increased cyst counts were observed after 72 hours of infection. Cysts formation was not prominently altered in PAA-treated myoblasts after 48 and 72 hours of infection compared to the mock control (Figure 3.16D). Together, these results indicate that inhibition of the pyruvate carboxylase has only a minor and ambiguous impact of *T. gondii* stage differentiation in SkMCs.

3.3.7 Dimethyl- α -ketoglutarate accelerates *T. gondii* BAG1 expression in myoblasts

As another approach to modulate TCA cycle activities in *T. gondii*-infected myotubes and myoblasts and to determine its impact on bradyzoite differentiation, dimethyl- α -ketoglutarate (DMKG) was used to fuel the TCA cycle activities (see Figure 3.12). RT-qPCR was performed on mRNA isolated from cells treated with 5 mM or 10 mM of DMKG or mock-treated. Results revealed no induction of BAG1 mRNA expression in *T. gondii* within myotubes treated with 5 mM DMKG but an increased BAG1 expression in those parasites within myotubes treated with 10 mM DMKG compared to mock. Interestingly, *T. gondii* within myoblasts clearly up-regulated BAG1 expression in both 5 mM and 10 mM DMKG-treated cells and this reached statistical significance after treatment with 10 mM DMKG compared to mock (Figure 3.17A). In order to evaluate the impact of DMKG on parasite replication, immunofluorescence staining was performed. To this end, both myotubes and myoblasts were treated with concentrations of DMKG as above or were mock-treated. Then, parasite replication was assessed in DMKG-treated versus mock-treated samples by immunolabeling of the parasite. Unexpectedly, parasite replication was increased two times in DMKG-treated myotubes compared to the solvent DMSO. In contrast, parasite replication was clearly and dose-dependently reduced in myoblasts treated with increasing amounts of DMKG. Thus, it appeared from these results that fueling the TCA cycle with DMKG enhances parasite replication in myotubes but inhibits replication in myoblasts (Figure 3.17C). Representative images of parasitophorous vacuoles within the different host cells are shown in Figure 3.17B.

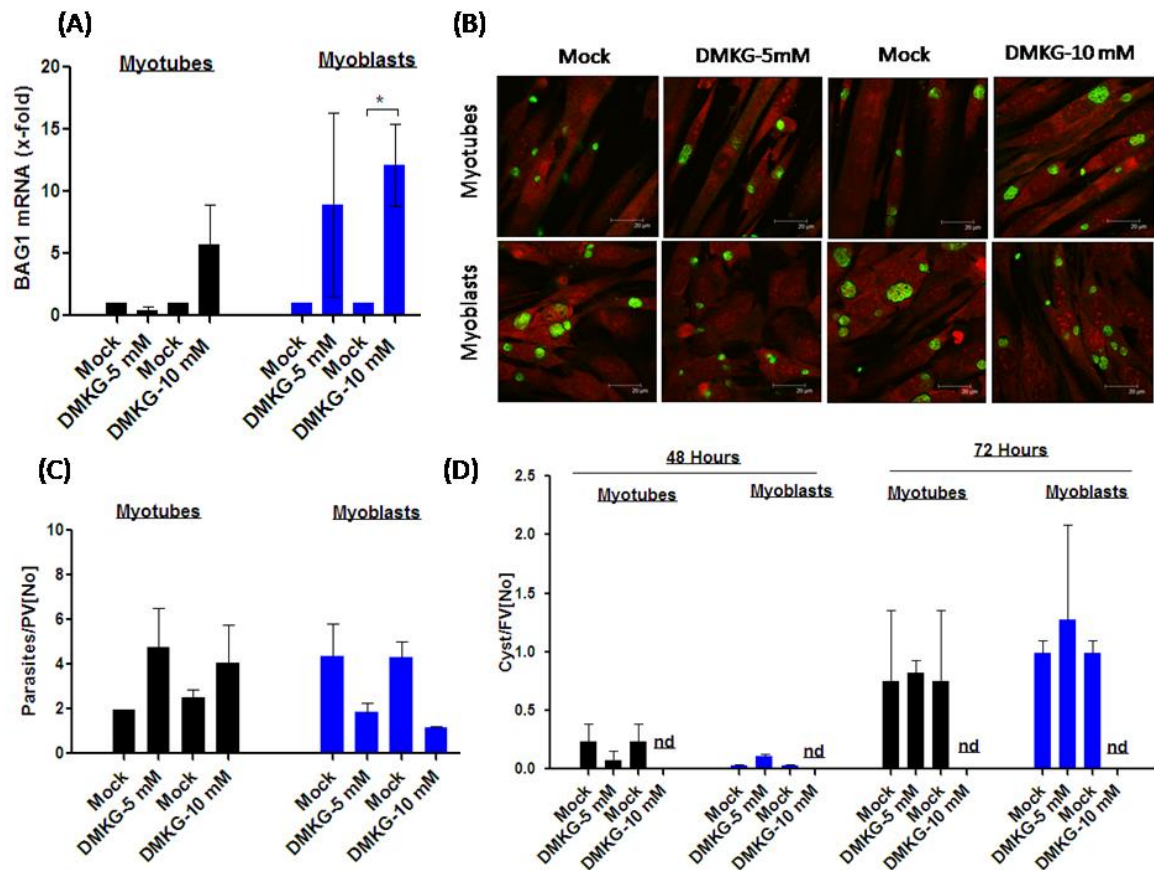


Figure 3.17: Dimethyl- α -ketoglutarate induces *T. gondii* BAG1 expression and reduces parasite replication in myoblasts. C2C12 myoblasts were induced to differentiate into myotubes. Both myotubes and myoblasts were treated with 5 mM and 10 mM of dimethyl- α -ketoglutarate (DMKG) or were DMSO-treated (mock). After 1 hour, cells were infected with *T. gondii* tachyzoites at a host cell-to-parasite ratio of 1:3.5. **(A)** After 48 hours of infection, total RNA was isolated, mRNA was reverse transcribed and cDNA was amplified using specific primers for *T. gondii* bradyzoite antigen 1 (BAG1) and *T. gondii* GAPDH (TgGAPDH) by quantitative real-time PCR. The fold increase in BAG1 mRNA between DMKG-treated and mock-treated cells was calculated using the $\Delta\Delta$ CP method in myotubes and myoblast and was normalized to TgGAPDH mRNA. Results are depicted as means \pm S.E.M. from three independent experiments. Significant differences were identified by Student's *t*-test (* $p < 0.05$). **(B)** Cells were fixed at 48 hours post infection with 4 % paraformaldehyde and parasites were immunolabeled (green fluorescence) using a polyclonal anti-*T. gondii* antiserum. Host cells were visualized using propidium iodide (red fluorescence). Representative images of both labelings were recorded by confocal laser scanning microscopy and were superimposed. **(C)** After cells had been fluorescently labeled as indicated in (B), the average size of parasitophorous vacuoles (PVs) in each sample was determined by counting the number of parasites in 100 PVs. Data represent means \pm S.E.M. from two independent experiments. **(D)** Cells were fixed at 48 and 72 hours post infection with 4 % paraformaldehyde. After fixation, tissue cyst of *T. gondii* were labeled with biotin-conjugated *Dolichos biflorus* lectin and Cy2-conjugated streptavidin, parasites were labeled with a polyclonal anti-*T. gondii* antiserum and Cy5-conjugated secondary antibodies and host cells were visualized using propidium iodide. The number of cysts were counted in 100 fields of vision (FV). Data represent means \pm S.E.M. from two independent experiments.

Finally, *T. gondii* cyst formation was evaluated in DMKG-treated versus DMSO-treated myotubes and myoblasts by staining the cyst wall with *Dolichos biflorus* lectin and the parasite population with a polyclonal antiserum. Data revealed a trend towards a decreased number of cysts in DMKG-treated myotubes compared to DMSO at 48 hours of infection. However, no differences were observed in cyst formation between DMKG-treated and mock-treated myoblasts at 48 hours of infection and in both cell types at 72 hours of infection (Figure 3.17D). Cyst counts could not be determined in cells treated with 10 mM DMKG due to a toxic effect on host cells during prolonged cultivation. Together, these data establish that fueling the TCA cycle in myoblasts with DMKG clearly increases BAG1 expression and reduces parasite replication but does not promote tissue cyst formation.

3.3.8 Sodium-L-lactate induces *T. gondii* BAG1 expression in myoblasts but not in myotubes

Through mass spectrometric analysis, it has been shown that myotubes and myoblasts do not considerably differ in the levels of carbon incorporation into metabolites of glycolysis irrespective of *T. gondii* infection (see Figure 3.10B). However, in a previous study it was shown that upregulation of glycolysis by the addition of glucose or forced expression of host kinase Akt release soluble metabolites including lactate from the cells which can inhibit bradyzoite differentiation in human foreskin fibroblasts (HFF) or Vero cells which are normally permissive for stage conversion under stress conditions (Weilhammer *et al.*, 2012). For this reason, anaerobic glycolysis was modulated here using sodium-L-lactate (see Figure 3.12) to determine its effect on BAG1 expression in *T. gondii* residing in either myotubes or myoblasts. RT-qPCR was performed on mRNA from *T. gondii*-infected myotubes and myoblasts treated with 1 and 3 mM of sodium-L-lactate or mock-treated. Sodium-L-lactate had no impact on BAG1 mRNA expression in myotubes as compared to mock-treated cells. In contrast, sodium-L-lactate-treated myoblasts clearly sustained increased BAG1 mRNA expression in *T. gondii* in a dose-dependent manner as compared to mock controls. However, this increase was not statistically significant due to high variances between individual experiments (Figure 3.18A).

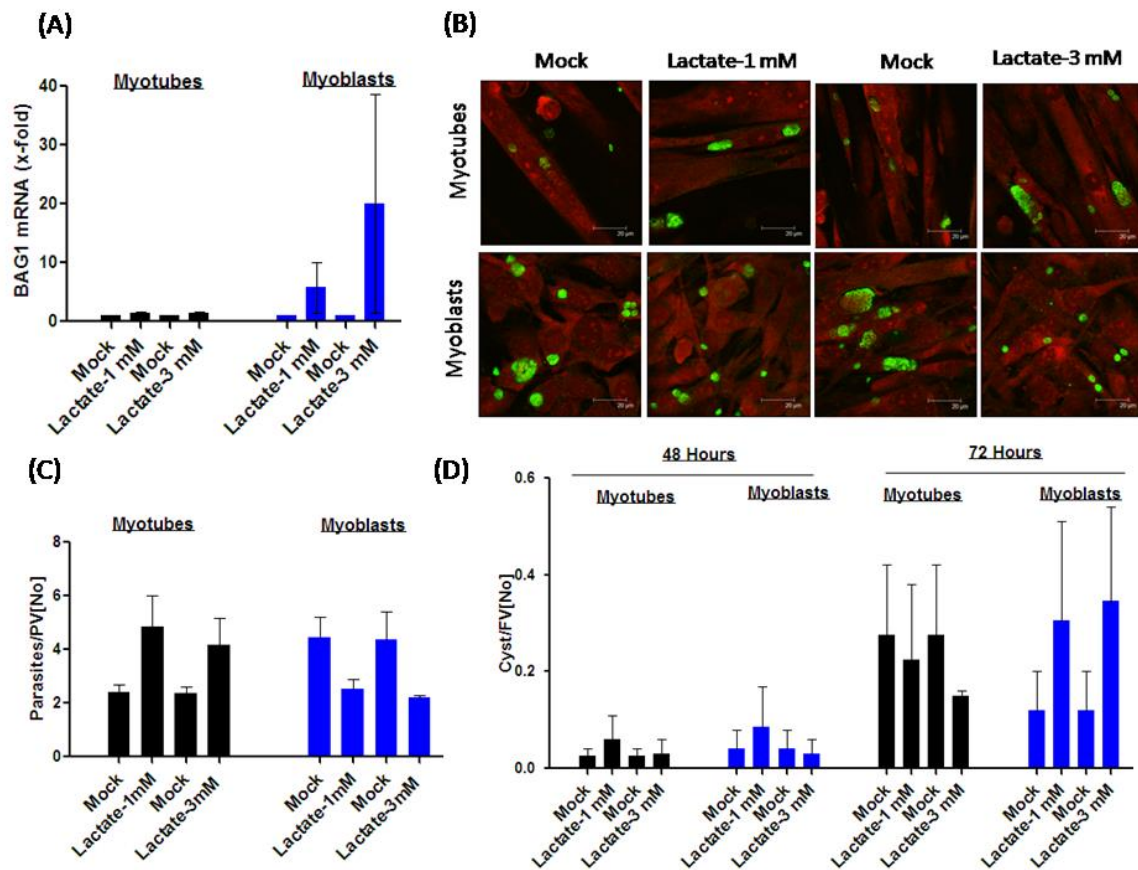


Figure 3.18: Lactate can increase BAG1 expression and cyst formation and can inhibit parasite replication in *T. gondii* within myoblasts but not in myotubes. C2C12 myoblasts were induced to differentiate into myotubes. Both myotubes and myoblasts were treated with 1 mM and 3 mM of sodium-L-lactate or were treated with water as solvent. After 1 hour, cells were then infected with *T. gondii* tachyzoites at a host cell-to-parasite ratio of 1:3.5. **(A)** Total RNA was isolated after 48 hours of infection and mRNA was reverse transcribed to cDNA which was amplified using specific primers for *T. gondii* bradyzoite antigen 1 (BAG1) and *T. gondii* GAPDH (TgGAPDH) as housekeeping gene by quantitative real-time PCR. The fold increase in BAG1 expression between sodium-L-lactate and mock-treated cells was calculated according to the $\Delta\Delta\text{CP}$ method and was normalized to TgGAPDH mRNA. Results were depicted as means \pm S.E.M. from four independent experiments. **(B)** Cells were fixed at 48 hours post infection with 4 % paraformaldehyde and parasites were immunolabeled (green fluorescence) using a polyclonal anti-*T. gondii* antiserum. Host cells were visualized using propidium iodide (red fluorescence). Representative images of both labelings were recorded by confocal laser scanning microscopy and were superimposed. **(C)** After cells had been fluorescently labeled as indicated above, the average size of parasitophorous vacuoles (PVs) in each sample was determined by counting the number of parasites in 100 PVs. Data represent means \pm S.E.M. from two independent experiments. **(D)** Cells were fixed at 48 and 72 hours post infection with 4 % paraformaldehyde. Tissue cysts of *T. gondii* were labeled with biotin-conjugated *Dolichos biflorus* lectin and Cy2-conjugated streptavidin, parasites were labeled with a polyclonal anti-*T. gondii* antiserum and Cy5-conjugated secondary antibodies and host cells were visualized using propidium iodide. The number of cysts was counted in 100 fields of vision (FV). Data represent means \pm S.E.M. from two independent experiments.

In order to determine the impact of sodium-L-lactate on parasite replication in myotubes and myoblasts, immunofluorescence stainings were performed. Results showed that parasite replication was increased in sodium-L-lactate treated myotubes compared to mock controls. Remarkably, the opposite effect was seen in myoblasts where parasite replication was dose-dependently decreased by sodium-L-lactate compared to mock thus being consistent with the increased BAG1 expression in these cells (Figure 3.18C). Immunofluorescence microscopy also indicated that parasitophorous vacuoles were larger in lactate-treated myotubes as compared to mock control whereas they were smaller in lactate-treated myoblasts (Figure 3.18B).

To determine the effect of sodium-L-lactate on *T. gondii* cysts formation in myotubes and myoblasts, staining of the cyst wall surrounding the parasitophorous vacuole was performed. Results showed similar patterns of cyst formation in sodium-L-lactate treated myotubes and myoblasts after 48 hours of infection with slightly higher cyst numbers in both myoblasts and myotubes treated with 1 mM sodium-L-lactate as compared to mock controls. After 72 hours of infection, cyst numbers had increased in myoblasts treated with 1 and 3 mM sodium-L-lactate compared to mock controls, whereas a trend towards lower cyst numbers were observed in sodium-L-lactate-treated myotubes (Figure 3.18D). Together, these results suggest that increased lactate concentrations can accelerate BAG1 mRNA expression and cyst formation in *T. gondii* residing in myoblasts but not myotubes.

3.4 Impact of redox homeostasis on *T. gondii* bradyzoite differentiation in SkMCs

Redox homeostasis is a balance between oxidative and reductive processes in a cell. Oxidative processes include formation of reactive oxygen species (ROS) that are normally produced as a byproduct of metabolic reactions. Reductive processes include formation of cellular antioxidants which are required in a cell for maintenance of redox homeostasis. It was observed that myotubes and myoblasts differ in glucose metabolic pathways as for instance myotubes had lower PPP activities than myoblasts (Figure 3.10A). Hence, myotubes may contain lower levels of NADPH which might lead to differences in redox potential in myotubes and myoblasts. The redox potential might also have a role in *T. gondii* bradyzoite differentiation in myotubes. Previously, it was shown that host cell-mediated ROS production suppresses *T. gondii* replication in human retinal pigment epithelial cell (ARPE-19). Subsequently, modulation of ROS level using siRNA knockdown of host NADPH oxidase-4 (NOX-4) therefore increased parasite replication (Zhou *et al.*, 2013). Hence, it was hypothesized that cellular ROS may play a role in parasite replication and *T. gondii* bradyzoite differentiation in myotubes.

3.4.1 Myotubes produce lower NADPH levels and higher ratio of NADP⁺/NADPH than myoblasts

As hypothesized above reduced activities of PPP enzymes in *T. gondii*-infected myotubes may lead to the formation of lower NADPH levels in these cells. The levels of NADPH and total NADP (NADP⁺ and NADPH) were measured colorimetrically in myotubes and myoblasts using a NADP⁺/NADPH quantification kit. Both myotubes and myoblasts were infected with *T. gondii* or were left non-infected and cells were extracted for isolation and measurement of total NADP and NADPH. As already indicated in 3.3.4, infected myotubes and myoblasts did not differ in total NADP concentrations (i.e. NADP⁺ and NADPH) and the same also applied to non-infected SkMCs. However, NADPH concentrations were clearly lower in both infected and non-infected myotubes as compared to myoblasts being in agreement with their decreased PPP activities (Figure 3.19A). Importantly, the ratio of NADP⁺ to NADPH was consequently two fold higher in both non-infected and *T. gondii*-infected myotubes than in myoblasts (Figure 3.19B). Thus, the

differences in the PPP as observed between myotubes and myoblasts resulted in significant differences in the levels of reducing equivalents in both cell types irrespective of infection.

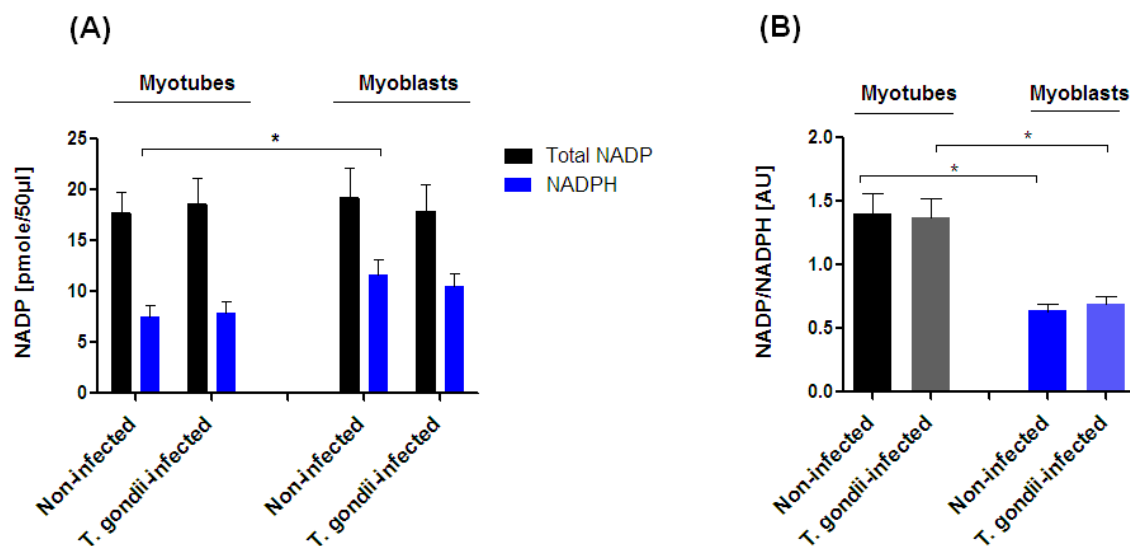


Figure 3.19: Myotubes produce reduced levels of NADPH as compared to myoblasts and have a higher NADP⁺/NADPH ratio. C2C12 myoblasts were induced to differentiate into myotubes. Both myotubes and myoblasts were infected with *T. gondii* tachyzoites at a host cell-to-parasite ratio of 1:3.5. After 48 hours of infection, cells were isolated and total NADP (i.e. NADP⁺ and NADPH) was extracted using NADP/NADPH extraction buffer. Then, samples were filtered through 10 kDa spin filters to deproteinize them in order to avoid consumption of NADPH by the enzymes. The samples along with standard NADPH were then used for colorimetric measurement of NADP total (NADP⁺ and NADPH) or NADPH at 450 nm using a multilabel plate reader. **(A)** Concentrations of total NADP (i.e. NADP⁺ and NADPH) and NADPH only were measured in samples by comparing with the absorbance of standard concentrations of NADPH. **(B)** Ratio of NADP⁺/NADPH was calculated from the concentration of NADP⁺ (i.e. total NADP minus NADPH) and NADPH only. Results are depicted as means \pm S.E.M. from four independent experiments. Significant differences were identified by Student's *t*-test (* $p < 0.05$).

3.4.2 CellROX staining indicates higher ROS levels in *T. gondii*-infected myoblasts than in myotubes

Higher NADP⁺/NADPH levels in *T. gondii*-infected and non-infected myotubes (see Figure 3.19) due to decreased PPP activities (see Figure 3.10A) might favor *T. gondii* bradyzoite formation due to increased oxidative stress in these cells (Kuehne *et al.*, 2015). I therefore wondered whether reduced levels of NADPH as observed in myotubes compared to myoblasts have any impact on the levels of reactive oxygen species (ROS) in myotubes.

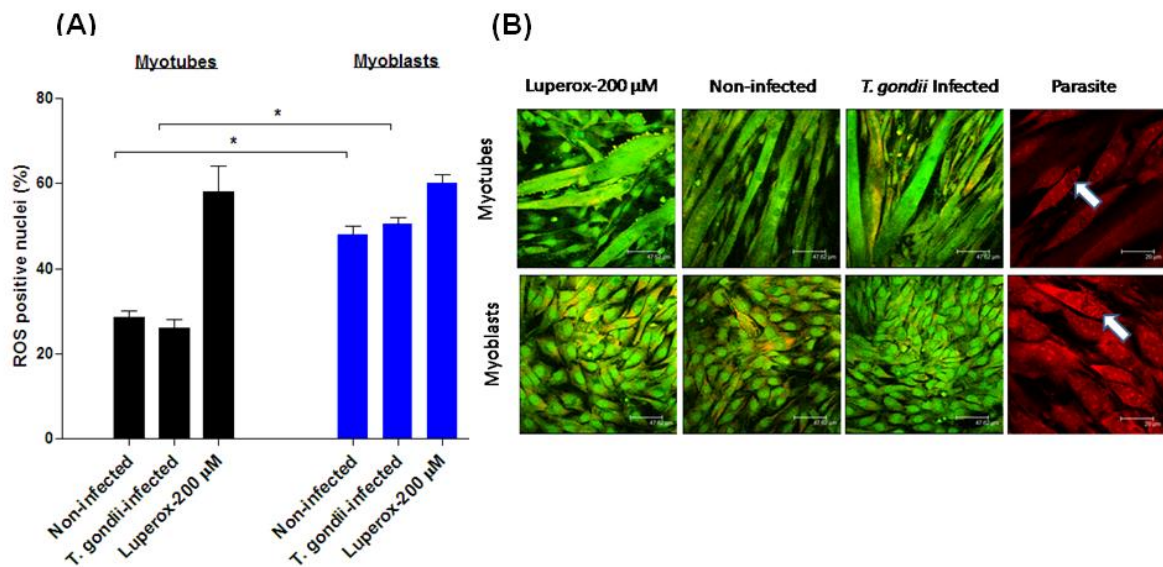


Figure 3.20: ROS staining in *T. gondii*-infected and non-infected myotubes and myoblasts. C2C12 myoblasts were induced to differentiate into myotubes. Both myotubes and myoblasts were infected with *T. gondii* tachyzoites at a host cell-to-parasite ratio of 1:3.5. After 48 hours of infection, non-infected cells were partially treated with the oxidant luperox at 200 μM for 60 minutes. Infected and non-infected cells were then stained with 5 μM CellROX green for 30 minutes. **(A)** After fixation with 4% paraformaldehyde for 15 minutes, cells were stained with propidium iodide (red fluorescence) and ROS-positive nuclei (green) per 200 nuclei were counted. Data are shown as mean percentages ± S.E.M. from three independent experiments. Significant differences were identified by Student's *t*-test (* $p < 0.05$). **(B)** Representative images of both labelings were recorded by confocal laser scanning microscopy and were superimposed. To identify parasite-positive cells (marked by arrows) images of the propidium iodide staining alone are also depicted.

To address this question, CellROX green staining was used to stain intracellular ROS in both non-infected and *T. gondii*-infected myotubes and myoblasts. CellROX green is a DNA dye that binds to the DNA primarily in the nucleus and mitochondria upon oxidation and thereby produces a green fluorescence predominantly within nuclei but also the cytoplasm. Results showed less than 30% ROS-positive nuclei in myotubes whereas up to 55% of the nuclei were ROS-positive in myoblasts. Percentages of ROS-positive nuclei differed between myoblasts and myotubes irrespective of whether cells had been infected with *T. gondii* or not (Figure 3.20A). Thus, ROS levels appeared higher in myoblasts than in myotubes despite increased NADPH in these cells. Luperox (tert-butyl-hydroperoxide) at 200 μM was used as a potent oxidant that led to ~60% ROS-positive nuclei in both cell types (Figure 3.20A). Representative images of Luperox-treated, non-infected and *T. gondii*-infected myoblasts and myotubes are shown in Figure 3.20B. Infected cells were identified by staining of parasite nuclei with propidium iodide (indicated by arrows in Figure 3.20B) although their identification was hampered by the concomitant staining of

the host cell. Together, this result suggests that reduced levels of ROS are present in myotubes as compared to myoblasts. Hence, it was important to determine whether this low level of intracellular ROS in myotubes may play role in *T. gondii* bradyzoite differentiation.

3.4.3 Modulation of ROS in SkMCs using antioxidants and its impact on *T. gondii* bradyzoite differentiation

Antioxidants are compounds that can detoxify free oxygen radicals and thereby protect against ROS in cells including SkMCs (Sriram *et al.*, 2011). I therefore aimed to modulate ROS levels in SkMCs in order to determine its putative impact on *T. gondii* bradyzoite differentiation in myotubes and myoblasts.

3.4.3.1 N-acetyl cysteine inhibits *T. gondii* bradyzoite differentiation in myotubes and myoblasts

Results presented above indicated ROS production in both myotubes and myoblasts irrespective of *T. gondii* infection but the level of ROS was lower in myotubes as compared to myoblasts (see Figure 3.20). Therefore, it was speculated that the lower level of endogenous ROS as observed in myotubes might provide an appropriate signal to the parasite for stage conversion. To further confirm a putative effect of intracellular ROS on *T. gondii* stage differentiation, ROS levels were modulated through scavenging by using a well known antioxidant, N-acetyl cysteine (NAC). NAC reduces intracellular ROS levels either by neutralizing hydroxyl radicals ($\bullet\text{OH}$) or by providing intracellular reduced glutathione (Aruoma *et al.*, 1989; Lasram *et al.*, 2015). To this end, RT-qPCR was performed with mRNA from NAC- or solvent-treated *T. gondii*-infected myotubes and myoblasts to examine BAG1 mRNA expression. Results showed that BAG1 mRNA expression was significantly reduced in both myotubes and myoblasts treated with 5 and 10 mM NAC as compared to mock-treated cells. Interestingly, a particularly strong reduction of BAG1 mRNA expression was observed in *T. gondii* residing in NAC-treated myoblasts as compared to the mock control (Figure 3.21A).

In order to determine the effect of NAC on parasite replication, immunofluorescence staining was performed in NAC- and solvent-treated, *T. gondii* infected myotubes and myoblasts after 48 hours of infection. Results showed that NAC (5 mM and 10 mM) strongly induced (3-fold) parasite replication in myotubes compared to mock treated cells. However, statistically significant increase of parasite growth was also observed in NAC-treated myoblasts compared to mock-treated but the induction of parasite replication was not as strong as seen in case of myotubes (Figure 3.21C). The microscopic images (Figure 3.21B) confirmed that the sizes of the parasitophorous vacuoles increased in myotubes and myoblasts that had been treated with 5 mM and 10 mM NAC compared to mock-treated cells.

Finally, the impact of NAC on *T. gondii* tissue cyst formation was evaluated after staining of the cyst wall with *Dolichos biflorus* lectin. Cyst formation was significantly inhibited in myotubes treated with 5 to 10 mM NAC compared to the mock controls at both after 48 and 72 hours of infection (Figure 3.21D). In myoblasts, however, there was no effect of NAC on cysts formation after 48 hours of infection and only a slightly reduced cysts formation was observed in NAC-treated samples compared to mock after 72 hours of infection (Figure 3.21D). Above results indicated that ROS scavenging in myotubes and myoblasts using antioxidant NAC inhibits *T. gondii* BAG1 expression in both myoblasts and myotubes but inhibits tissue cyst formation in myotubes only.

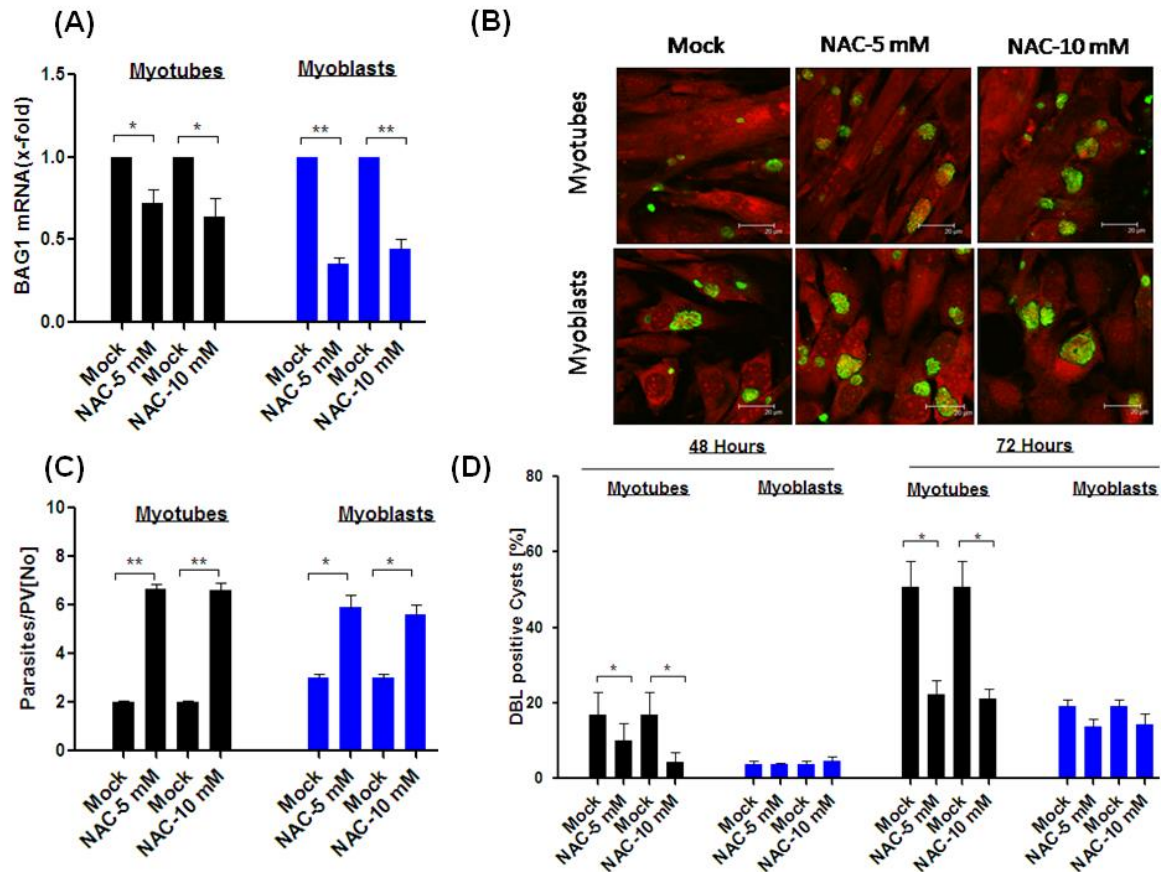


Figure 3.21: N-Acetyl cysteine inhibits *T. gondii* bradyzoite differentiation in myotubes and myoblasts but tissue cyst formation in myotubes only. C2C12 myoblasts were induced to differentiate into myotubes. Both myotubes and myoblasts were treated with 5 mM and 10 mM NAC or were mock-treated. After one hour, cells were infected with *T. gondii* tachyzoites at a host cell-to-parasite ratio of 1:3.5. (A) Total RNA was isolated at 48 hours post infection and mRNA was reverse transcribed to cDNA which was amplified using specific primers for *T. gondii* bradyzoite antigen 1 (BAG1) and *T. gondii* actin (TgActin) by quantitative real-time PCR. The fold increase in BAG1 mRNA between NAC-treated and mock-treated cells was calculated using the $\Delta\Delta\text{CP}$ method and was normalized to TgActin mRNA. Results are depicted as means \pm S.E.M. from five independent experiments. Significant differences were identified by Students *t*-test (* $p < 0.05$ and ** $p < 0.01$). (B) Cells were fixed at 48 hours post infection with 4 % paraformaldehyde and parasites were immunolabeled (green fluorescence) using a polyclonal *anti-T. gondii* antiserum. Host cells were visualized using propidium iodide (red fluorescence). Representative images of both labelings were recorded by confocal laser scanning microscopy and were superimposed. (C) After cells had been fluorescently labeled as described in (B), the average size of parasitophorous vacuoles (PVs) in each sample was determined by counting the number of parasites in 100 PVs. Data represent means \pm S.E.M. from three independent experiments. Significant differences were identified by Students *t*-test (* $p < 0.05$, ** $p < 0.01$). (D) Cells were fixed at 48 and 72 hours post infection with 4 % paraformaldehyde. After fixation, tissue cysts of *T. gondii* were labeled with biotin-conjugated *Dolichos biflorus* lectin and Cy2-conjugated streptavidin, parasites were labeled with a polyclonal *anti-T. gondii* antiserum and Cy5-conjugated secondary antibodies and host cells were visualized using propidium iodide. The numbers of DBL-positive cysts were counted in 100 parasitophorous vacuoles (PV) and were expressed as percentages. Data represent means \pm S.E.M. from three independent experiments. Significant differences were identified by Students *t*-test (* $p < 0.05$).

3.4.3.2 Tiron induces *T. gondii* BAG1 mRNA expression but not cyst formation in myotubes and myoblasts

Tiron is another antioxidant that can scavenge ROS (Taiwo, 2008). In this study, tiron was used to scavenge intracellular ROS in myotubes and myoblasts and to evaluate its effect on *T. gondii* bradyzoite differentiation in order to validate the effect of NAC (see Figure 3.21). RT-qPCR was performed with myoblasts and myotubes treated with tiron or solvent and infected with *T. gondii*. Results showed that tiron significantly and dose-dependently upregulated BAG1 mRNA expression in *T. gondii* within myotubes compared to mock. When *T. gondii* resided in myoblasts, tiron also induced BAG1 mRNA expression compared to mock controls but this did not reach statistical significance due to considerable variance between experiments (Figure 3.22A). However, the effect of tiron on BAG1 mRNA expression was clearly not consistent with the results obtained after NAC-treatment.

Next, the impact of tiron on parasite replication in myoblasts and myotubes was analysed. To this end, immunofluorescence staining was performed with tiron- or solvent-treated myotubes and myoblasts 48 hours after infection. Parasite replication was inhibited in myotubes and particularly in myoblasts after treatment with tiron compared to mock-treated cells. It has to be stressed however, that parasite replication was completely blocked in myotubes and myoblasts treated with tiron at 3 mM and 5 mM (Figure 3.22C). It can thus not be ruled out that tiron had a direct and adverse effect on the parasite that might have caused induction of BAG1 mRNA expression in *T. gondii* within both cell types. Representative microscopic images confirmed that parasitophorous vacuoles contained only very few or single parasites after treatment of myoblasts and myotubes with 1 to 5 mM tiron (Figure 3.22B). Finally, the effect of tiron on *T. gondii* cysts formation was determined. To this end, immunofluorescence and lectin-based staining of parasites and the cyst wall, respectively, was performed with tiron- (1 mM, 3 mM and 5 mM) or solvent-treated myoblasts and myotubes after infection with *T. gondii*. Despite induction of BAG1 expression and inhibition of replication, tiron clearly and dose-dependently inhibited *T. gondii* cyst formation in myotubes and myoblasts after 48 and 72 hours of infection (Figure 3.22D). The reduction of cyst numbers was particularly evident in myotubes and myoblasts at 72 hours of infection where high cyst numbers were present in mock-treated myotubes and to a lesser extent also in mock-treated myoblasts.

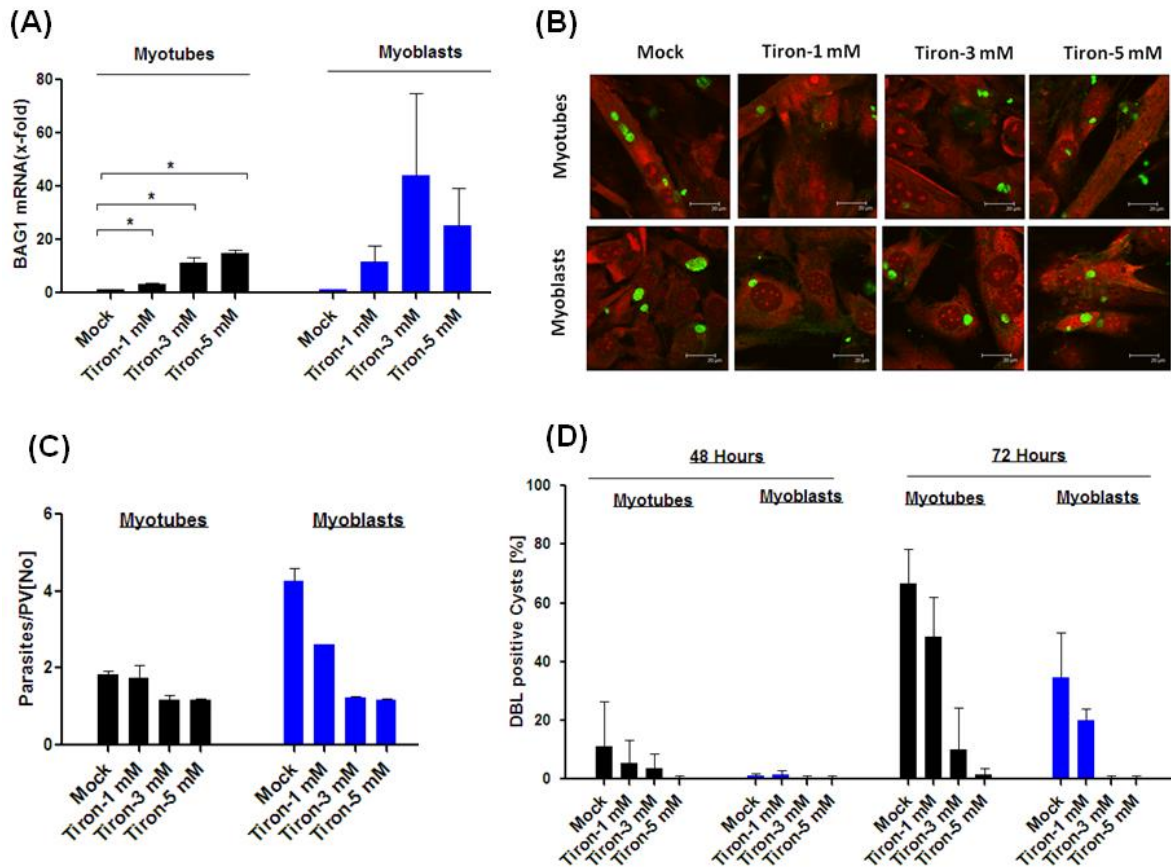


Figure 3.22: Tiron induces *T. gondii* BAG1 mRNA expression in myotubes and myoblasts but does not induce cyst formation. C2C12 myoblasts were induced to differentiate into myotubes. Both myotubes and myoblasts were treated with 1 mM, 3 mM and 5 mM of tiron or were mock-treated. After one hour, cells were infected with *T. gondii* tachyzoites at a host cell-to-parasite ratio of 1:3.5. **(A)** At 48 hours post infection, total RNA was isolated, mRNA was reverse transcribed and cDNA was amplified using specific primers for *T. gondii* bradyzoite antigen 1 (BAG1) and *T. gondii* actin (TgActin) by quantitative real-time PCR. The fold increase in BAG1 mRNA between tiron-treated and mock-treated cells was calculated by the $\Delta\Delta\text{CP}$ method and was normalized to TgActin mRNA. Results are depicted as means \pm S.E.M. from three independent experiments. Significant differences were identified by Students *t*-test (* $p < 0.05$). **(B)** Cells were fixed at 48 hours post infection with 4 % paraformaldehyde and parasites were immunolabeled using a polyclonal anti-*T. gondii* antiserum (green fluorescence). Host cells were visualized using propidium iodide (red fluorescence). Representative images of both labelings were recorded by confocal laser scanning microscopy and were superimposed. **(C)** After cells had been fluorescently labeled as described in (B), the average size of parasitophorous vacuoles (PVs) in each sample was determined by counting the number of parasites in 100 PVs. Data represent means \pm S.E.M. from two independent experiments. **(D)** Cells were fixed at 48 and 72 hours post infection with 4 % paraformaldehyde. After fixation, tissue cysts of *T. gondii* were labeled with biotin-conjugated *Dolichos biflorus* lectin and Cy2-conjugated streptavidin, parasites were labeled with a polyclonal anti-*T. gondii* antiserum and Cy5-conjugated secondary antibodies and host cells were visualized using propidium iodide. The number of DBL-positive cysts were counted in 100 parasitophorous vacuoles (PV) and were expressed as percentage of total PVs. Data represent means \pm S.E.M. from two independent experiments.

3.4.3.3 Tiron inhibits host cell proliferation

As Tiron possibly had a direct adverse effect on the parasite and thereby blocked parasite replication, I also tested its impact on the host cell, particularly on host cell proliferation. To this end, a BrdU incorporation assay which can visualize newly synthesized DNA was performed with myotubes and myoblasts treated with tiron or solvent as control. Results confirmed high levels of DNA synthesis in mock-treated myoblasts as sign of active proliferation whereas myotubes exhibited strongly reduced proliferation as expected. Importantly, tiron at 1 mM already strongly inhibited active SkMC proliferation as observed in mock-treated myoblasts (Figure 3.23A). As myotubes were already largely cell cycle arrested, the effect of tiron was less evident in these cells. Representative microscopic images confirmed high levels of proliferation in mock-treated myoblasts but not myotubes which was completely inhibited after tiron treatment (Figure 3.23B). This result indicated that tiron, beside its function as an antioxidant also strongly inhibited myoblast proliferation thereby possibly contributing to increased BAG1 expression in *T. gondii* residing in these cells.

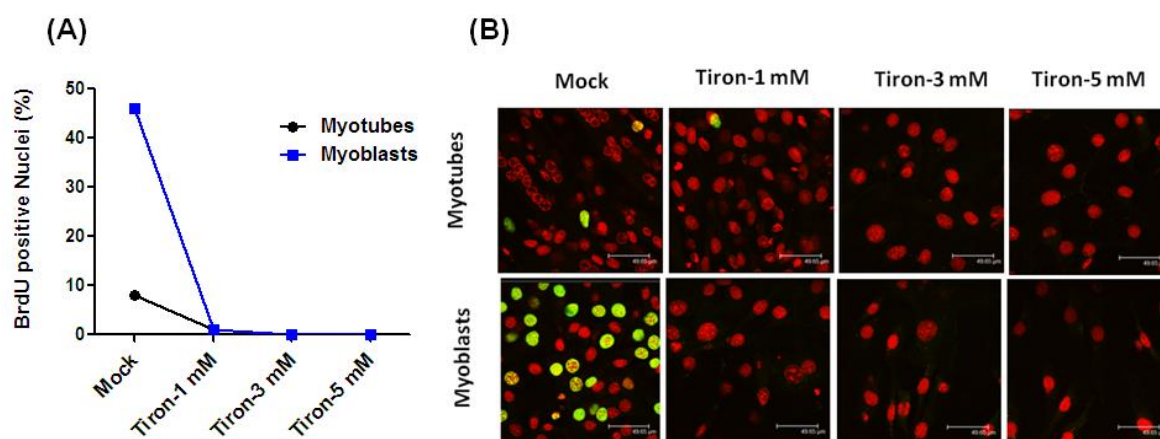


Figure 3.23: Tiron inhibits DNA synthesis and proliferation of SkMCs. C2C12 myoblasts were induced to differentiate into poly-nucleated myotubes. Both myotubes and myoblasts were treated with 1 mM, 3 mM and 5 mM of tiron or were mock-treated. Cells were treated with BrdU (10 μ g/ml) for 2 hours before fixation at 48 hours post infection. After fixation, proliferating cells were immunolabeled with antibodies recognizing BrdU followed by fluorescently labeled secondary antibodies (green fluorescence) and the total cell population was labeled with propidium iodide (red fluorescence). (A) The percentages of BrdU-labeled nuclei in tiron- and mock-treated myotubes and myoblasts were calculated by counting the number of BrdU-positive nuclei as compared to the number of total nuclei. Data represent percentages of BrdU-positive nuclei from one experiment. (B) Representative images of both labelings were recorded by confocal laser scanning microscopy and were superimposed.

3.4.4 N-acetyl cysteine induces extracellular *T. gondii* BAG1 mRNA expression

N-acetyl cysteine was found to inhibit *T. gondii* bradyzoite differentiation in infected myotubes and myoblasts (see Figure 3.21). In order to evaluate whether NAC had any direct effect on *T. gondii* thereby inhibiting stage conversion, its effect on extracellular parasite in the absence of host cells was determined. RT-qPCR was performed with NAC- or solvent-treated isolated *T. gondii* tachyzoites to quantify their BAG1 mRNA expression. Unexpectedly, results showed that NAC-treatment when compared to mock even induced BAG1 mRNA expression in the parasite in a dose-dependent fashion. This indicated an opposite effect of NAC when extracellular parasites were treated with NAC as compared to those treated intracellularly (Figure 3.24). From this data it can be concluded that NAC does not directly inhibit *T. gondii* stage conversion in infected myotubes and myoblasts but rather exerts its effect through modulation of the host cells.

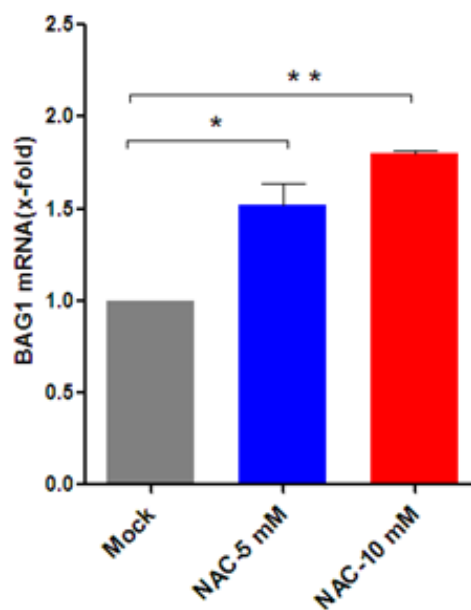


Figure 3.24: N-acetyl cysteine induces BAG1 mRNA expression in extracellular parasites. *T. gondii* tachyzoites were cultivated in the absence of host cells in C2C12 growth medium. Parasites were treated with 5 mM and 10 mM NAC or were mock-treated. Total RNA was isolated after 48 hours of adding NAC and mRNA was reverse transcribed into cDNA which was amplified using specific primers for *T. gondii* bradyzoite antigen 1 (BAG1) and *T. gondii* actin (TgActin) by quantitative real-time PCR. The increase in BAG1 mRNA was calculated between NAC-treated and mock-treated samples using the $\Delta\Delta\text{CP}$ method and was normalized to TgActin mRNA. Results are depicted as means \pm S.E.M. from three independent experiments. Significant differences were identified by Students *t*-test (* $p < 0.05$, ** $p < 0.01$).

3.4.5 Modulation of ROS in SkMCs using ROS inducer and its impact on *T. gondii* bradyzoite differentiation

It was shown above that scavenging endogenous ROS by NAC inhibits *T. gondii* bradyzoite differentiation in myotubes and myoblasts (Figure 3.21). Therefore, I wondered whether exogenous ROS can accelerate bradyzoite differentiation in *T. gondii* in SkMCs.

3.4.5.1 Luperox accelerates *T. gondii* BAG1 expression in myotubes and myoblasts

In order to accelerate ROS levels in myotubes and myoblasts, a well known ROS inducing agent, namely luperox (tert-butyl hydroperoxide) was used (Kučera *et al.*, 2014). To this end, both myotubes and myoblasts were treated with increasing concentrations of luperox in the presence or absence of 10 mM of the antioxidant NAC or were mock-treated and then infected with *T. gondii*. RT-qPCR was performed to examine upregulation of BAG1 mRNA by the parasite. Luperox clearly induces BAG1 mRNA in *T. gondii* within both myotubes and myoblasts in a concentration-dependent manner compared to the mock-treated controls. However, up-regulation of BAG1 mRNA as induced by luperox in myotubes was reduced by concomitant treatment with NAC. Unfortunately, BAG1 expression could not be determined in myoblasts treated with both luperox and NAC due to a toxic effect of NAC at 10 mM on these cells (Figure 3.25A). In order to determine the effect of luperox and NAC on parasite replication, immunofluorescence staining was performed. Parasites were immunolabeled with anti-*Toxoplasma* antibodies and parasite growth was evaluated by confocal microscopy. Results showed that parasite replication was inhibited in luperox-treated myoblasts whereas it was not clearly inhibited in luperox-treated myotubes as compared to mock control. Concomitant treatment with luperox and 10 mM NAC strongly accelerated parasite replication in myotubes to levels that were even higher than in mock-treated cells. In contrast, parasite replication was not induced by NAC-treatment of myoblasts due to its toxic effect on these cells (Figure 3.25C). The parasitophorous vacuoles were similarly small in luperox-treated and mock-treated myotubes but were clearly enlarged in myotubes treated with both luperox and NAC. However, vacuoles were of similar size in myoblasts treated with luperox with or without NAC (Figure 3.25B).

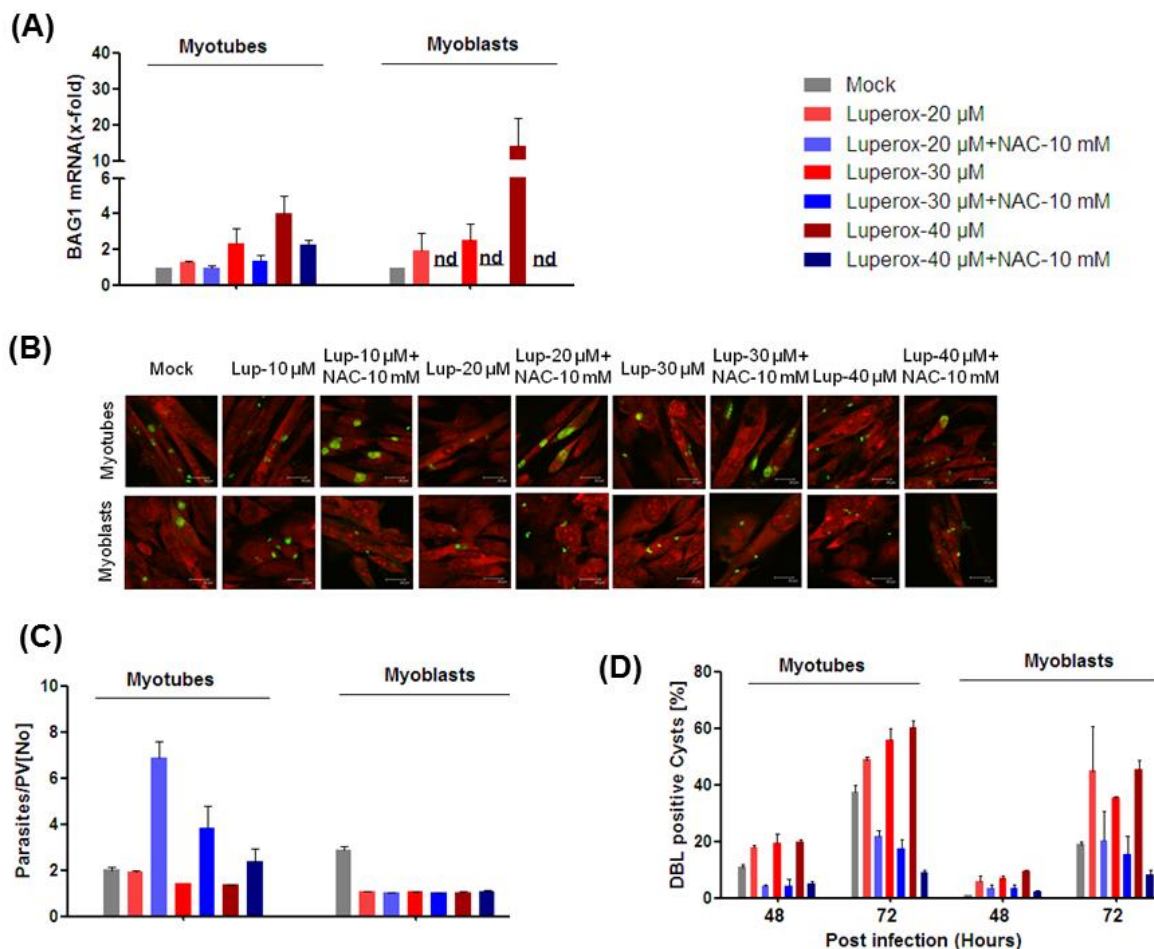


Figure 3.25: Luperox induces bradyzoite differentiation in myotubes and myoblasts. C2C12 myoblasts were induced to differentiate into myotubes. Both myotubes and myoblasts were treated with 20 μ M, 30 μ M or 40 μ M luperox (lup) in the presence or absence of 10 mM NAC, or also were mock-treated. After one hour, cells were then infected with *T. gondii* tachyzoites at a host cell-to-parasite ratio of 1:3.5. **(A)** Total RNA was isolated after 48 hours post infection and was reverse transcribed into cDNA which was amplified using specific primers for *T. gondii* bradyzoite antigen 1 (BAG1) and *T. gondii* actin (TgActin) by quantitative real-time PCR. The fold increase in BAG1 mRNA was calculated between luperox-treated and mock-treated myotubes and myoblasts using the $\Delta\Delta$ CP method and was normalized to TgActin mRNA. Results are depicted as means \pm S.E.M. from three independent experiments. **(B)** Cells were fixed at 48 hours post infection with 4 % paraformaldehyde and parasites were immunolabeled using a polyclonal *anti-T. gondii* antiserum (green fluorescence). Host cells were visualized using propidium iodide (red fluorescence). Representative images of both labelings were recorded by confocal laser scanning microscopy and were superimposed. **(C)** After cells had been fluorescently labeled as indicated above, the average size of parasitophorous vacuoles (PVs) in each sample was determined by counting the number of parasites in 100 PVs. Data represent means \pm S.E.M. from two independent experiments. **(D)** Cells were fixed at 48 and 72 hours post infection with 4 % paraformaldehyde. After fixation, tissue cyst of *T. gondii* were labeled with biotin-conjugated *Dolichos biflorus* lectin and Cy2-conjugated streptavidin, parasites were labeled with a polyclonal *anti-T. gondii* antiserum and Cy5-conjugated secondary antibodies and host cells were visualized using propidium iodide. The numbers of DBL-positive cysts were counted among 100 parasitophorous vacuoles (PV) and were expressed as percentages. Data represent means \pm S.E.M. from two independent experiments.

The impact of luperox alone or in combination with NAC on *T. gondii* cysts formation was then tested in myotubes and myoblasts. Immuno- and lectin-based fluorescence staining of *T. gondii* tissue cysts was achieved by using polyclonal anti-*T.gondii* antibodies and *Dolichos biflorus* lectin, respectively. Data showed higher numbers of DBL-positive cysts in luperox-treated myotubes as compared to mock-treated cells after 48 and 72 hours of infection but luperox-induced cyst formation was abrogated by concomitant treatment with NAC. On the other hand, cysts formation was also increased in luperox-treated myoblasts compared to mock after 48 and 72 hours of infection although cyst counts were very low at 48 hours post infection in these cells (Figure 3.25D). Again, NAC inhibited luperox-induced cyst formation. These results suggest that luperox can induce ROS concentrations in myotubes and myoblasts that are appropriate for accelerating *T. gondii* bradyzoite differentiation.

3.4.5.2 H₂O₂ induces BAG1 mRNA expression in myotubes and myoblasts

To further confirm that exogenous oxidants can accelerate *T. gondii* bradyzoite differentiation in myotubes and myoblasts, H₂O₂ was tested as another ROS species. RT-qPCR was performed with H₂O₂- or solvent-treated, parasite-infected myotubes and myoblasts and *T. gondii* BAG1 mRNA levels were determined. Data showed that H₂O₂ also induced BAG1 mRNA expression in *T. gondii* within both myotubes and myoblasts in a dose-dependent manner. Upregulation of BAG1 mRNA by H₂O₂ was higher in parasites residing in myoblasts than in myotubes. It has to be mentioned however, that upregulation of BAG1 mRNA expression did not reach statistical significance due to considerably variances (Figure 3.26). Addition of 10 mM of the ROS scavenger NAC inhibited BAG1 mRNA in both myotubes and myoblasts suggesting a role of ROS in induction of *T. gondii* BAG1 mRNA expression.

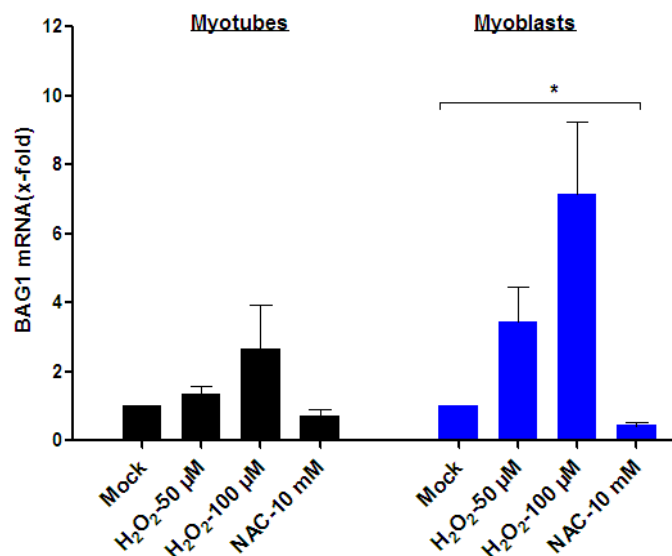


Figure 3.26: H₂O₂ induces BAG1 mRNA expression in *T. gondii* inside myotubes and myoblasts. C2C12 myoblasts were induced to differentiate into myotubes. Both myotubes and myoblasts were treated with 50 μM and 100 μM of H₂O₂ and 10 mM NAC or were mock-treated. After one hour, cells were infected with *T. gondii* tachyzoites at a host cell-to-parasite ratio of 1:3.5. Total RNA was isolated after 48 hours of infection and mRNA was reverse transcribed into cDNA which was amplified using specific primers for *T. gondii* bradyzoite antigen 1 (BAG1) and *T. gondii* actin (TgActin) by quantitative real-time PCR. The increase in BAG1 mRNA was calculated in H₂O₂/NAC-treated myotubes and myoblasts as compared to the mock controls using the $\Delta\Delta\text{CP}$ method and was normalized to TgActin mRNA. Results are depicted as means \pm S.E.M. from three independent experiments. Significant differences were identified by Student's *t*-test (* $p < 0.05$).

3.5 Impact of host cell cycle on *T. gondii* bradyzoite differentiation in SkMCs

The irreversible cell cycle arrest is one of the major differences between terminally differentiated myotubes and its proliferating precursor myoblasts (Huang and Thayer, 2002; Bentzinger *et al.*, 2012). Consequently, transcriptome analysis identified the cell cycle and a variety of cell cycle-associated genes being major differences between myotubes and myoblasts irrespective of *T. gondii* infection (see Figures 3.5, 3.8G, 3.9G and supplementary Table 3.9). Furthermore, previous results indicated that the host cell cycle may influence *T. gondii* stage differentiation (Swierzy and Lüder, 2014). Therefore, it was hypothesized that cell cycle regulation of SkMCs impacts *T. gondii* bradyzoite differentiation. To validate this hypothesis pharmacological and genetic approaches were used.

3.5.1 Pharmacological cell cycle inhibitors accelerate *T. gondii* bradyzoite differentiation in SkMCs

In order to arrest cell cycle progression in myoblasts, two well-known pharmacological cell cycle inhibitors, namely aphidicolin (APH) and mimosine (MIM) were used (Ji *et al.*, 1997). To assess the effect of APH and MIM on *T. gondii* BAG1 mRNA expression in myoblasts, quantitative real time RT-PCR was performed. For comparison, myotubes that are already cell-cycle arrested were also included in these analyses. Data showed that BAG1 mRNA was significantly upregulated in *T. gondii* within myoblasts treated with 250 or 500 ng/ml APH or those treated with 250 μ M MIM as compared to mock-treated cells. A trend of increasing BAG1 mRNA expression was also observed in *T. gondii* within myotubes treated with these inhibitors but significant upregulation was only detected after treatment with 500 ng/ml APH (Figure 3.27A).

I next addressed the question whether the cell cycle inhibitors APH and MIM had any effect on parasite replication in SkMCs. It has been reported previously that reduced parasite replication is necessary for induction of *T. gondii* bradyzoite differentiation in bone marrow-derived macrophages (Bohne *et al.*, 1994). In order to determine the impact of APH and MIM on parasite replication, immunofluorescence staining was performed. To this end, C2C12 myotubes and myoblasts were treated with 250-500 ng/ml APH and 100-

250 μ M MIM followed by infection with *T. gondii* tachyzoites four hours later. The parasite replication was then analyzed microscopically at 48 hours post infection. A dose-dependent inhibition of parasite replication was observed in both myotubes and myoblasts treated with APH and MIM compared to mock-treated cells (Figure 3.27C). Inhibition of parasite replication was particularly evident in myoblasts due to the higher parasite replication in mock-treated myoblasts. The higher concentrations of APH and MIM almost completely halted parasite replication in both cell types (Figure 3.27B).

It was then determined whether increased expression of BAG1 mRNA in parasites residing in APH- and MIM-treated myoblasts and to a lesser extent myotubes also leads to the formation of *T. gondii* tissue cysts. In order to determine tissue cysts formation, staining was performed where the wall of the parasite tissue cyst was fluorescently labeled with biotin-conjugated *Dolichos biflorus* lectin (DBL). Thereafter, DBL-reactive tissue cysts were identified and counted in APH- and MIM-treated myotubes and myoblasts at 48 and 72 hours post infection. Results showed only low numbers of cysts at 48 hours after infection in both mock- and inhibitors-treated myoblasts and myotubes, with the highest numbers observed in myotubes as expected. However, at 72 hours post infection, the number of cysts has strongly increased in myotubes and myoblasts treated with 250 ng/ml APH and 100 μ M MIM compared to mock-treated cells. In contrast, higher concentrations of both inhibitors were less effective or even completely failed in inducing tissue cyst formation by *T. gondii* (Figure 3.27D). Thus, an intermediate concentration of both cell cycle inhibitors appeared to be required to trigger tissue cyst formation whereas BAG1 mRNA levels were also increased by high inhibitor concentrations.

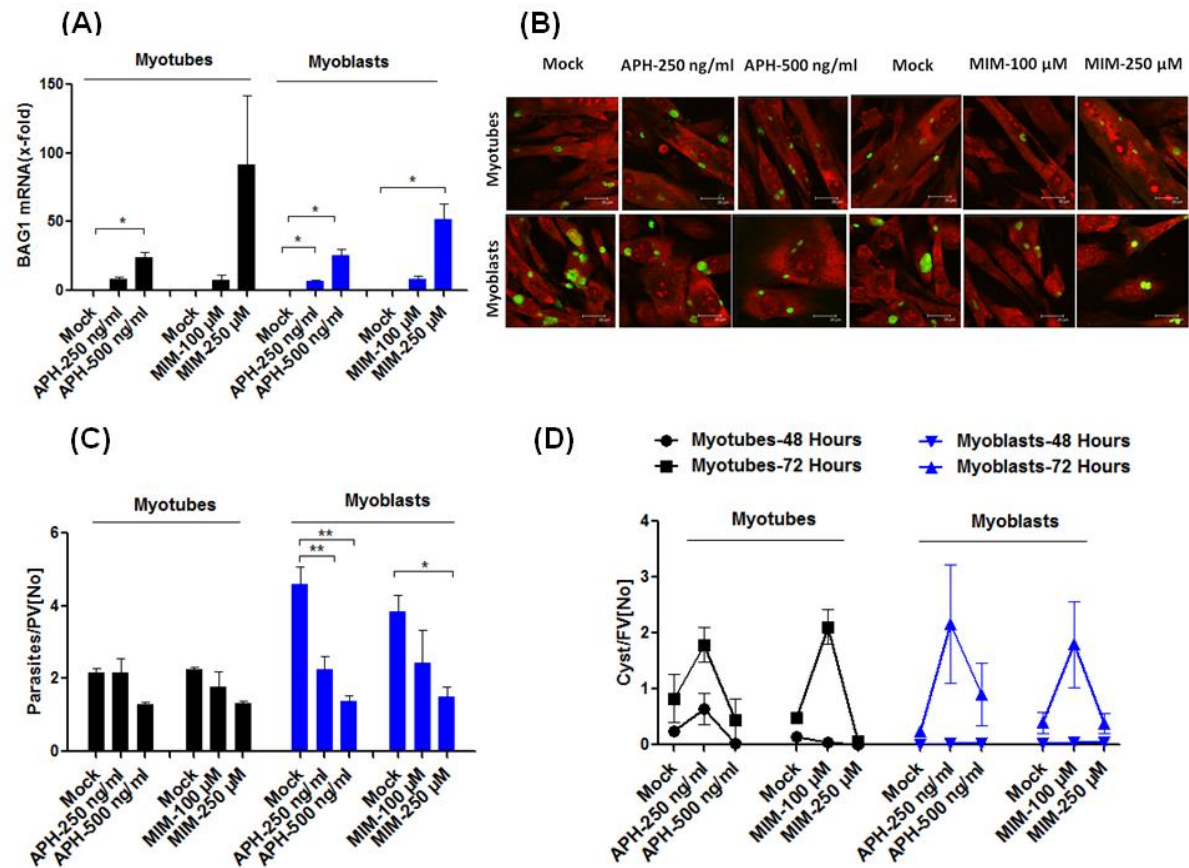


Figure 3.27: Cell cycle inhibitors can accelerate bradyzoite differentiation in myotubes and myoblasts. C2C12 myoblasts were induced to differentiate into poly-nucleated myotubes. Both myotubes and myoblasts were treated with 250 ng/ml or 500 ng/ml aphidicolin (APH), 100 μ M or 250 μ M mimosine (MIM) or with the respective solvents (mock). After 4 hours of treatment, cells were then infected with *T. gondii* tachyzoites at a host cell-to-parasite ratio of 1:3.5. **(A)** Total RNA was isolated after 48 hours of infection and mRNA was reverse transcribed into cDNA which was amplified using specific primers for *T. gondii* bradyzoite antigen 1 (BAG1) and *T. gondii* actin (TgActin) by quantitative real-time PCR. The increase of BAG1 mRNA in inhibitor-treated compared to solvent-treated cells was calculated according to the $\Delta\Delta$ CP method and was normalized to TgActin mRNA. Results are depicted as means \pm S.E.M. from three independent experiments. Significant differences were identified by Student's *t*-test (* $p < 0.05$). **(B)** Cells were fixed at 48 hours post infection with 4% paraformaldehyde and parasites were immunolabeled using a polyclonal *anti-T. gondii* antiserum and Cy2-conjugated secondary antibodies (green fluorescence). Host cells were visualized using propidium iodide (red fluorescence). Representative images of both parasite and host cell labeling were recorded by confocal laser scanning microscopy and were superimposed. **(C)** After cells had been fluorescently labeled as indicated above, the average size of parasitophorous vacuoles (PVs) in each sample was determined by counting the number of parasites in 100 PVs. Data represent means \pm S.E.M. from four independent experiments. Significant differences were identified by Student's *t*-test (* $p < 0.05$, ** $p < 0.01$). **(D)** Cells were fixed at 48 and 72 hours post infection with 4% paraformaldehyde. After fixation, tissue cysts of *T. gondii* were labeled with biotin-conjugated *Dolichos biflorus* lectin and Cy2-conjugated streptavidin, parasites were labeled with a polyclonal *anti-T. gondii* antiserum and Cy5-conjugated secondary antibodies and host cells were visualized using propidium iodide. The numbers of DBL-positive cyst were counted in 100 fields of vision (FV). Data represent means \pm S.E.M. from three independent experiments.

3.5.2 Cell cycle inhibitors strongly arrest host cell proliferation

In the experiments described above, host cell cycle progression was arrested by using APH and MIM in order to determine the effect of host cell cycle regulation on *T. gondii* bradyzoite differentiation (Figure 3.27). Therefore, it was important to validate whether or not the inhibitors APH and MIM arrested cell cycle progression in myoblasts and whether they had any effect of myotubes that are already cell cycle-arrested.

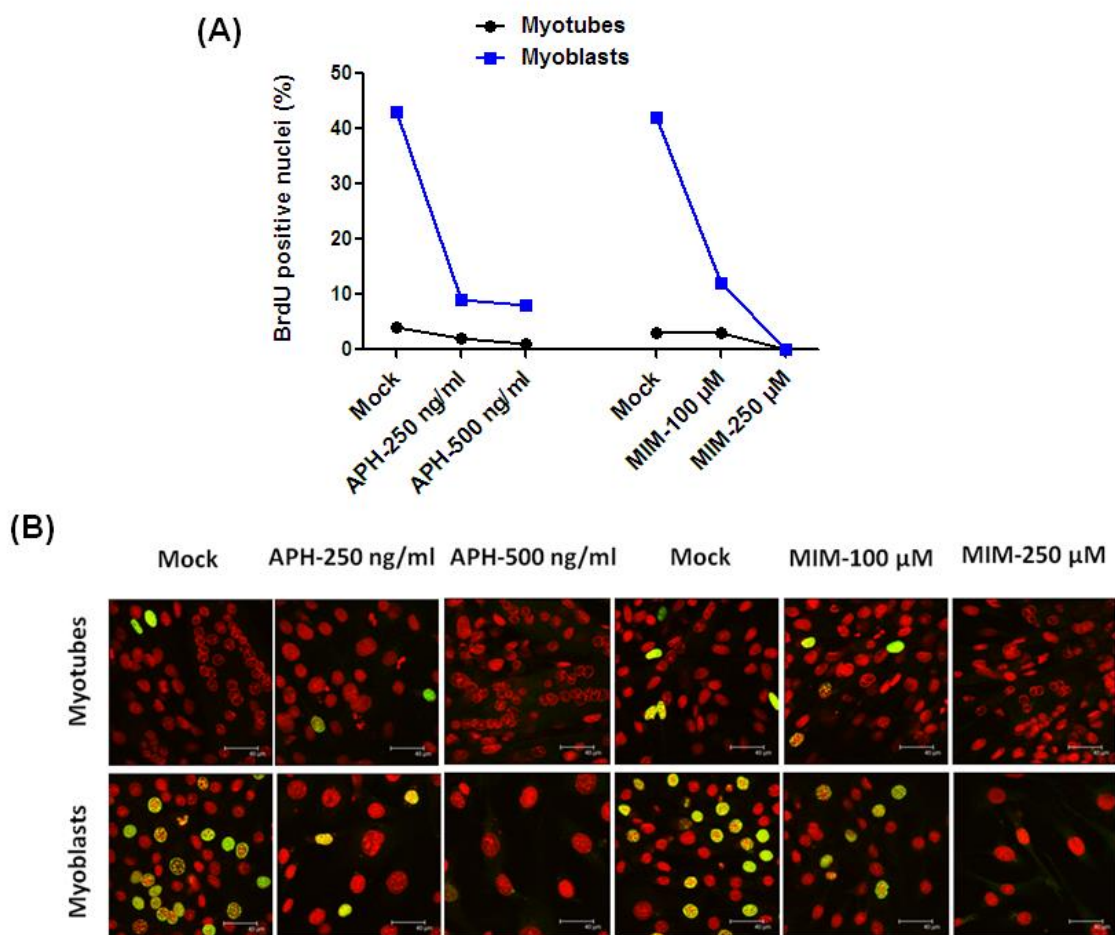


Figure 3.28: Cell cycle inhibitors inhibit host cells proliferation. C2C12 myoblasts were induced to differentiate into poly-nucleated myotubes. Both myotubes and myoblasts were treated with 250-500 ng/ml APH, 100-250 μ M MIM, or were mock-treated. Two hours prior to fixation, cells were treated with BrdU (10 μ g/ml). Then, cells were immunolabeled with antibodies recognizing BrdU followed by using DyLight488-conjugated secondary antibodies (green fluorescence) and the total cell population was labeled with propidium iodide (red fluorescence). (A) The percentages of BrdU-labeled nuclei in inhibitor-treated samples and controls were calculated by counting the number of BrdU-positive cells compared to total number of cells. Data represent percentages of BrdU-positive nuclei from one experiment. (B) Representative images of both labelings were recorded by confocal laser scanning microscopy and were superimposed.

To this end, cell proliferation was evaluated by using 5-Bromo-2-deoxyuridine (BrdU) which is a thymidine analogue which incorporates into newly synthesized DNA during cell cycle progression. Thus, both myotubes and myoblasts were treated with 250-500 ng/ml APH and 100 -250 μ M MIM or were mock treated and were cultivated in the presence of BrdU (10 μ g/ml) before fixation. Afterwards, the incorporated BrdU was identified using specific antibodies and cell cycle progression was analyzed by comparing inhibitor-treated samples with mock-treated ones. Data showed only minor differences in DNA synthesis between mock-treated and inhibitors-treated myotubes as determined by the lack of BrdU incorporation in the vast majority of cells. This was expected because myotubes are already cell cycle-arrested. In contrast, both APH and MIM strongly reduced BrdU incorporation and hence DNA synthesis in myoblasts compared to mock-treated controls thus confirming efficient inhibition of myoblast proliferation by both cell cycle inhibitors (Figure 3.28 A, B).

3.5.3 RNA interference mediated knock-down of cell cycle regulator p21^{Waf1/Cip1} and its impact on *T. gondii* bradyzoite differentiation on SkMCs

It has been previously described that terminally differentiated and cell cycle-arrested SkMCs, i.e. myotubes but not proliferating myoblasts support *T. gondii* bradyzoite differentiation (Swierzy and Lüder, 2014). The authors have also shown that inhibition of cell cycle withdrawal in SkMCs, i.e. inhibition of myotube formation by RNA interference mediated knockdown of a negative cell cycle regulator, namely testis-specific Y-encoded-like protein-2 (Tspyl2) abolished *T. gondii* bradyzoite differentiation and tissue cysts formation (Swierzy and Lüder, 2014). These data suggested that arresting the host cell cycle is an important signal for *T. gondii* bradyzoite differentiation in SkMCs. However, Tspyl2 knockdown may have other consequences on host cells than inhibiting cell cycle withdrawal as well. Therefore, in order to further validate an impact of host cell cycle arrest on bradyzoite formation in myotubes, I herein determined whether knockdown of the negative cell cycle regulator and downstream target of Tspyl2 p21^{Waf1/Cip1} would also abolish *T. gondii* bradyzoite differentiation in SkMCs.

3.5.3.1 Validation of p21^{Waf1/Cip1} knock-down in SkMCs and its impact on myotube formation

Since p21 mRNA levels are clearly higher in myotubes than in myoblasts irrespective of *T. gondii* infection as shown by both RNAseq (Figure 3.8G) and RT-qPCR analysis (Figure 3.9G), it was speculated that p21 protein might have a role on *T. gondii* bradyzoite development in myotubes. In order to test the role of p21 on *T. gondii* bradyzoite development, stable p21-shRNA knock-down C2C12 cell lines were constructed by transfection of myoblasts with plasmid vectors carrying five different p21-targeted shRNA sequences. As a negative control, a mutant control C2C12 cell line was constructed by transfection of cells with a p21-shRNA-negative pLKO.1-puro plasmid vector. The negative control plasmid had been previously propagated in *E. coli* 5-alpha competent cells. Successful transformation of *E. coli* 5-alpha was examined through qPCR of clones using specific primers (see 2.1.13) targeting the pLKO.1-puro plasmid. The presence of nucleic acid fragments of the correct size was confirmed after electrophoretic separation in an agarose gel (data not shown). After antibiotic selection of transfectants and cloning by limiting dilution, two different p21-shRNA knock-down clones (p21-shRNA1 and p21-shRNA2) and shRNA-negative control transfectants were selected for further analyses. Western blotting was used to examine p21 protein expression at day 3, 5, and 7 of differentiation from myoblasts to myotubes in p21-shRNA transfectants, shRNA-negative control transfectants and wildtype myotubes as well as in wildtype myoblasts at day 1 after seeding. P21 protein was highly expressed in wildtype myotubes at day 3 and 5 of differentiation compared to wildtype myoblasts (Figure 3.29A). In contrast to wildtype cells, p21-shRNA clones 1 and 2 expressed no or strongly reduced levels of p21 during incubation in differentiation medium for 3 to 7 days. On the other hand, negative control transfectant cells expressed p21 at similar levels during the differentiation period as wildtype cells. Control staining of Western blots with an anti-actin antibody confirmed equal protein loading (Figure 3.29A). These results thus indicated successful knockdown of p21 protein expression in p21-shRNA clones 1 and 2 but not negative control transfectants. In order to further evaluate p21 expression at the single cell level, immunofluorescence staining was performed by labeling of p21 with anti-p21 primary antibodies followed by Cy2-conjugated secondary antibodies.

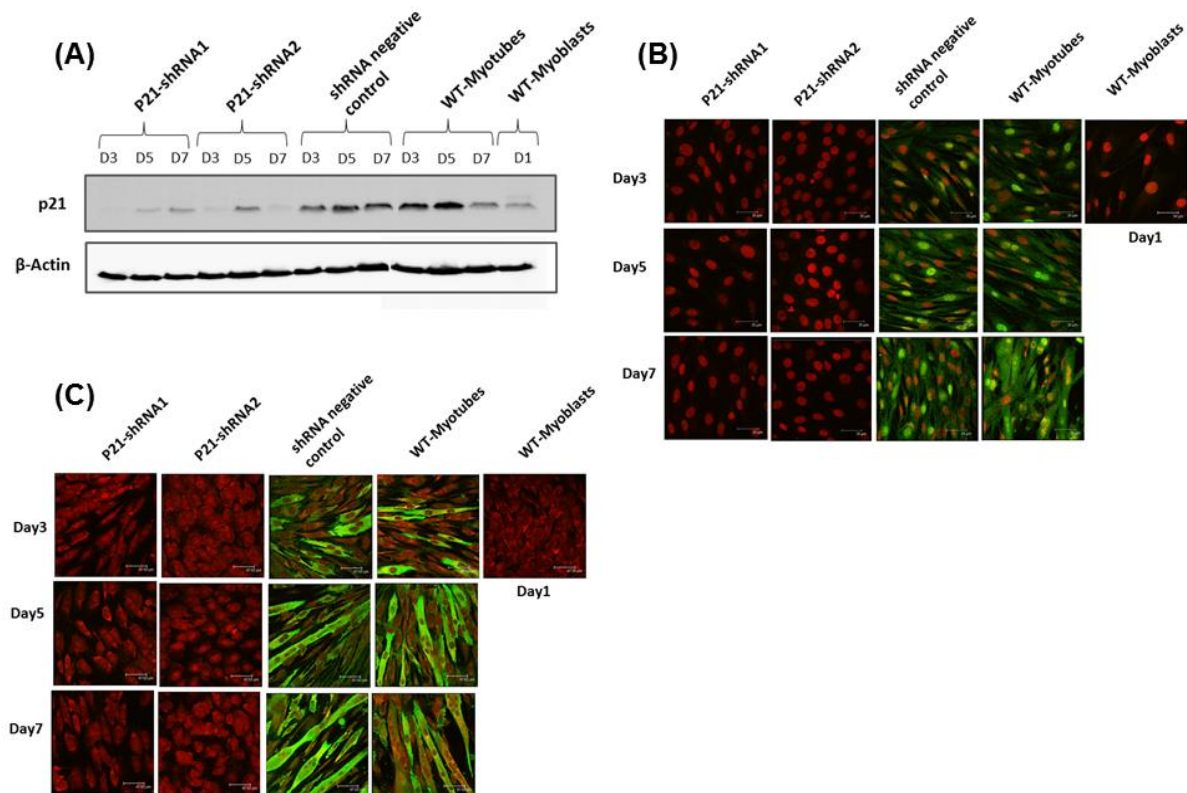


Figure 3.29: Validation of RNA interference-mediated knock-down of p21^{Waf1/Cip1} in SkMCs and its impact on myotube formation. C2C12 myoblasts were transfected with lentiviral plasmid vectors encoding different p21 specific shRNAs or a shRNA-negative control plasmid vector. Stable transfectants were selected by culturing cells in presence of puromycin and were cloned by limiting dilution. Two different clones carrying different p21-shRNAs (p21-shRNA1 and p21-shRNA2 which were derived from p21-targeted shRNA sequence #4) or carrying negative control plasmids were selected for further analyses. To this end, p21-shRNA knockdown clones, shRNA-negative control clone and wildtype C2C12 myoblasts were induced to differentiate for 3(D3), 5(D5), and 7(D7) days by using differentiation medium supplemented with 2% horse serum. Wildtype myoblasts at 1 day after seeding were included as additional control cell type. **(A)** Whole cell protein lysates were isolated from these clones and wildtype cells at the indicated time points along with wildtype myoblasts. Protein lysates were separated by SDS-PAGE and were analyzed by Western blot using antibodies recognizing p21^{Waf1/Cip1}. Immune complexes were visualized by enhanced chemiluminescence. Detection of mouse β -actin was used as loading control. **(B)** Cells were fixed at the indicated time points using 100% methanol for 15 minutes at -20°C and were immunolabeled with anti-p21^{Waf1/Cip1} primary antibodies and Cy2-conjugated secondary antibodies (green fluorescence). Host cells were labeled with propidium iodide (red fluorescence). Representative images of both labelings were recorded by confocal laser scanning microscopy and were superimposed. **(C)** Cells were fixed at the indicated time points using 4% PFA and mature myotubes were labelled with anti-myosin heavy chain-specific primary antibodies followed by Cy2-conjugated secondary antibodies (green fluorescence). Cells were also labeled with propidium iodide (red fluorescence). Representative images of both labelings were recorded by confocal laser scanning microscopy and were superimposed.

Results showed no p21 in nuclei and cytoplasm of p21-shRNA1 and p21-shRNA2 clones at any time during incubation in differentiation medium whereas shRNA-negative control transfectants and wildtype cells clearly expressed considerable amounts of p21 in nuclei and/or in the cytoplasm in all cells during differentiation. Proliferating C2C12 myoblasts at 1 day after seeding did also not express p21 at detectable levels using immunofluorescence staining (Figure 3.29B). Since p21 protein was highly expressed in C2C12 wildtype SkMCs during differentiation to myotubes as compared to proliferating myoblasts, immunofluorescence staining of p21-shRNA clones 1 and 2 was then performed to test its functional role in myogenic differentiation. After incubation of p21-shRNA1 and p21-shRNA2 transfectants, shRNA-negative control transfectants and wildtype C2C12 cells in differentiation medium containing 2% horse serum for 3, 5, and 7 days, and cultivation of wildtype myoblasts for 1 day in growth medium, the differentiation marker myosin heavy chain (MyHC) was immunolabeled and analyzed by immunofluorescence microscopy. Results showed that p21-shRNA transfectants were unable to differentiate from myoblasts to MyHC-positive myotubes whereas shRNA-negative control transfectants and wildtype C2C12 readily differentiated to poly-nucleated myotubes expressing MyHC. As expected, proliferating myoblasts did also not express detectable amounts of MyHC (Figure 3.29C).

3.5.3.2 P21 knockdown impact on host cell proliferation

In order to validate the impact of p21 knockdown on the host cell cycle, host cell proliferation was examined in p21-shRNA knockdown cells, shRNA-negative control transfectants and wildtype C2C12 cells. The BrdU incorporation assay was used to measure the cell proliferation capacity as BrdU (an analogue of thymidine) incorporates into newly synthesized DNA. Results showed 40% BrdU-positive nuclei at day1 after induction of differentiation in p21 knockdown clone 2, shRNA-negative transfectants and wildtype cells whereas p21-shRNA clone 1 had 20% BrdU positive nuclei. At day 3 after induction of differentiation, the proliferation of all cells decreased as the BrdU-positive nuclei decreased to a similar percentage of about 12%. At day 5 and day 7, cell proliferation was found to be similar in p21 knockdown clone 1, shRNA-negative control transfectants and wildtype cells whereas only p21-shRNA2 showed higher percentage of BrdU-positive nuclei compared to the other cell lines (Figure 3.30A, B).

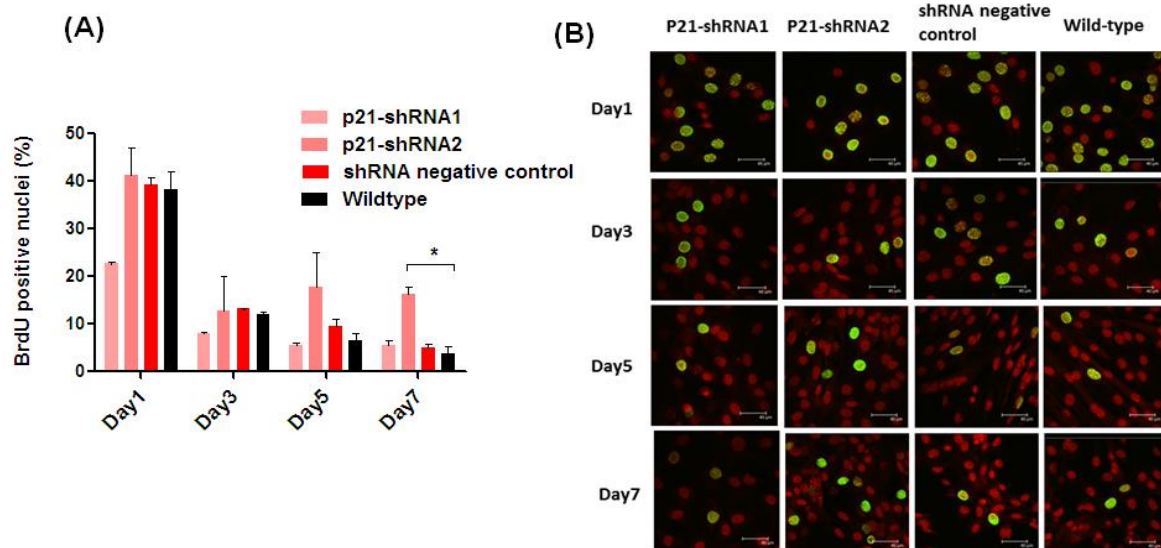


Figure 3.30: P21 knockdown in SkMCs does not generally accelerate host cell proliferation. P21-shRNA transfectant clones 1 and 2, shRNA-negative control transfectants and wild type C2C12 cells were induced to differentiate into myotubes using differentiation medium containing 2% HS for 1 to 7 days as indicated. During the last 2 hours of cultivation, cells were treated with BrdU (10 μ g/ml) before fixation using 70% ethanol. Thereafter, proliferating cells were immunolabeled with antibodies recognizing BrdU followed by Dylight-488 conjugated anti-mouse IgG secondary antibodies (green fluorescence). The total cell population was labeled with propidium iodide (red fluorescence). **(A)** The percentages of BrdU-labeled nuclei in p21-shRNA transfectants, shRNA-negative control transfectants and wildtype cells were calculated by counting the number of BrdU-positive nuclei as compared to the number of total nuclei. Data represent means \pm S.E.M. from two independent experiments. Significant differences were identified by Student *t*-test ($*p < 0.05$). **(B)** Representative images of both labelings were recorded by confocal laser scanning microscopy and were superimposed.

3.5.3.3 P21 knock-down does not affect *T. gondii* bradyzoite differentiation in SkMCs but strongly accelerates parasite replication

In order to investigate the functional role of p21 in myotubes on *T. gondii* bradyzoite development in SkMCs, upregulation of BAG1 mRNA expression was examined after infection of p21-shRNA1 and p21-shRNA2 transfectants, shRNA-negative control transfectants and wildtype myotubes induced to differentiate for 7 days as well as proliferating myoblasts with *T. gondii*. Remarkably, results indicated increased BAG1 mRNA expression in *T. gondii* residing in the p21-shRNA transfectants clone 1 and 2 compared to wildtype myotubes or shRNA-negative control transfectants but these differences were not statistically significant (Figure 3.31A). However, BAG1 mRNA expression was significantly lower in *T. gondii* within proliferating myoblasts as compared

to parasites within shRNA-negative control transfectants or wildtype myotubes as expected (see Figure 3.31A).

In order to determine the impact of p21 on parasite replication, immunofluorescence staining of the parasites was performed after infection of p21-shRNA1 and p21-shRNA2 knockdown cells, shRNA-negative control transfectants and wildtype SkMCs after 7 days of differentiation, along with infected proliferating wildtype myoblasts. Interestingly, both p21-shRNA1 and p21-shRNA2 transfectants sustained robust parasite replication compared to wildtype myotubes and shRNA-negative control transfectants after 48 hours of infection. At the same time, parasite replication was lower in myotubes and shRNA-negative control transfectants than in myoblasts (Figure 3.31C). Thus, parasitophorous vacuoles in p21-shRNA transfectants were clearly larger than in wildtype myotubes or shRNA-negative control transfectants, and they were even larger than in wildtype myoblasts (Figure 3.31B). Finally, cyst formation by *T. gondii* was compared within p21-shRNA knockdown cells, negative control transfectants and wildtype cells. The percentages of *T. gondii* tissue cysts generally increased within all cell types from 48 to 72 hours after infection. Furthermore, cyst formation was clearly lower in wildtype myoblasts than in myotubes and this was statistically significant at 72 hours after infection. However, while the formation of DBL-positive cysts was lower in p21-shRNA transfectant clone 1 at 48 hours of infection than in wildtype myotubes or shRNA-negative control transfectants, p21-shRNA clone 2 at 48 and 72 hours of infection showed nearly the same percentages of DBL-positive cysts than wildtype myotubes. Furthermore, at 72 hours after infection, p21-shRNA knockdown clone 1 showed cyst formation as shRNA negative control transfectants (Figure 3.31D).

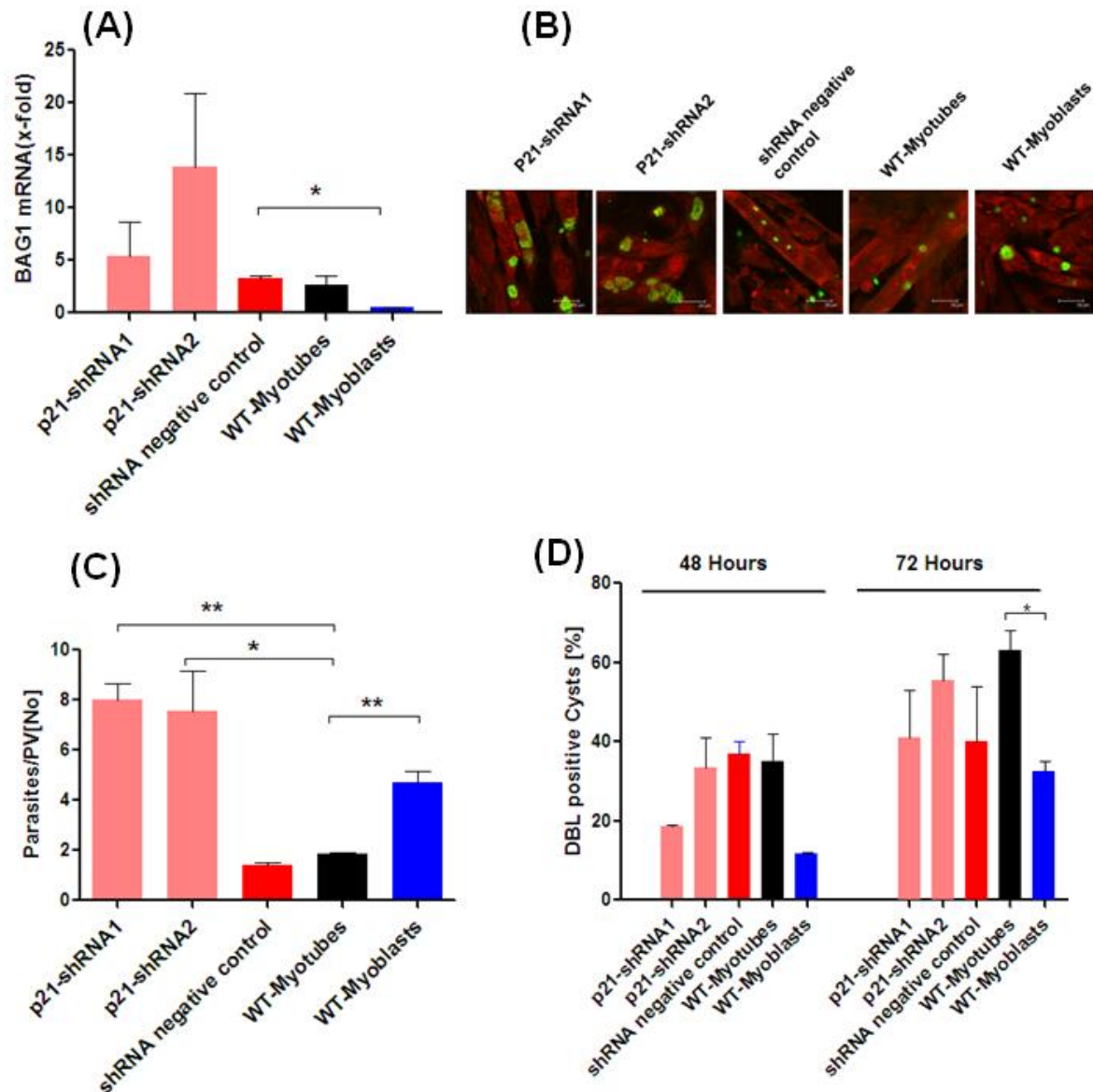


Figure 3.31: P21 knockdown in SkMCs does not impair bradyzoite differentiation but accelerates parasite replication. P21-shRNA transfectants clone 1 and 2, shRNA negative control transfectants and wildtype C2C12 cells were induced to differentiate into myotubes. Transfected cells, wildtype myotubes and proliferating myoblasts at day 1 after seeding were then infected with *T. gondii* tachyzoites at a host cell-to-parasite ratio of 1:3.5. **(A)** Total RNA was isolated at 4 and 48 hours post infection and was reverse transcribed for cDNA synthesis which was amplified using specific primers for *T. gondii* bradyzoite antigen 1 (BAG1) and *T. gondii* actin (TgActin) by quantitative real-time PCR. The fold increase in BAG1 mRNA in *T. gondii* between 4 and 48 hours was calculated using the $\Delta\Delta\text{CP}$ method and was normalized to TgActin mRNA. Results are depicted as means \pm S.E.M. from three independent experiments. Significant differences were identified by Students *t*-test (* $p < 0.05$). **(B)** Cells were fixed at 48 hours post infection with 4 % paraformaldehyde and parasites were immunolabelled (green fluorescence) using a polyclonal anti-*T. gondii* antiserum. Host cells were visualized using propidium iodide (red fluorescence). Representative images of both labelings were recorded by confocal laser scanning microscopy and were superimposed. **(C)** After cells had been fluorescently labeled as indicated above, the average size of parasitophorous vacuoles (PVs) in each sample was determined by counting the number of parasites in 100 PVs. Data represent means \pm S.E.M. from five independent experiments. Significant differences were identified by Students *t*-test (* $p < 0.05$, ** $p < 0.01$). **(D)** Cells were fixed at 48 and 72 hours post infection with 4 % paraformaldehyde. After fixation,

tissue cysts of *T. gondii* were labeled with biotin-conjugated *Dolichos biflorus* lectin (DBL) and Cy2-conjugated streptavidin, parasites were labeled with a polyclonal anti-*T. gondii* antiserum and Cy5-conjugated secondary antibodies and host cells were visualized using propidium iodide. The numbers of DBL-positive cysts were counted among 100 parasitophorous vacuoles (PV) and were expressed as percentages. Data represent means \pm S.E.M. from two independent experiments. Significant differences were identified by Student's *t*-test (* $p < 0.05$).

Chapter 4: Discussion

4.1 Terminally differentiated SkMCs support *T. gondii* stage conversion

Toxoplasma gondii stage conversion from its tachyzoite to its bradyzoite stage in skeletal muscle and/or neurons is considered a major cause of establishing long term chronic infections (Dubey *et al.*, 1998). Furthermore, persistence of the parasite in skeletal muscle cells (SkMCs) is associated with its transmission to new warm-blooded hosts including humans via eating raw and undercooked meat or meat products (Cook *et al.*, 2000; Jones *et al.*, 2009). Hence, it is an urgent need to understand the biology of *T. gondii* stage conversion in SkMCs. Recently, Swierzy and colleagues have demonstrated that the transcriptomes of four different heterogeneous host cell types, i.e SkMCs, neurons, astrocytes and fibroblasts differ substantially after infection with *T. gondii*, thus highlighting host cell-type specific parasite-host interactions (Swierzy *et al.*, 2017). This further argues for the necessity to determine stage differentiation specifically in SkMCs. C2C12 mouse SkMCs have been used as a suitable model to study the host-parasite interaction of *T. gondii* *in vitro* in skeletal muscle cells (Guimarães *et al.*, 2008; Ferreira-da-Silva *et al.*, 2009; Takács *et al.*, 2012; Swierzy and Lüder, 2014). It has to be stressed that *T. gondii* stage conversion spontaneously occurs in terminally differentiated mature SkMCs, i.e. in myotubes without any exogenous stress factor but not in proliferating myoblasts or fibroblasts (Ferreira-da-Silva *et al.*, 2009; Swierzy and Lüder, 2014). Consistent with these previous results, it was further confirmed here that *T. gondii* within myotubes but not in myoblasts upregulated BAG1 mRNA expression and increased tissue cysts formation, indicating preferred stage conversion of *T. gondii* in myotubes. However, the factors that induce stage conversion of *T. gondii* in myotubes are only partially known. Therefore, this study has been designed to unravel the host factors that might induce *T. gondii* stage conversion in myotubes but not in myoblasts. Myotubes and myoblasts differ largely in morphological aspects and in cell cycle regulation (Huang and Thayer, 2002; Shen *et al.*, 2003) as myotubes are poly-nucleated, terminally differentiated and irreversibly cell cycle-arrested cells whereas myoblasts are mononuclear actively proliferating cells. Besides, these cell types differ also in other molecular and cellular aspects as for instance their transcriptomes (Tomczak *et al.*, 2004; Rajan *et al.*, 2012), their proteomes including enzymes of glucose and lipid metabolism, structural proteins, transcription factors and cell signaling molecules (Kislinger *et al.*, 2005; Bentzinger *et al.*, 2012; Deshmukh *et al.*, 2015), and in expression of immune regulatory factors as for instance cytokines and chemokines (Wiendl *et al.*, 2005; Swierzy *et al.*, 2014). Obviously,

there might also be large metabolic differences between these two different states of the cells. Therefore, it was hypothesized that different cellular and metabolic characteristics of myotubes and myoblasts may play a role in the preferred triggering of *T. gondii* stage conversion within myotubes. Hence, this study aimed to uncover potential host factors that might induce *T. gondii* stage conversion in myotubes.

4.2 Transcriptome analyses provide candidates for experimental proof on *T. gondii* stage conversion in SkMCs

Transcriptome analysis of *T. gondii*-infected host cells may provide useful information for understanding underlying mechanisms of the host-parasite interaction. It provides the opportunity to determine the gene expression pattern of host cells, parasites and the effect of parasite infection on the host transcriptome on a genome-wide scale. It can also identify candidate genes expression of which may regulate *T. gondii* stage conversion in distinct cells. Such candidates can be subsequently tested for their functional impact on *T. gondii* stage conversion in SkMCs. Here, RNA sequencing-based transcriptome analysis of non-infected and *T. gondii*-infected myotubes and myoblasts were performed at 24 hours post infection to unravel their specific gene expression profiles before and after infection. Interestingly, infected and non-infected myotubes and myoblasts differed significantly in the expression of up to 6592 differentially regulated genes but surprisingly *T. gondii* infection had only a minor impact on host gene expression. It is important to note that *T. gondii* differentially modulated only 38 genes in myotubes after infection whereas 70 genes were differentially regulated in myoblasts by *T. gondii* infection. Surprisingly, most of the genes were identified as predicted or pseudogene. Nevertheless, the large differences in gene expression profiles of myotubes and myoblasts both before and after infection may provide important information for the host-parasite interaction within myotubes versus myoblasts. A recent study on the transcriptomes of four heterogeneous host cell types, namely differentiated SkMCs, neurons, astrocytes and fibroblasts identified more than 16,000 differentially expressed genes, and the large majority of them differed between host cell types but not between non-infected and infected cells. Thus, *T. gondii* also had only a minor impact on these transcriptomes (Swierzy *et al.*, 2017). Furthermore, *T. gondii* infection up- and downregulated largely different sets of genes in the different cell types, indicating cell type-specific responses of the host to *T. gondii*. In that study however, the

authors nevertheless identified 492 genes to be differentially expressed in myotubes after *T. gondii* infection (Swierzy *et al.*, 2017). The minor impact of *T. gondii* on host cell gene expression as observed in this study could be explained by two ways. First, although active and freshly egressed extracellular parasites, i.e. tachyzoites have been used for the infection experiments in this study, the presence of bradyzoites cannot be completely excluded. Due to the slower growth rate of bradyzoites, this parasite stage generally have a minor impact on the host cell transcriptome (Fouts *et al.*, 2007). Second, although parasite replication in both myotubes and myoblasts has been examined using immunofluorescent test, there might be a lack of equal distribution of parasite in host cells during the 24 hours infection period. Lack of efficient infection of host cells by the parasite might thus have contributed to the low impact of the parasite on host cell transcriptomes.

Gene ontology analysis confirmed that the large set of differentially expressed genes (6592) in *T. gondii*-infected myoblasts versus infected myotubes is associated with different biological pathways. Among these pathways, cellular component organization, mitotic cell cycle processes, cell cycle, metabolic processes and cellular metabolic processes were the most prominent differences between myotubes and myoblasts. The differences in cell cycle regulation between myotubes and myoblasts both before and after infection with *T. gondii* was expected because myotubes are terminally differentiated, cell cycle-arrested SkMCs which develop from their proliferating precursor myoblasts (Huang and Thayer, 2002; Bentzinger *et al.*, 2012). The differences between myotubes and myoblasts in metabolic pathways as identified herein were more surprising since the metabolism of C2C12 SkMCs before and after differentiation has not yet been thoroughly investigated. Therefore, differentially expressed genes involved in cell cycle regulation and metabolic processes in myotubes and myoblasts were selected for further in-depth analysis and their role in *T. gondii* stage conversion.

The group of genes that are involved in cell cycle regulation and that differed in expression between myotubes and myoblasts are shown in supplementary Table 3.9. The majority of them encode for different cyclins, cyclin-dependent kinases (CDKs), CDK inhibitors including p21, p18, p27, p57 and the cell cycle regulatory proteins i.e retinoblastoma (RB) 1, proliferating cell nuclear antigen (PCNA). Shen and colleagues have shown before that cell cycle arrest is one of the major differences between myotubes and myoblasts (Shen *et al.*, 2003). Here it was confirmed that p21, a cyclin-dependent kinase inhibitor of cell cycle

was 6.7-fold upregulated in differentiated myotubes compared to proliferating myoblasts irrespective of *T. gondii* infection (Figure 3.8G). This is consistent with other studies where p21 was also upregulated in the course of C2C12 myoblasts differentiation (Shen *et al.*, 2003; Swierzy and Lüder, 2014). It has to be noted that the level of p21 expression did not change after *T. gondii* infection in these studies and this was confirmed herein. P21 is a member of the CDK-interacting protein/kinase-inhibitory protein (CIP/KIP) family of CDK inhibitors that can arrest the cell cycle in two different ways. First, p21 can directly block cell cycle progression at G1/S through inactivating CDK2 or by interacting with multiple cyclin-CDK complexes (Starostina and Kipreos, 2012). Second, it can also arrest cell cycle progression during the G2 phase in certain tissues either by inhibiting cyclinB1-CDK1 and cyclinA-CDK1/2 complexes or by blocking the phosphorylation of retinoblastoma family proteins (Bunz *et al.*, 1998; Baus *et al.*, 2003). Gene expression data indicated that p27, p57 and RB1 were also upregulated in myotubes as compared to myoblasts while various cyclins as for instance cyclinA2, cyclinB1/B2, cyclinC, cyclinD1/D2, cyclin E1/E2, cyclin-dependent kinases i.e CDK1, CDK2, CDK4, CDK6, CDK8 along with p18 and PCNA were downregulated in myotubes as compared to myoblasts. In addition to p21, p27 and p57 are structurally similar and highly conserved CDK inhibitors that also induce cell cycle arrest of myotubes (Lee *et al.*, 1995; Zhang *et al.*, 1999; Myers *et al.*, 2004). Furthermore, RB1 is a protein regulator of G1/S transition of the cell cycle that acts through repression of E2F family members of transcription factors which are required for cell proliferation (Weinberg, 1995). Contrary, downregulation of cell cycle activators including various CDKs and their cyclins in myotubes are important for skeletal muscle differentiation (Kitzmann and Fernandez, 2001). Lower expression of p18 in myotubes indicated higher expression in proliferating myoblasts. P18 is a member of the INK4 family of CDK inhibitors which is differentially expressed during G1 exit by C2C12 cells (Phelps *et al.*, 1998). Phelps and colleagues have further shown that the p18 gene encodes two mRNA transcripts: one of 2.4 kb which is highly expressed in proliferating myoblasts and one of 1.2 kb which is expressed in differentiating myotubes (Phelps *et al.*, 1998). In addition, Broxmeyer and colleagues have shown that p18 positively influences the proliferation of hematopoietic progenitor cells as determined in p18^(-/-) mice (Broxmeyer *et al.*, 2012) which also justifies the presence of the higher level of p18 mRNA in proliferating myoblasts. Higher expression of PCNA in proliferating myoblasts accords with findings of previous studies in activated rat skeletal muscle

satellite cells where PCNA was highly expressed in the S phase of the cell cycle suggesting a role in DNA replication and cell proliferation (Johnson and Allen, 1993). Although many proteins of the cell cycle were differentially regulated in myotubes and myoblasts, p21 has been selected for functional analysis due to its high level of expression in myotubes as compared to myoblasts. In addition, p21 is a downstream molecule of Tspyl2, that has been previously shown to regulate *T. gondii* stage conversion in SkMCs (Swierzy and Lüder, 2014) (see below).

Along with transcriptome differences in cell cycle regulators between myotubes and myoblasts, differentially regulated genes related to metabolic processes were of particular interest in this study for testing their role on *T. gondii* stage conversion. Genes involved in the central carbohydrate metabolism, i.e. glycolysis, the TCA cycle, the pentose phosphate pathway (PPP) and glycogen metabolism were particularly enriched among the DEGs of myotubes and myoblasts irrespective of infection. Most genes encoding glycolytic enzymes were upregulated in myotubes as compared to myoblasts suggesting a higher rate of glycolysis in differentiated cells. Genes related to the TCA cycle itself were mostly similarly expressed in myotubes and myoblasts. However, the gene encoding the pyruvate carboxylase (PC) was 3.49-fold upregulated in myotubes as compared to myoblasts suggesting higher TCA cycle anaplerosis in myotubes. Pyruvate carboxylase is a mitochondrial enzyme that catalyzes the carboxylation of pyruvate to oxaloacetate, replenishing an important intermediate of TCA cycle. This anaplerotic reaction in skeletal muscle is important because the lack of oxaloacetate impairs TCA cycle activity and withdrawal of TCA cycle intermediates for other biosynthetic pathways as for instance synthesis of glucose, fatty acids, amino acids etc (Owen *et al.*, 2002; Jitrapakdee *et al.*, 2008). Minet and colleague have previously demonstrated the presence of PC in cultured human myotubes and human muscle tissue (Minet and Gaster, 2010). The absence of PC in human myotubes is fatal as shown by the fact that inhibition of PC using phenyl acetic acid abolishes enhanced glucose oxidation under high glucose concentration (Gaster, 2010) indicating the importance of PC-mediated anaplerotic reaction in human skeletal muscle.

Remarkably, many genes encoding for enzymes of both the oxidative and non-oxidative branches of the PPP were upregulated in myoblasts compared to myotubes irrespective of *T. gondii* infection (see supplementary Table 3.7). The oxidative phase of the PPP is important in eukaryotic cells because it converts glucose-6-phosphate into ribulose-5-

phosphate which is required for synthesis of nucleic acid and provides NADPH for the synthesis of anabolic macromolecules, i.e fatty acids, cholesterol and others as well as to maintain redox homeostasis under stress condition. On the other hand, the non-oxidative branch of the PPP uses glycolytic intermediates such as fructose-6-phosphate, glyceraldehyde-3-phosphate and sedoheptulose sugars for yielding ribose-5-phosphate for synthesis of nucleic acid, precursor of amino acids and *vice versa* depending on biochemical demand (Stincone *et al.*, 2015). Remarkably, expression of glucose-6-phosphate dehydrogenase (G6PDH)2, the rate limiting enzyme of PPP was clearly higher in myoblasts than in myotubes as determined by RNAseq and RT-qPCR. The results showed however discrepancy regarding the impact of parasite infection where *T. gondii* modulated its expression in both myoblasts and myotubes as determined by RNAseq analysis. This was not observed by RT-qPCR when G6PDH2 mRNA expression was compared between non-infected and *T. gondii*-infected myotubes and myoblasts. This might however be misleading in comparison to the absolute values obtained by RNAseq. G6PDH2 is an enzyme that catalyzes the conversion of glucose-6-phosphate to 6-phosphogluconolactone thereby shifting glucose into the PPP. Importantly, higher expression of G6PDH2 and other PPP enzymes in myoblasts indicated a higher influx of glucose into the PPP in myoblasts as compared to myotubes irrespective of *T. gondii* infection. This may provide larger amounts of the reducing equivalent NADPH in myoblasts which is required for several anabolic reactions including synthesis of fatty acids and cholesterol and to protect cells from oxidative stress. Though *T. gondii* is capable of synthesizing fatty acids *de novo*, they also scavenge it from host cells for organelle biogenesis and parasite survival (Charron and Sibley, 2002; Mazumdar *et al.*, 2006). On the other hand, *T. gondii* is auxotrophic for cholesterol and they must scavenge it from the host cells. Therefore, availability of cholesterol in *T. gondii*-infected myoblasts may affect parasite growth and stage conversion. Previous studies suggest that starvation of host cholesterol indeed induces tachyzoite-to-bradyzoite stage conversion in *T. gondii* in chinese hamster ovary cells (Ihara and Nishikawa, 2014). Higher NADPH in myoblasts may protect cells from ROS-induced oxidative stress through maintaining redox homeostasis. Higher ROS may damage lipids, proteins and nucleic acids of the parasite in *T. gondii*-infected cells which may hence affect parasite growth (see below).

Nonetheless, higher activity of enzymes of the PPP due to their increased expression may also provide higher amounts of ribose-5-phosphate in myoblasts for synthesis of nucleic

acids reflecting the proliferating nature of these cells. Importantly, higher incorporation of glucose-derived carbon atoms into ribulose-5-phosphate in myoblasts than in myotubes was indeed confirmed herein using GC-MS-mediated metabolome analysis (see below). Finally, in this study, genes related to glycogen metabolism including glycogen synthase-I and glycogen phosphorylase were upregulated in myotubes compared to myoblasts irrespective of *T. gondii* infection (see supplementary Table 3.8). Glycogen synthase-I and glycogen phosphorylase are two key enzymes associated with glycogen synthesis and glycogen degradation, respectively. This difference between C2C12 myoblasts and myotubes is not surprising because mature muscle cells use glycogen as a carbohydrate store for supplying energy during phases of starvation.

This study for the first time describes the gene expression profiles of myotubes and myoblasts infected with *T. gondii* or non-infected. The findings are similar to a previous studies where it has been shown that myogenic differentiation of myoblasts into myotubes is accompanied by changes of gene expression that are predominantly involved in muscle contraction and cytoskeleton organization, carbohydrate metabolism and cell cycle regulation (Moran *et al.*, 2002). However, the authors showed differential regulation of genes that are involved in carbohydrate metabolism including phosphofructokinase-1, glycogen phosphorylase, glycogenin, adenylosuccinate synthetase-1 and aldo-keto reductase family1 member B1 in 1-4 days differentiated myotubes. Besides, a number of genes were also differentially regulated in myotubes that are associated with cell cycle regulation as for instance p21, p57, p19, retinoblastoma-1, cyclinA2, cyclin B1-related sequence, cyclinG2, CDK4, CDK inhibitor3, PCNA, G1 to phase transition 1, cell division cycle 25 homolog C U58633, cyclin-dependent kinase regulatory subunit 2, cell division cycle 2 homolog, protein regulator of cytokinesis 1, protein phosphatase 1 and regulatory subunit 7 (Moran *et al.*, 2002). Importantly, Moran and colleagues used microarray based gene expression profiles of 1-4 days differentiated myotubes whereas RNAseq was used in this study to measure gene expression profiles of non-infected and *T. gondii*-infected 7 days differentiated myotubes and proliferating myoblasts. Together, the transcriptome analysis of myotubes and myoblasts provided thus initial guidelines for in-depth analysis of the impact of the host cell metabolism and cell cycle regulation in *T. gondii* stage conversion in myotubes.

4.3 Differences in host glucose metabolism impacts *T. gondii* stage conversion in SkMCs

SkMCs predominantly depend on glucose as a carbon source for their metabolic demands under normal physiological conditions. It has been shown that high levels of extracellular glucose accelerate proliferation of C2C12 myoblasts by inducing G1-cyclins which are important for cell cycle progression (Grabiec *et al.*, 2014). In addition, starvation for glucose inhibits differentiation from myoblasts to myotubes as indicated by reduced expression of myosin heavy chain, a marker of muscle differentiation (Fulco *et al.*, 2008; Brown *et al.*, 2012; Elkalaf *et al.*, 2013). Previous studies have also shown that undifferentiated C2C12 myoblasts largely depend on glycolysis as indicated by high lactate production, and it was estimated that 60% of energy comes from glucose in early stages of differentiation (Leary *et al.*, 1998). In contrast, increased expression of glycolytic enzymes was observed in myotubes (see above). These results suggest that glucose metabolism is important for myoblasts proliferation and differentiation as well. They also provide a link between metabolic activities of SkMCs and cell cycle regulation (Krylov *et al.*, 1999). From this point of view, it can be hypothesized that glucose metabolism in SkMCs may regulate *T. gondii* stage conversion.

Beside different metabolic demands of myoblasts and myotubes, *T. gondii* as an obligatory intracellular pathogen must meet all its metabolic demands for growth and survival within its host cells. For instance, *T. gondii* tachyzoites utilize glucose as a preferred carbon source for their energy production and synthesis of macromolecules (Polonais and Soldati-Favre, 2010; Macrae *et al.*, 2012) but they can also use glutamine as an alternative carbon source under both normal or glucose starvation conditions (Blume *et al.*, 2009; Macrae *et al.*, 2012). Previous findings confirm that the lack of glucose has only a minor impact on parasite growth and motility in human foreskin fibroblasts (HFF) cells (Blume *et al.*, 2009). Nevertheless, limited availability of glucose or its metabolic products in SkMCs may impact parasite growth and thereby favor tachyzoite-to-bradyzoite stage conversion. Therefore, the central glucose metabolism in non-infected and *T. gondii*-infected myotubes and myoblasts was of particular interest. For the first time, mass spectrometric analysis of the central carbohydrate metabolism in infected and non-infected myotubes and myoblasts was performed. The results indicated that myotubes and myoblasts significantly differ in their central glucose metabolism irrespective of *T. gondii* infection. Interestingly, whereas incorporation of glucose-derived carbon atoms into intermediates of the glycolysis did not

consistently differ between myotubes and myoblasts, higher incorporation into the PPP product ribulose-5-phosphate or into TCA cycle intermediates was measured in myoblasts and myotubes, respectively (Figure 3.10). Unexpectedly, myotubes and myoblasts did not show major differences of glucose metabolism through glycolysis in mass spectrometric analysis. Nevertheless, higher concentrations of lactic acid was found in the cell culture supernatant of myoblasts compared to myotubes irrespective of *T. gondii* infection suggesting indeed increased glycolysis in myoblasts than in myotubes (Blume & Lüder, unpublished). Although transcriptome analysis suggested higher expression of glycolytic enzymes in myotubes than in myoblasts, increased glycolytic activities in myoblasts was rather more expected because according to previous observations, myoblasts rely predominantly on glycolysis to provide rapid supply of energy (ATP) for their continuous proliferation (Leary *et al.*, 1998). The reason for the increased expression of glycolytic enzymes as observed here in myotubes is currently unknown. The evidences of higher TCA cycle activities in myotubes resemble results from other studies suggesting that differentiation of myoblasts into myotubes leads to a drastic increase of mitochondrial enzyme activities (Moyes *et al.*, 1997; Barbieri and Sestili, 2012). Transcriptome analysis of myotubes and myoblasts revealed higher expression of PC in myotubes (see above) suggesting higher influx of glucose-derived carbon atoms into the TCA cycle through replenishing the TCA cycle intermediate oxaloacetate (Figure 3.8D). It has to be stressed that GC-MS confirmed higher flux of glucose-derived carbon atoms via PC but not pyruvate dehydrogenase (PDH) complex pathway in myotubes as compared to myoblasts irrespective of *T. gondii* infection. This further suggested that myotubes channel glucose-derived carbon into TCA cycle through PC mediated TCA cycle anaplerosis. The functional significance of increased expression of glycogen metabolic enzymes was not validated by metabolomics and this would be an issue for future research.

A higher PPP activity in the proliferating myoblasts may be critical for providing sufficient amounts of ribose-5-phosphate to synthesize nucleotides and/or for providing the reducing equivalent NADPH for synthesis of macromolecules such as fatty acids and cholesterol. It may also be required for generating intermediates of glycolysis, i.e. glyceraldehyde-3-phosphate or fructose-6-phosphate through the non-oxidative phase of the PPP. Finally, it may serve maintaining cellular redox homeostasis by supplying reduced glutathione via NADPH (Barcia-Vieitez and Ramos-Martínez, 2014). The increased PPP activity in myoblasts as compared to myotubes correlates with the upregulation of enzymes of both

the oxidative and non-oxidative phases of the PPP in myoblasts as detected in the transcriptome analysis (see above). Importantly, infection with *T. gondii* did neither significantly modulate incorporation of glucose-derived carbon atoms into intermediates of the central carbohydrate metabolism nor gene expression of metabolic enzymes involved in these pathways except G6PDH2. Indeed, RNAseq analysis indicated up-regulation of that enzyme after infection of both myoblasts and to a lower extent also myotubes with *T. gondii*. However, this effect of *T. gondii* on G6PDH2 expression was not confirmed by RT-qPCR. The reasons for this discrepancy is not entirely clear (see above), but the measurement of ribulose-5-phosphate in infected versus non-infected myoblasts and myotubes did also not reveal any significant impact of the parasite. This suggests that even if *T. gondii* upregulates G6PDH2 expression in SkMCs, this appears do not affect the overall PPP activity. Together, transcriptome and metabolome analyses revealed clear differences between the central carbohydrate metabolism of myotubes and myoblasts whereas parasite infection did not considerably regulate metabolic traits of SkMCs. However, Blader and colleague previously showed *T. gondii*-mediated modulation of several glycolytic enzymes in HFF cells as for instance triose phosphate isomerase 1, phosphoglycerate kinase 1, phosphoglycerate mutase 1, and lactate dehydrogenase A (Blader et al. 2001). Findings in this study now suggest that *T. gondii* has only a minor, if any, impact on metabolic activities of myotubes and myoblasts.

Since myoblasts and myotubes significantly differed in their central carbohydrate metabolism, an important issue was then analyzing its impact on the differential *T. gondii* bradyzoite formation in both cell types. Among other factors, this study uncovered the impact of sodium-L-lactate on *T. gondii* bradyzoite differentiation in SkMCs. Transcriptome analysis indicated that lactate dehydrogenase-D was upregulated in myotubes compared to myoblasts irrespective of *T. gondii* infection. Lactate dehydrogenase-D is an important enzyme that catalyzes the reversible conversion of pyruvate to lactate, i.e. the last step of anaerobic glycolysis. Addition of lactate to the medium did not show any effect on *T. gondii* stage conversion in myotubes but it sustained bradyzoite differentiation in myoblasts. This is inconsistent with previous studies where lactate has been identified as a soluble metabolite that support parasite growth and inhibit *T. gondii* stage conversion in Vero cells but not in HFF cells which are normally permissive for bradyzoite differentiation under metabolic stress condition (Weilhammer *et al.*, 2012). The different impact of lactate on *T. gondii* stage conversion in Vero cells and

HFF cells was due to differences in efficient release of lactate through glucose catabolism in these cell types. Lactate-induced inhibition of *T. gondii* stage conversion was further confirmed after upregulation of glycolysis in permissive cells by either addition of glucose or by overexpression of the host kinase Akt (Weilhammer *et al.*, 2012). It is important to note that Weilhammer and colleagues investigated stress-induced stage conversion where lactate had an effect only in distinct cell types. The mechanism of lactate-induced stage conversion is not known but possibly other soluble mediators besides lactate are also involved in this process. Nevertheless, this study investigated spontaneous stage conversion of *T. gondii* in myotubes and lactate induced bradyzoite formation in myoblasts *in vitro*. Recently, Willkomm and colleagues demonstrated that lactate induces cell cycle withdrawal and initiates early but delays late differentiation of C2C12 myoblasts by increasing reactive oxygen species (Willkomm *et al.*, 2014). This could explain the finding of this study that lactate induced *T. gondii* bradyzoite differentiation in myoblasts, since *T. gondii* spontaneously convert from tachyzoites to bradyzoites in differentiated myotubes (Figure 3.1; Swierzy & Lüder 2014).

This study also uncovered the role of TCA cycle activities in *T. gondii* stage conversion in myotubes and myoblasts. TCA cycle was inhibited using phenyl acetic acid (PAA), an inhibitor of the PC which converts pyruvate into oxaloacetate, i.e. an important reaction of TCA cycle anaplerosis. Surprisingly, inhibition of PC slightly induced BAG1 mRNA expression in *T. gondii* residing within myotubes but not in those in myoblasts. This clearly suggests that increased fueling of pyruvate into the TCA cycle via PC as observed in myotubes is not important for triggering stage conversion of *T. gondii* in differentiated SkMCs. Importantly, the inhibition of the anaplerotic reaction exerted by the PC using PAA might not suffice for reducing total influx of glucose-derived carbon atoms into the TCA cycle because of the conventional conversion of pyruvate into citrate through the PDH complex. This view is indeed supported by our mass spectrometric analysis, indicating influx of glucose-derived carbon atoms into the TCA cycle through both the PC pathway and the PDH complex pathway. Thus, although myotubes channels carbon atoms derived from glucose more readily into the TCA cycle by an anaplerotic reaction than myoblasts, the inhibition of PC by PAA may not efficiently inhibit TCA cycle activities to subsequently reduce *T. gondii* stage conversion. Thus, increased total incorporation of carbon atoms into TCA cycle intermediates as observed in myotubes may nevertheless trigger *T. gondii* stage conversion. Interestingly, fueling of TCA cycle activities by

addition of the TCA cycle intermediate dimethyl- α -ketoglutarate (DMKG) indeed accelerated *T. gondii* BAG1 expression particularly in myoblasts and only to a lower extent in myotubes. Treatment of myoblasts with DMKG may hence have increased TCA cycle activities to levels as observed or similar to those observed in myotubes and this may have sustained *T. gondii* BAG1 expression in these cells. In contrast, further fueling of TCA cycle activities in myotubes might be inefficient to further support bradyzoite formation in *T. gondii*. It has to be mentioned that DMKG, although inducing BAG1 expression particularly in *T. gondii* residing in myoblasts, did not sustain tissue cyst formation. Thus, DMKG possibly accelerates only early steps of stage conversion in *T. gondii* but not later stages including cyst wall formation. How the inhibitors or modulators discussed above impact *T. gondii* stage conversion and whether they act on the host cells or the parasites carbohydrate metabolism needs to be further investigated in the future.

T. gondii stage conversion occurs spontaneously in myotubes which showed lower incorporation of glucose-derived carbon atoms into the PPP product ribulose-5-phosphate as compared to myoblasts. It was thus hypothesized that low PPP activities might have a role in inducing stage conversion or *vice versa* that increased PPP activities might favor parasite growth and inhibit parasite stage differentiation. In this study, a role of reduced PPP activities on *T. gondii* stage conversion has been established. Two structurally different inhibitors of critical PPP enzymes, namely dehydroepiandrosterone (DHEA) and 6-aminonicotinamide (6-AN) were used to inhibit PPP in *T. gondii*-infected myotubes and myoblasts. DHEA is a well-known uncompetitive inhibitor of the G6PDH, the rate limiting enzyme of the PPP (Gordon *et al.*, 1995; Schwartz and Pashko, 2004). 6-AN is a competitive inhibitor of NADP⁺-dependent enzyme 6-phosphogluconate dehydrogenase (Tyson *et al.*, 2000). Both inhibitors reduce intracellular NADPH levels by inhibiting the PPP in different cell types (Rawat *et al.*, 2012; Patel *et al.*, 2014). Herein, it was shown that inhibition of the PPP in *T. gondii*-infected myotubes and myoblasts using DHEA accelerated *T. gondii* BAG1 mRNA expression and tissue cyst formation and at the same time reduced parasite replication strongly indicating *T. gondii* stage conversion (Figure 3.13). A similar effect on *T. gondii* stage conversion was also found in myotubes and myoblasts treated with 6-AN to inhibit the 6-phosphogluconate dehydrogenase. Interestingly, the effect of DHEA and 6-AN was generally more pronounced on stage conversion of *T. gondii* in myoblasts although it was also measured in myotubes. This suggests that inhibiting the higher PPP activities as observed in myoblasts is more efficient

in inducing *T. gondii* stage conversion than a further decrease of the low PPP activities as observed in myotubes. The effect of DHEA on the inhibition of PPP has been demonstrated in myotubes and myoblasts by measuring NADPH. Reduced level of NADPH and higher ratios of $\text{NADP}^+/\text{NADPH}$ in DHEA-treated myotubes and myoblasts as compared to control confirmed the DHEA-mediated inhibition of PPP. Again, how these inhibitors impact stage conversion in *T. gondii* and whether they act on the host cell or rather the parasite itself needs further validation. However, the fact that two different inhibitors targeting different enzymes show similar results in these analyses rather argues for an effect via the validated targets of these drugs, i.e. on the mammalian enzymes but not the parasite enzymes.

Together, these functional results indicate that lower PPP and higher TCA cycle activities in myotubes can trigger *T. gondii* stage conversion in SkMCs.

4.4 Redox homeostasis modulate *T. gondii* stage conversion in SkMCs

The mechanism by which reduced PPP activities in myotubes support *T. gondii* stage conversion has also been investigated in this study. As discussed above, one of the main purposes of glucose metabolism through the PPP is the production of the reducing equivalent NADPH in the cytoplasm. Here, it was confirmed that the reduced PPP activities in myotubes lead to the production of lower levels of NADPH and higher $\text{NADP}^+/\text{NADPH}$ ratios as compared to myoblasts which catabolize more glucose through the PPP. Reduced levels of NADPH in myotubes may provide only insufficient cellular antioxidants, i.e. reduced glutathione for neutralization of ROS. It was therefore hypothesized that low levels of NADPH may lead to increased intracellular ROS in myotubes thereby affecting *T. gondii* stage conversion. Remarkably, this study revealed that ROS levels in myotubes were even lower as compared to myoblasts irrespective of *T. gondii* infection (Figure 3.20). However, this finding is consistent with other studies where the authors showed that differentiation of L6E9 myoblasts into myotubes is also accompanied by a decrease in intracellular ROS production (Lyons *et al.*, 2004; Jahnke *et al.*, 2009). Thus, despite harboring higher levels of NADPH as compared to myotubes, myoblasts showed increased intracellular ROS. Since myoblasts do not considerably sustain *T. gondii* stage conversion this clearly argues against a significant impact of the

higher ROS levels as observed in myoblasts in triggering parasite differentiation. The reason for higher ROS in myoblasts might be due to the high metabolic activity and the highly proliferative nature of the cells. Alternatively, high levels of cytosolic NADPH can act as substrate for the NADPH oxidase (NOX) to reduce molecular O₂ to superoxide anions (O₂⁻). This NADPH-dependent ROS production has been detected in skeletal muscle (Wang *et al.*, 2009; Barbieri and Sestili, 2012) and cardiac muscle (Heymes *et al.*, 2003). It has to be noted that intracellular ROS is considered an important regulatory factor in the differentiation of SkMCs (Barbieri and Sestili, 2012).

Although high levels of ROS do obviously not trigger stage conversion in *T. gondii* (see above), I wondered whether a distinct physiological range of concentrations of endogenous ROS has any impact on *T. gondii* stage conversion in myotubes. Modulation of endogenous ROS using the antioxidant N-acetyl cysteine (NAC) indeed inhibited bradyzoite-specific BAG1 mRNA expression and tissue cyst formation while supporting robust parasite replication (Figure 3.21). NAC is widely used as an antioxidant that scavenges intracellular ROS either by increasing levels of the cellular antioxidant reduced glutathione or by directly inactivating ROS through neutralization (Aruoma *et al.*, 1989; Lasram *et al.*, 2015). In previous studies, NAC has been recognized as effective antioxidant against the antitumor quinolone, 5-Nitroso-8-quinolinol (NSC3852) that also has anti-*T. gondii* activity *in vitro*. At low concentration (78.6 nM), NSC3852 is able to inhibit *T. gondii* tachyzoite growth in HFF cells by a ROS-dependent mechanism, since concomitant treatment with 5-20 mM NAC showed increased tachyzoite growth in presence of NSC3852 (Strobl *et al.*, 2009). In another study, it was shown that expression of the phosphoinositide-3-kinase (PI3K)/Akt-dependent NOX4 is required for controlling *T. gondii* proliferation by human retinal pigment epithelial cells. Consequently, decreasing ROS production using siRNA-mediated knockdown of host NOX4 strongly supported *T. gondii* replication (Zhou *et al.*, 2013). However, whether the increased parasite growth as observed in these studies after NAC treatment or NOX4 knockdown is accompanied with a decrease in bradyzoite formation has not been tested. Nevertheless, these results provide a clear link between ROS and *T. gondii* growth and this study also provides evidence that decreasing ROS in SkMCs by using NAC favor parasite growth and inhibits bradyzoite formation. It has to be stressed that NAC had not any direct effect on parasite for this inhibition of stage conversion as NAC showed increased BAG1 mRNA expression in extracellular *T. gondii*. The possible mechanism of ROS on inhibition of *T. gondii*

replication and induction of stage conversion could be explained by two ways. Firstly, ROS as for instance oxygen superoxide can react with essential lipids, proteins and nucleic acids of the parasite which may lead to parasite growth inhibition and induction of stage conversion. Secondly, low concentrations of ROS act as signaling molecules in various biological pathways as for instance the phosphoinositide-3-kinase (PI3K)/Akt pathway, the nuclear factor kappa-beta (NF- κ B) and mitogen-activated protein kinase (MAPK) pathways or may activate insulin like growth factor (IGF)-1 and peroxisome proliferator-activated receptor-gamma coactivator 1 alpha (PGC1- α) to control host or parasite gene expression which may affect *T. gondii* growth and stage conversion (Barbieri and Sestili, 2012; Zhang *et al.*, 2016).

Another antioxidant was also used in this study to further confirm an effect of ROS on *T. gondii* bradyzoite differentiation. Tiron (4,5- dihydroxy-1,3-benzene-disulfonic acid) has been selected because tiron is a vitamin E analog that can scavenge ROS by directly neutralizing hydroxyl radicals (\bullet OH) and superoxide anions (O_2^-). Tiron can also protect cells from oxidative stress by chelating metal ions (Krishna *et al.*, 1992). Surprisingly, data showed that tiron even accelerated BAG1 mRNA expression but not tissue cyst formation in both myotubes and myoblasts. Thus, with regard to BAG1 mRNA expression, tiron exerted an opposite effect on *T. gondii* than NAC. However, it was subsequently recognized that tiron at increased concentrations completely halted parasite cell cycle progression and also host cell proliferation. This suggested that tiron-induced BAG1 expression is not due to its effect on ROS modulation in the host cell, but rather to the inhibition of host and parasite replication. It has been previously reported that tiron inhibits cell cycle progression by increasing the percentage of cells in S-phase of cell cycle (Monticone *et al.*, 2014).

In addition to the NAC experiments discussed above, an additional functional link between ROS production and *T. gondii* stage conversion in myotubes has been established in this study. Thus, increasing ROS levels using the chemical agent luperox dose-dependently induced *T. gondii* BAG1 mRNA expression and tissue cyst formation in both myotubes and myoblasts. In addition, such stage differentiation was accompanied by reduced parasite growth. Similar effects of oxidants on *T. gondii* BAG1 mRNA expression were observed after treatment with another ROS inducing agent, i.e. H_2O_2 . Thus, increasing ROS in SkMCs can accelerate bradyzoite formation whereas scavenging ROS favors parasite

growth and reduces bradyzoite formation. Taken together, these studies suggest that host cell mediated endogenous ROS at physiological concentrations may trigger *T. gondii* stage conversion in myotubes.

4.5 Host cell cycle and its impact on *T. gondii* bradyzoite differentiation in SkMCs

Recently, it has been established that cell cycle withdrawal in myotubes is accompanied by increased expression of Testis specific Y-encoded like protein2 (Tspyl2) mRNA and thereby supports *T. gondii* bradyzoite differentiation and tissue cyst formation as observed in myotubes. Importantly, inhibiting host cell cycle withdrawal by knockdown of Tspyl2 abrogated bradyzoite formation in myotubes (Swierzy and Lüder, 2014). Since differential cell cycle regulation was also identified herein as a major difference in the transcriptomes of *T. gondii*-infected myotubes and myoblasts, the impact of the host cell cycle on *T. gondii* bradyzoite differentiation has been further investigated in this study. Indeed, the cell cycle is one of the major differences between terminally differentiated SkMCs, i.e. myotubes and its proliferating precursors, i.e. myoblasts (Shen *et al.*, 2003). Myotubes are permanently arrested at G1/G0 phase and this is also accompanied by the muscle differentiation process. Therefore, two different pharmacological cell cycle inhibitors, aphidicolin (APH) and mimosine (MIM) were selected to inhibit host cell proliferation in SkMCs and to thereby investigate their impact on *T. gondii* stage conversion in myotubes and myoblasts. APH and MIM are well-known reversible late G1/S inhibitors that have been used for studying different parasite-infected host cells (Bohne *et al.*, 1994; Naughton and Bell, 2007). Whereas APH prevents cell proliferation by inhibiting DNA polymerase- α (Krokan *et al.*, 1981), MIM, a plant-derived non-protein amino acid, blocks DNA synthesis by decreasing the cellular dNTP concentration through regulation of the ribonucleotide reductase (Dai *et al.*, 1994; Gilbert *et al.*, 1995). Herein, it was observed that *T. gondii* residing in both myotubes and myoblasts upregulated BAG1 mRNA expression in presence of APH and MIM (Figure 3.27A). Furthermore, APH and MIM inhibited both host and parasite cell cycle progression thereby leading to the induction of bradyzoite differentiation. However, from the results it was difficult to decide whether the both inhibitors triggered bradyzoite formation via inhibiting the host cell cycle or via a direct effect on parasite replication. Indeed, immunofluorescence analysis confirmed that parasite

replication was completely blocked in myotubes and myoblasts particularly at higher concentrations of these inhibitors. This resembles findings of Shaw and colleagues who showed that *T. gondii* DNA replication is blocked by these drugs even after a short treatment (Shaw *et al.*, 2001). Surprisingly, *T. gondii* tissue cyst formation was only induced by moderate concentrations of APH and MIM but was similar to control levels when treated with higher concentrations of the inhibitors. Thus, the relatively low number of tissue cysts as observed after treatment of myoblasts and myotubes with high concentrations of both cell cycle inhibitors appears to be inconsistent with the strongly increased BAG1 mRNA expression. It might indicate that *T. gondii* stage conversion as observed in the presence of APH and MIM is not only due to inhibiting the host cell cycle but possibly also to a direct effect on the parasite. Since reduced cell cycle progression is required for bradyzoite formation, this could increase BAG1 expression in APH- and MIM-treated myotubes and myoblasts. But exactly how APH and MIM induce bradyzoite differentiation in SkMCs through directly affecting the parasite is currently unknown.

This study highlighted that several cell cycle inhibitors including p21^{Waf1/Cip1} were upregulated in myotubes after 7 days of differentiation from myoblasts by differentiation medium containing 2% horse serum. P21 mRNA expression was 6.7-fold higher in myotubes as compared to myoblasts irrespective of infection as revealed by RNAseq. Similar patterns of increased expression of p21 in myotubes were also observed by RT-qPCR. P21 is an important cell cycle inhibitor of the CIP/KIP family that can inhibit proliferation at the G1 or G2 phase of the cell cycle by inactivating different cyclin-CDK complexes (Baus *et al.*, 2003; Gillis *et al.*, 2009). In addition, p21 has a strong affinity to bind with PCNA which is an essential cofactor of the DNA polymerase and thereby inhibits DNA synthesis in the S-phase of the cell cycle (Podust *et al.*, 1995; Gulbis *et al.*, 1996). The up-regulation of p21 in myotubes as compared to myoblasts irrespective of *T. gondii* infection accords with previous studies where p21 was highly regulated in the course of C2C12 differentiation (Shen *et al.*, 2003; Swierzy and Lüder, 2014). It clearly correlates with the fact that myotubes but not myoblasts are cell cycle arrested, terminally differentiated cells. Consequently, small interfering RNA (siRNA)-mediated knockdown of p21 in C2C12 myoblasts demonstrated that p21 is essential for myoblasts differentiation into myotubes. Indeed, p21-deficient myoblasts did not express myosin heavy chain (MyHC), a common marker of muscle differentiation thereby clearly indicating inhibition of myotubes formation. It has been shown that p21 deficiency increases cell cycle

progression and muscle cell proliferation in p21 knockout mice thereby delaying regeneration of skeletal muscle tissue after injury (Chinzei *et al.*, 2015). In contrast, *in vitro* studies have shown that p21 suppression does not impact on differentiation and fusion of primary mouse myoblasts into myotubes (Biferi *et al.*, 2015). In knockout mice, double mutants of p21 and p57 were required for inhibition of skeletal muscle differentiation while neither single mutant showed an effect on the differentiation process (Zhang *et al.*, 1999). These findings reinforce the conclusion that loss of p21 expression can be compensated by other cell cycle inhibitors including p57 and is not the only cell cycle regulator required for skeletal muscle differentiation.

Remarkably, p21 knockdown in SkMCs supported robust parasite replication but surprisingly did not inhibit BAG1 mRNA expression and tissue cysts formation. Conversely, p21 knockdown even induced BAG1 mRNA expression. This suggests that expression of the host cell cycle regulator p21 significantly regulates parasite growth but not *T. gondii* stage conversion. Surprisingly, higher parasite replication did not correlate with *T. gondii* BAG1 expression and tissue cysts formation. A previous study showed that reduced parasite replication is required for *T. gondii* stage conversion (Bohne *et al.*, 1994). Expression of BAG1 mRNA and sustained parasite growth might be due to the presence of a population of 'intermediate' bradyzoites which express both tachyzoite and bradyzoite markers and show 85% subpopulation at late S/G2 phase of the parasite cell cycle. Only mature bradyzoites arrest their cell cycle at the G1 or G0 phase, thereby developing into the non-replicating or slowly replicating parasite form (Radke *et al.*, 2003). However, to find out the exact mechanism of this unexpected result of increased BAG1 mRNA expression and concomitant parasite replication, p21 knockdown myoblasts and wildtype cells can be used to investigate in further detail the cell cycle stage of highly proliferative parasites that at the same time express relatively high levels of BAG1.

In a previous study by Swierzy and colleagues, the authors showed that knockdown of the host cell cycle regulator Tspyl2, i.e. an upstream molecule of p21 inhibits myotubes formation and concomitantly inhibits bradyzoite differentiation. At the same time, parasite replication was strongly supported by knockdown of Tspyl2 in SkMCs (Swierzy and Lüder, 2014). In another study, the human orthologue of Tspyl2, namely cell division autoantigen (CDA)-1 was identified as inhibitor of cell growth and proliferation by upregulation of p21 through either p53- or pERK1/2-dependent mechanisms (Tu *et al.*,

2007; Toh *et al.*, 2010). Therefore, the analysis of p21 knockdown in SkMCs as reported here now provides evidence that the function of Tspyl2 on *T. gondii* stage differentiation is mediated by a p21-independent mechanism. In addition to inhibition of the cell cycle, knockdown of Tspyl2 has been shown to inhibit differentiation of proliferating C2C12 myoblasts into poly-nucleated myotubes (Swierzy and Lüder, 2014). Furthermore, Tspyl2 also functions as a nucleosome assembly protein (NAP) thereby regulating gene expression in another terminally differentiated and cell cycle arrested cell type, i.e. neurons by interacting with calmodulin-associated serine/threonine kinase (Wang *et al.*, 2004; Tsang *et al.*, 2014). Recently, Tspyl2 has been identified as a positive regulator of transforming growth factor (TGF)- β dependent cell cycle arrest in human HaCaT cells through interacting with the transcriptional complex REST (Epping *et al.*, 2015). Therefore, the role of Tspyl2 on host cell cycle regulation and on *T. gondii* stage conversion in SkMCs may relate to these pathways as well. Which of these other Tspyl2-dependent pathways might regulate *T. gondii* stage conversion remains currently unclear and is an important issue for further analysis.

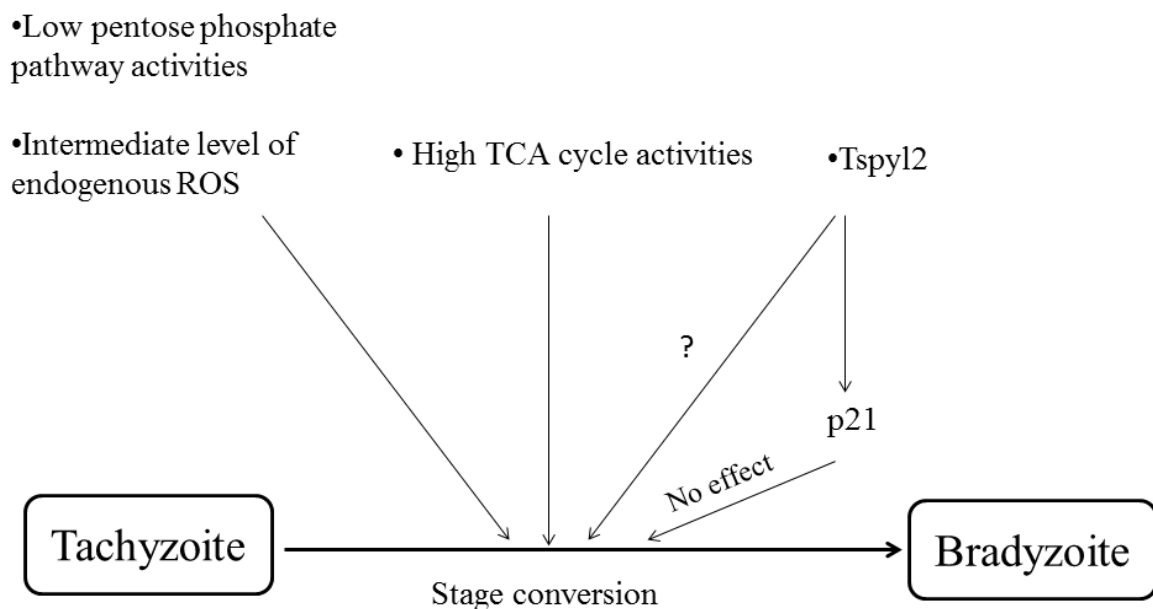


Figure 4.1: Scheme on factors that induce *T. gondii* bradyzoite differentiation in myotubes

Together, the results of the study establish that metabolic traits of myotubes as a reduced PPP activity, increased TCA cycle activities and distinct levels of endogenous ROS as observed in myotubes may impact *T. gondii* differentiation to the bradyzoite stage (Figure 4.1). Furthermore, it shows that *T. gondii* stage conversion in SkMCs occurs in a host cell p21-independent manner and suggests that Tspyl2 regulates bradyzoite formation by other means than p21 (Figure 4.1). However, the molecular mechanisms of how these factors regulate *T. gondii* stage differentiation in SkMCs needs to be further investigated in the future.

Chapter 5: References

1. **Abmayr, S. M. and Pavlath, G. K.** (2012) 'Myoblast fusion: lessons from flies and mice'. *Development*, 139(4), pp. 641–656.
2. **Acharya, S., Peters, A. M., Norton, A. S., Murdoch, G. K. and Hill, R. A.** (2013) 'Change in Nox4 expression is accompanied by changes in myogenic marker expression in differentiating C2C12 myoblasts'. *European Journal of Physiology*, 465(8), pp. 1181–1196.
3. **Aguilar, V. and Fajas, L.** (2010) 'Cycling through metabolism'. *EMBO Molecular Medicine*, 2(9), pp. 338–348.
4. **Aigner, C. P., Silva, A. V. da, Sandrini, F., Osório, P. de S., Poiares, L. and Largura, A.** (2010) 'Real-time PCR-based quantification of *Toxoplasma gondii* in tissue samples of serologically positive outdoor chickens'. *Memórias do Instituto Oswaldo Cruz*, 105(7), pp. 935–937.
5. **Ajzenberg, D., Cogné, N., Paris, L., Bessières, M., Thulliez, P., Filisetti, D., Pelloux, H., Marty, P. and Dardé, M.** (2002) 'Genotype of 86 *Toxoplasma gondii* Isolates Associated with Human Congenital Toxoplasmosis, and Correlation with Clinical Findings'. *The Journal of Infectious Diseases*, 186(5), pp. 684–689.
6. **Ajzenberg, D., Yera, H., Marty, P., Paris, L., Dalle, F., Menotti, J., Aubert, D., Franck, J., Bessières, M., Quinio, D., Pelloux, H., Delhaes, L., Desbois, N., Thulliez, P., Robert Gangneux, F., et al.** (2009) 'Genotype of 88 *Toxoplasma gondii* Isolates Associated with Toxoplasmosis in Immunocompromised Patients and Correlation with Clinical Findings'. *The Journal of Infectious Diseases*, 199(8), pp. 1155–1167.
7. **Araujo, F. G., Huskinson-Mark, J., Gutteridge, W. E. and Remington, J. S.** (1992) 'In vitro and in vivo activities of the hydroxynaphthoquinone 566C80 against the cyst form of *Toxoplasma gondii*.' *Antimicrobial Agents and Chemotherapy*, 36(2), pp. 326–330.
8. **Aruoma, O. I., Halliwell, B., Hoey, B. M. and Butler, J.** (1989) 'The antioxidant action of N-acetylcysteine: its reaction with hydrogen peroxide, hydroxyl radical, superoxide, and hypochlorous acid.' *Free Radical Biology & Medicine*, 6(6), pp. 593–597.
9. **Aubert, D., Ajzenberg, D., Richomme, C., Gilot-Fromont, E., Terrier, M. E., de Gevigney, C., Game, Y., Maillard, D., Gibert, P., Dardé, M. L. and Villena, I.** (2010) 'Molecular and biological characteristics of *Toxoplasma gondii* isolates from wildlife in France'. *Veterinary Parasitology*, 171(3–4), pp. 346–349.
10. **Bahl, J. J., Defronzo, A. and Bressler, R.** (1997) 'In Vitro and In Vivo Suppression of Gluconeogenesis by Inhibition of Pyruvate Carboxylase'. *Biochemical Pharmacology*, 53(1), pp. 67–74.

11. **Barbieri, E. and Sestili, P.** (2012) 'Reactive oxygen species in skeletal muscle signaling.' *Journal of SignalTransduction*, 2012(12), pp. 982794.
12. **Barcan, L. A., Dallurzo, M. L., Clara, L. O., Valledor, A., Macias, S., Zorkin, E., Gerona, S., Livellara, B., Barcan, L. A., Dallurzo, M. L., Clara, L. O., Valledor, A., Macias, S., Zorkin, E., Gerona, S., et al.** (2002) 'Toxoplasma gondii pneumonia in liver transplantation: survival after a severe case of reactivation'. *Transplant Infectious Disease*, 4(2), pp. 93–96.
13. **Barcia-Vieitez, R. and Ramos-Martínez, J. I.** (2014) 'The regulation of the oxidative phase of the pentose phosphate pathway: New answers to old problems'. *IUBMB Life*, 66(11), pp. 775–779.
14. **Barja, G.** (1999) 'Mitochondrial oxygen radical generation and leak: sites of production in states 4 and 3, organ specificity, and relation to aging and longevity.' *Journal of Bioenergetics and Biomembranes*, 31(4), pp. 347–366.
15. **Baum, J., Tim-WolfGilberger, Freddy Frischknecht and MarkusMeissner** (2008) 'Host-cell invasion by malaria parasites: insights from Plasmodium and Toxoplasma'. *Trends in Parasitology*, 24(12), pp. 557–563.
16. **Baus, F., Gire, V., Fisher, D., Piette, J. and Dulić, V.** (2003) 'Permanent cell cycle exit in G2 phase after DNA damage in normal human fibroblasts'. *The EMBO Journal*, 22(15), pp. 3992–4002.
17. **Bentzinger, C. F., Wang, Y. X. and Rudnicki, M. A.** (2012) 'Building muscle: molecular regulation of myogenesis.' *Cold Spring Harbor Perspectives in Biology*, 4(2), pp. a008342.
18. **Biferi, M. G., Nicoletti, C., Falcone, G., Puggioni, E. M. R., Passaro, N., Mazzola, A., Pajalunga, D., Zaccagnini, G., Rizzuto, E., Auricchio, A., Zentilin, L., De Luca, G., Giacca, M., Martelli, F., Musio, A., et al.** (2015) 'Proliferation of multiple cell types in the skeletal muscle tissue elicited by acute p21 suppression'. *Molecular Therapy*, 23(5), pp. 885–895.
19. **Blader, I. J. and Koshy, A. A.** (2014) 'Toxoplasma gondii Development of Its Replicative Niche: in Its Host Cell and Beyond'. *Eukaryotic Cell*, 13(8), pp. 965–976.
20. **Blader, I. J., Manger, I. D. and Boothroyd, J. C.** (2001) 'Microarray Analysis Reveals Previously Unknown Changes in Toxoplasma gondii-infected Human Cells'. *Journal of Biological Chemistry*, 276(26), pp. 24223–24231.
21. **Blume, M., Nitzsche, R., Sternberg, U., Gerlic, M., Masters, S. L. L., Gupta, N. and McConville, M. J. J.** (2015) 'A Toxoplasma gondii Gluconeogenic Enzyme Contributes to Robust Central Carbon Metabolism and Is Essential for Replication and Virulence'. *Cell Host & Microbe*, 18(2), pp. 210–220.

22. **Blume, M., Rodriguez-Contreras, D., Landfear, S., Fleige, T., Soldati-Favre, D., Lucius, R. and Gupta, N.** (2009) 'Host-derived glucose and its transporter in the obligate intracellular pathogen *Toxoplasma gondii* are dispensable by glutaminolysis.' *Proceedings of the National Academy of Sciences*, 106(31), pp. 12998–13003.
23. **Bohne, W., Heesemann, J. and Gross, U.** (1993) 'Induction of bradyzoite-specific *Toxoplasma gondii* antigens in gamma interferon-treated mouse macrophages'. *Infection and Immunity*, 61(3), pp. 1141–1145.
24. **Bohne, W., Heesemann, J. and Gross, U.** (1994) 'Reduced Replication of *Toxoplasma gondii* Is Necessary for Induction of Bradyzoite-Specific Antigens: a Possible Role for Nitric Oxide in Triggering Stage Conversion'. *Infection and Immunity*, 62(5), pp. 1761–1767.
25. **Brown, D. M., Parr, T. and Brameld, J. M.** (2012) 'Myosin heavy chain mRNA isoforms are expressed in two distinct cohorts during C2C12 myogenesis.' *Journal of Muscle Research and Cell Motility*, 32(6), pp. 383–90.
26. **Broxmeyer, H. E., Franklin, D. S., Cooper, S., Hangoc, G. and Mantel, C.** (2012) 'Cyclin Dependent Kinase Inhibitors Differentially Modulate Synergistic Cytokine Responsiveness of Hematopoietic Progenitor Cells'. *Stem Cells and Development*, 21(10), pp. 1597–1603.
27. **De Buhr, K., Ludewig, M. and Fehlhaber, K.** (2008) 'Toxoplasma gondii-seroprevalence – current results in German swine herds'. *Journal of Food Safety and Food Quality*, 59(1), pp. 5–8.
28. **Bunz, F., Dutriaux, A., Lengauer, C., Waldman, T., Zhou, S., Brown, J. P., Sedivy, J. M., Kinzler, K. W. and Vogelstein, B.** (1998) 'Requirement for p53 and p21 to sustain G2 arrest after DNA damage.' *Science*, 282(5393), pp. 1497–501.
29. **Burattini, S., Ferri, R., Battistelli, M., Curci, R., Luchetti, F. and Falcieri, E.** (2004) 'C2C12 murine myoblasts as a model of skeletal muscle development: Morpho-functional characterization'. *European Journal of Histochemistry*, 48(3), pp. 223–233.
30. **Casadei, L., Vallorani, L., Gioacchini, A. M., Guescini, M., Burattini, S., D'Emilio, A., Biagiotti, L., Falcieri, E. and Stocchi, V.** (2009) 'Proteomics-based investigation in C2C12 myoblast differentiation.' *European Journal of Histochemistry*, 53(4), pp. 261–268.
31. **Charron, A. J. and Sibley, L. D.** (2002) 'Host cells: mobilizable lipid resources for the intracellular parasite *Toxoplasma gondii*.' *Journal of Cell Science*, 115(15), pp. 3049–3059.

32. **Chaudhary, K., Darling, J. A., Fohl, L. M., Sullivan, W. J., Donald, R. G. K., Pfefferkorn, E. R., Ullman, B. and Roos, D. S.** (2004) 'Purine Salvage Pathways in the Apicomplexan Parasite *Toxoplasma gondii*'. *Journal of Biological Chemistry*, 279(30), pp. 31221–31227.
33. **Chaudhary, K. and Roos, D. S.** (2005) 'Protozoan genomics for drug discovery'. *Nature Biotechnology*, 23(9), pp. 1089–1091.
34. **Chinzei, N., Hayashi, S., Ueha, T., Fujishiro, T., Kanzaki, N., Hashimoto, S., Sakata, S., Kihara, S., Haneda, M., Sakai, Y., Kuroda, R. and Kurosaka, M.** (2015) 'P21 deficiency delays regeneration of skeletal muscular tissue'. *PLoS ONE*, 10(5), pp. 1–14.
35. **Cook, A. J., Gilbert, R. E., Buffolano, W., Zufferey, J., Petersen, E., Jenum, P. A., Foulon, W., Semprini, A. E. and Dunn, D. T.** (2000) 'Sources of toxoplasma infection in pregnant women: European multicentre case-control study'. *British Medical Journal (Clinical Research Ed.)*, 321(7254), pp. 142–147.
36. **Cook, T., Roos, D., Morada, M., Zhu, G., Keithly, J. S., Feagin, J. E., Wu, G. and Yarlett, N.** (2007) 'Divergent polyamine metabolism in the Apicomplexa'. *Microbiology*, 153(4), pp. 1123–1130.
37. **Coppens, I. and Joiner, K. A.** (2003) 'Host but not parasite cholesterol controls *Toxoplasma* cell entry by modulating organelle discharge.' *Molecular Biology of the Cell*, 14(9), pp. 3804–20.
38. **Crawford, M. J., Thomsen-Zieger, N., Ray, M., Schachtner, J., Roos, D. S. and Seeber, F.** (2006) '*Toxoplasma gondii* scavenges host-derived lipoic acid despite its de novo synthesis in the apicoplast'. *The EMBO Journal*, 25(13), pp. 3214–3222.
39. **Curci, R., Battistelli, M., Burattini, S., D'Emilio, A., Ferri, P., Lattanzi, D., Ciuffoli, S., Ambrogini, P., Cuppini, R. and Falcieri, E.** (2008) 'Surface and inner cell behaviour along skeletal muscle cell in vitro differentiation'. *Micron*, 39(7), pp. 843–851.
40. **Dai, Y., Gold, B., Vishwanatha, J. K. and Rhode, S. L.** (1994) 'Mimosine Inhibits Viral DNA Synthesis through Ribonucleotide Reductase'. *Virology*, 205(1), pp. 210–216.
41. **Daniel, C. R., Cross, A. J., Koebnick, C. and Sinha, R.** (2011) 'Trends in meat consumption in the USA.' *Public Health Nutrition*, 14(4), pp. 575–83.
42. **Davies, K. J., Quintanilha, A. T., Brooks, G. A. and Packer, L.** (1982) 'Free radicals and tissue damage produced by exercise.' *Biochemical and Biophysical Research Communications*, 107(4), pp. 1198–205.

43. **Deshmukh, A. S., Murgia, M., Nagaraj, N., Treebak, J. T., Cox, J. and Mann, M.** (2015) 'Deep proteomics of mouse skeletal muscle enables quantitation of protein isoforms, metabolic pathways, and transcription factors.' *Molecular & Cellular Proteomics*, 14(4), pp. 841–53.
44. **Dubey, J. P.** (1997) 'Bradyzoite-induced murine toxoplasmosis: stage conversion, pathogenesis, and tissue cyst formation in mice fed bradyzoites of different strains of *Toxoplasma gondii*.' *The Journal of Eukaryotic Microbiology*, 44(6), pp. 592–602.
45. **Dubey, J. P.** (1998) 'Advances in the life cycle of *Toxoplasma gondii*.' *International Journal for Parasitology*, 28(7), pp. 1019–24.
46. **Dubey, J. P.** (2010a) 'Toxoplasma gondii Infections in Chickens (*Gallus domesticus*): Prevalence, Clinical Disease, Diagnosis and Public Health Significance'. *Zoonoses and Public Health*, 57(1), pp. 60–73.
47. **Dubey, J. P.** (2010b) 'Toxoplasmosis of animals and humans'. *CRC Press* 336. 2nd edition, pp. 49.
48. **Dubey, J. P. and Frenkel, J. K.** (1972) 'Cyst-induced toxoplasmosis in cats.' *The Journal of Protozoology*, 19(1), pp. 155–177.
49. **Dubey, J. P., Hill, D. E., Jones, J. L., Hightower, A. W., Kirkland, E., Roberts, J. M., Marcet, P. L., Lehmann, T., Vianna, M. C. B., Miska, K., Sreekumar, C., Kwok, O. C. H., Shen, S. K. and Gamble, H. R.** (2005) 'Prevalence of viable *Toxoplasma gondii* in beef, chicken, and pork from retail meat stores in the United States: risk assessment to consumers.' *Journal of Parasitology*, 91(5), pp. 1082–1093.
50. **Dubey, J. P., Hill, D. E., Rozeboom, D. W., Rajendran, C., Choudhary, S., Ferreira, L. R., Kwok, O. C. H. and Su, C.** (2012) 'High prevalence and genotypes of *Toxoplasma gondii* isolated from organic pigs in northern USA'. *Veterinary Parasitology*, 188(1–2), pp. 14–18.
51. **Dubey, J. P., Lindsay, D. S. and Speer, C. A.** (1998) 'Structures of *Toxoplasma gondii* Tachyzoites, Bradyzoites, and Sporozoites and Biology and Development of Tissue Cysts'. *Clinical Microbiology Review*, 11(2), pp. 267–267.
52. **Dubey, J. P., Rajendran, C., Ferreira, L. R., Martins, J., Kwok, O. C. H., Hill, D. E., Villena, I., Zhou, H., Su, C. and Jones, J. L.** (2011) 'High prevalence and genotypes of *Toxoplasma gondii* isolated from goats, from a retail meat store, destined for human consumption in the USA'. *International Journal for Parasitology*, 41(8), pp. 827–833.
53. **Dunn, D., Wallon, M., Peyron, F., Petersen, E., Peckham, C. and Gilbert, R.** (1999) 'Mother-to-child transmission of toxoplasmosis: risk estimates for clinical counselling'. *The Lancet*, 353(9167), pp. 1829–1833.

54. **Dzierszinski, F., Nishi, M., Ouko, L. and Roos, D. S.** (2004) 'Dynamics of *Toxoplasma gondii* differentiation.' *Eukaryotic cell*, 3(4), pp. 992–1003.
55. **Elkalaf, M., Andě L, M. and Trnka, J.** (2013) 'Low Glucose but Not Galactose Enhances Oxidative Mitochondrial Metabolism in C2C12 Myoblasts and Myotubes'. *PLoS ONE*, 8(8), pp. e70772.
56. **Epping, M. T., Lunardi, A., Nachmani, D., Castillo-Martin, M., Thin, T. H., Cordon-Cardo, C. and Pandolfi, P. P.** (2015) 'TSPYL2 is an essential component of the REST/NRSF transcriptional complex for TGFβ signaling activation.' *Cell Death and Differentiation*, 22(8), pp. 1353–62.
57. **Fajas, L.** (2013) 'Re-thinking cell cycle regulators: the cross-talk with metabolism'. *Frontiers in Oncology*, 3(4), pp. 1–6.
58. **Ferguson, D.** (2002) 'Toxoplasma gondii and sex: essential or optional extra?' *Trends in Parasitology*, 18(8), pp. 355–359.
59. **Ferguson, D.** (2004) 'Use of molecular and ultrastructural markers to evaluate stage conversion of *Toxoplasma gondii* in both the intermediate and definitive host'. *International Journal for Parasitology*, 34(3), pp. 347–360.
60. **Ferguson, D., Huskinson-Markt, J., Araujot, F. G. and Remington, J. S.** (1994) 'An ultrastructural study of the effect of treatment with atovaquone in brains of mice chronically infected with the ME49 strain of *Toxoplasma gondii*'. *International Journal of Experimental Pathology*, 75(2), pp. 111–116.
61. **Ferreira-da-Silva, M. F., Rodrigues, R. M., Andrade, E. F. De, Carvalho, L. De, Gross, U., Lüder, C. G. K. and Barbosa, H. S.** (2009) 'Spontaneous stage differentiation of mouse-virulent *Toxoplasma gondii* RH parasites in skeletal muscle cells : an ultrastructural evaluation'. *Mem Inst Oswaldo Cruz, Rio de Janeiro*, 104(2), pp. 196–200.
62. **Ferreira da Silva, M. da F., Barbosa, H. S., Groß, U., Lüder, C. G. K., Ho-Yen, D. O., Tomavo, S., Dubremetz, J. F. and Angel, S. O.** (2008) 'Stress-related and spontaneous stage differentiation of *Toxoplasma gondii*'. *Molecular BioSystems*, 4(8), pp. 824–834.
63. **Flegr, J., Prandota, J., Sovičková, M. and Israili, Z. H.** (2014) 'Toxoplasmosis - A global threat. Correlation of latent toxoplasmosis with specific disease burden in a set of 88 countries'. *PLoS ONE*, 9(3), pp. e90203.
64. **Fouts, A. E., Boothroyd, J. C., Fouts, A. E. and Boothroyd, J. C.** (2007) 'Infection with *Toxoplasma gondii* Bradyzoites Has a Diminished Impact on Host Transcript Levels Relative to Tachyzoite Infection'. *Infection and Immunity*, 75(2), pp. 634–642.

65. **Fox, B. A., Gigley, J. P. and Bzik, D. J.** (2004) 'Toxoplasma gondii lacks the enzymes required for de novo arginine biosynthesis and arginine starvation triggers cyst formation'. *International Journal for Parasitology*, 34(3), pp. 323–331.
66. **Fulco, M., Cen, Y., Zhao, P., Hoffman, E. P., McBurney, M. W., Sauve, A. A. and Sartorelli, V.** (2008) 'Glucose Restriction Inhibits Skeletal Myoblast Differentiation by Activating SIRT1 through AMPK-Mediated Regulation of Nampt'. *Developmental Cell*, 14(5), pp. 661–673.
67. **Fux, B., Nawas, J., Khan, A., Gill, D. B., Su, C. and Sibley, L. D.** (2007) 'Toxoplasma gondii Strains Defective in Oral Transmission Are Also Defective in Developmental Stage Differentiation'. *Infection and Immunity*, 75(5), pp. 2580–2590.
68. **Gail, M., Gross, U. and Bohne, W.** (2001) 'Transcriptional profile of Toxoplasma gondii-infected human fibroblasts as revealed by gene-array hybridization.' *Molecular Genetics and Genomics*, 265(5), pp. 905–912.
69. **Gail, M., Gross, U. and Bohne, W.** (2004) 'Transferrin receptor induction in Toxoplasma gondii-infected HFF is associated with increased iron-responsive protein 1 activity and is mediated by secreted factors'. *Parasitology Research*, 94(3), pp. 233–239.
70. **Gaster, M.** (2010) 'Substrate overload: Glucose oxidation in human myotubes conquers palmitate oxidation through anaplerosis'. *Biochemical and Biophysical Research Communications*, 391(3), pp. 1369–1373.
71. **Gilbert, D., Neilson, A., Miyazawa, H., DePamphilis, M. and Burhans, W.** (1995) 'Mimosine arrests DNA synthesis at replication forks by inhibiting deoxyribonucleotide metabolism'. *Journal of Biological Chemistry*, 270(16), pp. 9597–9606.
72. **Gillis, L. D., Leidal, A. M., Hill, R. and Lee, P. W. K.** (2009) 'p21Cip1/WAF1 mediates cyclin B1 degradation in response to DNA damage'. *Cell Cycle*, 8(2), pp. 253–256.
73. **Goebel, S., Gross, U. and Lüder, C. G. K.** (2001) 'Inhibition of host cell apoptosis by Toxoplasma gondii is accompanied by reduced activation of the caspase cascade and alterations of poly (ADP-ribose) polymerase expression'. *Journal of Cell Science*, 114(19), pp. 3495–3505.
74. **Gordon, G., Mackow, M. C. and Levy, H. R.** (1995) 'On the Mechanism of Interaction of Steroids with Human Glucose 6-Phosphate Dehydrogenase'. *Archives of Biochemistry and Biophysics*, 318(1), pp. 25–29.
75. **Gottlieb, E.** (2011) 'P53 Guards the Metabolic Pathway Less Travelled.' *Nature Cell Biology*, 13(3), pp. 195–197.

76. **Grabiec, K., Blaszczyk, M., Milewska, M., Gajewska, M. and Grzelkowska-Kowalczyk, K.** (2014) 'The Effect of High Glucose on Mechanisms Controlling Proliferation of Mouse C2C12 Myoblasts'. *International Journal of Diabetes & Clinical Diagnosis*, 1(106), pp. 1–5.
77. **Gross, U., Holpert, M. and Goebel, S.** (2004) 'Impact of stage differentiation on diagnosis of toxoplasmosis'. *Ann Ist Super Sanita*, 40(1), pp. 65–70.
78. **Gross, U., Muller, W. A., Knapp, S. and Heesemann, J.** (1991) 'Identification of a virulence-associated antigen of *Toxoplasma gondii* by use of a mouse monoclonal antibody'. *Infection and Immunity*, 59(12), pp. 4511–4516.
79. **Gross, U. and Pohl, F.** (1996) 'Influence of antimicrobial agents on replication and stage conversion of *Toxoplasma gondii*.' *Current Topics in Microbiology and Immunology*, 219, pp. 235–245.
80. **Grosu, I., Ghekiere, O., Layios, N., Hantson, P. and Cosnard, G.** (2007) 'Toxoplasma encephalitis after autologous stem cell transplantation'. *Leukemia & Lymphoma*, 48(1), pp. 201–203.
81. **Guimarães, E. V., Carvalho, L. De and Barbosa, H. S.** (2009) 'Interaction and cystogenesis of *Toxoplasma gondii* within skeletal muscle cells in vitro'. *Mem Inst Oswaldo Cruz Rio de Janeiro*, 104(2), pp. 170–174.
82. **Guimarães, E. V., de Carvalho, L. and Santos Barbosa, H.** (2008) 'Primary Culture of Skeletal Muscle Cells as a Model for Studies of *Toxoplasma gondii* Cystogenesis'. *Journal of Parasitology*, 94(1), pp. 72–83.
83. **Gulbis, J. M., Kelman, Z., Hurwitz, J., O'Donnell, M. and Kuriyan, J.** (1996) 'Structure of the C-terminal region of p21(WAF1/CIP1) complexed with human PCNA.' *Cell*, 87(2), pp. 297–306.
84. **Halos, L., Thébault, A., Aubert, D., Thomas, M., Perret, C., Geers, R., Alliot, A., Escotte-Binet, S., Ajzenberg, D., Dardé, M.-L., Durand, B., Boireau, P. and Villena, I.** (2010) 'An innovative survey underlining the significant level of contamination by *Toxoplasma gondii* of ovine meat consumed in France'. *International Journal for Parasitology*, 40(2), pp. 193–200.
85. **Havelaar, A. H., Kemmeren, J. M. and Kortbeek, L. M.** (2007) 'Disease Burden of Congenital Toxoplasmosis'. *Clinical Infectious Diseases*, 44(11), pp. 1467–1474.
86. **Heiden, M. G. Vander, Cantley, L. C., Thompson, C. B., Mammalian, P., Exhibit, C. and Metabolism, A.** (2009) 'Understanding the Warburg Effect: Cell Proliferation'. *Science*, 324(5930), pp. 1029–1033.

87. Heymes, C., Bendall, J. K., Ratajczak, P., Cave, A. C., Samuel, J.-L., Hasenfuss, G. and Shah, A. M. (2003) 'Increased myocardial NADPH oxidase activity in human heart failure'. *Journal of the American College of Cardiology*, 41(12), pp. 2164–2171.
88. Hill, D. E. and Dubey, J. P. (2013) 'Toxoplasma gondii prevalence in farm animals in the United States'. *International Journal for Parasitology*, 43(2), pp. 107–113.
89. Howe, D. K. and Sibley, L. D. (1995) 'Toxoplasma gondii comprises three clonal lineages: correlation of parasite genotype with human disease.' *The Journal of Infectious Diseases*, 172(6), pp. 1561–1566.
90. Huang, J. and Thayer, M. J. (2002) 'Interactions between the cell cycle and the myogenic program'. *Advances in Developmental Biology and Biochemistry*, 11, pp. 53–74.
91. Hunter, C. A. and David Sibley, L. (2012) 'Modulation of innate immunity by Toxoplasma gondii virulence effectors'. *Nature Reviews Microbiology*, 10(11), pp. 766–78.
92. Ibrahim, H. M., Bannai, H., Xuan, X. and Nishikawa, Y. (2009) 'Toxoplasma gondii Cyclophilin 18-Mediated Production of Nitric Oxide Induces Bradyzoite Conversion in a CCR5-Dependent Manner'. *Infection and Immunity*, 77(9), pp. 3686–3695.
93. Ihara, F. and Nishikawa, Y. (2014) 'Starvation of low-density lipoprotein-derived cholesterol induces bradyzoite conversion in Toxoplasma gondii'. *Parasites and Vectors*, 7(1), pp. 1–5.
94. Jahnke, V. E., Sabido, O. and Freyssenet, D. (2009) 'Control of mitochondrial biogenesis, ROS level, and cytosolic Ca²⁺ concentration during the cell cycle and the onset of differentiation in L6E9 myoblasts'. *AJP: Cell Physiology*, 296(5), pp. C1185–C1194.
95. Ji, C., Marnett, L. J. and Pietenpol, J. A. (1997) 'Cell cycle re-entry following chemically-induced cell cycle synchronization leads to elevated p53 and p21 protein levels'. *Oncogene*, 15(22), pp. 2749–2753.
96. Jitrapakdee, S., St Maurice, M., Rayment, I., Cleland, W. W., Wallace, J. C. and Attwood, P. V (2008) 'Structure, mechanism and regulation of pyruvate carboxylase.' *The Biochemical Journal*, 413(3), pp. 369–87.
97. Johnson, S. E. and Allen, R. E. (1993) 'Proliferating cell nuclear antigen (PCNA) is expressed in activated rat skeletal muscle satellite cells'. *Journal of Cellular Physiology*, 154(1), pp. 39–43.

98. **Jokelainen, P., Isomursu, M., Näreaho, A. and Oksanen, A.** (2011) 'Natural toxoplasma gondii infections in European brown hares and mountain hares in Finland: proportional mortality rate, antibody prevalence, and genetic characterization.' *Journal of Wildlife Diseases*, 47(1), pp. 154–163.
99. **Jones, J. L., Dargelas, V., Roberts, J., Press, C., Remington, J. S. and Montoya, J. G.** (2009) 'Risk Factors for *Toxoplasma gondii* Infection in the United States'. *Clinical Infectious Diseases*, 49(6), pp. 878–884.
100. **Jones, J. L. and Dubey, J. P.** (2012) 'Foodborne Toxoplasmosis'. *Clinical Infectious Diseases*, 55(6), pp. 845–851.
101. **Kim, K. and Weiss, L. M.** (2004) 'Toxoplasma gondii: The model apicomplexan'. *International Journal for Parasitology*, 34(3), pp. 423–432.
102. **Kirkman, L. A., Weiss, L. M. and Kim, K.** (2001) 'Cyclic Nucleotide Signaling in *Toxoplasma gondii* Bradyzoite Differentiation'. *Infection and Immunity*, 69(1), pp. 148–153.
103. **Kislinger, T., Gramolini, A. O., Pan, Y., Rahman, K., MacLennan, D. H. and Emili, A.** (2005) 'Proteome Dynamics during C2C12 Myoblast Differentiation'. *Molecular & Cellular Proteomics*, 4(7), pp. 887–901.
104. **Kitzmann, M. and Fernandez, A.** (2001) 'Crosstalk between cell cycle regulators and the myogenic factor MyoD in skeletal myoblasts'. *Cellular and Molecular Life Sciences*, 58(4), pp. 571–9.
105. **Krishna, C. M., Liebmann, J. E., Kaufman, D., DeGraff, W., Hahn, S. M., McMurry, T., Mitchell, J. B. and Russo, A.** (1992) 'The catecholic metal sequestering agent 1,2-dihydroxybenzene-3,5-disulfonate confers protection against oxidative cell damage.' *Archives of Biochemistry and Biophysics*, 294(1), pp. 98–106.
106. **Krokan, H., Wist, E. and Krokan, R. H.** (1981) 'Aphidicolin inhibits DNA synthesis by DNA polymerase alpha and isolated nuclei by a similar mechanism.' *Nucleic Acids Research*, 9(18), pp. 4709–19.
107. **Krug, E. C., Marr, J. J. and Berens, R. L.** (1989) 'Purine metabolism in *Toxoplasma gondii*.' *The Journal of Biological Chemistry*, 264(18), pp. 10601–10607.
108. **Krylov, S. N., Zhang, Z., Chan, N. W. C., Arriaga, E., Palcic, M. M. and Dovichi, N. J.** (1999) 'Correlating cell cycle with metabolism in single cells: Combination of image and metabolic cytometry'. *Cytometry*, 37(1), pp. 14–20.
109. **Kučera, O., Endlicher, R., Rouar, T., Lotkov, H., Garnol, T., Drahota, Z. and Ervinkov, Z.** (2014) 'The effect of tert -butyl hydroperoxide-induced oxidative stress on lean and steatotic rat hepatocytes in vitro'. *Oxidative Medicine and Cellular Longevity*, 2014(3), pp. 1–12.

110. **Kuehne, A., Emmert, H., Soehle, J., Lucius, R., Hildebrand, J. and Zamboni, N.** (2015) 'Acute Activation of Oxidative Pentose Phosphate Pathway as First-Line Response to Oxidative Stress in Human Skin Cells'. *Molecular Cell*, 59(3), pp. 359–371.
111. **Lange, K. and Proft, E. R.** (1970) 'Inhibition of the 6-phosphogluconate dehydrogenase in the rat kidney by 6-aminonicotinamide'. *Naunyn-Schmiedeberg's Archiv Für Pharmakologie*, 267(2), pp. 177–180.
112. **Lasram, M. M., Dhouib, I. B., Annabi, A., El Fazaa, S. and Gharbi, N.** (2015) 'A review on the possible molecular mechanism of action of N-acetylcysteine against insulin resistance and type-2 diabetes development'. *Clinical Biochemistry*, 48(16–17), pp. 1200–1208.
113. **Leary, S. C., Battersby, B. J., Hansford, R. G. and Moyes, C. D.** (1998) 'Interactions between bioenergetics and mitochondrial biogenesis'. *Biochimica et Biophysica Acta - Bioenergetics*, 1365(3), pp. 522–530.
114. **Lee, M. H., Reynisdóttir, I. and Massagué, J.** (1995) 'Cloning of p57KIP2, a cyclin-dependent kinase inhibitor with unique domain structure and tissue distribution.' *Genes & Development*, 9(6), pp. 639–49.
115. **Lu, N., Liu, C., Wang, J., Ding, Y. and Ai, Q.** (2015) 'Toxoplasmosis complicating lung cancer: a case report.' *International Medical Case Reports Journal*, 8(1), pp. 37–40.
116. **Lüder, C. G. K., Giraldo-Velásquez, M., Sendtner, M., Gross, U., Lüder, C. G. K. and -Velásquez, G.** (1999) 'Toxoplasma gondii in Primary Rat CNS Cells: Differential Contribution of Neurons, Astrocytes, and Microglial Cells for the Intracerebral Development and Stage Differentiation'. *Experimental Parasitology*, 93(1), pp. 23–32.
117. **Lüder, C. G. K. and Rahman, T.** (2017) 'Impact of the host on Toxoplasma stage differentiation'. *Microbial Cell*, 4(7), pp. 203–211.
118. **Luft, B. J. and Remington, J. S.** (1992) 'Toxoplasmic encephalitis in AIDS.' *Clinical Infectious Diseases*, 15(2), pp. 211–22.
119. **Lyons, C. N., Leary, S. C. and Moyes, C. D.** (2004) 'Bioenergetic remodeling during cellular differentiation: changes in cytochrome c oxidase regulation do not affect the metabolic phenotype'. *Biochemistry and Cell Biololgy*, 82(3), pp. 391–399.
120. **Lyons, R. E., Mcleod, R. and Roberts, C. W.** (2002) 'Toxoplasma gondii tachyzoite – bradyzoite interconversion'. *Trends in Parasitology*, 18(5), pp. 198–201.

121. **Macrae, J. I., Sheiner, L., Nahid, A., Tonkin, C., Striepen, B. and Mcconville, M. J.** (2012) 'Article Mitochondrial Metabolism of Glucose and Glutamine Is Required for Intracellular Growth of *Toxoplasma gondii*'. *Cell Host and Microbe*. Elsevier Inc., 12(5), pp. 682–692.
122. **Mahamed, D. A., Mills, J. H., Egan, C. E., Denkers, E. Y., Bynoe, M. S. and Thomas Wellems, by E.** (2012) 'CD73-generated adenosine facilitates *Toxoplasma gondii* differentiation to long-lived tissue cysts in the central nervous system'. *Proceedings of the National Academy of Sciences*, 109(40), pp. 16312–16317.
123. **Maksimov, P., Zerweck, J., Maksimov, A., Hotop, A., Groß, U., Spekker, K., Däubener, W., Werdermann, S., Niederstrasser, O., Petri, E., Mertens, M., Ulrich, R. G., Conraths, F. J. and Schares, G.** (2012) 'Analysis of Clonal Type-Specific Antibody Reactions in *Toxoplasma gondii* Seropositive Humans from Germany by Peptide-Microarray'. *PLoS ONE*, 7(3), pp. e34212.
124. **Mazumdar, J., H Wilson, E., Masek, K., A Hunter, C. and Striepen, B.** (2006) 'Apicoplast fatty acid synthesis is essential for organelle biogenesis and parasite survival in *Toxoplasma gondii*.' *Proceedings of the National Academy of Sciences*, 103(35), pp. 13192–7.
125. **McHugh, T., Gbewonyo, A., Johnson, J., Holliman, R. and Butcher, P.** (1993) 'Development of an in Vitro Model of *Toxoplasma Gondii* Cyst Formation'. *FEMS Microbiology Letters*, 114(3), pp. 325–332.
126. **Minet, A. D. and Gaster, M.** (2010) 'Pyruvate carboxylase is expressed in human skeletal muscle'. *Biochemical and Biophysical Research Communications*, 402(2), pp. 196–197.
127. **Moncada, P. A. and Montoya, J. G.** (2012) 'Toxoplasmosis in the fetus and newborn: an update on prevalence, diagnosis and treatment'. *Expert Review of Anti-infective Therapy*, 10(7), pp. 815–828.
128. **Monticone, M., Taherian, R., Stigliani, S., Carra, E., Monteghirfo, S., Longo, L., Daga, A., Dono, M., Zupo, S., Giaretti, W. and Castagnola, P.** (2014) 'NAC, tiron and trolox impair survival of cell cultures containing glioblastoma tumorigenic initiating cells by inhibition of cell cycle progression.' *PloS ONE*, 9(2), p. e90085.
129. **Montoya, J. G. and Liesenfeld, O.** (2004) 'Toxoplasmosis'. *Lancet*, 363(9425), pp. 1965–1976.
130. **Moran, J. L., Hill, A. A., Mounts, W. M., Miller, C. P., Li, Y., Hill, A. A., Mounts, W. M., Miller, C. P., Moran, J. L., Li, Y., Hill, A. A., Mounts, W. M., Miller, C. P., Jennifer, L., Li, Y., et al.** (2002) 'Gene expression changes during mouse skeletal myoblast differentiation revealed by transcriptional profiling'. *Physiological Genomics*, 10(2), pp. 103–111.

131. **de Moura, L., Bahia-Oliveira, L. M. G., Wada, M. Y., Jones, J. L., Tuboi, S. H., Carmo, E. H., Ramalho, W. M., Camargo, N. J., Trevisan, R., Graça, R. M. T., da Silva, A. J., Moura, I., Dubey, J. P. and Garrett, D. O.** (2006) 'Waterborne Toxoplasmosis, Brazil, from Field to Gene'. *Emerging Infectious Diseases*, 12(2), pp. 326–329.
132. **Moyes, C. D., Mathieu-Costello, O. A., Tsuchiya, N., Filburn, C. and Hansford, R. G.** (1997) 'Mitochondrial biogenesis during cellular differentiation.' *The American Journal of Physiology*, 272(4 Pt 1), pp. C1345-51.
133. **Muller, F. L., Liu, Y. and Van Remmen, H.** (2004) 'Complex III Releases Superoxide to Both Sides of the Inner Mitochondrial Membrane'. *Journal of Biological Chemistry*, 279(47), pp. 49064–49073.
134. **Myers, T. K., Andreuzza, S. E. and Franklin, D. S.** (2004) 'p18INK4c and p27KIP1 are required for cell cycle arrest of differentiated myotubes'. *Experimental Cell Research*, 300(2), pp. 365–378.
135. **Naughton, J. a and Bell, A.** (2007) 'Studies on cell-cycle synchronization in the asexual erythrocytic stages of Plasmodium falciparum.' *Parasitology*, 134(Pt 3), pp. 331–337.
136. **Nicolle and Manceaux** (1908) 'Sur une infection à corps de Leishman (ou organismes voisins) du gondi'. *C R Seances Acad Sci*, (147), pp. 763–766.
137. **Owen, O. E., Kalhan, S. C. and Hanson, R. W.** (2002) 'The Key Role of Anaplerosis and Cataplerosis for Citric Acid Cycle Function'. *Journal of Biological Chemistry*, 277(34), pp. 30409–30412.
138. **Pappas, G., Roussos, N. and Falagas, M. E.** (2009) 'Toxoplasmosis snapshots: Global status of Toxoplasma gondii seroprevalence and implications for pregnancy and congenital toxoplasmosis'. *International Journal for Parasitology*, 39(12), pp. 1385–1394.
139. **Patel, D., Kandhi, S., Kelly, M., Neo, B. H. and Wolin, M. S.** (2014) 'Dehydroepiandrosterone promotes pulmonary artery relaxation by NADPH oxidation-elicited subunit dimerization of protein kinase G 1'. *AJP: Lung Cellular and Molecular Physiology*, 306(4), pp. L383–L391.
140. **Pfefferkorn, E. R.** (1984) 'Interferon gamma blocks the growth of Toxoplasma gondii in human fibroblasts by inducing the host cells to degrade tryptophan.' *Proceedings of the National Academy of Sciences*, 81(3), pp. 908–912.
141. **Phelps, D. E., Hsiao, K. M., Li, Y., Hu, N., Franklin, D. S., Westphal, E., Lee, E. Y. and Xiong, Y.** (1998) 'Coupled transcriptional and translational control of cyclin-dependent kinase inhibitor p18INK4c expression during myogenesis.' *Molecular and Cellular Biology*, 18(4), pp. 2334–43.

142. **Piao, Y. J., Seo, Y. H., Hong, F., Kim, J. H., Kim, Y.-J., Kang, M. H., Kim, B. S., Jo, S. A., Jo, I., Jue, D.-M., Kang, I., Ha, J. and Kim, S. S.** (2005) 'Nox 2 stimulates muscle differentiation via NF- κ B/iNOS pathway'. *Free Radical Biology and Medicine*, 38(8), pp. 989–1001.
143. **Podust, V. N., Podust, L. M., Goubin, F., Ducommun, B. and Hiibscher, U.** (1995) 'Mechanism of Inhibition of Proliferating Cell Nuclear Antigen-Dependent DNA Synthesis by the Cyclin-Dependent Kinase Inhibitor p21'. *Biochemistry*, 34(27), pp. 8869–8875.
144. **Polonais, V. and Soldati-Favre, D.** (2010) 'Versatility in the acquisition of energy and carbon sources by the Apicomplexa.' *Biology of the Cell*, 102(8), pp. 435–445.
145. **Radke, J. R., Donald, R. G., Eibs, A., Jerome, M. E., Behnke, M. S., Liberator, P. and White, M. W.** (2006) 'Changes in the Expression of Human Cell Division Autoantigen-1 Influence *Toxoplasma gondii* Growth and Development'. *PLoS Pathogens*, 2(10), p. e105.
146. **Radke, J. R., Guerini, M. N., Jerome, M. and White, M. W.** (2003) 'A change in the premitotic period of the cell cycle is associated with bradyzoite differentiation in *Toxoplasma gondii*'. *Molecular and Biochemical Parasitology*, 131(2003), pp. 119–127.
147. **Radke, J. R., Striepen, B., Guerini, M. N., Jerome, M. E., Roos, D. S. and White, M. W.** (2001) 'Defining the cell cycle for the tachyzoite stage of *Toxoplasma gondii*'. *Molecular and Biochemical Parasitology*, 115(2), pp. 165–175.
148. **Rajan, S., Dang, H. C. P., Djambazian, H., Zuzan, H., Fedyshyn, Y., Ketela, T., Moffat, J., Hudson, T. J. and Sladek, R.** (2012) 'Analysis of early C2C12 myogenesis identifies stably and differentially expressed transcriptional regulators whose knock-down inhibits myoblast differentiation'. *Physiological Genomics*, 44(2), pp. 183–197.
149. **Rawat, D. K., Hecker, P., Watanabe, M., Chettimada, S., Levy, R. J., Okada, T., Edwards, J. G. and Gupte, S. A.** (2012) 'Glucose-6-Phosphate Dehydrogenase and NADPH Redox Regulates Cardiac Myocyte L-Type Calcium Channel Activity and Myocardial Contractile Function'. *PLoS ONE*, 7(10), pp. 1–10.
150. **Schlüter, D., Däubener, W., Schares, G., Groß, U., Pleyer, U. and Lüder, C.** (2014) 'Animals are key to human toxoplasmosis'. *International Journal of Medical Microbiology*, 304(7), pp. 917–929.
151. **Schwartz, A. and Pashko, L. L.** (2004) 'Dehydroepiandrosterone, glucose-6-phosphate dehydrogenase, and longevity'. *Ageing Research Reviews*, 3(2), pp. 171–187.

152. **Sehgal, A., Bettiol, S., Pypaert, M., Wenk, M. R., Kaasch, A., Blader, I. J., Joiner, K. A. and Coppens, I.** (2005) 'Peculiarities of Host Cholesterol Transport to the Unique Intracellular Vacuole Containing *Toxoplasma*'. *Traffic*, 6(12), pp. 1125–1141.
153. **Shaw, M. K., Roos, D. S. and Tilney, L. G.** (2001) 'DNA replication and daughter cell budding are not tightly linked in the protozoan parasite *Toxoplasma gondii*'. *Microbes and Infection*, 3(5), pp. 351–362.
154. **Shen, X., Collier, J. M., Hlaing, M., Zhang, L., Delshad, E. H., Bristow, J. and Bernstein, H. S.** (2003) 'Genome-Wide Examination of Myoblast Cell Cycle Withdrawal During Differentiation'. *Developmental Dynamics*, 226(1), pp. 128–138.
155. **Sibley, L. D. and Ajioka, J. W.** (2008) 'Population Structure of *Toxoplasma gondii*: Clonal Expansion Driven by Infrequent Recombination and Selective Sweeps'. *Annual Review of Microbiology*, 62(1), pp. 329–351.
156. **Soète, M., Camus, D. and Dubremetz, J. F.** (1994) 'Experimental induction of bradyzoite-specific antigen expression and cyst formation by the RH strain of *Toxoplasma gondii* in vitro.' *Experimental parasitology*, 78(4), pp. 361–370.
157. **Sousa, S. de, Ajzenberg, D., Canada, N., Freire, L., Costa, J. M. C. da, Dardé, M. L., Thulliez, P. and Dubey, J. P.** (2006) 'Biologic and molecular characterization of *Toxoplasma gondii* isolates from pigs from Portugal'. *Veterinary Parasitology*, 135(2), pp. 133–136.
158. **Spooner, R. and Yilmaz, Ö.** (2011) 'The role of reactive-oxygen-species in microbial persistence and inflammation'. *International Journal of Molecular Sciences*, 12(1), pp. 334–352.
159. **Sriram, S., Subramanian, S., Sathiakumar, D., Venkatesh, R., Salerno, M. S., Mcfarlane, C. D., Kambadur, R. and Sharma, M.** (2011) 'Modulation of reactive oxygen species in skeletal muscle by myostatin is mediated through NF- κ B.' *Aging Cell*, 10(6), pp. 931–948.
160. **Starostina, N. G. and Kipreos, E. T.** (2012) 'Multiple degradation pathways regulate versatile CIP/KIP CDK inhibitors'. *Trends in Cell Biology*, 22(1), pp. 33–41.
161. **Steinbacher, P. and Eckl, P.** (2015) 'Impact of Oxidative Stress on Exercising Skeletal Muscle'. *Biomolecules*, 5(2), pp. 356–377.
162. **Stincon, A., Prigione, A., Cramer, T., Wamelink, M. M. C., Campbell, K., Cheung, E., Olin-Sandoval, V., Grüning, N. M., Krüger, A., Tauqeer Alam, M., Keller, M. A., Breitenbach, M., Brindle, K. M., Rabinowitz, J. D. and Ralser, M.** (2015) 'The return of metabolism: Biochemistry and physiology of the pentose phosphate pathway'. *Biological Reviews*, 90(3), pp. 927–963.

163. **Strobl, J. S., Seibert, C. W., Li, Y., Nagarkatti, R., Mitchell, S. M., Rosypal, A. C., Rathore, D. and Lindsay, D. S.** (2009) 'Inhibition of *Toxoplasma gondii* and *Plasmodium falciparum* infections in vitro by NSC3852, a redox active antiproliferative and tumor cell differentiation agent.' *The Journal of Parasitology*, 95(1), pp. 215–223.
164. **Suzuki, Y., Orellana, M. A., Schreiber, R. D. and Remington, J. S.** (1988) 'Interferon-gamma: the major mediator of resistance against *Toxoplasma gondii*.' *Science*, 240(4851), pp. 516–518.
165. **Swierzy, I. J., Händel, U., Kaefer, A., Scharfe, M., Schlüter, D. and Lüder, C. G. K.** (2017) 'Divergent co-transcriptomes of different host cells infected with *Toxoplasma gondii* reveal cell type-specific host- parasite interactions'. *Nature Scientific Reports*, 7(7229), pp. 1–14.
166. **Swierzy, I. J. and Lüder, C. G. K.** (2014) 'Withdrawal of skeletal muscle cells from cell cycle progression triggers differentiation of *Toxoplasma gondii* towards the bradyzoite stage'. *Cellular Microbiology*, 17(1), pp. 2–17.
167. **Swierzy, I. J., Muhammad, M., Kroll, J., Abelmann, A., Tenter, A. M. and Lüder, C. G. K.** (2014) 'Toxoplasma gondii within skeletal muscle cells: A critical interplay for food-borne parasite transmission'. *International Journal for Parasitology*, 44(2), pp. 91–98.
168. **Taiwo, F. A.** (2008) 'Mechanism of tiron as scavenger of superoxide ions and free electrons'. *Spectroscopy*, 22(6), pp. 491–498.
169. **Takács, A. C., Swierzy, I. J., Lü Der, C. G. K. and Blader, I.** (2012) 'Interferon- γ Restricts *Toxoplasma gondii* Development in Murine Skeletal Muscle Cells via Nitric Oxide Production and Immunity-Related GTPases'. *PLoS ONE*, 7(9), pp. e45440.
170. **Tao, K. P., Fong, S. W., Lu, Z., Ching, Y. P., Chan, K. W. and Chan, S. Y.** (2011) 'TSPYL2 is important for G1 checkpoint maintenance upon DNA damage'. *PLoS ONE*, 6(6), pp. 1–8.
171. **Tenter, A. M.** (2009) 'Toxoplasma gondii in animals used for human consumption'. *Memórias do Instituto Oswaldo Cruz*, 104(2), pp. 364–369.
172. **Tenter, A. M., Heckeroth, A. R. and Weiss, L. M.** (2000) 'Toxoplasma gondii: from animals to humans'. *International Journal for Parasitology*, 30(12–13), pp. 1217–1258.
173. **Toh, B. H., Tu, Y., Cao, Z., Cooper, M. E. and Chai, Z.** (2010) 'Role of cell division Autoantigen 1 (CDA1) in cell proliferation and fibrosis'. *Genes*, 1(3), pp. 335–348.

174. **Tomavo, S. and Boothroyd, J. C.** (1995) 'Interconnection between organellar functions, development and drug resistance in the protozoan parasite, *Toxoplasma gondii*.' *International Journal for Parasitology*, 25(11), pp. 1293–1299.
175. **Tomczak, K. K., Marinescu, V. D., Ramoni, M. F., Sanoudou, D., Montanaro, F., Han, M., Kunkel, L. M., Kohane, I. S. and Beggs, A. H.** (2004) 'Expression profiling and identification of novel genes involved in myogenic differentiation'. *The FASEB Journal*, 18(2), pp. 403–405.
176. **Tsang, K. H., Lai, S. K., Li, Q., Yung, W. H., Liu, H., Mak, P. H. S., Ng, C. C. P., McAlonan, G., Chan, Y. S. and Chan, S. Y.** (2014) 'The Nucleosome Assembly Protein TSPYL2 Regulates the Expression of NMDA Receptor Subunits GluN2A and GluN2B'. *Scientific Reports*, 4(1), pp. 3654.
177. **Tu, Y., Wu, W., Wu, T., Cao, Z., Wilkins, R., Toh, B. H., Cooper, M. E. and Chai, Z.** (2007) 'Antiproliferative autoantigen CDA1 transcriptionally up-regulates p21 Waf1/Cip1 by activating p53 and MEK/ERK1/2 MAPK pathways'. *Journal of Biological Chemistry*, 282(16), pp. 11722–11731.
178. **Tyson, R. L., Perron, J. and Sutherland, G. R.** (2000) '6-Aminonicotinamide inhibition of the pentose phosphate pathway in rat neocortex.' *Neuroreport*, 11(9), pp. 1845–1848.
179. **Voth, J.** (2015) 'An Evaluation of Sustainable Consumption in the German Meat Market'. *NIL Sustainability in Food Retailing*, pp. 21–29.
180. **Wagatsuma, A. and Sakuma, K.** (2013) 'Mitochondria as a potential regulator of myogenesis.' *The Scientific World Journal*, 2013(1), pp. 1–9.
181. **Wang, G.-S., Hong, C.-J., Yen, T.-Y., Huang, H.-Y., Ou, Y., Huang, T.-N., Jung, W.-G., Kuo, T.-Y., Sheng, M., Wang, T.-F. and Hsueh, Y.-P.** (2004) 'Transcriptional modification by a CASK-interacting nucleosome assembly protein.' *Neuron*, 42(1), pp. 113–28.
182. **Wang, H.-J., Pan, Y.-X., Wang, W.-Z., Zucker, I. H. and Wang, W.-Z.** (2009) 'NADPH oxidase-derived reactive oxygen species in skeletal muscle modulates the exercise pressor reflex'. *Journal of Applied Physiology*, 107(2), pp. 450–459.
183. **Weilhammer, D. R., Iavarone, A. T., Villegas, E. N., Brooks, G. a, Sinai, A. P. and Sha, W. C.** (2012) 'Host metabolism regulates growth and differentiation of *Toxoplasma gondii*.' *International Journal for Parasitology*, 42(10), pp. 947–959.
184. **Weinberg, R. A.** (1995) 'The retinoblastoma protein and cell cycle control.' *Cell*, 81(3), pp. 323–30.

185. **Weiss, L. M., Laplace, D., Takvorian, P. M., Tanowitz, H. B., Cali, A. and Wittner, M.** (1995) 'A cell culture system for study of the development of *Toxoplasma gondii* bradyzoites.' *The Journal of Eukaryotic Microbiology*, 42(2), pp. 150–157.
186. **Wiendl, H., Hohlfeld, R. and Kieseier, B. C.** (2005) 'Immunobiology of muscle: advances in understanding an immunological microenvironment'. *Trends in Immunology*, 26(7), pp. 373–380.
187. **Wilking, H., Thamm, M., Stark, K., Aebischer, T. and Seeber, F.** (2016) 'Prevalence, incidence estimations, and risk factors of *Toxoplasma gondii* infection in Germany: a representative, cross-sectional, serological study'. *Nature Scientific Reports*, 6(3), p. 22551.
188. **Willkomm, L., Schubert, S., Jung, R., Elsen, M., Borde, J., Gehlert, S., Suhr, F. and Bloch, W.** (2014) 'Lactate regulates myogenesis in C2C12 myoblasts in vitro'. *Stem Cell Research*, 12(3), pp. 742–753.
189. **Zhang, J., Wang, X., Vikash, V., Ye, Q., Wu, D., Liu, Y. and Dong, W.** (2016) 'ROS and ROS-Mediated Cellular Signaling'. *Oxidative Medicine and Cellular Longevity*, 2016(12), pp. 1–18.
190. **Zhang, P., Wong, C., Liu, D., Finegold, M., Harper, J. W. and Elledge, S. J.** (1999) 'p21 CIP1 and p57 KIP2 control muscle differentiation at the myogenin step'. *Genes and Development*, 13(2), pp. 213–224.
191. **Zhou, W., Quan, J. H., Lee, Y. H., Shin, D. W. and Cha, G. H.** (2013) 'Toxoplasma gondii Proliferation Require Down-Regulation of Host Nox4 Expression via Activation of PI3 Kinase/Akt Signaling Pathway'. *PLoS ONE*, 8(6), p. e66306.
192. **Zuo, L., Christofi, F. L., Wright, V. P., Bao, S. and Clanton, T. L.** (2004) 'Lipoxygenase-dependent superoxide release in skeletal muscle'. *Journal of Applied Physiology*, 97(2), pp. 661–668.

Supplementary Tables:**Supplementary Table 3.1: Top30 uniquely upregulated DEGs in *T. gondii*-infected myoblasts versus myotubes**

Ensemble ID	gene name	description	log2Fold Change	p-value
ENSMUSG00000095419	Gm14328	predicted gene 14328	2.53	4.5208E-06
ENSMUSG00000042607	Asb4	ankyrin repeat and SOCS box-containing 4	2.51	0.0015546
ENSMUSG00000004872	Pax3	paired box 3	2.49	0.00105264
ENSMUSG00000044103	Il1f9	interleukin 1 family, member 9	2.41	0.00031793
ENSMUSG00000096755	Gm20746	predicted gene, 20746	2.35	0.00216651
ENSMUSG00000092819	Gm23639	predicted gene, 23639	2.31	0.00106358
ENSMUSG00000029372	Ppbp	pro-platelet basic protein	2.27	0.00086012
ENSMUSG00000084331	Gm8163	predicted gene 8163	2.23	0.00537326
ENSMUSG00000079008	Gm14124	predicted gene 14124	2.22	0.00587077
ENSMUSG00000091623	Gm17092	predicted gene 17092	2.14	0.00473877
ENSMUSG00000075478	Slitrk1	SLIT and NTRK-like family, member 1	2.11	0.00969976
ENSMUSG00000043782	Ccdc64b	coiled-coil domain containing 64B	2.09	0.01048871
ENSMUSG00000071715	Ncf4	neutrophil cytosolic factor 4	2.05	0.00216474
ENSMUSG00000043340	6530409C15Rik	RIKEN cDNA 6530409C15 gene	2.05	0.00710414
ENSMUSG00000064023	Klk8	kallikrein related-peptidase 8	2.04	0.00499059
ENSMUSG00000093245	Mir677	microRNA 677	2.03	0.01249689
ENSMUSG00000054568	Usp17la	ubiquitin specific peptidase 17-like A	2.03	0.00012613
ENSMUSG00000087017	4930417H01Rik	RIKEN cDNA 4930417H01 gene	1.98	0.01100347
ENSMUSG00000087819	Gm25117	predicted gene, 25117	1.98	0.00127121
ENSMUSG00000079304	4933413G19Rik	RIKEN cDNA 4933413G19 gene	1.97	0.00669523
ENSMUSG00000065663	Gm22579	predicted gene, 22579	1.97	0.00316963
ENSMUSG00000090362	Vmn2r79	vomer nasal 2, receptor 79	1.97	0.01061651
ENSMUSG00000093548	Gm6407	predicted gene 6407	1.96	0.00893079
ENSMUSG00000082408	Gm13545	predicted gene 13545	1.95	0.01722413
ENSMUSG00000034764	1700006J14Rik	RIKEN cDNA 1700006J14 gene	1.95	0.01794258
ENSMUSG00000041134	Cyyr1	cysteine and tyrosine-rich protein 1	1.93	0.02026058
ENSMUSG00000052504	Epha3	Eph receptor A3	1.92	0.00406016
ENSMUSG00000083291	Gm13679	predicted gene 13679	1.91	0.00156182
ENSMUSG00000071658	Gng3	guanine nucleotide binding protein (G protein), gamma 3	1.91	0.01564742
ENSMUSG00000081302	Gm12020	predicted gene 12020	1.91	2.0329E-06

Supplementary Table 3.2: Top30 uniquely downregulated DEGs in *T. gondii*-infected myoblasts versus myotubes

Ensemble ID	gene name	description	log2Fold Change	p-value
ENSMUSG00000086449	9030204H09Rik	RIKEN cDNA 9030204H09 gene	-2.89	0.000182875
ENSMUSG00000043029	Trpv3	transient receptor potential cation channel, subfamily V, member 3	-2.87	2.13361E-05
ENSMUSG00000038738	Shank1	SH3/ankyrin domain gene 1	-2.76	0.000334785
ENSMUSG00000068348	Gm10238	predicted pseudogene 10238	-2.67	0.000390624
ENSMUSG00000028354	Fmn2	formin 2	-2.49	0.000851051
ENSMUSG00000055865	Fam19a3	family with sequence similarity 19, member A3	-2.48	0.001958978
ENSMUSG00000021313	Ryr2	ryanodine receptor 2, cardiac	-2.45	0.001314366
ENSMUSG00000073052	D130052B06Rik	RIKEN cDNA D130052B06 gene	-2.42	0.002594387
ENSMUSG00000076897	Traj32	T cell receptor alpha joining 32	-2.40	5.2548E-05
ENSMUSG00000051225	Fam83a	family with sequence similarity 83, member A	-2.40	0.00141186
ENSMUSG00000057723	Krt33b	keratin 33B	-2.38	0.003216406
ENSMUSG00000021953	Tdh	L-threonine dehydrogenase	-2.35	0.003425066
ENSMUSG00000047343	Mettl21c	methyltransferase like 21C	-2.35	0.00321369
ENSMUSG00000087028	Gm13387	predicted gene 13387	-2.34	0.003750199
ENSMUSG00000039661	Dusp26	dual specificity phosphatase 26 (putative)	-2.30	0.004655933
ENSMUSG00000021490	Slc34a1	solute carrier family 34 (sodium phosphate), member 1	-2.24	0.005531173
ENSMUSG00000063681	Crb1	crumbs family member 1, photoreceptor morphogenesis associated	-2.21	0.005767139
ENSMUSG00000097860	Gm26857	predicted gene, 26857	-2.20	0.003592543
ENSMUSG00000050201	Otop2	otopetrin 2	-2.17	0.002750153
ENSMUSG00000004609	Cd33	CD33 antigen	-2.14	0.008952032
ENSMUSG00000086607	4930511M06Rik	RIKEN cDNA 4930511M06 gene	-2.13	0.005891531
ENSMUSG00000007279	Scube2	signal peptide, CUB domain, EGF-like 2	-2.12	0.001609105
ENSMUSG00000071392	Ect1	epithelial cell transforming sequence 2 oncogene-like	-2.12	0.004192352
ENSMUSG00000096948	Gm4221	predicted gene 4221	-2.11	0.003519203
ENSMUSG00000030336	Cd27	CD27 antigen	-2.09	0.001688153
ENSMUSG00000087600	Pmepa1os	prostate transmembrane protein, androgen induced 1, opposite strand	-2.09	0.005689734
ENSMUSG00000032572	Col6a4	collagen, type VI, alpha 4	-2.08	0.000137108
ENSMUSG00000050097	Ces2b	carboxyesterase 2B	-2.08	0.010970546
ENSMUSG00000023153	Tmem52	transmembrane protein 52	-2.08	0.011110238
ENSMUSG00000020830	Vmo1	vitelline membrane outer layer 1 homolog (chicken)	-2.07	0.010777209

Supplementary Table 3.3: List of differentially regulated genes in *T. gondii*-infected myotubes versus non-infected myotubes

Ensemble ID	gene name	description	log2Fold Change	p-value
ENSMUSG00000071419	Rps15-ps2	ribosomal protein S15, pseudogene 2	3.26	6.9311E-22
ENSMUSG00000068240	Gm11808	predicted gene 11808	2.73	1.1944E-14
ENSMUSG00000084817	Gm5526	predicted pseudogene 5526	2.83	1.4118E-14
ENSMUSG00000082536	Gm13456	predicted gene 13456	1.60	3.2711E-13
ENSMUSG00000080921	Rpl38-ps2	ribosomal protein L38, pseudogene 2	3.57	6.2048E-13
ENSMUSG00000090243	Gm16103	predicted gene 16103	2.86	4.6324E-08
ENSMUSG00000083621	Gm14586	predicted gene 14586	2.73	9.3046E-08
ENSMUSG00000082456	Gm11598	predicted gene 11598	3.41	1.7094E-06
ENSMUSG00000083327	Vcp-rs	valosin containing protein, related sequence	1.07	1.0493E-05
ENSMUSG00000043192	Gm1840	predicted gene 1840	1.17	1.0493E-05
ENSMUSG00000091449	Gm10269	predicted gene 10269	2.67	2.8868E-05
ENSMUSG00000043618	Eif5a13-ps	eukaryotic translation initiation factor 5A-like 3, pseudogene	2.48	3.0077E-05
ENSMUSG00000043483	Gm6863	predicted gene 6863	1.64	3.4035E-05
ENSMUSG00000067344	Rps25-ps1	ribosomal protein S25, pseudogene 1	2.45	0.00012335
ENSMUSG00000082420	Gm6517	predicted gene 6517	1.35	0.00013623
ENSMUSG00000080875	Gm7332	predicted gene 7332	2.41	0.00017536
ENSMUSG00000045690	Wdr89	WD repeat domain 89	0.72	0.00080566
ENSMUSG00000074479	Gm10704	predicted pseudogene 10704	1.89	0.00089356
ENSMUSG00000069682	Gm10275	predicted pseudogene 10275	1.56	0.00089356
ENSMUSG00000066554	Gm10167	predicted pseudogene 10167	1.29	0.0013283
ENSMUSG00000063902	Gm7964	predicted gene 7964	0.66	0.00217238
ENSMUSG00000059970	Hspa2	heat shock protein 2	0.69	0.00282959
ENSMUSG00000081999	Gm13461	predicted gene 13461	1.58	0.00282959
ENSMUSG00000058809	Hspd1-ps3	heat shock protein 1 (chaperonin), pseudogene 3	1.97	0.00308245
ENSMUSG00000039684	Gm5422	predicted pseudogene 5422	1.32	0.0032471
ENSMUSG00000084280	Gm11972	predicted gene 11972	2.72	0.0032471
ENSMUSG00000084163	Gm11901	predicted gene 11901	1.60	0.00465211
ENSMUSG00000060068	Gm12222	predicted gene 12222	2.45	0.00536265
ENSMUSG00000079139	Gm4204	predicted gene 4204	0.86	0.00614431

ENSMUSG00000079297	Gm2223	predicted pseudogene 2223	1.65	0.00984243
ENSMUSG00000049494			1.16	0.0159097
ENSMUSG00000020178	Adora2a	adenosine A2a receptor	1.56	0.01947589
ENSMUSG00000074800	Gm4149	predicted pseudogene 4149	2.18	0.01947589
ENSMUSG00000046341	Gm11223	predicted gene 11223	1.97	0.01973754
ENSMUSG00000097245	Gm5421	predicted gene 5421	1.14	0.02101872
ENSMUSG00000064317	Gm10146	predicted gene 10146	2.48	0.02101872
ENSMUSG00000071141	Rpl36a-ps3	ribosomal protein L36A, pseudogene 3	2.11	0.02222175
ENSMUSG00000083240	Gm13453	predicted gene 13453	2.38	0.02573356

Supplementary Table 3.4: List of differentially regulated genes in *T. gondii*-infected myoblasts versus non-infected myoblasts

Ensemble ID	gene name	description	log2Fold Change	p-value
ENSMUSG00000071419	Rps15-ps2	ribosomal protein S15, pseudogene 2	3.32	7.85E-28
ENSMUSG00000082536	Gm13456	predicted gene 13456	1.85	3.94911E-18
ENSMUSG00000080921	Rpl38-ps2	ribosomal protein L38, pseudogene 2	3.47	2.8401E-15
ENSMUSG00000084817	Gm5526	predicted pseudogene 5526	2.53	2.8401E-15
ENSMUSG00000083621	Gm14586	predicted gene 14586	2.91	1.41679E-11
ENSMUSG00000090243	Gm16103	predicted gene 16103	3.15	5.74158E-11
ENSMUSG00000068240	Gm11808	predicted gene 11808	2.15	4.16872E-10
ENSMUSG00000058809	Hspd1-ps3	heat shock protein 1 (chaperonin), pseudogene 3	2.56	6.20514E-10
ENSMUSG00000043618	Eif5a13-ps	eukaryotic translation initiation factor 5A-like 3, pseudogene	2.33	1.15634E-09
ENSMUSG00000043192	Gm1840	predicted gene 1840	1.54	3.99799E-09
ENSMUSG00000083327	Vcp-rs	valosin containing protein, related sequence	1.21	3.58062E-08
ENSMUSG00000069682	Gm10275	predicted pseudogene 10275	1.96	1.2285E-07
ENSMUSG00000066554	Gm10167	predicted pseudogene 10167	1.38	1.51298E-07
ENSMUSG00000095419	Gm14328	predicted gene 14328	3.53	2.14701E-07
ENSMUSG00000058126	Tpm3-rs7	tropomyosin 3, related sequence 7	1.26	4.98655E-07
ENSMUSG00000067344	Rps25-ps1	ribosomal protein S25, pseudogene 1	2.44	1.46785E-06
ENSMUSG00000043483	Gm6863	predicted gene 6863	1.67	1.49389E-06
ENSMUSG00000082456	Gm11598	predicted gene 11598	3.04	2.98958E-06
ENSMUSG00000045690	Wdr89	WD repeat domain 89	0.79	9.59556E-06
ENSMUSG00000063902	Gm7964	predicted gene 7964	0.74	1.03599E-05
ENSMUSG00000084280	Gm11972	predicted gene 11972	3.16	2.01534E-05

ENSMUSG00000091449	Gm10269	predicted gene 10269	2.19	3.64408E-05
ENSMUSG00000084163	Gm11901	predicted gene 11901	1.75	8.95066E-05
ENSMUSG00000082420	Gm6517	predicted gene 6517	1.33	0.000116755
ENSMUSG00000025225	Nfkb2	nuclear factor of kappa light polypeptide gene enhancer in B cells 2, p49/p100	0.52	0.000120184
ENSMUSG00000080875	Gm7332	predicted gene 7332	2.01	0.000120184
ENSMUSG00000017737	Mmp9	matrix metalloproteinase 9	3.03	0.000143602
ENSMUSG00000079139	Gm4204	predicted gene 4204	0.92	0.000239843
ENSMUSG00000081308	Gm14480	predicted gene 14480	3.35	0.000266767
ENSMUSG00000049494			1.23	0.000276971
ENSMUSG00000095908	Gm5576	predicted pseudogene 5576	2.90	0.000349203
ENSMUSG00000081792	Anp32b-ps1	Basic (leucine-rich) nuclear phosphoprotein 32 family, member B, pseudogene 1	1.96	0.000443491
ENSMUSG00000051255	Gm6563	predicted pseudogene 6563	1.10	0.000608142
ENSMUSG00000089764	Gm16580	predicted gene 16580	1.07	0.000608142
ENSMUSG00000076999	Gm22426	predicted gene, 22426	2.67	0.000626824
ENSMUSG00000043889	Gm8399	predicted gene 8399	1.24	0.000701962
ENSMUSG00000020178	Adora2a	adenosine A2a receptor	1.80	0.000881955
ENSMUSG00000046341	Gm11223	predicted gene 11223	1.58	0.00133387
ENSMUSG00000081999	Gm13461	predicted gene 13461	1.43	0.002059009
ENSMUSG00000082044	Gm14284	predicted gene 14284	2.01	0.002093637
ENSMUSG00000079297	Gm2223	predicted pseudogene 2223	1.65	0.002478247
ENSMUSG00000084384	Gm12251	predicted gene 12251	2.20	0.002478247
ENSMUSG00000044751	Gm12231	predicted gene 12231	1.92	0.003009955
ENSMUSG00000071041	Gm15210	predicted gene 15210	1.06	0.00424674
ENSMUSG00000081603	Gm14681	predicted gene 14681	1.31	0.004965718
ENSMUSG00000085783	Gm9816	predicted pseudogene 9816	1.27	0.005982894
ENSMUSG00000081302	Gm12020	predicted gene 12020	1.52	0.006793115
ENSMUSG00000068631	Gm7676	predicted gene 7676	1.66	0.009511183
ENSMUSG00000039684	Gm5422	predicted pseudogene 5422	1.12	0.009511183
ENSMUSG00000080966	Gm6263	predicted gene 6263	2.14	0.010630767
ENSMUSG00000075268	Gm10819	predicted gene 10819	1.96	0.012875706
ENSMUSG00000060214			1.19	0.013999197
ENSMUSG00000068706	Gm10250	predicted pseudogene 10250	1.37	0.015244317
ENSMUSG00000083477	Gm5555	predicted pseudogene 5555	1.76	0.016790782
ENSMUSG00000030735	Gm9755	predicted pseudogene 9755	1.48	0.016890583
ENSMUSG00000071141	Rpl36a-ps3	ribosomal protein L36A, pseudogene 3	1.87	0.019070742
ENSMUSG00000083899	Gm12346	predicted gene 12346	0.89	0.029460631
ENSMUSG00000080776	Gm12174	predicted gene 12174	1.82	0.029460631
ENSMUSG00000084416	Rpl10a-ps1	ribosomal protein L10A, pseudogene 1	0.99	0.029460631
ENSMUSG00000079225	Gm9531	predicted gene 9531	1.78	0.032012533
ENSMUSG00000083396	Gm15542	predicted gene 15542	2.13	0.039258034
ENSMUSG00000074800	Gm4149	predicted pseudogene 4149	1.86	0.039258034
ENSMUSG00000063696	Gm8730	predicted pseudogene 8730	1.49	0.039258034
ENSMUSG00000064317	Gm10146	predicted gene 10146	1.94	0.042426496
ENSMUSG00000078238	Gm12854	predicted gene 12854	1.40	0.044005604

ENSMUSG00000081578	Gm12611	predicted gene 12611	2.34	0.045880403
ENSMUSG00000062093	Gm10110	predicted gene 10110	1.13	0.045880403
ENSMUSG00000024164	C3	complement component 3	2.63	0.049628066
ENSMUSG00000081406	Rps6-ps4	ribosomal protein S6, pseudogene 4	2.37	0.049628066
ENSMUSG00000089999	Gm6485	predicted gene 6485	1.60	0.049865068

Supplementary Table 3.5: List of DEGs involved in glycolysis in non-infected and *T. gondii*-infected myotubes and myoblasts

Name of Enzyme	Ninf-MTs (RPKM)	Inf-MTs (RPKM)	Ninf-MBs (RPKM)	Inf-MBs (RPKM)	FC (Inf-MTs vs Inf-MBs)	<i>p</i> -value
Hexokinase-II	3843.84	3874.96	2391.08	2495.12	1.55	0.00158687
Glucose phosphate isomerase-I	14177.17	14704.36	9846.05	9601.52	1.53	4.26657E-05
Phosphofruktokinase-I	25088.74	24814.43	2274.60	2232.22	11.12	1.48889E-52
Aldolase-A	65565.43	66298.06	35486.08	32972.81	2.01	8.35789E-08
Glyceraldehyde-3P-dehydrogenase	682.54	626.26	690.25	702.93	0.89	0.261487467
Triphosphate isomerase-I	24513.19	25013.36	21443.78	20423.83	1.23	0.135664454
Phosphoglycrate kinase-I	2036.55	2126.56	1929.35	1788.71	1.19	0.372127957
Phosphoglycerate mutase-II	3313.57	3115.43	106.21	83.41	37.35	5.11824E-34
Enolase 3, beta-muscle	51401.92	47390.09	19764.94	16469.75	2.88	3.33734E-19
Pyruvate kinase	56685.11	56932.92	64899.77	60942.09	0.93	0.576795898
Lactate dehydrogenase-D	11.47	12.76	2.68	3.29	3.88	0.002190597

Note: **Ninf:** Non-infected, **Inf:** *T. gondii*-infected, **MTs:** Myotubes, **MBs:** Myoblasts, **FC:** Fold change, RPKM (Average RPKM from three independent biological replicates)

Supplementary Table 3.6: List of DEGs involved in TCA cycle in non-infected and *T. gondii*-infected myotubes and myoblasts

Name of Enzyme	Ninf-MTs (RPKM)	Inf-MTs (RPKM)	Ninf-MBs (RPKM)	Inf-MBs (RPKM)	FC (Inf-MTs vs Inf-MBs)	<i>p</i> -value
Pyruvate dehydrogenase complex	1465.98	1439.76	921.79	921.90	1.56	4.11758E-15
Citrate synthase	12121.37	12617.61	17264.04	17571.94	0.72	2.71997E-08
Aconitase-II	15883.56	15802.30	11676.62	11639.58	1.36	5.60364E-06
Isocitrate dehydrogenase 2	4216.30	4203.16	3451.13	3396.40	1.05	1.39938E-05
Ketoglutarate dehydrogenase	7309.51	7317.74	7374.97	7399.76	0.99	0.938729615
Succinate COA ligase(alpha)	3950.17	3799.33	3458.94	3147.43	1.21	0.190789113
Succinate dehydrogenase	8532.70	8158.17	7870.85	7644.87	1.07	0.357196406
Fumarate hydratase-I	3532.83	3600.27	4211.05	4092.49	0.88	0.197569596
Malate dehydrogenase-II	12400.33	12079.20	15547.65	14652.56	0.82	0.214493466
Pyruvate carboxylase	1759.70	1622.82	497.34	464.49	3.49	7.05465E-14
PEP carboxykinase2	1590.14	1703.32	3550.36	3483.44	0.49	3.47131E-11

Note: **Ninf:** Non-infected, **Inf:** *T. gondii*-infected, **MTs:** Myotubes, **MBs:** Myoblasts, **FC:** Fold change, RPKM (Average RPKM from three independent biological replicates)

Supplementary Table 3.7: List of DEGs involved in the pentose phosphate pathway in non-infected and *T. gondii*-infected myotubes and myoblasts

Name of Enzyme	Ninf-MTs (RPKM)	Inf-MTs (RPKM)	Ninf-MBs (RPKM)	Inf-MBs (RPKM)	FC (Inf-MTs vs Inf-MBs)	<i>p</i> -value
Glucose-6-phosphate dehydrogenase2	0	0.88	0.69	5.03	0.17	0.04198657
Glucose-6-phosphate dehydrogenase(X-linked)	1151.64	1161.26	4002.39	4318.99	0.27	8.52947E-61
6-phospho-gluconolactonase	2285.01	2288.07	2714.66	2355.19	0.97	0.917819246
6-phosphogluconate dehydrogenase	4508.70	4259.35	10217.70	9879.02	0.43	2.46997E-13
Ribose-5-phosphate isomerase	496.18	482.39	628.25	619.27	0.78	0.016798579
Transketolase	1049.58	1124.96	2828.63	2828.78	0.40	3.29912E-08
Transaldolase-I	3507.40	3399.36	4717.46	4097.25	0.83	0.325393781

Note: Ninf: Non-infected, Inf: *T. gondii*-infected, MTs: Myotubes, MBs: Myoblasts, FC: Fold change, RPKM (Average RPKM from three independent biological replicates)

Supplementary Table 3.8: List of DEGs involved in glycogen metabolism in non-infected and *T. gondii*-infected myotubes and myoblasts

Name of Enzyme	Ninf-MTs (RPKM)	Inf-MTs (RPKM)	Ninf-MBs (RPKM)	Inf-MBs (RPKM)	FC (Inf-MTs vs Inf-MBs)	<i>p</i> -value
Hexokinase-II	3843.84	3874.96	2391.08	2495.12	1.55	0.00158687
Phosphoglucomutase-II	5382.57	5333.61	3962.40	3599.70	1.48	0.003926753
UDP-glucose pyrophosphorylase2	4236.06	4268.94	3400.56	3088.90	1.38	4.51381E-05
Glycogenin	4430.68	4441.82	1653.29	1518.17	2.92	1.67296E-35
Glycogen synthase-I	8084.66	8069.19	1951.75	1837.02	4.39	1.48889E-52
Branching enzyme	764.14	809.71	687.59	723.33	1.12	0.281891944
Glycogen phosphorylase	8609.45	8544.74	229.01	235.53	36.28	3.95621E-14
Debranching enzyme	4833.23	4946.81	1796.73	1872.06	2.64	3.02017E-09

Note: Ninf: Non-infected, Inf: *T. gondii*-infected, MTs: Myotubes, MBs: Myoblasts, FC: Fold change, RPKM (Average RPKM from three independent biological replicates)

Supplementary Table 3.9: List of DEGs involved in cell cycle regulation in non-infected and *T. gondii*-infected myotubes and myoblasts

Name of protein	Ninf-MTs (RPKM)	Inf-MTs (RPKM)	Ninf-MBs (RPKM)	Inf-MBs (RPKM)	FC (Inf-MTs vs Inf-MBs)	<i>p</i> -value
P21	57791.013	55664.455	8631.226	8302.2580	6.704	6.97541E-52
P53 and DNA damage regulated-I	2665.479	2514.2973	1508.159	1329.9731	1.890	2.35322E-06
P57	294.561	256.21666	93.7548	84.61721	3.027	1.47466E-10
P27	2307.542	2401.2136	2077.2920	2055.0977	1.168	0.012060258
Retinoblastoma 1 (RB1)	3728.590	3861.1401	1661.973	1735.7367	2.224	2.06244E-05
CyclinA2	1392.712	1492.968	6962.999	7262.305	0.205	2.71989E-87
CyclinB1	281.709	288.22866	1525.5039	1533.8542	0.187	3.22722E-55
CyclinB2	850.556	893.039	3356.735	3023.042	0.295	5.75517E-18
CyclinC	901.763	866.0563	1293.018	1269.509	0.682	1.55291E-09
CyclinD1	1753.484	2008.287	10498.170	10800.078	0.185	2.46947E-28
CyclinD2	604.857	682.1955	1863.534	2302.278	0.296	2.6401E-06
CyclinE1	330.487	358.3018	1518.631	1551.325	0.230	1.05932E-34
CyclinE2	274.060	360.7402	1147.27	1321.349	0.273	1.18921E-33
CDK1	1560.276	1718.158	8968.375	8376.256	0.205	1.9079E-23
CDK2	1650.460	1646.989	2136.575	2143.399	0.768	8.09482E-05
CDK4	6699.051	6730.020	15583.254	15474.768	0.435	4.7623E-13
CDK6	162.473	219.006	492.603	718.746	0.305	5.2045E-05
CDK8	531.157	551.841	1059.251	1065.921	0.518	5.5133E-12
P18	961.992	1000.329	1683.769	1573.919	0.636	1.04844E-06
TSPY-like2	740.515	712.086	862.742	807.013	0.88	0.058085214

CWF-19 like1	347.582	332.963	561.456	580.418	0.574	1.64422E-10
Proliferating cell nuclear antigen	983.010	954.0822	2944.851	3006.691	0.317	2.23211E-37

Note: **Ninf:** Non-infected, **Inf:** *T. gondii*-infected, **MTs:** Myotubes, **MBs:** Myoblasts, **FC:** Fold change, RPKM (Average RPKM from three independent biological replicates)

Curriculum Vitae

PERSONAL INFORMATION:

Name: Md. Taibur Rahman

Father's Name: Md. Abdus Samad

Mother's Name: Amena Begum

Gender: Male, Date of birth: 04 November 1985

Birth place: Dinajpur, Nationality: Bangladeshi

Present address: Robert Koch Str. 38, App.-1021, 37075, Göttingen

Contact address: Department of Biochemistry and Molecular Biology,

University of Dhaka, Dhaka-1000, Bangladesh. Email: taibur@du.ac.bd



EDUCATIONAL BACKGROUND:

Degree	Subject	Year of Award	Result	University/ Institution
Doctor of Philosophy (Ph.D)	Molecular Microbiology	2017 (Expected)	Not completed	Georg-August Universität Göttingen, Germany
Master of Science (M.Sc)	Biochemistry and Molecular Biology	2009	First class 2nd (74%)	University of Dhaka, Bangladesh
Bachelor of Science (B.Sc)	Biochemistry and Molecular Biology	2008	First class 2nd (73%)	University of Dhaka, Bangladesh
Higher Secondary School Certificate (HSC)	Science	2002	First Division (81%)	Fulbari Govt. College, Bangladesh
Secondary School Certificate (SSC)	Science	2000	First Division (79%)	Kushdaha M. U High School, Bangladesh

EMPLOYMENT EXPERIENCES:

September 2014 to present: PhD student, Institute of Medical Microbiology, University of Goettingen, Germany

May 2013 to present (on leave): Assistant Professor and Researcher, Department of Biochemistry and Molecular Biology, University of Dhaka, Bangladesh.

July 2010 to April 2013: Lecturer and Researcher, Department of Biochemistry and Molecular Biology, University of Dhaka, Bangladesh.

April 2009 to June 2010: Research Officer, Immunology Laboratory, International Centre for Diarrheal Disease Research, Bangladesh

March 2008 to March 2009: Thesis student (MSc), Immunology Laboratory, International Centre for Diarrheal Disease Research, Bangladesh.

STUDENT SUPERVISION:

Supervision of student for laboratory rotation (6 weeks) prior Master thesis in the Laboratory of Professor Dr. Carsten Lüder of the institute for Medical Microbiology, Göttingen.

MEMBERSHIP ASSOCIATION:

1. Member, German Society for Hygiene and Microbiology, Germany
2. Member, Graduate Biochemist Association (GBA), Bangladesh.
3. Member, Bangladesh Society for Biochemistry and Molecular Biology (BSBMB), Bangladesh.

LANGUAGE PROFICIENCY:

Bengali (Native), English (Good), Deutsch (Basic A1)

COMPUTER SKILLS:

Computer fundamentals, MS office, program C++, SPSS, Sigma-Stat, Sigma-Plot, Mega-4, Graph Pad, Bioinformatics tools: NCBI, Venn diagram, DAVID analysis tools.

ACADEMIC TRAINING/COURSES:

- 2015: German language certificate courses A1.2, winter semester 2015, University of Gottingen, Germany.
- 2015: German language certificate courses A1.1, summer semester 2016, University of Gottingen, Germany.
- 2012: Training program on Bioinformatics, Online teaching, Microsoft Office, Photoshop, High Performance Liquid Chromatography (HPLC), Department of Biochemistry and Molecular Biology, University of Dhaka, Bangladesh.
- 2012: Training program on Statistical Package for the Social Sciences (SPSS Software), Institute of Statistics and Research Training, University of Dhaka, Bangladesh.
- 2009: Training program on Bio-safety and Bio-security, International Centre for Diarrheal Disease Research, Bangladesh.
- 2009: Training program on Gender issue and awareness, International Centre for Diarrheal Disease Research, Bangladesh.
- 2008: Laboratory visit, International Center for Diarrheal Disease Research in Bangladesh (ICDDR, B) and SQUARE pharmaceuticals Ltd.

SCHOLARTSHIP/ AWARDS:

- 2014: PhD fellowship, Erasmus Mundus (Interweave), University of Göttingen, Germany.
- 2012: Travel grant, German Cancer Research Center, University of Heidelberg, Germany.
- 2010: Travel award, International Summer program 2010 “Infection and immunity” Tokyo Medical and Dental University, Japan.
- 2009: Dean’s Award, Faculty of Biological Science, University of Dhaka, Bangladesh.
- 2002: Board Scholarship, Ministry of Education, Bangladesh

LIST OF PUBLICATIONS:

- 2017: Lüder, Carsten G.K., and **Taibur Rahman**. "Impact of the Host on Toxoplasma Stage Differentiation." *Microbial Cell* 4.7 (2017): 203–211.
- 2014: Sajib Chakraborty, **Taibur Rahman**, and Rajib Chakravorty, "Characterization of the Protective HIV-1 CTL Epitopes and the Corresponding HLA Class I Alleles: A Step towards Designing CTL Based HIV-1 Vaccine," *Advances in Virology*, vol. 2014.
- 2013: **Taibur Rahman**, Ismail Hosen and Sajib Chakraborty. A Rapid glimpse on Typhoid fever: An updated minireview. "Journal of Life medicine" October 2013, 1(3) 83-92.
- 2013: M.M. Towhidul Islam, Arnab Talukder, **Taibur Rahman**, Jahid M M Islam, Shahadat Hossain Hossain, Hossain Uddin Shekhar. Food functionality of popular and commonly consumed indigenous vegetables and fruits from Bangladesh. *Food and Nutrition Sciences*, 2013, 4, 741-747.
- 2012: Q Shazia, Z H Mohammad, **Taibur Rahman**, and Hossain Uddin Shekhar "Correlation of Oxidative Stress with Serum Trace Element Levels and antioxidant enzyme status in Beta Thalassemia Major Patients: A Review of the literature" *Anemia*. 2012;2012:270923. Epub 2012 May 9.
- 2012: M. Mesbah Uddin, Sharif Akhteruzzaman, **Taibur Rahman**, A.K.M. Mahbub Hasan, and Hossain U. Shekhar "Pattern of β -Thalassemia and Other Haemoglobinopathies: A cross sectional study in Bangladesh" *ISRN Hematology*, Volume 2012, Article ID 659191,6 Pages.
- 2012: Sajib Charaborty and **Taibur Rahman**. "Difficulties in cancer treatment" Editorials in *ecancermedicalsecience*, 14 Nov 2012, <http://ecancer.org/ecms/editorials>]
- 2012: Sajib Chakraborty*, **Taibur Rahman**, Rajib Chakravorty, Alison Kuchta, Atai Rabby and Munsai Shaiuzzaman. HLA supertypes contribute in HIV-1 Cytotoxic T lymphocyte (CTL) epitope clustering in Nef and Gag proteins, *AIDS Res Hum Retroviruses*. 2012 Oct 12.
- 2012: **Rahman, T.**, Hosen, I., Islam, M. and Shekhar, H. (2012) Oxidative stress and human health. *Advances in Bioscience and Biotechnology*, 3,997-1019. doi:10.4236/abb.2012.327123.
- 2011: Kuchta A*, **Rahman T***, Sennott EL, Bhuyian TR, Uddin T, Rashu R, Chowdhury F, Kahn AI, Arifuzzaman M, Weil AA, Podolsky M, Larocque RC, Ryan ET, Calderwood SB, Qadri F, Harris JB. *Vibrio cholerae* O1 Infection Induces Pro-inflammatory CD4+ T Cell Responses in Blood and Intestinal Mucosa of Infected Humans. *Clin Vaccine Immunol*. 2011 Jun 22. [* indicate equally contributed First Author]

2011: Sheikh A, Khanam F, Sayeed MA, **Rahman T**, Pacek M, Hu Y, Rollins A, Bhuiyan MS, Rollins S, Kalsy A, Arifuzzaman M, Leung DT, Sarracino DA, Krastins B, Charles RC, Larocque RC, Cravioto A, Calderwood SB, Brooks WA, Harris JB, Labaer J, Qadri F, Ryan ET. Interferon- γ and Proliferation Responses to Salmonella enterica Serotype Typhi Proteins in Patients with S. Typhi Bacteremia in Dhaka, Bangladesh. PLoS Negl Trop Dis. 2011 Jun;5(6):e1193.

CONFERENCE REPORTS:

2016: **Taibur Rahman**¹, Izabela Swierzy¹, Bryan Downie², Gabriela Salinas-Riester², Martin Blume³, Carsten G.K. Lüder¹. Impact of host cell carbohydrate metabolism on *Toxoplasma gondii* bradyzoite formation in skeletal muscle cells. Abstract submitted on 68th Annual Meeting of the German Society for Hygiene and Microbiology' 11-14 September 2016. Ulm, Germany

2016: **Taibur Rahman**¹, Izabela Swierzy¹, Bryan Downie², Gabriela Salinas-Riester², Martin Blume³, Carsten G.K. Lüder¹ Regulation of *Toxoplasma gondii* bradyzoite formation in skeletal muscle cells – insights from host cell metabolome and transcriptome analyses. Abstract submitted on 27th Annual Meeting of the German Society for Parasitology, 9–12 March 2016. Göttingen, Germany.

2016: **Taibur Rahman**¹, Izabela Swierzy¹, Bryan Downie², Gabriela Salinas-Riester², Martin Blume³, Carsten G.K. Lüder¹ Intrinsic host factors triggers *Toxoplasma gondii* bradyzoite formation in terminally differentiated skeletal muscle cells-A study on the host cell transcriptome and metabolome. Abstract submitted on Workshop of the DGHM ' Eukaryotic pathogens' 28-29 January 2016. Aachen, Germany.

2012: Nabi AHMN, **Taibur Rahman**, Sajib Chakraborty, AKM Mahbub Hasan, Sonia Tamanna, Rajib Chakravorty, Fumiaki Suzuki. Conservation of (pro) renin receptor gene among different species: an evolutionary perspective. Abstract published in the proceedings of the Bangladesh Society for Biochemistry and Molecular Biology, 2012; p39

2011: Mohammad Arifuzzaman, Alison Kuchta, Taufiqur R. Bhuyian, Taibur Rahman, Erica L. Sennott, Taher Uddin, Rasheduzzaman Rashu, Fahima Chowdhury, Ashraf I. Kahn, Ana A. Weil, Regina C. LaRocque, Edward T. Ryan, Stephen B. Calderwood, Jason B. Harris, and Firdausi Qadri. *Vibrio cholerae* O1 infection induces robust pro-inflammatory CD4+ T-cell responses in blood and intestinal mucosa of infected humans. Abstract published in the proceedings of 13th Annual Scientific Conference, 2011, p247

2011: Alison L. Kuchta¹, **Taibur Rahman**¹, Taufiqur R. Bhuiyan¹, Mohammad Arifuzzaman¹, Rasheduzzaman Rashu¹, Ashraf I. Khan¹, Fahima Chowdhury¹, Amit Saha¹, Edward T. Ryan², Stephen B. Calderwood² Firdausi Qadri¹, Jason B. Harris¹ Proliferation of cytokine producing T cells in response to *Vibrio cholerae*

O1 infection or vaccination in Bangladeshi Adults. Abstract published in the preceding of American Society of Tropical Medicine and Hygiene.

- 2011: Alaullah Sheikh^{1,2}, Farhana Khanam¹, **Taibur Rahman**¹, Marcin Pacek³, Yanhui Hu³, Andrea Baresch², Md. Saruar Bhuiyan^{1,2}, Sean Rollins², Robert Citorik², Anuj Kalsy², Richelle Charles², Regina C. LaRocque², Joshua LaBaer³, Stephen B. Calderwood^{2,4}, Jason B. Harris², Firdausi Qadri¹, Edward T Ryan^{2,5,6} Evaluation of interferon- γ responses in patients with Salmonella enterica serovar Typhi bacteremia in Dhaka, Bangladesh. Abstract published in the preceding of American Society of Tropical Medicine and Hygiene.
- 2010: **Taibur Rahman**, Alison Kuchta, Taufiqur R Bhuiyan, Arifuzzaman M, Rasheduzzaman Rashu, Ashraful Khan, Fahima Chowdhury, Amit Saha, Edward T Ryan, Stephen B Calderwood, Firdausi Qadri, Jason B Harris. Cytokine responses in Vibrio cholerae O1 infected patients and oral cholera vaccine recipients. Presented to International summer program "Infection and Immunity" 4-8th September 2010, Tokyo Medical and Dental University, Japan.
- 2009: Weil AA¹, Arifuzzaman M¹, Bhuiyan TR¹, Thakkar H^{1,4}, Kuchta A¹, **Rahman T**¹, Harris JB^{2,3}, LaRocque RC^{2,4}, Banerjee KK⁷, Clements JD⁸, Ryan ET^{2,4,6}, calderwood SB^{2,4,5}, Qadri F¹ The contribution of T cells to the adaptive immune response in patients with dehydrating diarrhea caused by Vibrio cholerae O1. CHOLERA AND OTHER BACTERIAL ENTERIC INFECTIONS' 44th Annual joint panel Meeting, United States-Japan cooperative medical science program, San Diego, California, October 12-14, 2009

TECHNICAL EXPERTISE:

Cell culture, RNA/DNA isolation, RT-qPCR, PCR, Transformation and transfection, Gel electrophoresis, Gene knockdown, plasmid isolation, protein isolation, SDS-PAGE, Western Blotting, Immunofluorescence staining, Confocal microscopy, Victor kinetic assay, Blood cell isolation, Antibody in lymphocyte supernatant (ALS) assay, enzyme-linked immunosorbent assay (ELISA), Enzyme-linked immunospot (ELISPOT), Tritiated thymidine Assay, Flow cytometry based Intracellular cytokine assay (ICS), Flow cytometric assay of specific cell-mediated immune response in activated whole blood (FASCIA), Widal assay etc.

I confirm that the information provided in this CV is truthful and correctly describes my qualifications.

Göttingen, 25-09-2017

Md. Taibur Rahman